ASSESSMENT OF SEISMIC VULNERABILITY INDEX OF GAS NETWORK AREA IN DHAKA CITY USING MICROTREMOR MEASUREMENTS

Md. Arshadull Kabir

Department of Civil Engineering
BANGLADESH UNIVERSITY OF ENGINEERING AND TECHNOLOGY
DHAKA, BANGLADESH

2018

ASSESSMENT OF SEISMIC VULNERABILITY INDEX OF GAS NETWORK AREA IN DHAKA CITY USING MICROTREMOR MEASUREMENTS

A Project Report Submitted

by

Md. Arshadull Kabir

In partial fulfillment of the requirements for the degree of

MASTER OF ENGINEERING IN CIVIL ENGINEERING

(GEOTECHNICAL)

Department of Civil Engineering

BANGLADESH UNIVERSITY OF ENGINEERING AND TECHNOLOGY

DHAKA, BANGLADESH

March, 2018

The project titled **"Assessment of Seismic Vulnerability Index of Gas Network Area in Dhaka City using Microtremor Measurements"** submitted by Md. Arshadull Kabir, Roll No. 0413042236 (P), Session: April 2013 has been accepted as satisfactory in partial fulfillment of the requirement for the degree of Master of Engineering in Civil Engineering (Geotechnical) on 27th March, 2018.

BOARD OF EXAMINERS

Dr. Mehedi Ahmed Ansary — Chairman (Supervisor)
Professor
Department of Civil Engineering
Bangladesh University of Engineering and Technology.

Dr. Abu Siddique — Member
Professor
Department of Civil Engineering
Bangladesh University of Engineering and Technology.

Dr. Mohammad Shariful Islam — Member
Professor
Department of Civil Engineering
Bangladesh University of Engineering and Technology.

DECLARATION

It is hereby declared that except for the contents where specific references have been made to the work of others, the studies contained in this project report are the result of investigation executed by the author under the supervision of Dr. Mehedi Ahmed Ansary, Professor, Department of Civil Engineering, Bangladesh University of Engineering and Technology.

Neither the thesis nor any part thereof has been submitted or is being concurrently submitted to any other university or other educational institute for the award of any degree or diploma, except for publication.

(Signeture of the Author)

ACKNOWLEDGEMENT

The author conveys utmost gratitude to ALLAH, the Almighty, without His mercy and blessing, this work would not been possible. The author is grateful and would like to express his sincere gratitude to his supervisor, Dr. Mehedi Ahmed Ansary, Professor, Department of Civil Engineering, Bangladesh University of Engineering & Technology (BUET), Dhaka, for sharing his vision, experience, dynamic assistance, constant guidance, invaluable suggestions, enthusiastic encouragement, strong support, generous help, persistent simulation and unfailing enthusiasm at all stages that enabled him to successfully complete this research. Most helpful was his patience and ingenious ways of steering in the right direction, as the author often tended to drift during the course of this research.

The author wishes to express his gratefulness and sincere appreciation to his respected teachers Dr. Abu Siddique, Professor of the Department of Civil Engineering, BUET and Dr. Mohammad Shariful Islam, Professor of the Department of Civil Engineering, BUET for their valuable advice and directions in completing the project report.

The author conveys special thanks to Bangladesh Network Office for Urban Safety (BNUS) staffs for providing microtremor equipment as well as assistance to fulfill this research. The author is also very grateful to the Civil Engineering Department, BUET for providing all the necessary supports and funds for this whole work.

The author also gradually acknowledges towards his colleagues, friends and well-wishers, who have helped him, suggested him with a view to accomplishing the project work.

The author acknowledges the sacrifice of his parents and others of the family that has enabled him to attain this level.

ABSTRACT

The aim of this study is to assess seismic vulnerability index (K_g) of gas network area within Dhaka city by utilizing H/V spectral ratio method. Fifty eight locations in and around gas network area of Dhaka city have been selected for microtremor observation. Microtremor data has been collected and analyzed in order to determine predominant frequency and amplification factor according to the guideline of SESAME. Finally, seismic vulnerability index (K_g) of site soil using Nakamura's technique has been calculated from predominant frequency and amplification factor parameter for the purpose of this research. Microtremor measurements of 46 sites have produced reliable curves and peaks of H/V spectral ratio to determine the site predominant frequency and amplification factor. It is not possible to determine the predominant frequency and amplification factor for 12 sites since unreliable and flat curve. The predominant frequencies of the study area are relatively uniform, ranging from 0.36 to 1.5 Hz. The frequencies of the study area have been grouped ranges of $0.36Hz \leq f_0 \leq 0.50Hz$, $0.51Hz \leq f_0 \leq 1.0Hz$ and $1.0Hz < f_0 \leq 1.5Hz$. It has been observed a consistent peak in a frequency range $0.36Hz \leq f_0 \leq 0.50Hz$ covered the most part of the study area. The main reason for such a small range of results arises from the small differences in the near surface geological conditions of the study area. The observed frequencies can be related to the total thickness of soft sediments, deposited on the hard strata built of Madhupur tract. The low frequencies are obtained to soft soil sites in maximum measurements and the high frequencies are obtained to stiff soil sites in a few measurements. The amplification factor (A_0) or peak of H/V spectral ratio is in investigation sites ranging from 2.05 to 12.1. In the majority of the study area, the H/V spectral ratio peak amplitudes are between 2 and 6. Low values are measured for stiff soil sites and high values for soft soil sites. Finally, Seismic vulnerability index (K_g) is calculated from the predominant frequency and amplification factor for 46 sites. Seismic vulnerability index (K_g) is an index indicating the level of vulnerability of a layer of soil to deform at the time of occurrence of earthquakes. Damaging earthquakes will occur when the limits are exceeded due to the shear strain deformation surface layer of soil. The seismic vulnerability index (K_g) for 46 sites varies between 4.41 and 186.14. The low seismic vulnerability index indicates that the areas are very stiff as well as thick sediment deposit. Seismic vulnerability index (K_g) in the study area has been found that the high values are scattered in the soft alluvial deposits area having a high seismic vulnerability indication. Based on the basement ground acceleration, a_b = 0.2 g and the bedrock shear wave velocity, v_b = 800 m/s, about 17.4% of the study area will face very high damage during earthquake. On the other hand, while a_b = 0.2 g and engineering bed rock shear wave velocity, v_b = 500 m/s, about 28.3% of the study area will face very high damage during earthquake.

TABLE OF CONTENTS

LIST OF FIGURES

LIST OF TABLES

ABBREVIATIONS AND ACRONYMS

AR	Amplitude Ratio
BNBC	Bangladesh National Building Code
CGS	City Gate Station
DRS	District Regulatory Station
EW	East-West
GPS	Global Position System
GSB	Geological Survey of Bangladesh
HVSR	Horizontal to Vertical Spectral Ratio
H/V	Horizontal to Vertical
Hz	Hertz
MSL	Mean sea Level
NS	North-South
SCS	Segmental Cross-Spectrum
SESAME	Site EffectS assessment using AMbient Excitations
SPR	Standard Spectral Ratio
TBS	Town Border Station
UD	Up-Down
d	Seismic Displacement of Basement
f	Natural Frequency
g	Acceleration due to Gravity
h	Thickness of Surface Layer
H	Thickness of soil deposit
γ	Shear strain deformation
A_g , A_0	Horizontal to Vertical Spectral Ratio Peak /Amplitude/Amplification Factor
F_g , f_0	Predominant Frequency
K_g	Seismic Vulnerability Index
σ_f	Standard deviation of the peak frequency
$\sigma_A(f_0)$	Standard deviation of the amplitude at the peak frequency
α_b, a_b	Acceleration of basement
V_s	Shear Wave Velocity
V_b, v_b	Velocity of Basement
Vs	Velocity of Surface
S_T	Standard Spectral Ratio
S_{HS}	Horizontal Spectrum on a soft site
S_{HB}	Horizontal Spectrum on a hard site
S_{TT}	Modified Spectral Ratio
S_{VS}	Vertical Spectrum on a soft site
S_{VB}	Vertical Spectrum on a hard site
E_T	Effect of Source
Hs	Site Effect
Hr	Source Effect

CHAPTER 1
INTRODUCTION

1.1 GENERAL

Bangladesh is a small country situated in South Asia and bordered by India, Bhutan, and Myanmar. Its geography makes it unlike any other place on Earth. The Himalayas, the world's largest mountain range are to the north of Bangladesh. The Brahmaputra, Ganges and Meghna flow from the Himalayas and other nearby mountain ranges and amalgamate in Bangladesh. These rivers deposit huge amounts of mud and sand. All this sediment forms the world's largest delta. Much of the region's geography is shaped by what's happening beneath the surface-between the tectonic plates that make up Earth's crust. Bangladesh is one of the most tectonically active regions in the world. It sits where three tectonic plates meet: the Indian Plate, the Eurasian Plate, and the Burmese Plate. As the Indian Plate moves gradually northeast, it is slowly colliding with the Eurasian Plate, causing the Himalayas to rise. Active faults are found along this boundary, particularly the 300km-long Dauki fault that borders northern Bangladesh. Here, the large Shillong Plateau is slowly folding over the Indian Plate. To the east, the Burmese Plate pushes west against (and over) the Indian Plate. As these plates collide, rocks fold and buckle to form the hills and valleys of the Burma Arc. Bangladesh has a long history of earthquakes. In 1762, a major earthquake caused the submergence of 150 square kilometers of land, and killed 500 people in Dhaka, then only a small town. Between 1850 and 1950, there have been another 7 significant earthquake in the region, ranging in magnitude from 7.0 to 8.7 on the Richter scale. Since the last significant earthquake, Bangladesh has changed quite significantly. The greater Dhaka area has a population of over 15 millions. A study (CDMP, 2011) conducted a few years ago predicted over 120,000 casualties in Dhaka due to a 7.5M earthquake. Bilham et al. (2001) pointed out that there is high possibility that a huge earthquake will occur around the Himalayan region based on the difference between energy accumulation in this region and historical earthquake occurrence. The population increase around this region is at least 50 times than the population of 1897 and city like Dhaka has population exceeding several millions. The infrequent occurrence of destructive earthquakes does not permit the compilation of enough data to support the estimation of the distribution of damages in the future. To overcome this lacking, different authors

proposed the use of alternative sources of excitation, such as, distant earthquakes, small near earthquakes, explosions, aftershocks and microtremors.

The use of microtremor, an idea pioneered by Kanai et al. (1954) turns into one of the most appealing approaches in the site effects studies, due to its relatively low economic cost, and the possibility of recordings without strict spatial or time restrictions (Rodriguez and Midorikawa, 2002). The H/V spectral ratio technique of microtremors has gained popularity in the early nineties, after the publication of several papers (Nakamura, 1989; Field and Jacob, 1993; Lermo and Chávez-García, 1994; Asskar Choobbasti et al., 2015) claiming the ability of this technique to estimate the site response of soft sedimentary deposits satisfactorily. This method is rather attractive in developing countries characterized by a moderate seismicity, where only very limited resources are available for seismic hazard studies. The H/V spectral ratio determined from microtremors has shown a clear peak that is well correlated with the fundamental resonance frequency at "soft" soil sites (Bard, 2004; Horike et al., 2001; Field et al., 1995; Lachet and Bard, 1994; Lermo and Chávez-García, 1993). Based on numerical calculations, many other researchers (Lermo and Chávez-García, 1993, 1994; Lachet and Bard, 1994; Dravinski et al., 1996) have shown that the H/V ratio method is obviously able to predict fundamental resonant frequency well. Huang et al. (2002) has found that the ground vulnerability index (K_g) values in the liquefied areas are higher than those in the neighboring areas without liquefaction at 42 points in central Taiwan. By using the fundamental frequency and amplification factor of microtremor measurement, the value of vulnerability index (K_g) has been calculated and the liquefaction potential has been evaluated in Babol city. For controlling the accuracy of this method, its output has been compared with the results of Seed and Idriss method in 30 excavated boreholes and these two methods show an acceptable conformity with each other (Asskar Choobbasti et al., 2015).

Although it is not possible to prevent earthquake, it is however, possible to mitigate the impacts of this disaster. Specific roles and responsibilities relating to earthquake hazard should be emphasized in our disaster mitigation plan. Bangladesh is a country characterized by a moderate seismicity with almost no resources available for large scale seismic hazard studies. The objective of this study is to evaluate the seismic vulnerability index (K_g) using H/V spectral ratio of microtremor in terms of predominant frequency and corresponding amplification within the gas network area of Dhaka city.

1.2 STUDY AREA AND GEOLOGY

The gas is supplied through pipe of different diameter under the ground soil to gas network area of Dhaka City by Titas Gas Transmission & Distribution Company Limited. The gas network of Dhaka city consists of the length of 16 inch, 14 inch, 12 inch, 10 inch, 8 inch, 6 inch, 4 inch, 3 inch and ≤ 2 inch diameter pipe is found to be 248.09 km, 173.16 km, 453.04 km, 188.01 km, 473.44 km, 371.72 km, 826.76 km, 810.64 km and 9382.01 km respectively laying beneath the ground soil about 1 m to 3 m (Figure 1.1). There are total 23 gas supply District Regulatory Station (DRS), Town Border Station (TBS) and City Gate Station (CGS) in the gas network of Dhaka city. To assess seismic vulnerability index (K_g) of gas network area in Dhaka city, fifty eight locations have been selected to obtain microtremor observation. These microtremor observation sites are situated at latitude from 23˚40′ N to 23˚55′ N and longitude from 90˚18′ E to 90˚27′ E.

1.2.1 Geological Subdivisions of Dhaka city

The geology of various locations of Bangladesh is shown in Figure 1.2. More than 80% of Bangladesh is underlain by quarternary sediments consisting deltaic and alluvial deposits of the Ganges, Brahmaputra and Meghna rivers and their tributaries. The sediments of Bangladesh Geology has been classified into five major groups, which are Coastal deposits, Deltaic deposits, Paludal deposits, Alluvial deposits and Residual deposits. These five major groups are sub-divided into seventeen different geological units. Dhaka is located between the Megna and Brahmaputra Flood Plains. The soil deposits mainly consist of the Alluvial Silt and Clay; Madhupur Clay Residuum and Marsh Clay and Peat of soil. The geology of the study area is located in three major groups, which are paludal deposits, Residual deposits and Alluvial deposits. The geological units are ppc (Marshy clay and peat), asd (Alluvial sand), asl (Alluvial silt), asc (Alluvial silt and clay) and rm (Modhupur clay residium). The brief descriptions of these five geological units are given below:

(a) Marshly clay and peat: ppc is generally Marsh clay and peat-gray or bluish gray clay, black herbaceous peat and yellowish-gray silt. Alternating beds of peat and peat clay common in bills and large structurally controlled depression; peat is thickest in different parts.

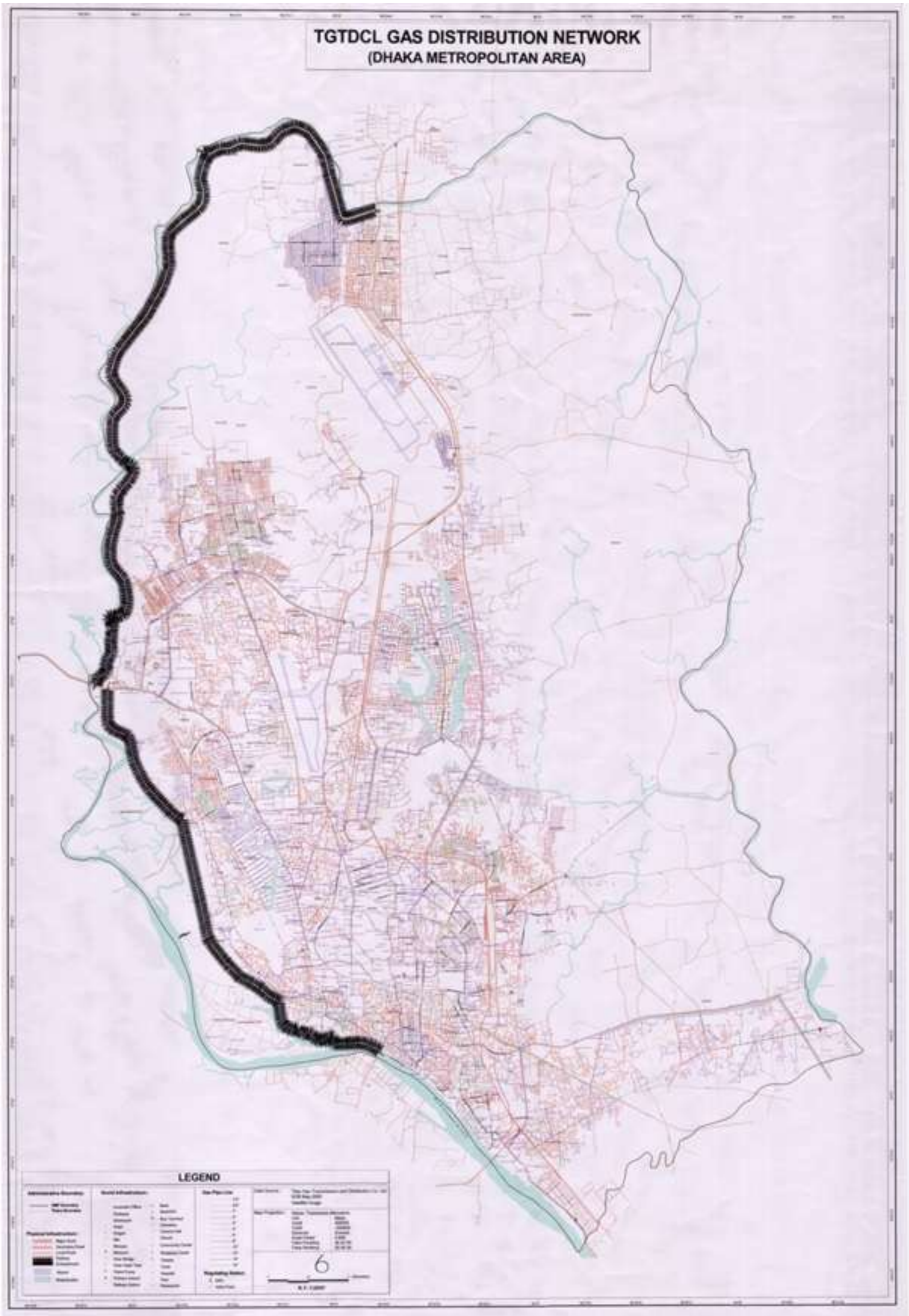

Figure 1.1: Gas pipe line network of Dhaka City (Source: Titas Gas Transmission & Distribution Co. Ltd. SOB Map, 2000)

(b) Alluvial sand: The common asd is Alluvial Sand-Light to brownish grey, coarse sand to fine silty sand. Sand is generally subrounded; constitutes channel, bar and levee deposits along rivers and larger tributaries; small and medium-scale crossbeds and laminations are common Brahmaputra river sand is medium to fine. Grain size decreases generally from North to South and away from channels. Brahmaputra sand contains mostly quartz, feldspar, mica, and significant amount of heavy minerals, indicating that the sand is first cycle sediments from the Himalayan Mountains and the Indian shield. Meghna sand contains quartz-rich, reworked sediments from sandy tertiary rocks in the Fold Belt embedded with sediment derived from igneous rocks of the Shillong Plateaus.

(c) Alluvial Silt: The asl is alluvial silt- Light to medium grey, fine sandy to clayey silt. Commonly poorly stratified; average grain size decreases away from main channels, chiefly deposited in flood basins and interstream areas. Unit includes small block swamp deposits during episodic or unusually large floods. Illite is the most abundant clay flooded annually, included in this unit are thin western of sand spread by episodic large floods over flood plain silts.

(d) Alluvial silt and clay: The asl is generally Medium dark gray to clay; colour is darker as amount of organic material increases. Map unit is a combination of alluvial and paludal deposits; includes flood-basin silt, back swamp silty clay and organic rich clay is sag ponds and large depressions. Some depressions contain peat. Large area underlain by this unit is dry only a few months of the year; the deeper part of depressions and bills (bhils) contain water throughout the year.

(e) Madhupur clay residuum: Madhupur Clay is the oldest sediment exposed in and around the city area having characteristic topography and drainage. Madhupur Clay characterized by Light yellowish-grey, orange, light to brick-red, and grayish white, micaceous silty clay to sandy clay; plastic and abundantly motted in upper 8 m; contains dominantly quartz, minor feldspar (orthoclase greater than plagioclase) and mica; sand content increases with depth, Dominantly clay minerals are kaolinite and illite. Iron manganese oxide nodules concentrated in zones; calcium carbonate nodules rare. Locally, a cohesive, 35 cm thick iron oxide zone is preserved near the surface of residuum.

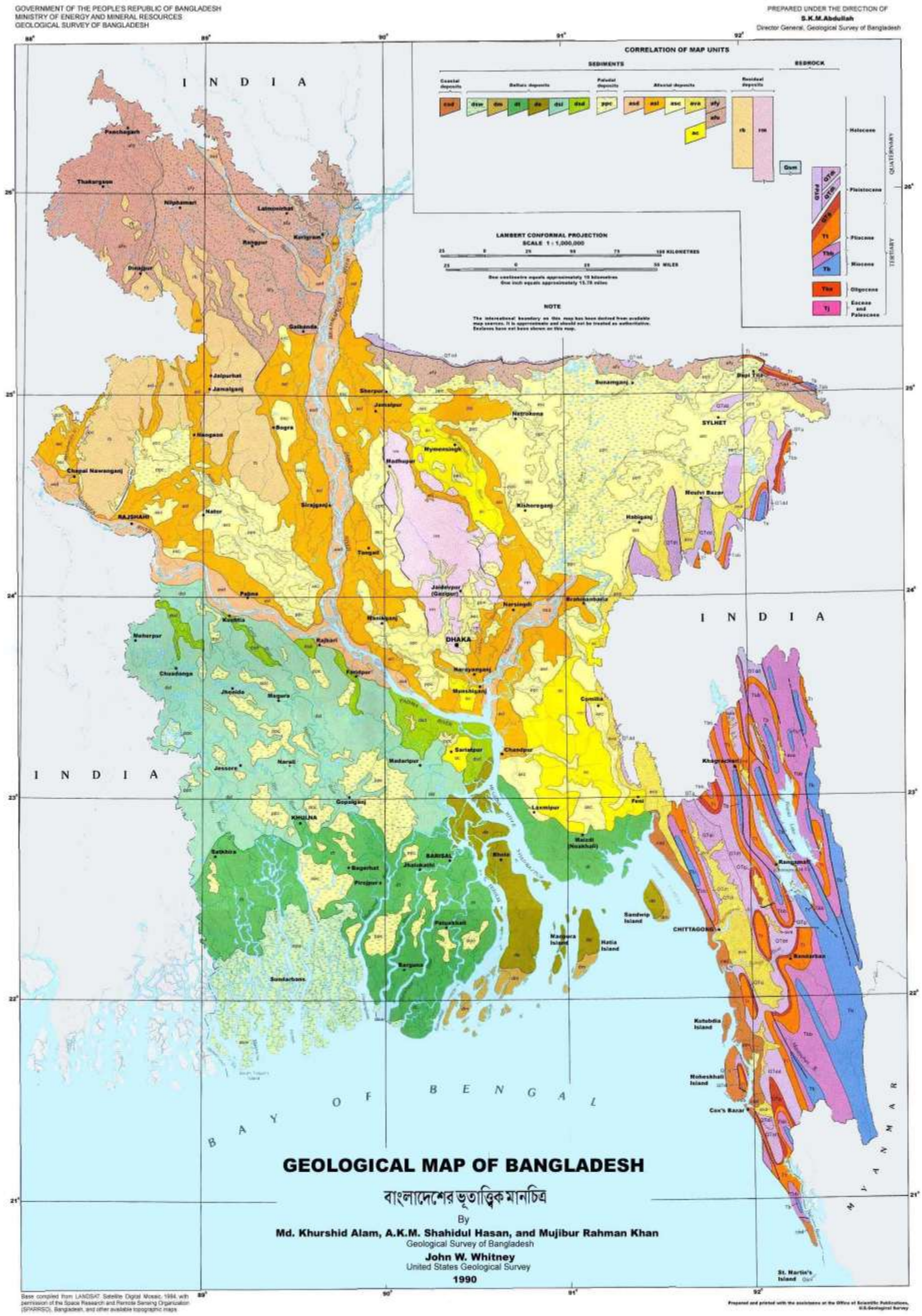

Figure 1.2: Geology Map of Bangladesh. (Source: Geological Survey of Bangladesh, Alam et al., 1990)

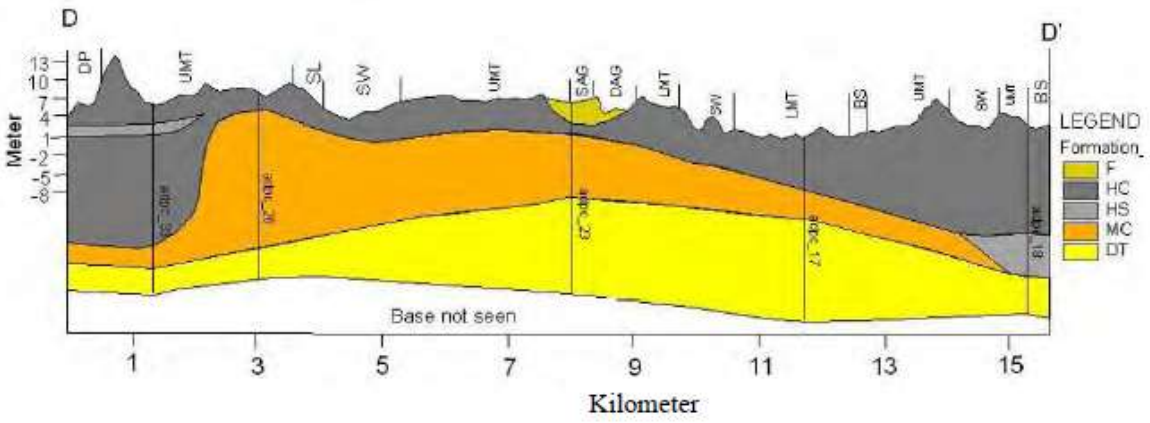

(Note: F-Fill, HC-Holocene Clay, HS-Holocene Sand, MC-Madhupur Clay and DT-Dupi Tila)

Figure 1.3: Schematic geological cross section of Dhaka (after CDMP, 2011)

Schematic geological cross section of Dhaka is presented in Figure 1.3. In the section, it is shown that the strata of Dhaka generally consists of 3 layers, which are Holocene soil including Fill, *Modhupur* Clay and *Dupi Tila*. Thickness of *Modhupur* Clay gradually becomes thin or is disappeared towards boundary of Dhaka. *Dupi Tila* distributes whole Dhaka, and surface of *Dupi Tila* in the central part and its surroundings are encountered in shallow portion (shallower than 20 m in depth from ground surface) and in the deeper portion (deeper than 30 m in depth beside the boundary of Dhaka).

1.3 OBJECTIVE OF THE PROJECT

The specific objectives of this project are

i. To estimate predominant frequency (f_0) and amplification factor (A_0) for each selected location within gas network area in Dhaka city using the H/V Spectral Ratio technique from microtremor observation.
ii. To calculate seismic vulnerability index (K_g) of the gas network area in Dhaka city using predominant frequency (f_0) and amplification factor (A_0).
iii. To identify site soil damage level during earthquake from the value of seismic vulnerability index (K_g) of the study area.

1.4 OVERVIEW OF THE PROJECT

The main purpose of this project is to estimate seismic vulnerability index (K_g) of soil at different locations of gas network area in Dhaka City from predominant frequency and amplification factor using Horizontal to Vertical (H/V) spectral ratio technique of microtremor observation.

Chapter 1 presents a short background of the study, study area and geology as well as objectives of the study.

Chapter 2 presents Regional Tectonics; Relevant literature review that includes past researches on HVSR and microtremor; relationship between microtremor and earthquake; Horizontal to Vertical (H/V) spectral ratio technique; Analysis approach of Horizontal to Vertical Spectral Ratio (HVSR), development of HVSR and Reliability of HVSR according to SESAME. In addition to this, application of microtremor H/V ratio technique for damage assessment of any site soil from vulnerable index value has been included.

Chapter 3 represents location, geology and geomorphological classification of selected sites of the study area. This chapter includes microtremor data collection guidelines; precautionary measures; constraints of data acquisition in the field and data recording according to SESAME.

Chapter 4 consists of detailed H/V spectral ratio analysis methodology, Criteria of The H/V Spectral Ratio Analysis, H/V Spectral Ratio Analysis, Results and Discussions as well as calculation of seismic vulnerability index (K_g) of the study area.

Chapter 5 presents the specific conclusions of the results and the findings resulting from this research. It includes recommendations for future research.

CHAPTER 2
LITERATURE REVIEW

2.1 GENERAL

Damages due to seismic vibration are depended on the local geological conditions, infrastructure, the combination of local geology and structure, the seismic characteristic and the distance between structure and earthquake epicenter. Maximum damages due to seismic vibration can be controlled assessing local geology as well as local site effect. The site effects can be determined using analytical and empirical methods. The analytical calculation of the site response requires a very good knowledge of the geotechnical parameters to constrain the results. Empirical methods are also more effective as the frequency spectrum calculated directly from the recorded ground motion. Among the empirical methods, the spectral ratio of a sedimentary site to a bedrock site, known as the *standard spectral ratio technique*, is a widely used approach (e.g., Borcherdt, 1970; Borcherdt and Gibbs, 1976; Rogers et al., 1984). Effective use of this technique is demonstrated at different sites and geological conditions following large destructive earthquakes (e.g., Singh et al., 1988; Lermo et al., 1988; Borcherdt et al., 1989; Hough et al., 1990).

Among empirical methods, a reflexive method increasing in popularity for site response analysis is the HVSR (H/V spectral ratio method), also commonly referred to as the Nakamura's method. The HVSR method is effective to determine site response by removing source effects by dividing the horizontal component of ambient noise by the vertical component. This method has been applied by many researchers, like, Gosar, A, 2010; Kelli et al., 2010; Dwa Desa et al., 2011; Rahman Md. Saidur, 2011; Elcin Gok and Orhan Polat, 2012; Asskar et al., 2013, 2015; Bouranta et al., 2013; Pyi Soe et al., 2014; Khalda Y. et al., 2015; Sayed SR Moustafa, 2015; Qadri et al., 2015; Hatem F. A., 2016 Andrej Gosar, 2017 and Raymond Ng, 2017 to identify the fundamental resonant frequency, amplification factor, depth and vulnerability index of sediments. Microtermors are very important and useful measurements in site response that will compensate the shortage and deficiency of the seismic record data. Many studies of H/V method to check and evaluate the consistency of the technique with the analysis of strong motion records such as, Chavez-Garcia & Cuenca, 1996, Teves-Costa et al., 1996, Bour et al., 1998, Jensen, 2000, Chavez-Garcia and Tejeda-Jacome, 2010; Surve & Mohan, 2010.

Microtremors are used to estimate local site effects due to its simple approach and applicability by using a single three-component seismograph. Microtremors can be performed at various site conditions, the instruments and the analysis are simple, and it does not have any environmental consequence. Microtremor and Earthquake consists of different types of waves producing in soil from various sources. The common noise sources are vibrating machine, traffic, environment and human movement. Microtremor observation is carried out to record time history of ambient noise of ground at certain location. Ambient noise is known by many synonyms: microtremor, ambient vibration, seismic noise, ambient wavefield, etc. Ambient noise is produced by random sources, a combination of both natural and anthropic signals as categorized by Gutenberg (1958), and contains both surface and body waves. Natural signals, microseisms, originate from the ocean and are predominantly Rayleigh waves as theorized by Longuet-Higgins (1950), while anthropic signals which originate from industry or human activity are mainly Love and Rayleigh waves as categorized by Gutenberg (1958); Asten (1978) and SESAME WP12 (2004). Typically, the boundary between microseisms and anthropic signals is at the 1 Hz frequency as suggested by various authors (e.g., Gutenberg, 1958; Asten, 1978; Frantti et al., (1962) and Frantti (1963). However, Seo (1997) found the boundary between microseisms and anthropic signals can be at a lower frequency in a deep and soft basin. Microseisms are generated by ocean wave energy coupling with the earth and are commonly observed in ambient noise data by a primary peak at 0.07 Hz and secondary peak at 0.15 Hz as discussed in Longuet-Higgins (1950). According to Bonnefoy-Claudet et al. (2004) low frequencies are predominately fundamental modes of Rayleigh waves, while at higher energies; Love waves begin to have a higher proportion. Figure 2.1 shows various sources of microtremor for site response analysis. Microtremor is composed of fundamental mode of Rayleigh wave (Sato et al., 1991; Tokimatsu and Miyadera, 1992). Higher frequency microtremor bears resemblance to Shear Wave characteristics (Nakamura, 1989; Wakamatsu and Yasui, 1995). On the other hand, microtremors can also be dominated by Love-wave (Tamura et al. 1993). Suzuki et al. (1995) has applied microtremor measurements to the estimation of earthquake ground motions based on a hypothesis that the amplitude ratio defined by Nakamura can be regarded identical with half of the amplification factor from bedrock to the ground surface. However, the real generation and nature of microtremors have not yet been established.

This chapter presents regional tectonics and the past researches related to H/V technique using microtremor. The reliability with application of Horizontal to Vertical Spectral Ratio (H/V) has been discussed from different points of view. The relationship between microtremor analysis and seismic activity has also been included in this chapter. The characteristics of various types of microtremor waves have been illustrated using mathematical expressions. Finally, seismic damage assessment of Nakamura's vulnerability index for damage estimation of soil has been discussed.

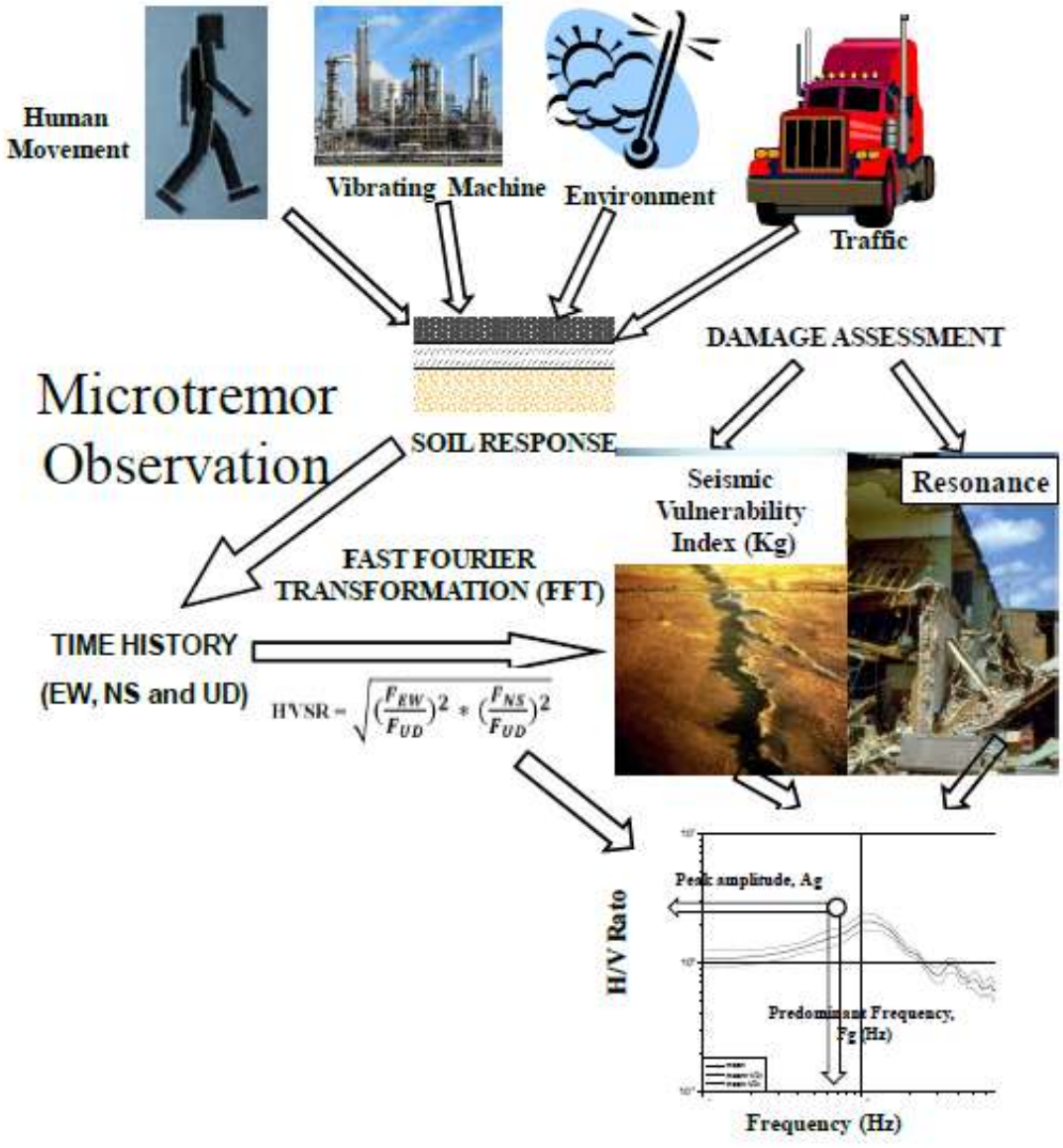

Figure 2.1: Microtremor observation and damage assessment (after Rahman et al., 2011)

2.2 REGIONAL TECTONICS

Plate tectonics provide a physically simple mechanism for large-scale horizontal motions of separate portions of the earth's crust. One of the central concepts of plate tectonics is that a small number of large plates of high strength lithosphere, move rigidly with respect to one another at rates of 1 to 20 cm/year over the low-strength asthenosphere. According to Molnar and Tapponnier (1975), for the past 40 million years the Indian subcontinent has been pushing northward against the Eurasian plate at a rate of 5 cm/year, giving rise to the severest earthquakes and most diverse land forms known. Figure 2.2 Estimated slip potential along the Himalaya (after Bilham et al., 2001) and Figure 2.3 shows India's northward drift over the last 70 million years (after Molnar and Tapponnier, 1975).

The region of northeastern India, northern Burma and Southwestern China is tectonically and seismically one of the most interesting active plate boundaries. The region comprises the Himalayas, the Indo-Burma Ranges, the Tripura folded belt, the Bengal Basin, the Shillong Plateau and the Assam Valley. Figure 2.4 shows the Generalized tectonic map of Bangladesh and adjoining areas (After GSB, Alam et al., 1990). It is a rifted eastern marginal basin of Indian plate that is gradually shortening due to the subduction of the Indian plate and overriding of the Burmese plate from the east.

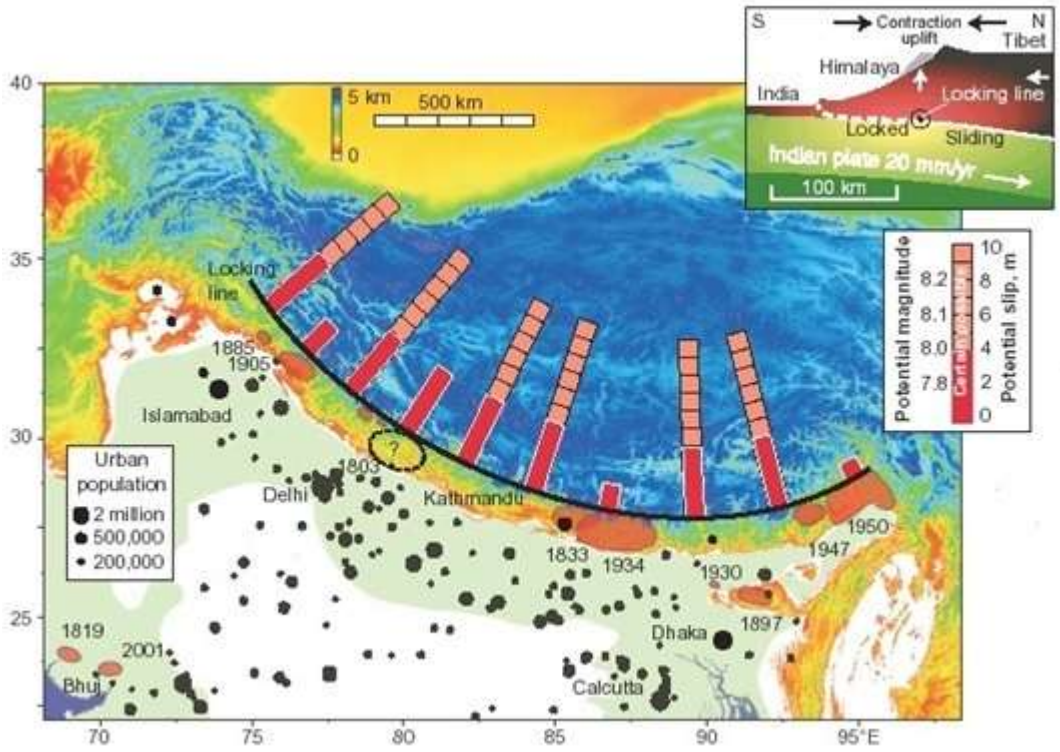

Figure 2.2: Estimated slip potential along the Himalaya (after Bilham et al., 2001)

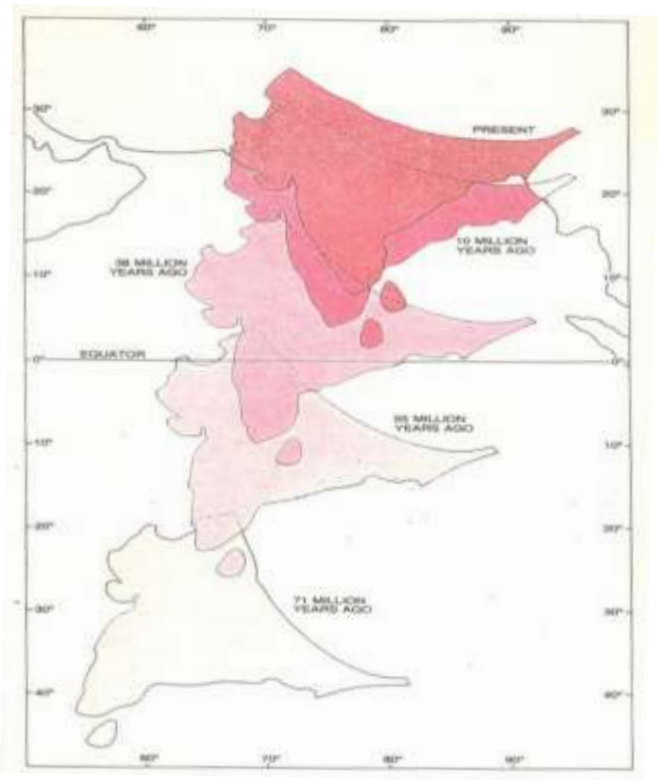

Figure 2.3: India's northward drift over the last 70 million years (after Molnar and Tapponnier, 1975)

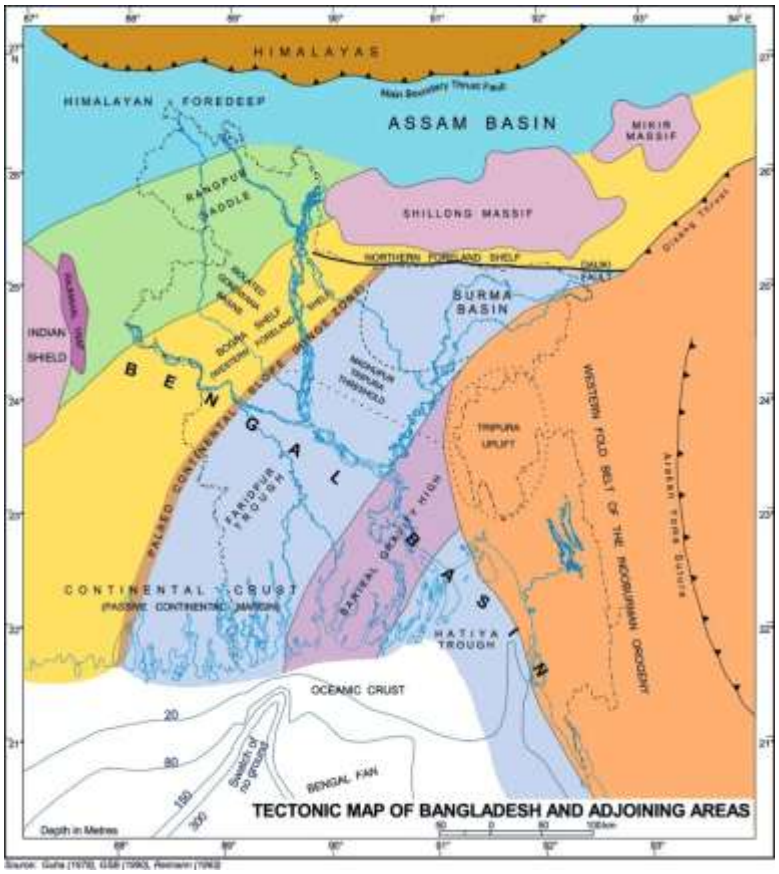

Figure 2.4: Generalized tectonic map of Bangladesh and adjoining areas (After GSB, Alam et al., 1990)

2.2.1 Seismotectonic Setup

Bangladesh has been divided into three major tectonic zones (Khandaker, 1989):

(1) *The Shelf zone*: It consists of mainly the northwestern part of the country including the districts of Rangpur, Dinajpur and Bogra.

(2) *The Hinge zone*: It passes through Calcutta, Pabna, Mymensingh and extend further NE across the Dauki fault.

(3) *The Bengal Foredeep zone*: It comprises of the rest of area of the country and occupies the area between the Shelf zone in the west and Arakan-Yoma Hill range in the east. The deep basin area of the foredeep is composed of the Surma Basin or Sylhet Trough, Faridpur Trough and the Hatia Trough.

The junction between the platform and the foredeep running southwest from Mymensingh to Calcutta (the Hinge line) is considered to be a zone of weakness. However, no association of the hinge with earthquakes has so far been established. The Foredeep is terminated in the northeast by a major fault, the Dauki fault at the southern margin of the Shillong Plateau. Some major earthquakes can be related to this fault. There are numerous faults particularly in the eastern part of the folded flank of the Foredeep. Here again there is no association with any major earthquake. Most recorded earthquakes had epicenter further east in Burma.

The eastern margin of the Indian plate is supposed to run through Myanmar, not far from the Bangladesh border, and northeast Assam (Arunachal Pradesh) is considered to be a corner of the northern and eastern margins of the plate.

The Himalayan arc can be regarded as one of the most intensely active seismic regions of the world. In northeast India, the Shillong plateau and adjacent syntaxis between the two arcuate structures is one of the most unstable regions in the Alpine-Himalayan belt and faced three major earthquakes of magnitude greater than 8.0 within the last two hundred years (1897, 1934, and 1950).

At present, the southernmost thrusting in the Himalaya-Shillong Plateau region could be taking place along the southern fringe of the plateau coinciding with the Dauki fault.

Currently, it is believed that the Shillong plateau has a thrust plane beneath it and is undergoing southward thrusting against a concept of vertical tectonism along the Dauki fault.

The Shillong plateau and its adjoining region including the northeastern part of Bangladesh have high seismic status. The seismic activity along the Dauki-Haflong fault zone is comparatively lower and a seismic gap has been postulated along this fault zone. The major earthquakes that have affected Bangladesh since the middle of the last century are presented in Table 2.1.

Table 2.1 Great historical earthquakes in and around Bangladesh

Date	Name	Epicenter	Magnitude (M)
10-01-1869	Cachar Earthquake	Jantia Hill, Assam	7.5
14-07-1885	Bengal Earthquake	Sirajgonj, Bangladesh	7.0
12-06-1897	Great Indian Earthquake	Shillong Plateau	8.7
18-07-1918	Srimangal Earthquake	Srimangal, Sylhet	7.6
02-07-1930	Dhubri Earthquake	Dhubri, Assam	7.1
15-01-1934	Bihar-Nepal Earthquake	Bihar, India	8.3

2.2.2 Major Seismic Sources

The seismic hazard is typically determined using a combination of seismological, morphological, geological and geotechnical investigations, combined with the history of earthquake in the region. Bolt (1987) analyzed different seismic sources in and around Bangladesh and arrived at conclusions related to maximum likely earthquake magnitude. Bolt identified the following four major sources:

i. Assam fault zone
ii. Tripura fault zone
iii. Sub- Dauki fault zone
iv. Bogra fault zone

A brief description of geology, tectonics of the individual fault zone is given below:

(i) Assam fault zone: The east-west fault separates the Assam fault zone from sub-Dauki fault zone. This zone consists of Archaean Proterozoic basement complex and characterized by the maximum concentration earthquake events. The hypocenter beneath the Shillong plateau is shallow focus in origin and are scattered. Only a few epicenters appear on or close to Dauki fault indicate that this fault is relatively seismically inactive during the recent time. But it was active since the Jurassic and was the main architect for the evolution of Shillong plateau. The great earthquake of 1897 originated in the Assam fault zone. Number morphotectonic lineaments have been identified from the study of the satellite imagery. Most of the lineaments trend NE-SW with a few trending N-S. The N-S trending Brahmaputra fault is present along the course of Brahmaputra River. The fault dips steeply to the north. This zone is characterized by scattered shallow depth earthquake probably due to prevalent upward forces existing below the Shillong Plateau.

ii) Tripura fault zone: This zone is characterized by high concentration of earthquake events. A number of morphotectonic lineaments have been identified. Among these the Kopili lineament trending NW-SE is remarkable and is geologically recent in origin. Seismic section reveals that this lineament is the surface expression of deep-seated subvertical fault and termed as the Kopili fault, which belongs to the category of high angle reverse fault. At the north of this zone Halflong-Dissang thrust is present. Morphotectonic lineaments around the Halflong-Dissang thrust zone trend NE-SW, E-W and NW-SE. Mikir hill is present to the northeast corner of the Halflong-Dissang thrust, which separates the Shillong plateau by Kopili fault.

iii) Sub-Dauki fault zone: This zone covers the southern part of Dauki fault and eastern part of Bogra fault zone and bounded by longitude 90ºE and 92ºE. The morphotectonic lineaments trend NNW- SSE and NW-SE. The Sylhet plain covers the area and comprises the vast alluvial tract and the linear belts of folded Tertiary rocks trending N-S and NNE-SSW. Sylhet lineament of 180 km long trending NE-SW is the subsurface expression of deep seated high angle reverse fault having a dip of about 70º towards southeast and as named as Sylhet fault. A number of epicenteres fall on or close to this fault and some of them were of damaging character. Among them the earthquake of 1845 and Srimangal earthquake of 1918 are remarkable.

iv*) *Bogra fault zone: This is the westernmost area bounded by latitude 20ºN and 28ºN, and longitude 87ºE and 90ºE. The area is covered with thick deposits of alluvium. The main boundary fault of Himalayan ranges occurs in the north of this fault zone. A number of morphotectonic lineaments have been identified from the study of satellite imagery. These are mostly oriented NW/ NNW- SE/SSE. One such lineament is Teesta lineament. Gupta and Nandi seismic activity in the Garo-Rajmahal gap is related to the activity along the Jamuna fracture which is the surface manifestation of apparently deep-seated sub-vertical fault. Most of the earthquakes along this fault are shallow in depth. But one earthquake had a depth of hypocentre of 100 km. The 1885 earthquake of magnitude 7.0 was originated in this fault.

The magnitudes of earthquake suggested by Bolt, (1987) (Table 2.2) are the maximum magnitude generated in these blocks as recorded in the historical seismic catalogue. The historical seismic catalogue of the regions covers approximately 250 years of (starting 1762) recent seismicity of the region and such a meagre database does not provide true picture of seismicity of the tectonic provinces. For example, the Assam and Tripura fault zones contain significant faults capable of producing magnitude 8.6 and 8.0 earthquakes respectively in future. Similarly maximum magnitude of 7.5 in Sub- Dauki fault zone and Bogra fault zones are not unlikely event.

Table 2.2 Significant Seismic Sources and Maximum Likely Earthquake Magnitude in Bangladesh (After Bolt, 1987)

Location	**Maximum likely earthquake magnitude**
A. Assam fault zone	8.0
B. Tripura fault zone	7.0
C. Sub-Dauki fault zone	7.3
D. Bogra fault zone	7.0

After a thorough review of available data, Ali and Choudhury (1992) recommended magnitudes of Operational Basis Earthquakes and Maximum Credible Earthquakes in Table.2.3.

Table 2.3 Operational Basis Earthquakes, Maximum Credible Earthquake and Depth of Focus of Earthquakes for Different Seismic Sources (After Ali And Chowdhury, 1992)

Location	Operational basis Earthquakes (Richter)	Maximum Credible Earthquakes	Depth of focus (km)
A. Assam fault zone	8.0	8.7	0-70
B. Tripura fault zone	7.0	8.0	0-75
C. Sub-Dauki fault zone	7.3	7.5	0-75
D. Bogra fault zone	7.0	7.5	0-70

Reliable historical data for seismic activity affecting Indian subcontinent is available only for the last 450 years (Gupta et al., 1982). Recently developed earthquake catalogue for Bangladesh and surrounding area (Sharfuddin, 2001) showed that 66 earthquakes with Ms ≥4.0 occurred from 1885 to 1995 within a 200 km radius of Dhaka City. The most prominent historical earthquakes affecting of Bangladesh was listed in Table 2.4.

Table 2.4 Magnitude, EMS Intensities and distances of some major historical earthquakes around Dhaka (after Ansary, 2001)

Name of Earthquake	Magnitude	Intensity at Dhaka	Distance (km)
1869 Cachar Earthquake	7.5	V	250
1885 Bengal	7.0	VII	170
1897 Great Indian Earthquake	8.7	VIII+	230
1918 Srimangal Earthquake	7.6	VI	150
1930 Dhubri Earthquake	7.1	V+	250

2.3 PAST RESEARCHES ON H/V SPECTRAL RATIO AND MICROTREMOR

The infrequent occurrence of destructive earthquakes does not permit the compilation of enough data to support the estimation of the distribution of damages in the future. To overcome this lacking, different authors proposed the use of alternative sources of excitation, such as, distant earthquakes, small near earthquakes, explosions, aftershocks and microtremors. Wave propagation mechanism of microtremor and its relation with ground vibration characteristics have been studied from the beginning of microtremor studies (Aki, 1957; Kanai and Tanaka, 1961). Meanwhile, practical application of microtremor in the field of engineering has advanced tremendously. One of the powerful and simplest applications of microtremor observation is in seismic micro-zoning.

The use of microtremors, an idea pioneered by Kanai et al. (1954) turns into one of the most appealing approaches in site effects studies, due to its relatively low economic cost and the possibility of recordings without strict spatial or time restrictions (Rodriguez and Midorikawa, 2002). In recent studies, ambient noise measurements have been widely applied (Seo, 1994). The results obtained from the application of long period ambient noise measurements (Ohta et al., 1978; Yamanaka et al., 1993, 1994) allow the application microtremor for site effects. Short period ambient noise measurements have been applied to a wide range of seismic settings (Morales et al., 1991, 1993; Lermo and Chavez-Garcia, 1993; Field and Jacob, 1993; Field et al., 1995; Seo, 1994). The H/V spectral ratio method (Nakamura 1989) has been discussed at great length and proven to be a suitable, quick and effective method (Konno and Ohmachi, 1998; Bard, 1999; Enomoto et al., 2002) for determining the predominant period of soil. This method has been applied to different Spanish cities exposed to a moderate seismic hazard (Vidal et al., 1996; Seo, 1994; Pujades et al., 2000; Alfaro et al., 2001; Navarro et al., 2001).

Dividing the research area into regions in line with material conditions is a very useful way of reducing the number of sites whose effect has to be considered. The first step is the geological and geotechnical identification of the materials, after which the obtained soil conditions have been extrapolated. Due to close relation between microtremors and the fundamental dynamic behavior of the surface soil layer Taga (1993), microtremor measurements can prove a useful tool for evaluating the properties of earthquake ground motion and also for extrapolating the seismic motion observed at a given point to its surrounding area.

The concentration of human activity in urban areas implies an accumulation of risk elements, to which traditional seismic hazard studies do not devote enough attention. This is why specific studies based on very detailed research of close sources are essential, as are in situ measurements that take into account local effects. Priority has to be given to this sort of studies in order to prevent, mitigate and manage seismic risks. The superficial geology of an urban area has a remarkable influence on the distribution of the damages caused by an earthquake. It has been proved that soil movement during an earthquake can be amplified by local landform conditions (Aki, 1993 and Bard, 1999) and in some cases it amplifies the seismic shake in a range of periods that coincide with the period of vibration of the damaged structures (Seo, 1994), showing the relationship between the amplification caused by surface geology and the degree of destruction. Even though urban geomorphology is a term that appeared only recently, its use has spread significantly over the last few years.

The H/V spectral ratio technique of microtremors gained popularity in the early nineties, after the publication of several papers (Nakamura, 1989; Field and Jacob, 1993; Lermo and Chavez-Garcia, 1994) claiming the ability of this technique to estimate the site response of soft sedimentary deposits satisfactorily. The mathematical expression of Microtremor H/V Technique is discussed in section 2.4 of this Chapter. The method is rather attractive in developing countries characterized by a moderate seismicity, where only very limited resources are available for seismic hazard studies.

The single-instrument microtremor method has been widely applied across southwestern British Columbia, Canada. This area exhibits a high level of seismic hazard due to its close proximity to the deep earthquakes under the Strait of Georgia/Puget Sound. The moderate seismicity combined with the majority of the provincial population, building stock and infrastructure creates great concern for earthquake engineering. Microtremors are short period vibrations that result from coastal effects, atmospheric loading, wind interaction with structures and vegetation, and cultural sources. The single-instrument microtremor method initially proposed by Nogoshi and Igarashi (1971), and popularized by Nakamura (1989), produces an estimate of site geological conditions by providing the peak period of amplification from the horizontal to vertical (H/V) spectral ratio (amplification occurs where the ratio amplitude is greater than one). Site response has been presented by H/V ratio for a site, shown as a function of frequency (Hz) and generated from Fourier

amplitude spectra. In Canada, the single-instrument microtremor method has been used most extensively by studies across SW British Columbia (Molnar et al., 2007; Molnar et al., 2006a; Molnar et al., 2006b; Molnar and Cassidy, 2006; Onur et al., 2004; Ventura et al., 2004), along with a study of the seismic microzonation for Montreal, Quebec (Chouinard et al., 2004) and at seismic instrument sites across Ontario (Sneider et al., 2005). The ground's responses from microtremors at strong-motion instrument sites have been compared with all possible earthquakes recorded at these sites to validate whether or not microtremors can be used as a proxy for linear earthquake response.

An important question refers to the composition of the elastic waves which make up ambient seismic noise. In the original Nakamura's explanation, horizontal component of microtremors consists of multi-reflected S-waves whereas the vertical component is mainly dominated by P-waves which is not suffer amplification in a thin sedimentary layer because of its higher wavelength. Amplification of vertical motion is due, under this hypothesis, to the effects of Rayleigh waves. Considering that H/V ratio is 1 at bedrock, Nakamura (1989) concludes that spectral ratio at surface is a reliable estimation for transfer function of surface layers corrected of the effects of Rayleigh waves.

Current researches show that Nakamura's explanation, based on body waves, does not really demonstrate that spectral ratio is the soil response for horizontal oscillations neither around predominant frequency (Bard, 1999). Better results have been obtained supposing that microtremors are composed by a high ratio of surface waves. This assumption is supported on the presence of dispersion in seismic noise which is a typical characteristic of Rayleigh waves and Love waves. That evidence has been obtained from multiple experiments using arrays of sensors (Flores et al., 2003; Enomoto et al., 2002). The general agreement between ellipticity curves of Rayleigh waves and microtremor spectral ratio is established (Nogoshi and Igarashi (1971); Lachet and Bard (1994); Konno and Ohmachi, 1998). Ellipticity curves represent the horizontal to vertical ratio for the motion of a particle due to a plane Rayleigh wave. In case of a soft layer over a stiff half space, exist enough impedance contrast (upper than 2.5-3), these theoretical functions show a well defined peak which position is in fairly good accord with the fundamental resonant frequency of vertically incident S-waves f_0.

Although the real contribution of surface and body waves is still discussed (Nakamura, 2000; Konno and Ohmachi, 1998; Arai and Tokimatsu, 2004), all they recognize that Nakamura's method provides a reliable estimation of the fundamental frequency for this kind of geological structure. Lachet and Bard (1994) show from simulations using surface sources that this agreement appears again for many layered profiles. Other interesting matter is the possibility that information about the level of amplification for the case of earthquake could be obtained from microtremor spectral ratio. In the case of high contrast of impedance between sedimentary layer and basement the ellipticity curve of fundamental Rayleigh mode suffer a divergence for a frequency near to f_0. So, the identification of amplification factors seems difficult for this approach.

Though, Konno and Ohmachi (1998) developed a smoothing function in order to deal with these infinite peaks and found reasonable correlations with the theoretical maximum amplification for vertically incident S-waves. On the other hand, Lachet and Bard (1994) found, taking simulations of body and surface waves into account, worse correlation and a high influence of Poisson's ratio for the upper layer on the peak amplitude. Several recent works have been executed to obtain more information than the fundamental frequency from the whole shape of the spectral ratio and not only from the region around f_0. In Konno and Ohmachi (1998) is already noticed that this function shows a trough for a frequency about 2 f_0 which can be used to obtain the resonant frequency. The possibility of a good characterization for the sedimentary structure is analyzed by Fäh et al. (2003) by using genetic algorithms in order to invert the soil profile from a fitting of the measured H/V. The fundamental Rayleigh mode is used in the forward calculation and the method fails for some particular structures in which higher modes of surface waves and body waves should be considered. Arai and Tokimatsu (2004) improve that method taking all modes for surface waves and the relative contribution of Rayleigh and Love waves as 40% and 60% respectively for the entire considered frequency band. It has been used the scheme developed by Arai and Tokimatsu (2000, 2004) in order to check the reliability of this technique for a known soil profile which characteristics have been obtained from downhole and from S-wave refraction surveys.

When recordings of microtremors are analyzed using Nakamura's method Nakamura (1989), the Horizontal to Vertical Spectral Ratio (HVSR) plots for certain soft sites have

the characteristic appearance of a peak, with a height of more than five, followed by a trough with a height of less than one, at a higher frequency. According to Haskell (1953), in the course of changing from retrograde to prograde particle orbits as frequency increases, the particle motion theoretically becomes a horizontal line, and in changing from prograde to retrograde particle orbits at a higher frequency, the motion theoretically becomes a vertical line. These transitions would result in an infinite and a zero HVSR, respectively. It has therefore been suggested (Lachet and Bard, 1994; Lermo and Chavez-Garcia, 1994a, 1994b; Konno and Ohmachi, 1998) that the mechanism which governs Nakamura's method is the propagation of Rayleigh waves, contrary to the original view (Nakamura, 1989) that any Rayleigh wave contribution detracts from the method. Accepting this interpretation of the origin of the peak/trough structure of many HVSR plots, it becomes important to investigate the geotechnical circumstances under which prograde Rayleigh wave orbits (and therefore an HVSR peak and trough structure) may arise.

A Rayleigh wave travelling along the interface between a homogeneous half space and the empty space above it has a particle motion which is elliptical in a plane containing vertical and the propagation direction (Bullen and Bolt, 1985). In contrast to water waves, the particle motion is always retrograde, that is, if a Rayleigh wave is travelling from left to right the particle motion describes an anti clockwise ellipse. However, when the Rayleigh wave travels in a more flexible layer on top of the half space, there may be a range of frequencies for which the particle motion is prograde, that is, if a wave is travelling from left to right the particle motion describes a clockwise ellipse. In changing between prograde and retrograde the motion must at some frequency become a straight line (which is neither retrograde nor prograde). It sometimes happens (Haskell, 1953) that for one transition the straight line is vertical and for the other it is horizontal. If the motion is completely horizontal at some frequency, the HVSR will be infinite at that frequency, and if the motion is completely vertical at some other frequency, the HVSR will be zero at that frequency. It has been shown (Lachet and Bard, 1994) that the peak of a Nakamura's ratio plot corresponds to the resonant frequency of the layer. Further modeling (Lermo and Chavez-Garcia, 1994a, 1994b) showed the theoretical existence of a trough as well, but the significance of the trough has not been remarked upon.

Subsequently the peak/trough structure has been noted (Konno and Ohmachi, 1998), with the comment that the frequency ratio between trough and peak is approximately two, and that the frequency of the trough could be used as an additional control on the natural frequency of the layer. It has been also asserted (Konno and Ohmachi, 1998) that some layer/half space stratigraphies can result in a trough structure. Such a result has also been encountered in the investigations described here, but it is a relatively rare occurrence. The HVSR predicted by a simple one-layer model has a close correspondence to the actual frequencies at which the HVSR peak and trough occur. The very existence of sharp resonant peaks in some HVSR plots is suggestive of an abrupt change in shear wave velocity at some depth, and therefore a suitable tactic to start investigations must lie in exploring the properties of a simple homogeneous layer lying on top of a stiffer half space, even though such simple circumstances must seldom occur in nature. Accordingly, a uniform layer upon a half space, is the model adopted for this work. In addition, it is useful to adopt likely values for the layer and half space properties. A typical soft site has a superficial layer of saturated soil, which has a high P-wave velocity and a low S-wave velocity (Poisson ratio n approaching 0.5). By contrast rock is closer to being a poisson solid.

The Nakamura technique (Nakamura, 1989), first proposed by Nogoshi and Igarashi (1970, 1971), is today one of the most commonly applied methods for microzonation studies of large areas (Parolai et al., 2001). A large number of studies using this rapid, economical and therefore attractive technique have been published (Field and Jacob, 1993; Mucciarelli, 1998; Bard, 1999; Fah et al., 2001). More recent studies (Fah et al., 2003; Scherbaum et al., 2003; Arai and Tokimatsu, 2004; Parolai et al., 2005; Picozzi et al., 2005; Parrolai et al., 2006) proposed and tested the possibility of inverting the Horizontal to Vertical (H/V) spectral ratio of noise (alone or in a joint inversion scheme) for investigating the S-wave subsoil structure. All these studies require the assumption that the noise wave field is generally dominated by surface waves. Moreover, attempts to provide standards for the analysis of seismic noise have only recently been carried out (Bard, 1999; SESAME, 2004; Picozzi et al., 2005). To this regard, a point frequently debated by the seismological community is whether only the stationery part of the recorded signal should be considered in the analysis, or could transients (due to human activities) also be considered (excluding obviously very strong and clipped signals). Most authors disregarded the non-stationery noise from the analysis (Horike et al., 2001), while others (Mucciarelli et al., 2003)

showed that the H/V ratio of non-stationery noise might be more similar, especially in amplitude, to the H/V ratio of non-stationery noise might be more similar, especially in amplitude, to the H/V spectral ratio determined for small-size earthquakes. By applying an optimal filtering procedure to empirical data and using numerical simulations, Parolai and Galiana-Merino (2006) showed that transients might cause large variability in the H/V shape, depending on source type and distance from the receiver relative to the thickness of the sedimentary cover. However, they showed that when dealing with a sufficient number of real data, the H/V technique is not biased by including transients. Recently, Chatelian et al. (2007) suggested to avoid the use of transients in the H/V analysis. Nevertheless, they showed that H/V does not significantly change if the sensor is located just a few meters from the major sources of transients (in their case, cars on a highway). Furthermore, at only 2 m from the highway, the peak in the H/V spectral ratio is still visible, when it disappears when the sensor is placed directly on the highway. These results (except for those from the stations located directly on the highway) seem to be in agreement with the pioneering study of Taniguchi and Sawada (1979) who made systematic noise measurements close to a highway under constructions and observed that (1) the frequency peak in the transient spectra has been stable independent of the mass of the source (a truck), hinting to the fact that the frequency of the traffic-induced vibration is mainly determined by ground soil conditions, and (2) traffic-generated vibrations have been dominated by Rayleigh waves. A recent investigation of seismic noise wave field induced by several source types can be found in Kim and Lee (2007).

Additional evidence of the role played by transients has been reported by Mucciarelli (1998) who showed that when generating transients with a sledge hammer near the recording sensor, the H/V peak becomes clearer. This result, probably too often overlooked, stimulates many intriguing questions. Since the energy released by the blow of sledge hammer peaks at frequencies much higher (50-70 Hz) than the fundamental resonance frequency of the site (1 Hz), how can the transients modify the H/V? Similarly, human generated seismic noise mainly affects frequencies higher than 1-2 Hz, with cars generating signals with frequencies mainly between 10-20 Hz (Toniguchi and Sawada. 1979; McNamara and Buland, 2004). Therefore, the question arises if there is any important information carried by the transients that one could try to extract.

2.3.1 Earthquake and Microtremor Spectral Ratio

Worldwide, microtremor studies have shown that the peak amplitude of the microtremor H/V ratio tends to underestimate the peak amplitude of earthquake spectral ratios with respect to a reference (bedrock) site (Bard, 1999). The H/V spectral ratio determined from microtremors has shown a clear peak that is well correlated with the fundamental resonance frequency at "soft" soil sites (Bard, 2004; Horike et al., 2001; Lachet et al., 1996; Field and Jacob, 1995; Lachet and Bard, 1994; Lermo and Chavez-Garcia 1994a, 1994b). Numerical analysis suggests that microtremor site response can only be generated when the impedance contrast is greater than 3.5 (Malischewsky and Scherbaum, 2004), thus the good correlation at "soft" soil sites. Only a few studies claim rough agreement between the peak amplitude of the microtremor H/V ratio and earthquake site-to-reference spectral ratios (Molnar and Cassidy, 2006; Mucciarelli et al., 2003; Horike et al., 2001; Lermo and Chavez-Garcia, 1994a, 1994b). In general, the site response shown by the earthquake site-to-reference spectral ratio method is regarded as the best approximation for engineering use, whereas H/V spectral ratios from earthquakes and/or microtremors are regarded as providing the fundamental peak and lower bound estimate of amplification for a soil site.

Figure 2.5 demonstrates the remarkable similarity between the earthquake site-to-reference and H/V ratio response, with the microtremor H/V ratio response at three strong-motion earthquake recording sites in greater Victoria. Traditionally strong-motion instrument has been used for earthquake recordings, rather than recordings from weak-motion sensors, as these instruments are designed to record the largest ground motions, and are generally present at sites of geologic interest (i.e. not bedrock). There are six BC Hydro substations in greater Victoria with a permanent strong-motion instrument. Since 1996, up to seven weak motion (peak ground acceleration $\leq$ 5.5 % g) earthquakes, ranging in magnitude from ML 3.6 to MW 6.8, have been recorded at these sites.

All six BC Hydro instrument sites show similar response regardless of excitation source (weak-motion earthquakes or microtremors) and spectral ratio method (Molnar and Cassidy, 2006). This suggests that microtremor recordings are valid for estimation of linear earthquake response at sites in greater Victoria.

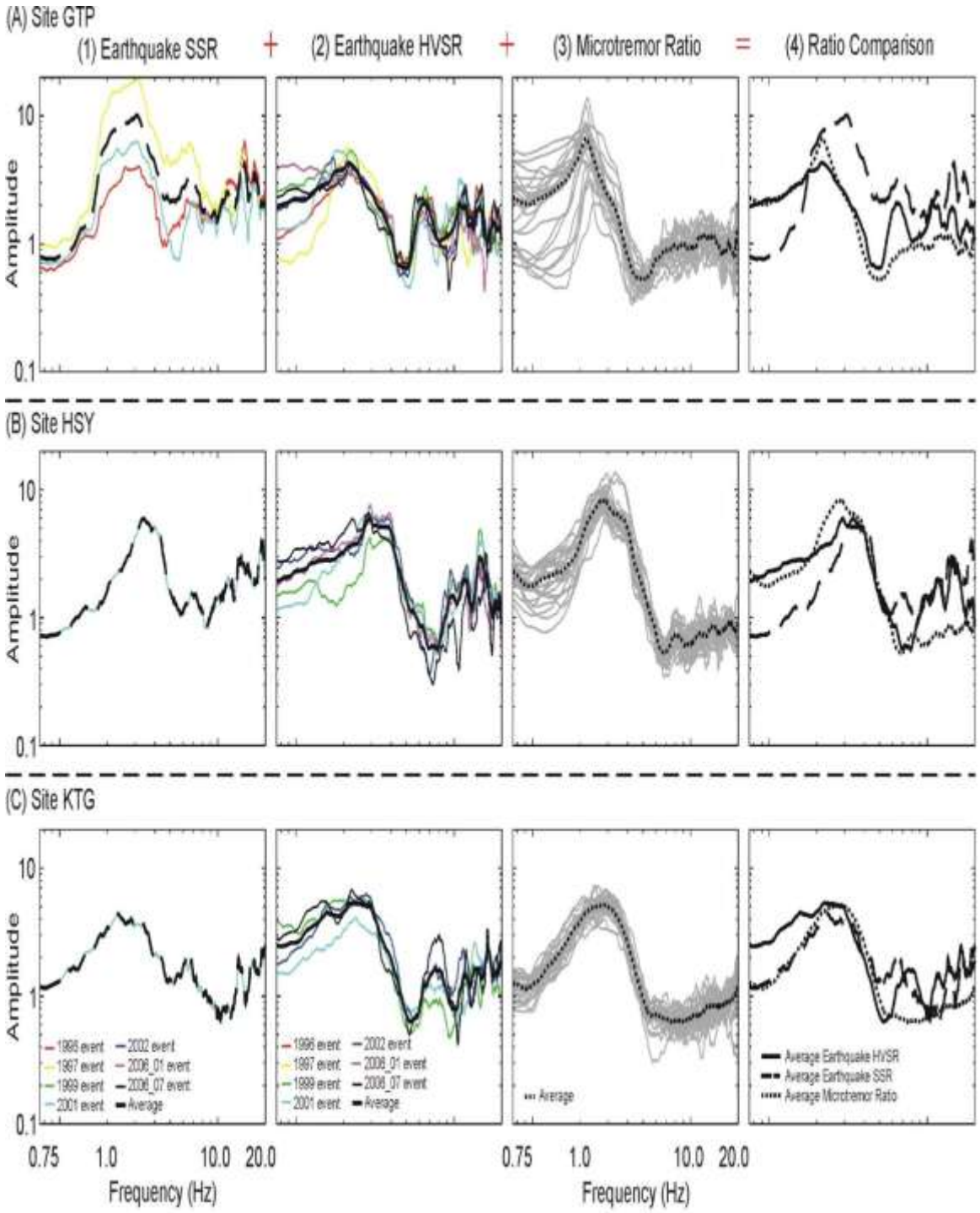

Figure 2.5: Comparison of (1) the average earthquake site-to-reference spectral ratios (SSR) with (2) the average earthquake H/V spectral ratios (HVSR) of up to seven earthquakes, and (3) the average microtremor H/V spectral ratio at three strong-motion instrument sites in greater Victoria. (After Molnar et al., 2007)

Another source of strong-motion earthquake recordings comes from the Geological Survey of Canada. In 2002, they began to operate strong-motion instruments that continuously record and communicate in near real-time over the Internet (Rosenberger et al., 2007, Molnar et al., 2006b, Molnar et al., 2006c). These new instrumentation features have provided around 500 earthquake acceleration recordings across SW British Columbia (Cassidy et al., 2007) from only four earthquakes ranging in magnitude from MW 4.0 to MW 6.4. However, the recordings are all relatively low-level, varying in peak ground accelerations between 0.6 and 3.9%g. Figure 2.6 shows good similarity of the fundamental period of the H/V spectral ratio response from these earthquake recordings with the microtremor response at four strong-motion instrument sites across SW British Columbia (Molnar et al., 2006d).

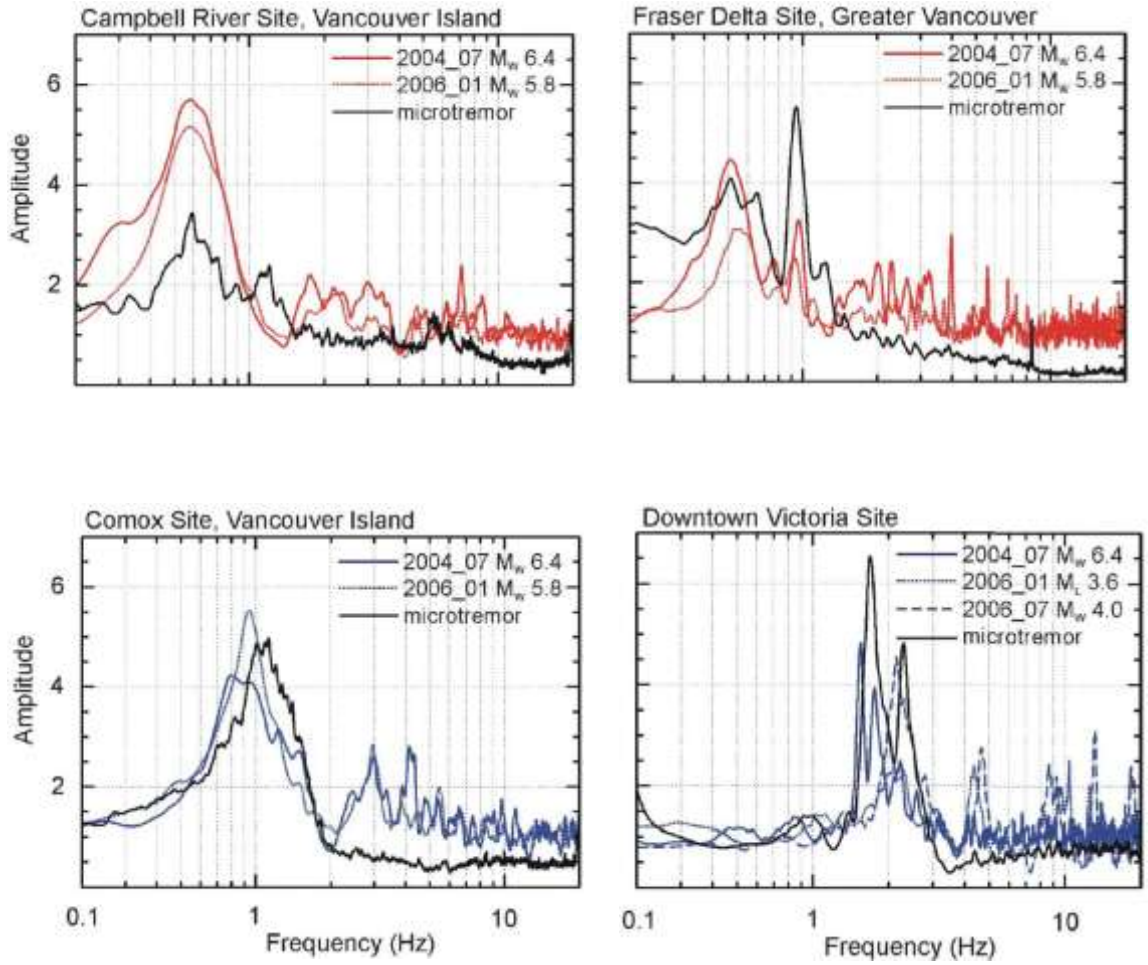

Figure 2.6: Comparison of the H/V spectral ratio from up to four weak-motion earthquakes and microtremors at four sites across SW British Columbia. (After Molnar et al, 2007)

Overall, for SW British Columbia excellent agreement has been observed in the fundamental period of a site 413 between earthquake and microtremor spectral ratio responses, and good agreement in the level of amplification, especially at sites in greater Victoria. The microtremor response at higher modes is always lower than that of the earthquake response. The microtremor underestimates earthquake response amplitude at frequencies greater than 2 to 3 Hz. Figures 2.5 and 2.6 demonstrate the validity of the single-instrument microtremor method as a proxy for earthquake site response across SW British Columbia.

2.3.2 Observed and Analytical Amplitude Ratio

A microtremor research has been carried out at thirteen locations in Japan (Ansary et al, 1996). Soil model has been developed for theoretical analysis using the existing boreholes and PS loggings. The transfer function of the shear wave (The surface motion versus the incidental motion at some depth) and the amplitude ratio for the fundamental mode of Rayleigh wave have been calculated at the sites using those soil models. For the calculation of transfer function of shear wave, a damping ratio of 2 % has been used, assuming input motion at the outcrop.

Figure 2.7 shows the transfer function of shear wave, amplitude ratios of Rayleigh wave and microtremor for six locations in Japan. During the comparision of theoretical curves, the amplitude ratio, AR (T), of microtremor used have been expressed by the following equation:

$$\mathrm{AR}\ (\mathrm{T}) = \frac{\sqrt{\mathrm{F_{NS}(T)F_{EW}(T)}}}{\mathrm{F_{UD}(T)}} \qquad (2.1)$$

Where,$\mathrm{F_{NS}(T)}$, $\mathrm{F_{EW}}$ (T) and $\mathrm{F_{UD}(T)}$are average Fourier spectra of six time instants.

The trend of three curves, i.e., two theoretical and one observed, somewhat resembles each other for these sites. Ansary et al. (1996) found that the period at which the Rayleigh wave amplitude ratio either suddenly drops or peaks, microtremor amplitude ratio closely resembles it. In a general sense, amplitude ratio for pure Rayleigh wave is always lower than the amplitude ratio of microtremor. The reason is that microtremor may contain some shear wave and Love wave contents as well as Rayleigh wave. Ansary et al. (1996)

concluded that the characteristics of the microtremors amplitude ratio are similar to that of Rayleigh wave and the period corresponding to the peak amplitude ratio corresponds to the peak periods of Rayleigh wave amplitude ratio and Shear wave transfer function.

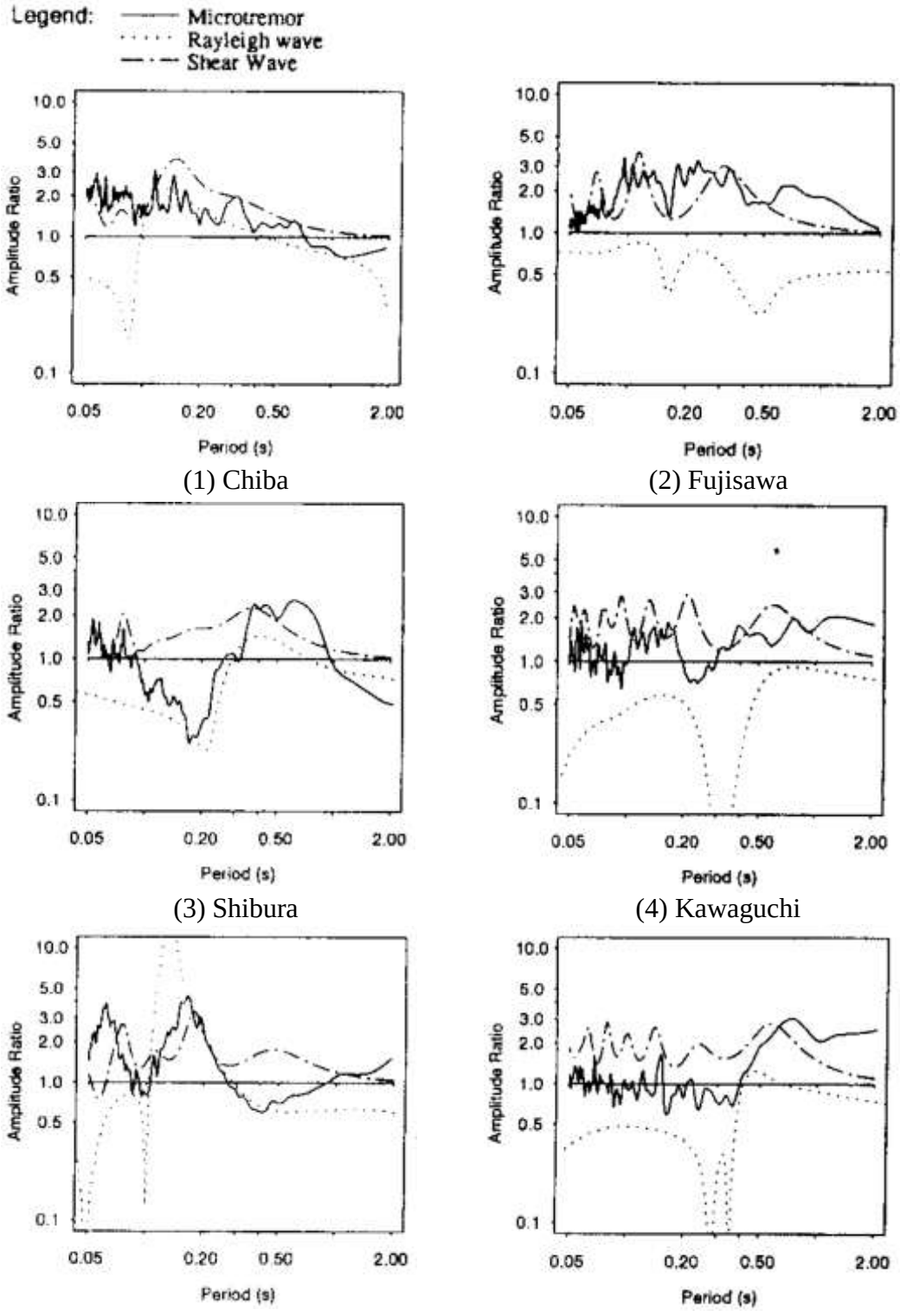

(1) Chiba (2) Fujisawa

(3) Shibura (4) Kawaguchi

(5) Kodaira (6) Sasamegawa

Figure 2.7: Amplitude ratios of microtremor and theoretical Rayleigh-wave plotted with transfer function of shear wave. (After Ansary et al., 1996)

2.4 MICROTREMOR H/V TECHNIQUE

Damages caused by the recent earthquakes are concluded as a direct result of local geological conditions affecting the ground motion. Best approach for understanding ground conditions is through direct observation of seismic ground motion, but such studies are restricted to areas with relatively high rates of seismicity. Because of these restrictions in other methods, such as high rates of seismicity and the availability of an adequate reference site, non-reference site methods have been applied to site response studies. Microtremor is a very convenient tool to estimate the effect of surface geology on seismic motion without needing other geological information. H/V technique fits very well to this description and it has received great attention from all over the world with its simplicity together with quick information about dynamic characteristics of ground and structures. Although several researchers claimed that theoretical background of this technique is not clear, there have been many successful experimental studies performed. Method is attractive since it gives the ease of data collection and it can be applied in areas of low or even no seismicity.

2.4.1 Method of H/V Technique

Techniques for analyzing microtremors are generally divided into two main categories: non-reference site (H/V) and reference site (Hs/Hr) techniques. In Hs/Hr method, assumptions are that at nearby sites, source and path effects are believed to be identical and reference site is free of any site effect. Therefore, motion recorded at the reference station is representative of the excitation arriving at the interface sediments under the soft soil site and spectral ratio, Hs/Hr, constitute a reliable estimate of site response. This technique, introduced first by Borcherdt (1970), is still widely used and is very popular for the analysis of weak or strong motion records. It has been applied to microtremor measurements by Kagami et al. (1986) with good results. In the traditional spectral ratio method, Hs/Hr, site and source effects are estimated from observations at a reference site. In practice, adequate reference site are not always available especially in flat areas. Therefore, methods have been developed that do not need reference sites (Bard, 2004).

A technique using horizontal to vertical spectral ratios (H/V) of the microtremors, which was first applied by Nogoshi and Igarashi (1970, 1971) and popularized by Nakamura

(1989), has been widely used to estimate the site effects. Several recent applications of this technique have proved to be effective in estimating fundamental periods as well as relatively amplification factors. Several methods have been proposed for spectral calculation of ground motions including microtremors. Fourier spectrum is the most convenient one that is used widely. Some investigations showed that different methods give similar results (Dimitriu et al., 1998). However some researchers declare that a suitable spectral method gives more reliable results. Ghayamghamian and Kawakami (1997) introduced segmental cross-spectrum (SCS), as an effective tool for compensating unknown effects like source effects and noise in input and output measurements. They evaluated the performance of SCS in contrast with the conventional methods, i.e. Fourier or power spectra through the mathematical modeling and numerical simulations. Results of their studies indicated that SCS gives more reliable results for both amplification factor and predominant resonance frequency of the site than the conventional methods.

Two approaches for determining the site effect are the standard spectral ratio (S_T) and the H/V spectral ratio methods (Katz, 1976; Nakamura, 1989; Huang and Teng, 2002) as shown in Figure 2.8. The standard spectral ratio is determined by taking the ratio of the horizontal spectrum of ground motion on a soft sediment site, S_{HS}, relative to the horizontal spectrum on a hard (or reference) site S_{HB},

$$S_T = \frac{S_{HS}}{S_{HB}} \qquad (2.2)$$

Nakamura (1989) investigated the use of microtremors for estimating site effect by first looking at seismic waveforms of different earthquakes at various observation points. He observed that regardless of earthquake magnitude or propagation path, waveforms recorded at the same observation point shared similarities. Based on this observation, Nakamura (1989) proposed using a spectral ratio of the vertical spectrum of ground motion on a soft site, S_{VS}, and hard site, S_{VB}, to estimate the effect of the source, E_S , on amplitude of recorded motion, where,

$$E_S = \frac{S_{VS}}{S_{VB}} \qquad (2.3)$$

To compensate for the source effect, Lermo and Chavez-Garcia (1993) and Nakamura (1989) proposed a modified spectral ratio, S_{TT}, where,

$$S_{TT} = \frac{S_T}{E_S} \approx \frac{S_{HS}}{S_{VS}} \qquad (2.4)$$

Several studies have shown empirically that the ratio of S_{HB}/S_{VB} is approximately 1, thus yielding a transfer function based only on ground motion at a soft sediment site (Nakamura, 1989; Lermo and Chavez-Garcia, 1993; Huang, 2002). This technique eliminates the need for a reference site, which is important for studies a site, where a hard rock reference is not locally accessible. In application, this quantity is known as the H/V spectral ratio (HVSR),

$$\text{HVSR} = \frac{\frac{H_N + H_E}{2}}{V_Z} \qquad (2.5)$$

Where, H_N and H_E are the power spectra of the recorded horizontal components (NS, EW) of ground motion and V_Z is the vertical component. The HVSR method assumes that the vertical component is uninfluenced by low-velocity sediments and that the Rayleigh wave affects the vertical and horizontal components equally (Nakamura, 1989; Woolery and Street, 2002). The resulting spectrum is assumed to be independent of source and path and can be used to determine resonant frequencies, which appear in the HVSR as peak amplitudes.

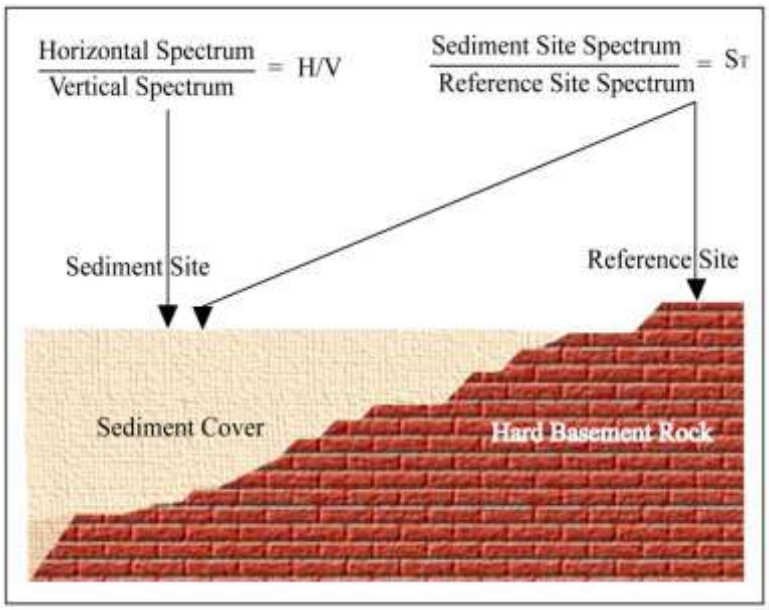

Figure 2.8: Assumptions of microtremor method to derive transfer function for sedimentary basins using H/V (Nakamura, 1989) and standard spectral ratios (modified from Ibs-von Seht and Wohlenberg, 1999).

2.4.2 Analysis Approach: Horizontal to Vertical Spectral Ratio (HVSR)

The method use for data analysis is the Horizontal to Vertical Spectral Ratio (HVSR) approach developed by Nakamura (1989). The HVSR approach is applied to ambient noise and generates a Fourier spectral ratio of amplitude versus frequency. The HVSR method divides the horizontal component of noise to the vertical component to remove source effects as shown in Figure 2.9. The spectral ratio is calculated by taking the Fourier transform (Welch, 1967) of the ambient noise recordings. This resulting function shows how the amplitude of motion is distributed with respect to frequency. A narrow spectral peak at a particular frequency (range) implies that a large component of the energy of motion falls within that frequency range.

Lachet & Bard (1994) investigated the HVSR approach on ambient noise recordings to clarify if this method reflected characteristics of the site as opposed to the source. Their study concluded the HVSR approach was able to clearly show the HVSR peak of a sedimentary site independent of source effects. The HVSR analysis is considered to remove the source effect by dividing the horizontal by the vertical component as described by Nakamura (1989); Lachet & Bard (1994); Bard (1999); Nakamura (2000); Panou et al. (2005) and Nakamura (2008).

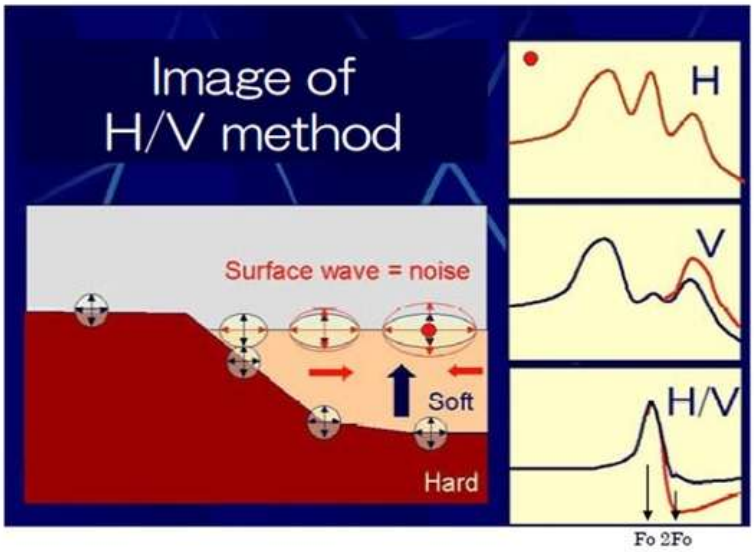

Figure 2.9: Cartoon of the HVSR method, where Rayleigh wave ellipticity of the basement and ground surface is shown in the left panel. The Fourier transform of the horizontal (top) and vertical (center) component, and the resulting HVSR (bottom) are shown on the right. The image is from Nakamura (2008).

2.4.3 The Development of HVSR

The HVSR approach is an empirical technique for determining site characteristics and has been shown to be effective by comparing its results with the results of various other approaches as described in Zhao et al. (2000); Mucciarelli et al. (2003); Bard et al. (2004); Koller et al. (2004); Bard et al. (2005) and Guillier et al. (2007). There are various ways to explain the HVSR method. Initially proposed by Nogoshi & Igarashi (1971) and developed by Nakamura (1989), HVSR assumes the ambient noise field to be composed of S and Rayleigh waves. Later, the HVSR approach was theoretically substantiated for the fundamental mode of a Rayleigh wave by Lachet & Bard (1994); Konno & Ohmachi (1998) and Bard (1999). Bard et al. (2004) explained the HVSR theory based on the primary peaks of the spectral graphs referring to the ellipticity of the Rayleigh wave. Also, Arai & Tokimatsu (2000) suggested the frequencies in the HVSR approach are controlled by Rayleigh waves and the amplitudes are controlled by Love waves. More recently, the HVSR analysis was also verified based on the diffuse field, developed by Sanchez-Sesma et al. (2011).

2.4.4 Reliability of the HVSR Approach

The HVSR approach has been popular for site response investigations due to its ease of use, low cost, and flexibility in the use of data that is not dependent on strong ground motion or an active source. Ambient noise HVSR studies have been conducted extensively and compared for reliability against other methods, as discussed by Zhao et al. (2000); Mucciarelli et al. (2003); Bard et al. (2004); Koller et al. (2004); Bard et al. (2005) and Guillier et al. (2007). Nakamura (1989); Koller et al. (2004); Lachet & Bard (1994) and Guillier et al. (2007) have shown that the HVSR spectral peak frequency represents the fundamental frequency of the site soil column. This has been confirmed by later studies which tested the accuracy and reliability of the HVSR approach, as described in papers such as Ducellier et al. (2013); Cara et al. (2010); Nakamura (2008); Guillier et al. (2007) and Parolai et al. (2004). Further investigation by SESAME WP12, (2004) and Bard & SESAME Participants (2004) in the Site Effects Assessment Using Ambient Excitation project (SESAME) compared the ambient noise HVSR results with those from earthquake-based HVSR analysis and these results were further verified in Bard et al. (2004) and Bard et al. (2005). The primary objectives of the SESAME project were to

better understand the physical basis of the HVSR approach, determine its purpose in site response, and propose guidelines for correct analysis. As shown in Figure 2.10, the SESAME project demonstrated a strong linear correlation between the spectral peak frequency determined through ambient noise HVSR and those determined at the same site through Standard Spectral Ratio (SPR) measurements from earthquake data. This result clearly demonstrates that ambient noise HVSR results for the spectral ratio peak frequency may be interpreted as indicating the expected peak frequency in case of strong ground motion due to earthquakes. Based on this SESAME frequency comparison and investigations mentioned earlier, we will refer to the peak frequency measured from the HVSR graph as the site fundamental frequency in this thesis.

The amplitude of the spectral ratio has been used by some authors as a representation of amplification relative to hard rock site as in for example, Nakamura (1989); Lachet & Bard (1994); Siddiqqi & Atkinson (2002); Theodulidis et al. (2004); Bard & SESAME Participants (2004). Thus, the HVSR method is a simple and effective technique for determining the first fundamental frequency of soil resonance. However, its use in determining higher resonance modes has been controversial. Bonnefoy-Claudet et al. (2009) suggest the HVSR approach is inadequate for determining higher resonance modes, while other authors such as Lermo & Chavez-Garcia (1994) suggested otherwise.

It is important that, before calculating the HVSR, filter out microtremor data, any short duration, close (10-60 m depending on the size of the source), local sources (footsteps, cars, trains, and other transient sources) and monochromatic signals (construction machines, pumps, industrial machines, etc.) from our data set. Monochromatic signals are evident in the 3 component seismogram in Figure 2.11, which shows how the uniform amplitudes of ambient noise data are interrupted by sharp high peaks of induced signal of a single frequency.

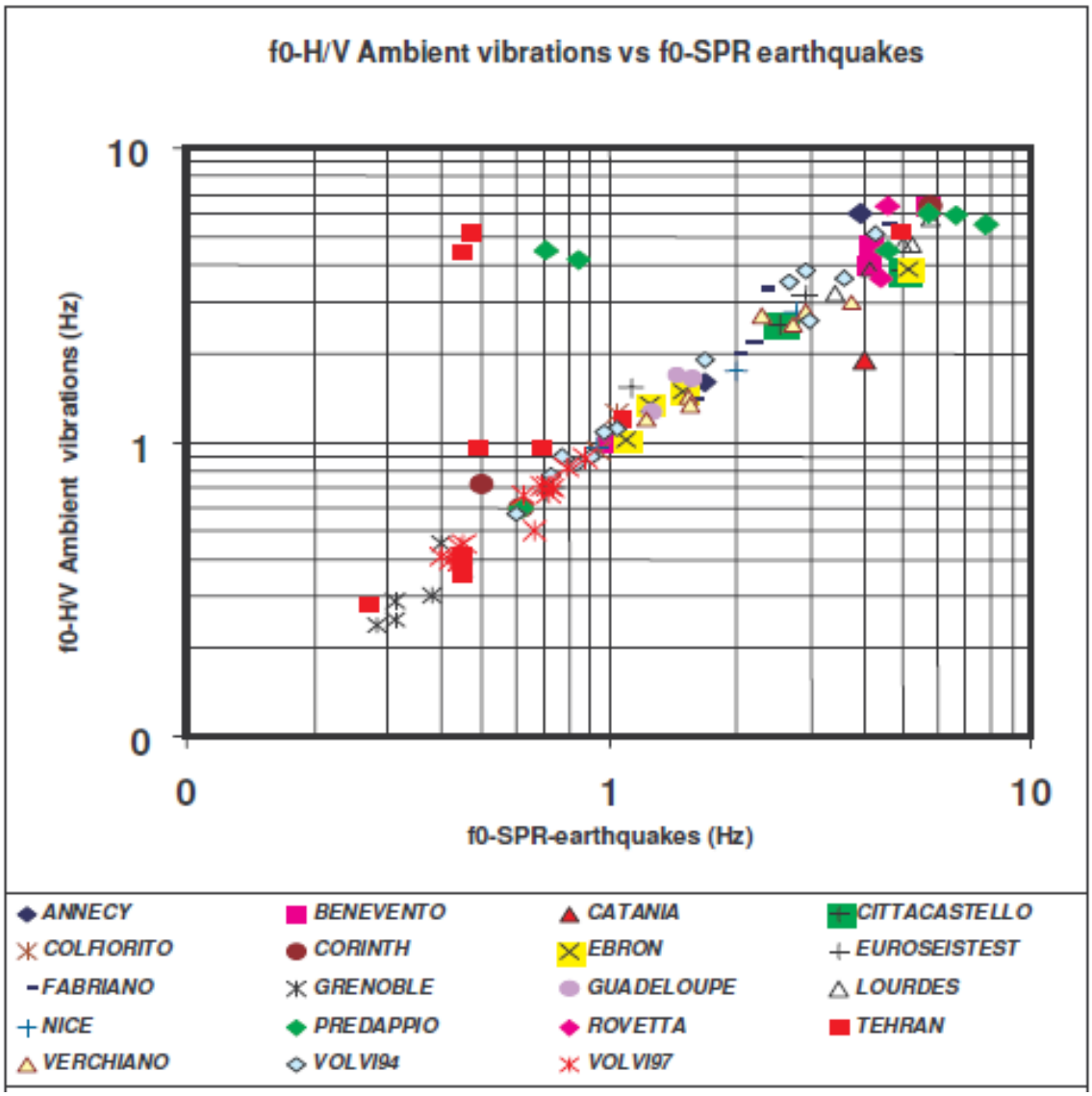

Figure 2.10: Ambient noise HVSR frequency comparison with earthquake SPR frequency measurements. The vertical axis depicts HVSR frequency values while the horizontal axis shows SPR frequency values for corresponding sites. A strong linear correlation in spectral ratio peak frequency from both methods is shown. Image is from SESAME WP12, (2004).

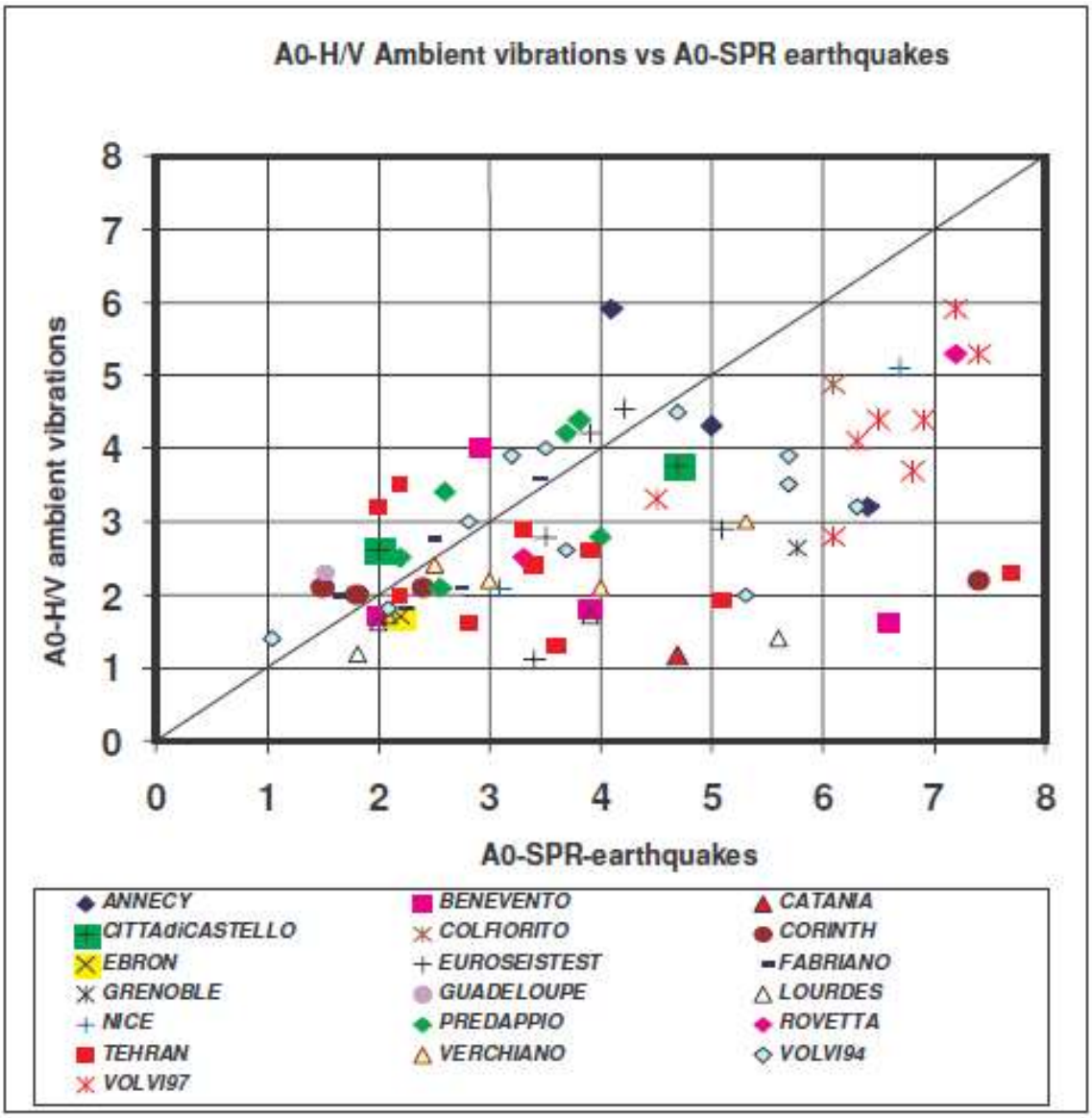

Figure 2.11: HVSR amplitude comparison with earthquake SPR amplitude measurements. The vertical axis depicts HVSR amplitude values, while the horizontal axis shows SPR amplitude values for corresponding sites. The comparison of amplitudes between the two methods shows overall higher SPR amplitudes than HVSR amplitudes. Image is from SESAME WP12, (2004).

2.5 DAMAGE ASSESSMENT

Soil conditions are often variable even inside of a relatively small area as a town. So it is necessary to find a low-cost method to obtain a detailed dynamic characterization of soil. Microtremor is the most convenient, reliable and low-cost technique to assess the damage of any site and building. Damage assessment of any building and site can be done in two ways. First one is Resonance Criteria, which is assessed from the analysis microtremor data in both building and site. Second one is Nakamura's Seismic Vulnerability Index; K_g has been discussed in this section.

2.5.1 Resonance Criteria

Fundamental frequency is a parameter that describes the resonance of the soil column for site response. Resonance is the phenomenon in which the amplitude of a system may be dramatically increased as a cyclical force is applied at a specific frequency. The frequency of the cyclical force at which this dramatic increase occurs is known as the natural frequency, fundamental frequency, or resonance frequency of the system. When this internal resonance frequency matches an external applied frequency, the system is considered to be in resonance. A system in resonance responds with increasing amplitude to the driving force. In harmonics, the first harmonic of the natural frequency is half the standing wavelength, where higher order harmonics are multiples of the fundamental frequency. The occurrence of resonance in a system may result in an increase of oscillation amplitudes to tremendous magnitudes which, in a rigid body, may be violent and could result in a catastrophic system failure.

If the predominant frequency of any building coincides with the predominant frequency of soil, resonance is said to occur. Ground motions that are not influenced by the presence of structures are referred to as free-field motions. When a structure founded on solid rock is subjected to an earthquake, the extremely high stiffness of the rock is considered to be fixed-base structures.

On the other hand, the same structure would respond differently if supported on a soft soil deposit. First, the inability of the foundation to conform to the deformations of the free-field motion would cause the motion of the base of the structure to deviate from the free

field motion. Second, the dynamic response of the structure itself would induce deformation of the supporting soil. This process, in which the response of the soil influences the motion of the structure and the response of the structure influences the motion of the soil, is referred to as soil-structure interaction.

Soil-structure interaction has little effect on the dynamic response of many structures and foundation systems (Kramer, 1996). In other cases, however, its effects can be significant. Whether the neglect of its effect can be significant, whether the neglect of its effects is conservative or unconservative depends on the details of the problem at hand and must be evaluated on a case-by-case basis. Simplified relationships to establish natural frequency of site/structure are given in Equation 2.6 and 2.7.

$$f_{Structure} = \frac{N}{10} \quad (2.6)$$

$$f_{Site} = \frac{V_S}{4H} \quad (2.7)$$

f = natural frequency, N = the number of stories in the structure, V_S = the shear wave velocity of the site, H = the thickness of the soil deposit.

2.5.2 Nakamura's Seismic Vulnerability Index (K_g)

Earthquake damage of structural members occurs at the time of exceeding the limit of the strain caused by deformation, and it causes the collapse if the stability of the structure lacked. Nakamura (1997) proposed use of a vulnerability index, K_g, to represent the degree to which a site or area might experience destructive ground motions, or high shear strains, during earthquakes. High shear strains ($> 10^{-6}$) can lead to soil liquefaction, landslide, and settlement. Since Nakamura (1997) introduced the technique, others have used it to assess vulnerability in areas that have experienced intense liquefaction due to strong ground motion (Konno and Ohmachi, 1998; Huang and Tseng, 2002; Gosar, A, 2010; Kelli et al., 2010; Dwa Desa et al., 2011; Elcin Gok and Orhan Polat, 2012; Asskar et al., 2013, 2015; Bouranta et al., 2013; Pyi Soe et al., 2014; Khalda Y. et al., 2015; Sayed SR Moustafa, 2015; Qadri et al., 2015).

Nakamura (1997) investigated two areas in Japan, one largely occupied by railway lines and the other occupied by rigid-frame viaducts. Microtremor measurements were taken along railway sections that were damaged in an earthquake. These railway sections were repaired but damaged again by another earthquake. Results corresponding to K_g values along the railway line indicate that damage occurred where K_g values were relatively large (Nakamura, 1997). Similar results were also observed in another area, where large K_g values corresponded to the amount of damage to viaducts. Nakamura (1997) asserts that the K_g values obtained prior to earthquakes can be expected to predict accurately the future earthquake damage at a site.

Huang and Tseng (2002) investigated liquefaction vulnerability for sites in Taiwan that experienced severe liquefaction resulting from the 1999 Chi-Chi earthquake. They took microtremor data in an alluvial fan setting at 42 sites and applied Nakamura's method of estimating liquefaction potential by use of K_g values. Sites that revealed a higher calculated K_g value corresponded with sites that had experienced serious liquefaction.

For ground, shear strain γ of surface ground is noticed. Table 2.5 shows relationship of γ to ground disasters compiled by Ishihara (1978). It indicates that from $\gamma \cong 1000 \times 10^{-6}$; ground begins to show non-linear character and in $\gamma > 10{,}000 \times 10^{-6}$ large deformation and collapse occur.

Table 2.5 Strain Dependences of Dynamic Properties of Soil (Ishihara, 1978)

Size of Strain γ	**10^{-6} 10^{-5}**	**10^{-4} 10^{-3}**	**10^{-2} 10^{-1}**
Phenomena	Wave, Vibration	Crack, Settlement	Landslide, Soil Compaction, Liquefaction
Dynamic Properties	Elasticity	Elasto-Plasticity	Collapse Repeat- Effect, Speed-Effect of Loading

Seismic vulnerability index, K_g is derived from predominant frequencies and amplification factor as determined from the H/V Ratios. The amplitude of the predominant frequency observed in the HVSR is considered the amplification factor. The predominant frequency is $F_g = \frac{V_s}{4\,H}$ and the amplification factor A_g for this frequency is related with impedance

ratio. If densities for basement and surface layer are same then, $A_g = \frac{V_b}{V_s}$ and depth of basement H is, $H = \frac{V_b}{4\,A_g\,F_g}$ where, V_b is S wave velocity of basement.

For calculating K_g, shear strain of the ground is considered. Simplifying the shear strain deformation of surface ground as shown in Figure 2.12, average shear strain γ of surface ground can be estimated by following formula, namely

$$\gamma = A_g \frac{d}{H} \qquad (2.8)$$

Where, A_g is amplification factor of surface layer, H is thickness of surface layer and d is seismic displacement of the basement ground.

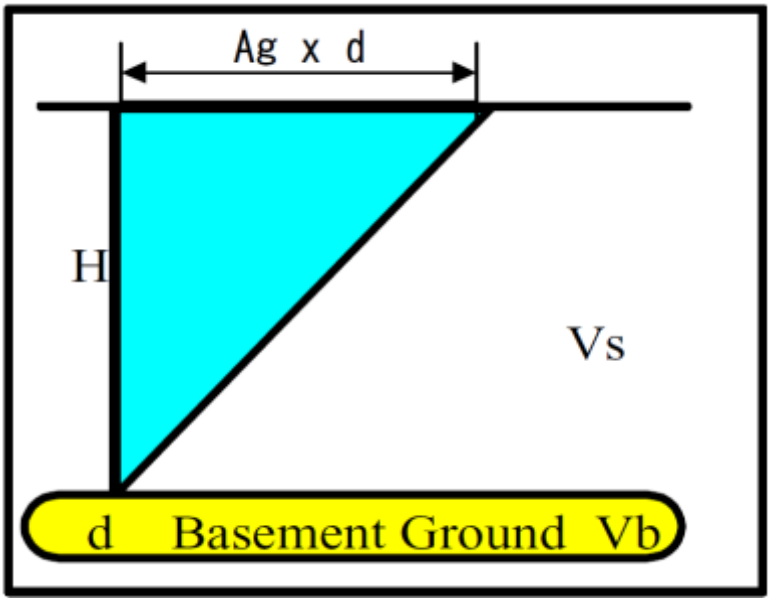

Figure 2.12: Surface ground deformation.

Putting S-wave velocities of basement ground and surface ground as V_b and V_s respectively, proper predominant frequency F_g of surface ground is approximately expressed as,

$$F_g = \frac{V_b}{4A_gH} \qquad (2.9)$$

Acceleration of basement ground α_b is expressed as,

$\alpha_b = (2\pi F_g)^2 d$

and shear strain γ is expressed by F_g, A_g and V_b as follows,

$$\gamma = \frac{A_g \alpha_b}{(2\pi F_g)^2} \times 4A_g \frac{F_g}{V_b} \quad (2.10)$$

$$= \frac{{A_g}^2}{F_g} \times \frac{\alpha_b}{\pi^2 V_b}$$

$$= K_g \times \frac{\alpha_b}{\pi^2 V_b} \quad (2.11)$$

If efficiency of applied dynamic force is assumed to be e % of static force, effective γ_e is

$$\gamma_e = K_g(e)\alpha_b \quad (2.12)$$

Where, $K_g(e) = \frac{e}{100} \times \frac{{A_g}^2}{F_g} \times \frac{1}{\pi^2 V_b}$ (2.13)

The value of V_b is expected to be nearly constant in a broad area and K_g is a proper value for measured point. Thus K_g can be considered as an index to indicate easiness of deformation of measured points which is expected useful to detect weak points of the ground. As we can consider V_b = 600 m/s, we obtain $\frac{1}{\pi^2 V_b} = 1.69 \times 10^{-6}$ (s/cm). If we put e = 60 %, then $K_g(e) \cong \frac{{A_g}^2}{F_g}$ and the effective strain can be estimated by multiplying $K_g(e)$ value with maximum acceleration of basement ground in Gal (= cm/s^2).

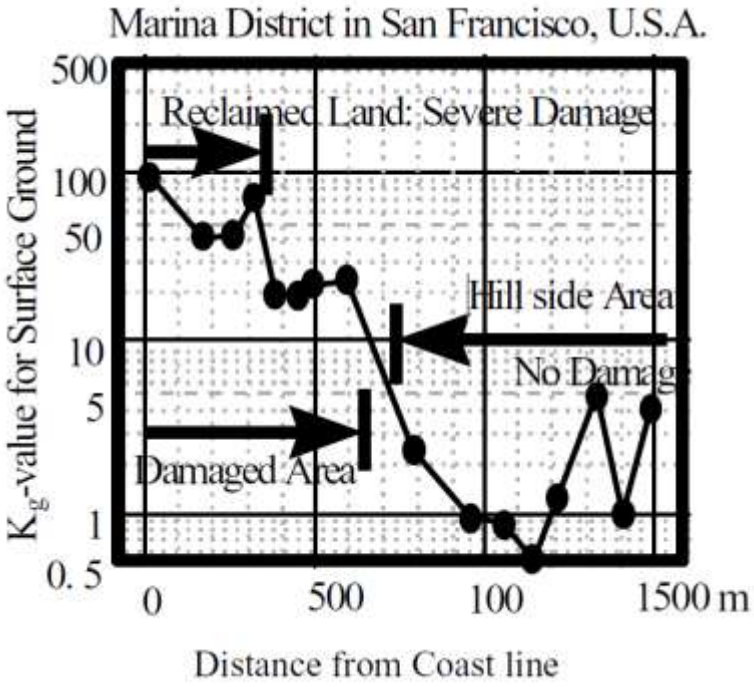

Figure 2.13: K_g values calculated for Loma Prieta Earthquake. (After Nakamura et al., 1990)

Figure 2.13 indicates K_g-values obtained in San Francisco Bay Area after the 1989 Loma-Prieta Earthquake. For Marina district the result along a line from sea coast to hillside is shown. It shows K_g at the sites where grounds deform much are bigger than 20 and K_g at the sites with no damage are very small. Considering the maximum basement accelerations around the area are estimated as 50 Gal based on observations, $Kg = 1000 \times 10^{-6}$ separates the areas liquefied or not. The result shows the similarity between actual damage and theoretical damage assessment using K_g value.

2.6 CONCLUDING REMARKS

In this chapter definition of spectral ratio technique, ambient noise, its sources and regional tectonics have been discussed. Relevant literatures on H/V spectral ratio and microtremor, relationship between microtremor and earthquake, method of H/V ratio technique and application of H/V spectral ratio have been reviewed. Analysis approach of Horizontal to Vertical Spectral Ratio (HVSR), development of HVSR and Reliability of HVSR according to SESAME, WP12, (2004) has been included in this chapter.

Finally, the literature related to damage assessment using H/V spectral ratio technique has been described in this chapter. The theory of the vulnerability of site soil according to Nakamura's (1997) Vulnerability Index (K_g) has been discussed. The application of seismic Vulnerability index in various places also included.

All the above discussions are relevant to the current study and has been referred in Chapter 3 and 4.

CHAPTER 3
EXPERIMENTAL PROGRAM

3.1 GENERAL

Local site conditions substantially affect the characteristics of seismic waves during earthquakes. Soft alluvial deposits tend to amplify certain frequencies of ground motion and extend the duration of motion which may cause further earthquake damage. The expected variation in the ground motion, according to the geological site conditions, make it necessary to perform a more detailed seismic hazard assessment for a metropolitan area. To accurately identify the variation of seismic hazards as well as vulnerable index at different locations within the metropolis, one may conduct seismic microzonation that requires subdividing an area into zones with respect to the geological characteristics of the sites. The study is conducted in Dhaka city, which is densely populated with critical buildings and infrastructures and it is built upon ppc (Marshy clay and peat), asd (Alluvial sand), asl (Alluvial silt), asc (Alluvial silt and clay) and rm (Modhupur clay residium) soft sediments of the Megna and Brahmaputra River. There are two aspects for safety against earthquake hazards: firstly, safety against potentially destructive dynamic forces and secondly, the safety of a site itself related with geotechnical phenomena such as amplification, land sliding and liquefaction (Ansary et al., 2004). With regards Nakamura's method, H/V spectral ratios, predominant frequency, amplification factor and finally vulnerability index (K_g) are calculated for 58 microtremor measurements.

3.2 LOCATION, GEOLOGY AND GEOMORPHOLOGY

Microtremor measurements at 58 selected locations in and around Gas network area of Dhaka city has been executed in consideration of diversified geological and geomorphological units. The selected locations in and around Dhaka city are situated in various geological units as discussed in Chapter 1. Figure 3.1 shows microtremor observation of 58 selected locations in Gas network area map of Dhaka city. As surface sedimentary deposits amplify the seismic waves and geomorphological map units represent the surface geology, these detailed delineated geomorphic units are used to estimate the seismic response of the ground. A geomorphological map with appropriate geomorphic units has been developed by GSB (2014) for Dhaka city. Microtremor

measurement points have been superimposed on the geomorphological map of greater Dhaka city (GSB, 2014) is shown Figure 3.2. Geomorphic units of study points from the geomorphological map are discussed below in Table 3.1 The selected site location, their ID, latitude, longitude and geomorphic unit of these locations have been presented in Table 3.2.

From Table 3.1, it can be seen that 58 selected locations are situated in 10 different geomorphologic units according to Figure 3.2. According to Figure 3.2, 58 selected locations have been classified into following groups:

28-Madhupur Terrace (High) [MT2; MT4; MT9; MT10; MT11; MT13; MT14; MT17; MT18; MT19; MT20; MT24; MT26; MT27; MT28; MT30; MT31; MT32; MT33; MT36; MT37; MT38; MT41; MT42; MT43; MT44; MT45; MT58], 6-Madhupur Terrace (Middle) [MT1; MT3; MT5; MT16; MT35; MT52], 4-Madhupur Terrace (Low) [MT15; MT22; MT40; MT46], 4-Narrow Valley/Gully [MT12; MT21; MT25; MT39], 1-Broad Valley [MT29], 3-High Flood plain [MT48; MT50; MT56], 3-Low Flood plain [MT47; MT53; MT55], 3-Marshy Land [MT6; MT34; MT54], 2-Younger Natural Levee [MT49; MT57], 4-Pointbar Complex [MT7; MT8; MT23; MT51].

Out of 58 selected locations, 28 selected locations have been classified into Madhupur Terrace (High) geomorphologic unit, which is the most predominant geomorphologic unit of the study area. The second most common geomorphologic unit is Madhupur Terrace (Middle).

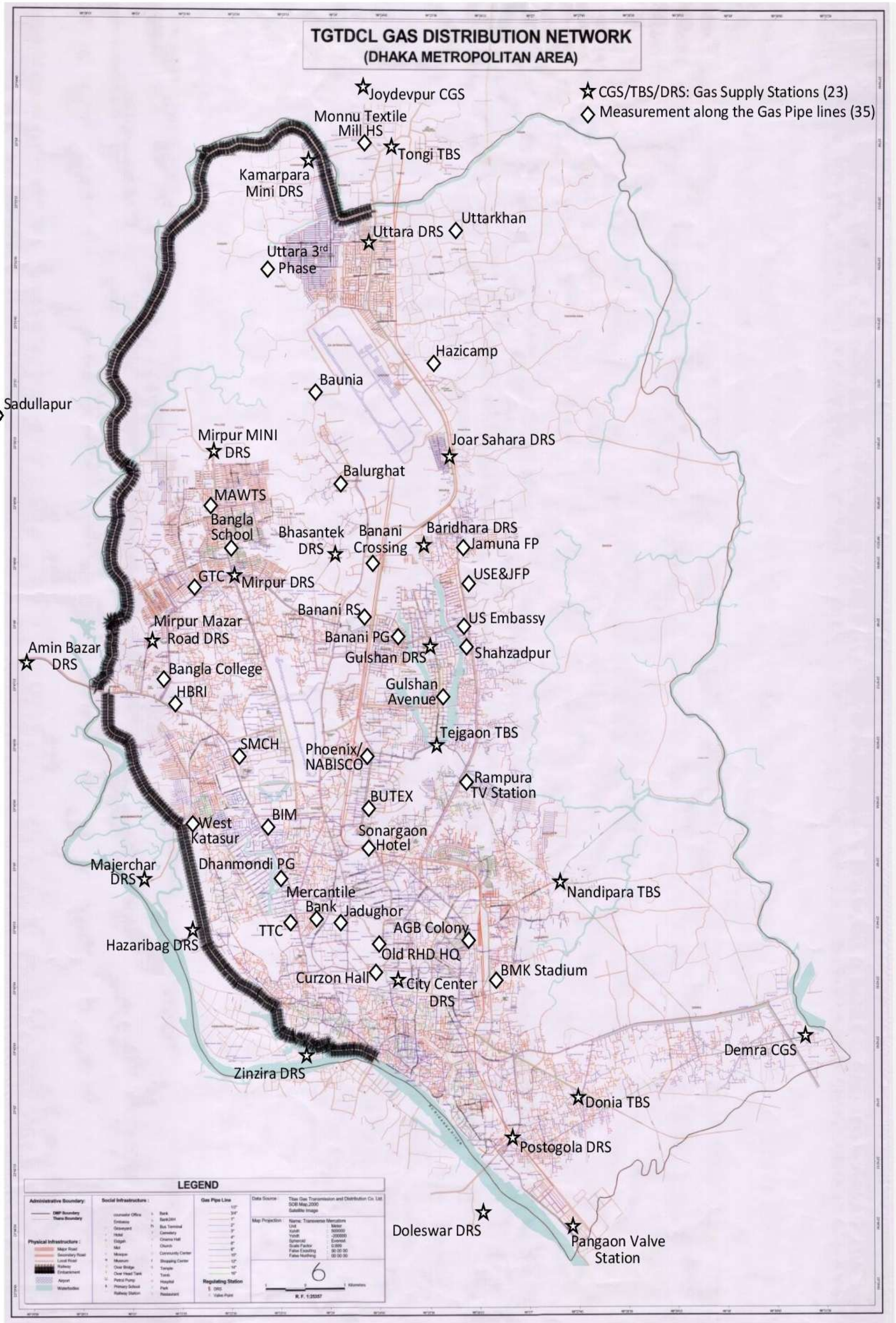

Figure 3.1: Microtremor observation at fifty eight selected locations in and around Gas Network of Dhaka City.

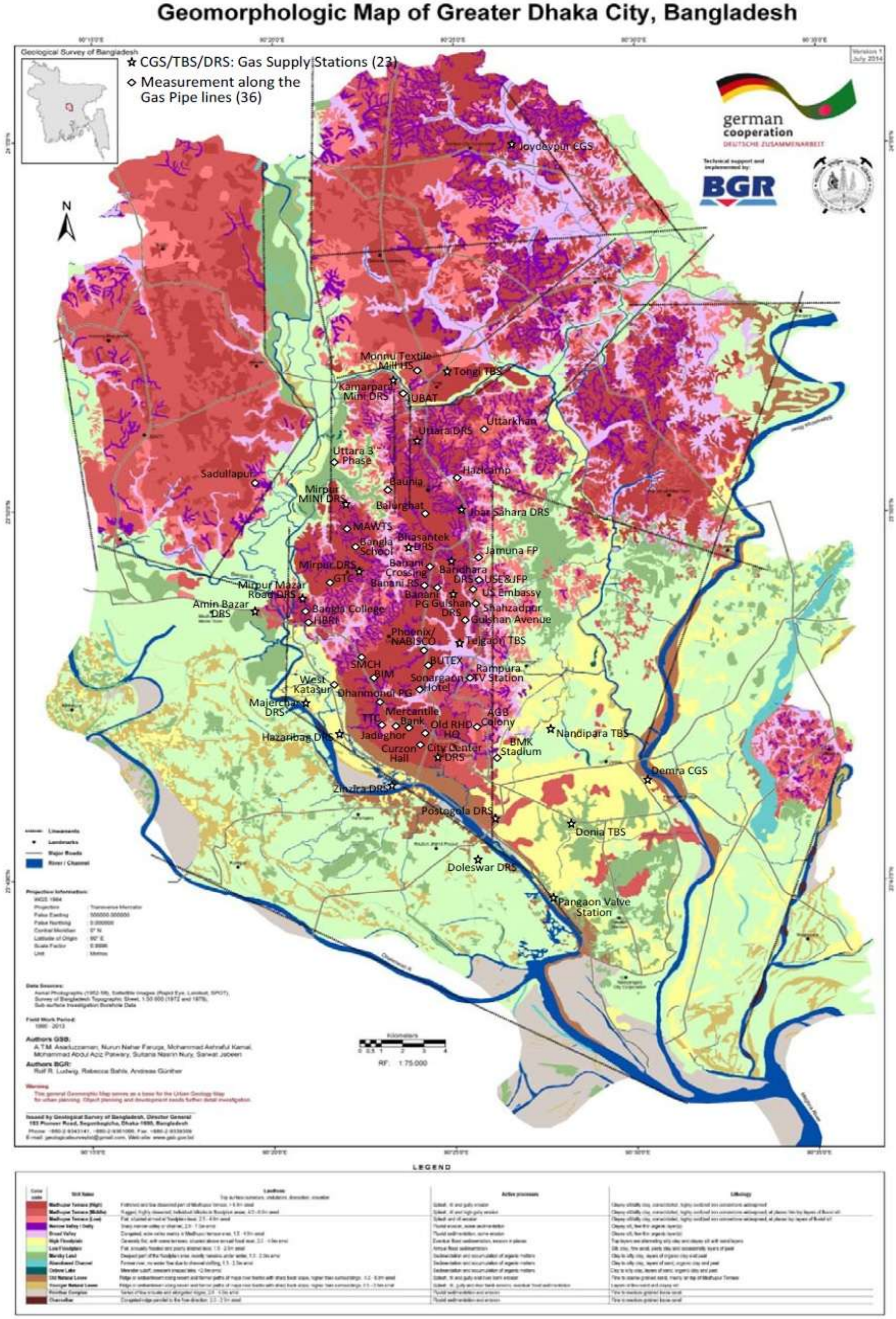

Figure 3.2: Superimposed study points on Geomorphological Map of Dhaka City

Table 3.1 Geomorphic unit of the study area

Geomorphic unit	**Landform:** Top surface curvature, undulation, dissection, elevation	**Active processes**	**Lithology**
Madhupur Terrace (High)	Flattened and low dissected part of Madhupur terrace, > 6.0m amsl	Splash, rill and gully erosion	Clayey silt/silty clay, consolidated, highly oxidized iron concretions widespread
Madhupur Terrace (Middle)	Rugged, highly dissected, individual hillocks in floodplain areas, 4.0-6.0m amsl	Splash, rill and high gully erosion	Clayey silt/silty clay, consolidated, highly oxidized iron concretions widespread, at places thin top layers of fluvial silt
Madhupur Terrace (Low)	Flat, situated almost at floodplain level, 2.5-4.0m amsl	Splash and rill erosion	Clayey silt/silty clay, consolidated, highly oxidized iron concretions widespread, at places top layers of fluvial silt
Narrow Valley/Gully	Sharp narrow valley or channel, 2.0-7.0m amsl	Fluvial erosion, some sedimentation	Clayey silt, few thin organic layer(s)
Broad Valley	Elongated, wide valley mainly in Madhupur terrace area, 1.5-4.0m amsl	Fluvial sedimentation, some erosion	Clayey silt, few thin organic layer(s)
High Floodplain	Generally flat, with some terraces, situated above annual flood level, 2.0-4.0m amsl	Eventual flood sedimentation, erosion in places	Top layers are alternating silty clay and clayey silt with sand layers
Low Floodplain	Flat, annually flooded and poorly drained land, 1.5-2.5m amsl	Annual-flood sedimentation	Silt, clay, fine sand, peaty clay and occasionally layers of peat
Marshy Land	Deepest part of the floodplain area, mostly remains under water, 1.3-2.0m amsl	Sedimentation and accumulation of organic matters	Clay to silty clay, layers of organic clay and peat
Younger Natural Levee	Ridge or embankment along resent and former paths of major river banks with shrap back slope, higher than surroundings, 2.5-3.5m amsl	Splash, rill, gully and river bank erosion, eventual flood sedimentation	Layers of fine sand and clayey silt
Pointbar Complex	Series of low arcuate and elongated ridges, 2.0-4.0m amsl	Fluvial sedimentation and erosion	Fine to medium grained loose sand

Table 3.2 Location of Microtremor Observation of the study area

Sl. No.	ID	Location	Latitude	Longitude	Geomorphologic Unit
1	MT1	Monnu Textile Mill High School	23°53'39.8"N	90°24'01.9"E	Madhupur Terrace (Middle)
2	MT2	Tongi TBS	23°54'17.47"N	90°24'18.71"E	Madhupur Terrace (High)
3	MT3	Kamarpara Mini DRS	23°52'50.8"N	90°24'00.9"E	Madhupur Terrace (Middle)
4	MT4	Uttara DRS	23°52'26.8"N	90°23'58.3"E	Madhupur Terrace (High)
5	MT5	Uttarkhan	23°52'45.0"N	90°25'29.3"E	Madhupur Terrace (Middle)
6	MT6	Uttara 3rd Phase	23°50'55.3"N	90°22'22.0"E	Marshy Land
7	MT7	Hazi Camp	23°51'04.1"N	90°24'41.3"E	Pointbar Complex
8	MT8	Baunia	23°50'57.0"N	90°23'18.7"E	Pointbar Complex
9	MT9	Joarsahara DRS	23°49'48.9"N	90°25'08.0"E	Madhupur Terrace (High)
10	MT10	Balurghat	23°49'46.4"N	90°23'19.1"E	Madhupur Terrace (High)
11	MT11	Mirpur Mini DRS	23°49'57.6"N	90°21'49.2"E	Madhupur Terrace (High)
12	MT12	Sadullapur	23°51'26.2"N	90°18'35.2"E	Narrow Valley/Gully
13	MT13	MAWTS	23°49'30.3"N	90°21'51.0"E	Madhupur Terrace (High)
14	MT14	Mirpur Bangla School	23°48'51.8"N	90°22'02.6"E	Madhupur Terrace (High)
15	MT15	Bhasantek DRS	23°48'22.3"N	90°23'16.2"E	Madhupur Terrace (Low)
16	MT16	Mirpur 10 DRS	23°48'25.5"N	90°22'08.1"E	Madhupur Terrace (Middle)
17	MT17	German Technical Training Center	23°48'08.2"N	90°21'28.9"E	Madhupur Terrace (High)
18	MT18	Banani Rail Crossing	23°48'44.0"N	90°24'13.7"E	Madhupur Terrace (High)
19	MT19	Banani Rail Station	23°47'44.8"N	90°24'03.7"E	Madhupur Terrace (High)
20	MT20	Banani Play Ground	23°47'37.0"N	90°24'29.7"E	Madhupur Terrace (High)
21	MT21	Baridhara DRS	23°48'58.7"N	90°24'58.7"E	Narrow Valley/Gully
22	MT22	Jamuna Future Park	23°48'47.8"N	90°25'16.5"E	Madhupur Terrace (Low)
23	MT23	Between US Embassy & JFP	23°48'24.5"N	90°25'18.4"E	Pointbar Complex
24	MT24	US Embassy	23°47'48.8"N	90°25'24.2"E	Madhupur Terrace (High)

Table 3.2 Location of Microtremor Observation of the study area (Continue)

Sl. No.	ID	Location	Latitude	Longitude	Geomorphologic Unit
25	MT25	Shahzadpur	23°46'29.8"N	90°25'34.2"E	Narrow Valley/Gully
26	MT26	Gulshan Avenue	23°46'59.6"N	90°25'01.2"E	Madhupur Terrace (High)
27	MT27	Gulshan DRS	23°47'33.1"N	90°24'54.4"E	Madhupur Terrace (High)
28	MT28	Tejgaon TBS	23°46'24.0"N	90°25'01.2"E	Madhupur Terrace (High)
29	MT29	Nabisco (Phoenix)	23°46'16.1"N	90°24'03.9"E	Broad Valley
30	MT30	BUTEX	23°45'37.8"N	90°23'58.6"E	Madhupur Terrace (High)
31	MT31	Mirpur Bangla College	23°47'05.1"N	90°21'11.6"E	Madhupur Terrace (High)
32	MT32	HBRI	23°46'52.5"N	90°21'11.7"E	Madhupur Terrace (High)
33	MT33	Mirpur Mazar Road DRS	23°47'35.3"N	90°21'01.3"E	Madhupur Terrace (High)
34	MT34	Amin Bazar DRS	23°47'20.7"N	90°19'05.8"E	Marshy Land
35	MT35	SMCH	23°46'06.8"N	90°22'09.1"E	Madhupur Terrace (Middle)
36	MT36	BIM	23°45'24.2"N	90°22'30.6"E	Madhupur Terrace (High)
37	MT37	Dhanmondi Play Ground	23°44'45.8"N	90°22'52.1"E	Madhupur Terrace (High)
38	MT38	Sonargaon Hotel	23°45'10.1"N	90°23'59.5"E	Madhupur Terrace (High)
39	MT39	Rampura TV Station	23°46'00.1"N	90°25'28.2"E	Narrow Valley/Gully
40	MT40	Teachers Training College	23°44'11.3"N	90°23'01.6"E	Madhupur Terrace (Low)
41	MT41	Elephant Road (Mercantile Bank)	23°44'20.3"N	90°23'14.3"E	Madhupur Terrace (High)
42	MT42	Old RHD HQ	23°44'01.6"N	90°24'08.0"E	Madhupur Terrace (High)
43	MT43	Jadughor	23°44'17.4"N	90°23'41.2"E	Madhupur Terrace (High)
44	MT44	Curzon Hall	23°43'41.0"N	90°24'07.2"E	Madhupur Terrace (High)
45	MT45	City Center DRS	23°43'30.1"N	90°24'35.3"E	Madhupur Terrace (High)
46	MT46	AGB Colony	23°43'59.4"N	90°25'23.6"E	Madhupur Terrace (Low)
47	MT47	BMK Stadium	23°43'34.3"N	90°25'43.7"E	Low Flood plain
48	MT48	West Katasur	23°45'03.8"N	90°21'28.3"E	High Flood plain

Table 3.2 Location of Microtremor Observation of the study area (Continue)

Sl. No.	ID	Location	Latitude	Longitude	Geomorphologic Unit
49	MT49	Majerchar DRS	23°44'09.2"N	90°20'06.0"E	Younger Natural Levee
50	MT50	Hazaribag DRS	23°43'55.0"N	90°21'42.5"E	High Flood plain
51	MT51	Zinzira DRS	23°47'33.1"N	90°23'52.9"E	Pointbar Complex
52	MT52	Postogola DRS	23°41'17.3"N	90°26'04.0"E	Madhupur Terrace (Middle)
53	MT53	Nandipara TBS	23°44'44.5"N	90°26'41.1"E	Low Flood plain
54	MT54	Donia TBS	23°42'01.2"N	90°27'24.4"E	Marshy Land
55	MT55	Doleswar DRS	23°40'25.4"N	90°26'21.0"E	Low Flood plain
56	MT56	Pangaon Valve Station	23°39'47.5"N	90°26'58.3"E	High Flood plain
57	MT57	Demra CGS	23°42'46.7"N	90°30'11.7"E	Younger Natural Levee
58	MT58	Joydevpur CGS	24°00'31.5"N	90°24'54.4"E	Madhupur Terrace (High)

3.3 MICROTREMOR DATA COLLECTION

Microtremors are ambient vibrations of the ground caused by natural or artificial disturbances such as wind, sea waves, traffic, human activities and industrial machinery. In this research, Microtremor measurements have been performed in Dhaka city during the period January, 2015 to April, 2017. The measurements have been carried out often Friday and Saturday, the distance between sites is approximately two kilometer. Microtremor measurements have been taken at District Regulating Station (DRS), Town Bordering Station (TBS), City Gate Station (CGS) and along gas pipe lines of gas network area. Site selection and Microtremor measurements have been executed according to guideline of SESAME, WP12 (2004).

In this research broad band sensor type of seismograph microtremor measurement apparatus has been used to acquire data. The name of seismograph is Central Recording System CR-6plus produced by GeoSIG Ltd. The CR-6plus seismograph consists of the 15 channel, 24 bit acquisition box system with built-in computer with all its auxiliary peripherals such as keyboard, mouse controls, USB inlets and outlets, 8 GB recording memory, Sensor, Cable, Battery, GPS and a high resolution screen for seismic data previews. GeoDAS software is used to record microtremor data. Five sensors have been used for data recording. Sensors have been used in consideration of surface condition,

weather, time and geology of sites. Sensors comprise of three components, which can record the horizontal motion (in Latitude and Longitude directions) and the vertical motions (up and down). The sampling frequency has been used 200 Hz. The amplification factor used is 20 db in observation system. Figure 3.3 shows some pictures of microtremor measurement at different locations. These pictures have been taken at different time during microtremor data observation.

3.3.1 Guidelines of Field Data Acquisition

The information of the guidelines and criteria for the implementation of the H/V spectral ratio technique on ambient noise vibrations measurements, processing and interpretation, is currently available at the following website address:http://sesame-fpsiobs.ujf-grenoble.fr/papers/HVUserGuidelines.pdf. The reliability of the H/V technique using ambient vibrations has been investigated by SESAME European project (Site EffectS assessment using AMbient Excitations). The seismological community agrees that the H/V technique gives valuable results if applied “with care” or “appropriately” (Martin et al. 2004). H/V measurements require both reliability of the results and rapidity of data collection. Therefore avoiding the possible influence of recording parameters, asphalt, grass, cement and concrete interfaces, that of nearby buildings, that of weather conditions and stability of the results over time are very important for data quality and reliability (SESAME, WP12, 2004).

3.3.2 Precautionary Measures in the Field

Some of the main points of precautionary measures have been taken for data acquisition from the field gathered from many experiences and the guidelines of SESME project:

i. Avoiding use of nonstandard recording/instrument/sensor setting parameters that influence on the H/V curves.
ii. Avoiding measurements on soft/irregular soils such as mud, grass, ploughed soil, ice, gravel, not compacted snow etc.
iii. Avoiding Artificial soil/sensor coupling
iv. Avoiding measurements under wind or strong rain
v. Avoiding high-voltage underground lines.

Figure 3.3: Microtremor data recording in and around Dhaka city.

vi. Avoiding rainy and windy days, extreme temperatures and low pressures to minimize the unstable distortions of frequencies.

vii. Avoid using long cables wiring to minimize the electronic and mechanical interferences.

viii. Avoiding some noise of short period local sources during measurement, such as footsteps, cars, tractors, engines etc.

ix. Avoiding working times of factory and heavy activities.

x. Keeping away a sufficient distances from infrastructure such as water pipes and electricity lines.

xi. Keeping away from buildings and big structures.

xii. Keeping away from trees and high plantation areas.

xiii. Avoiding waterlogged and highly water saturation areas.

Base on the SESAME program, the guidelines for the field data survey that has been reported in the official manual, are listed in Table 3.3**.**

Table 3.3 The guidelines for the field data survey based on SESAME program

Type of parameter	Main recommendations	
Recording duration	Minimum expected f_0 [Hz]	Recommended minimum recording duration [min]
	0.2	30' **(Selected)**
	0.5	20'
	1	10'
	2	5'
	5	3'
	10	2'
Measurement spacing	→ Microzonation: start with a large spacing (for example a 500 m grid) and, in case of lateral variation of the results, densify the grid point spacing, down to 250 m, for example. → Single site response: never use a single measurement point to derive an f_0 value, make at least three measurement points.	
Recording parameters	→ level the sensor as recommended by the manufacturer. → fix the gain level at the maximum possible without signal saturation.	
In situ soil-sensor coupling	→ set the sensor down directly on the ground, whenever possible. → avoid setting the sensor on "soft grounds" (mud, ploughed soil, tall grass, etc.), or soil saturated after rain.	
Artificial soil-sensor coupling	→ avoid plates from "soft" materials such as foam rubber, cardboard, etc. → on steep slopes that do not allow correct sensor levelling, install the sensor in a sand pile or in a container filled with sand. → on snow or ice, install a metallic or wooden plate or a container filled with sand to avoid sensor tilting due to local melting.	
Nearby structures	→ Avoid recording near structures such as buildings, trees, etc. in case of wind blowing (faster than approx. 5 m/s). It may strongly influence H/V results by introducing some low frequencies in the curves → Avoid measuring above underground structures such as car parks, pipes, sewer lids, etc.	
Weather conditions	→ Wind: Protect the sensor from the wind (faster than approx. 5 m/s). This only helps if there are no nearby structures. → Rain: avoid measurements under heavy rain. Slight rain has no noticeable influence. → Temperature: check sensor and recorder manufacturer's instructions. → Meteorological perturbations: indicate on the field sheet whether the measurements are performed during a low-pressure meteorological event.	
Disturbances	→ Monochromatic sources: avoid measurements near construction machines, industrial machines, pumps, generators, etc. → Transients: In case of transients (steps, cars,...), increase the recording duration to allow for enough windows for the analysis, after transient removal.	

The field sheet provided the detailed information about the circumstances and descriptions of the site. Such sheet is important to keep all the needed information about the site survey during the analysis and interpretation of the results. Table 3.4 shows the detailed information sheet.

Table 3.4 Sheet details information about site survey

<table>
<tr><td colspan="2">DATE:</td><td colspan="2">HOUR:</td><td colspan="2">PLACE:</td></tr>
<tr><td colspan="3">OPERATOR</td><td colspan="3">GPS TYPE and #</td></tr>
<tr><td colspan="2">LATITUDE</td><td colspan="2">LONGITUDE</td><td colspan="2">ALTITUDE</td></tr>
<tr><td colspan="2">STATION TYPE</td><td colspan="2">SENSOR TYPE</td><td colspan="2"></td></tr>
<tr><td colspan="2">STATION #</td><td colspan="2">SENSOR #</td><td colspan="2">DISK #</td></tr>
<tr><td colspan="4">FILE NAME:</td><td colspan="2">POINT #</td></tr>
<tr><td>GAIN</td><td colspan="2">SAMPL. FREQ. Hz</td><td colspan="3">REC. DURATION minutes seconds</td></tr>
<tr><td>WEATHER CONDITIONS</td><td colspan="5">Wind ☐ none ☐ weak (5 m/s) ☐ medium ☐ strong
Measurement (if any)……
Rain ☐ none ☐ weak ☐ medium ☐ strong
Measurement (if any)……
Temperature (approx): ……Remarks……</td></tr>
<tr><td>GROUND TYPE</td><td colspan="5">☐ earth ☐ hard ☐ soft ☐ gravel ☐ sand ☐ rock ☐ grass ☐ short ☐ tall
☐ asphalt ☐ cement ☐ concrete ☐ paved ☐ other
☐ dry soil ☐ wet soil Remarks……</td></tr>
<tr><td colspan="6">ARTIFICIAL GROUND-SENSOR COUPLING ☐ no ☐ yes, type…..…….</td></tr>
<tr><td colspan="6">BUILDING DENSITY ☐ none ☐ scattered ☐ dense ☐ other, type……</td></tr>
<tr><td>TRANSIENTS</td><td>none</td><td>few</td><td>moderate</td><td>many</td><td>very dense</td><td>distance</td></tr>
<tr><td>cars</td><td></td><td></td><td></td><td></td><td></td><td></td></tr>
<tr><td>trucks</td><td></td><td></td><td></td><td></td><td></td><td></td></tr>
<tr><td>pedestrians</td><td></td><td></td><td></td><td></td><td></td><td></td></tr>
<tr><td>other……..</td><td></td><td></td><td></td><td></td><td></td><td></td></tr>
<tr><td colspan="4" rowspan="2">OBSERVATIONS</td><td colspan="3">Monochromatic noise sources (factories, works, pumps, rivers,…)
☐ no ☐ yes, type……</td></tr>
<tr><td colspan="3">NEARBY STRUCTURES (trees, polls, buildings, bridges, underground structures,…..) (description, height, distance)</td></tr>
<tr><td colspan="4"></td><td colspan="3">FREQUENCY: Hz
(if completed in the field)</td></tr>
</table>

3.3.3 Constraints of Data Acquisition in the Field

Microtrmor data acquisition has been subjected to the following constraints:

i. High temperatures; especially in summer because the Dhaka city located within the warm dry climate region.
ii. Constraints associated with difficulties to take permission of the access to the selected site.
iii. Traffic conditions near the selected site especially with high traffic rates.
iv. Some industrial activities in the local area which have effects on certain times of data acquisition.
v. Some issues that are associated with especially closed agricultural areas such issues make it hard to follow up the points according to the supposed divisions of the study.
vi. Technical problems associated with the use of seismograph and seismometer in the field.
vii. Construction and drilling works in the surrounding area.
viii. The presence of infrastructure underground pipelines.
ix. Difficulty in choosing the quiet peak times such as dawn and night because of security conditions.

3.3.4 Data Recording

Before collection of data, some preparation has been checked, as follows:

i. Checking the equipment and making sure that it work efficiently before going to the field.
ii. Ensure the safety of the battery. It is preferred to take a backup battery to the field.
iii. Having a mobile high-precision GPS in order to determine the coordinates of measured points.
iv. Forming a team and selecting a vehicle appropriate to the field in order to conduct the study.
v. Taking a Picture of the study site with camera.
vi. Preparing a drawing of sensor setup indicating direction for the study area in order to collect field readings.

After determining the starting point for the data acquisition and before installing the devices, the recommended guidelines as outlined in section 3.3.2 are followed in order to get a clear, good and appropriate data for reliable results.

The total recording duration should be increased; in order to remove some transients occurred during the recording, from the signal for processing for "good quality" signal windows (SESAME, WP12, 2004). In this study microtremor data has been recorded for 30 minute according to SESAME recommendation as shown in Table 3.5.

Table 3.5 Recommended recording duration

f_0 [Hz]	Minimum value for l_w [s]	Minimum number of significant cycles (n_c)	Minimum number of windows	Minimum useful signal duration [s]	Recommended minimum record duration [min]
0.2	50	200	10	1000	30'
0.5	20	200	10	400	20'
1	10	200	10	200	10'
2	5	200	10	100	5'
5	5	200	10	40	3'
10	5	200	10	20	2'

Velocity-time history field microtremor data has been recorded in GeoDAS software with suitable five number of observation channels/sensors, 15 m observation length, 200 Hz observation frequency, specific low or high pass filter code, amplification ratio, observation latitude and longitude, observation time and observation channel mode. Figure 3.4 shows a typical time history field data recording of MT16-Mirpur 10 DRS at 11:30 PM on 6 February, 2016. The content of all input data are 2 CR-6plus velocity type sensors, 360000 observation points, 200Hz sampling frequency, 0.05 Hz Low-pass filter, 20db amplification ratio, Latitude-23°48'25.5"N and Longitude-90°22'08.1"E (Figure 3.4).

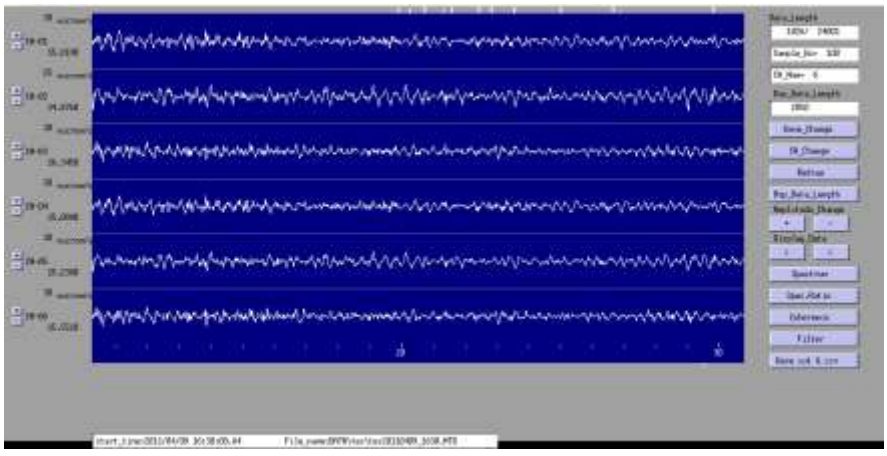

Figure 3.4: Time history of Microtremor observation at MT16-Mirpur 10 DRS

3.4 CONCLUDING REMARKS

Chapter 3 shows location and geomorphology of the study area. Also data collection method has been explained in details. The microtremor observations have been carried out at 58 locations in and around gas network area of Dhaka city which falls on different geological and geomorphological units. According to SESAME WP12, (2004), microtremor data collection guidelines; precautionary measures; constraints of data acquisition in the field and data recording have been included in this chapter.

CHAPTER 4
RESULTS AND DISCUSSIONS

4.1 GENERAL

Damage in recent earthquakes showed that local site conditions have a significant effect on ground motion. Site response studies play an important role in seismic microzonation studies. The application of microtremor is to determine dynamic characteristics (predominant frequency and amplification factor). Nowadays microtremor measurements are used in site characterization due to their simplicity, low cost and minimal disturbance to other activities.

In the traditional spectral ratio method, Hs/Hr, site and source effects are estimated from observation at a reference site. In practice, adequate reference site are not always available especially in flat areas where exposed rock is not available. Therefore, methods have been developed that do not need reference sites (Bard 1994). Several recent applications of this technique have proved to be effective in estimating predominant frequency (Field and Jacob 1993; Ohmachi et al. 1991) and amplification factors (Lermo and Chavez-Garcia 1994; Konno and Ohmachi 1998). The application of microtremor H/V technique for site response analysis has been discussed in Chapter 2.

Several methods have been proposed for spectral calculation of ground motions including microtremor. Fourier spectrum is the most convenient one that is used widely. Some investigations showed that different methods give similar results (Dimitriu et al. 1998). However, some researchers declare that a suitable spectral method gives more reliable results (Ghayamghamian and Kawakami 1997). That's why minimum twenty five windows have been selected from time history to compute amplitude spectrum of all three components, amplitude spectral ratios and the mean spectral ratio. Standard deviation of mean has also been calculated to show the deviation of mean value from twenty five spectral ratios.

4.2 H/V SPECTRAL RATIO METHODOLOGY

After the collection of data using the acquisition software with recommendations, precautions and any other requirements from SESAME guidelines and from other experts, the data has been compiled for each site in order to analyze them using DPLOT software. DPLOT is a windows program that lets engineers create presentation quality graphs from a wide variety of data sources. However, SESAME has developed a software for data analysis applying the H/V technique. The name of the software is J-SESAME to be used as a standard procedure in processing the microtremor data using H/V technique (SESAME, WP03, 2003).

Microtremor data composed of three components known as time domain data has been analyzed in accordance with the Site Effects Assessment Using Ambient Excitations (SESAME) guidelines for implementing the H/V spectral ratio approach (SESAME WP12, 2004). The H/V spectral ratio method has been used to show how to do the analysis for the interpretation of measured data from a single station summarized as following:

i. Recording the field data as three components; two horizontal and one vertical.
ii. Decomposition of the signal in time windows, aiming to isolate the part of the recording in which the signal is more stationary and to eliminate transient noise.
iii. Calculation and smoothing of the amplitude spectrum obtained by the Fourier Transform for each of the selected windows on all three components.
iv. Combination with an average of the two horizontal components for each of the selected windows. Merging the horizontal (NS and EW) components with a quadratic mean, $H = \frac{\sqrt{NS^2+EW^2}}{2}$ (4.1)
v. Calculation of the ratio between amplitudes of combined horizontal signal to the vertical signal (H/V) for each window. Thus, in each of the $n_{windows}$ windows the distribution of $Log_{10}(H/V)$ is obtained as a function of the frequency.
vi. Calculation of the average of the ratios H/V of all windows which is represented as the final H/V curve. The geometric mean of H/V is calculated: H/V is averaged over all window results; $H/V_{average} = \frac{\sum Log_{10}(H/V)}{n_{windows}}$ (4.2)

    H/V standard deviation is calculated:

$$\sigma_{H/V} = \sqrt{\frac{\sum \mathrm{Log}_{10}^2(H/V) - n_{windows} \times \mathrm{Log}_{10}^2(H/V_{average})}{(n_{windows} - 1)}} \qquad (4.3)$$

$H/V_{average}$ and $\sigma_{H/V}$ are set back to a linear scale by calculating $\overline{H/V} = 10^{H/V_{average}}$ and $\sigma_{\overline{H/V}} = 10^{\sigma_{H/V}}$.

MS Excel and DPLOT effectively are used to perform all the other steps from two to six mentioned above, to obtain simple and fast H/V Curve. The data processing has been carefully conducted to ensure the quality and reliability of the H/V curve. The steps of the data analysis using DPLOT software by applying H/V method are summarized as follows:

Loading the files

The format for the data of surveys HVSR was the mini seed file, which is the default format of data acquisition program "CR-6plus GeoDAS". DPLOT software can read .txt, excel and csv file. The data of mini seed file has been converted to text file and then excel file. The best sensor data of excel file format has been used in DPLOT software for graphical presentation of time domain data as time vs velocity in linear scale. Figure 4.1 shows time history microtremor data of 30 minute with 360000 observed data length at Mirpur 10 DRS. There are three components of this time history data as two horizontal directions (North-South and East-West) and the vertical component (Up-Down).

Window selection

The window length according to SESAME guidelines is based on the formula of $f_0 > 10/l_w$, where l_w is the minimum window length and f_0 is the expected natural frequency. This condition requires that at the frequency of interest, each window must have 10 significant cycles at least. Again the total number of significant cycles is $n_c = l_w \times n_w \times f_0$ must be greater than 200. In order to fulfill above criteria, minimum twenty five number of windows of 40.96 sec each window length with 8192 observed data length have been truncated from this time history data length to be analyzed. The window length 40.96 sec is large enough to ensure a good resolution at low frequency. This 25 number of windows may be enough to provide statistical confidence for the evaluation of the predominant frequency. Figure 4.1 shows 25 windows of 40.96 sec on time history microtremor data of 30 minute for two horizontal directions (North-South and East-West) and the vertical component (Up-Down) at Mirpur 10 DRS site.

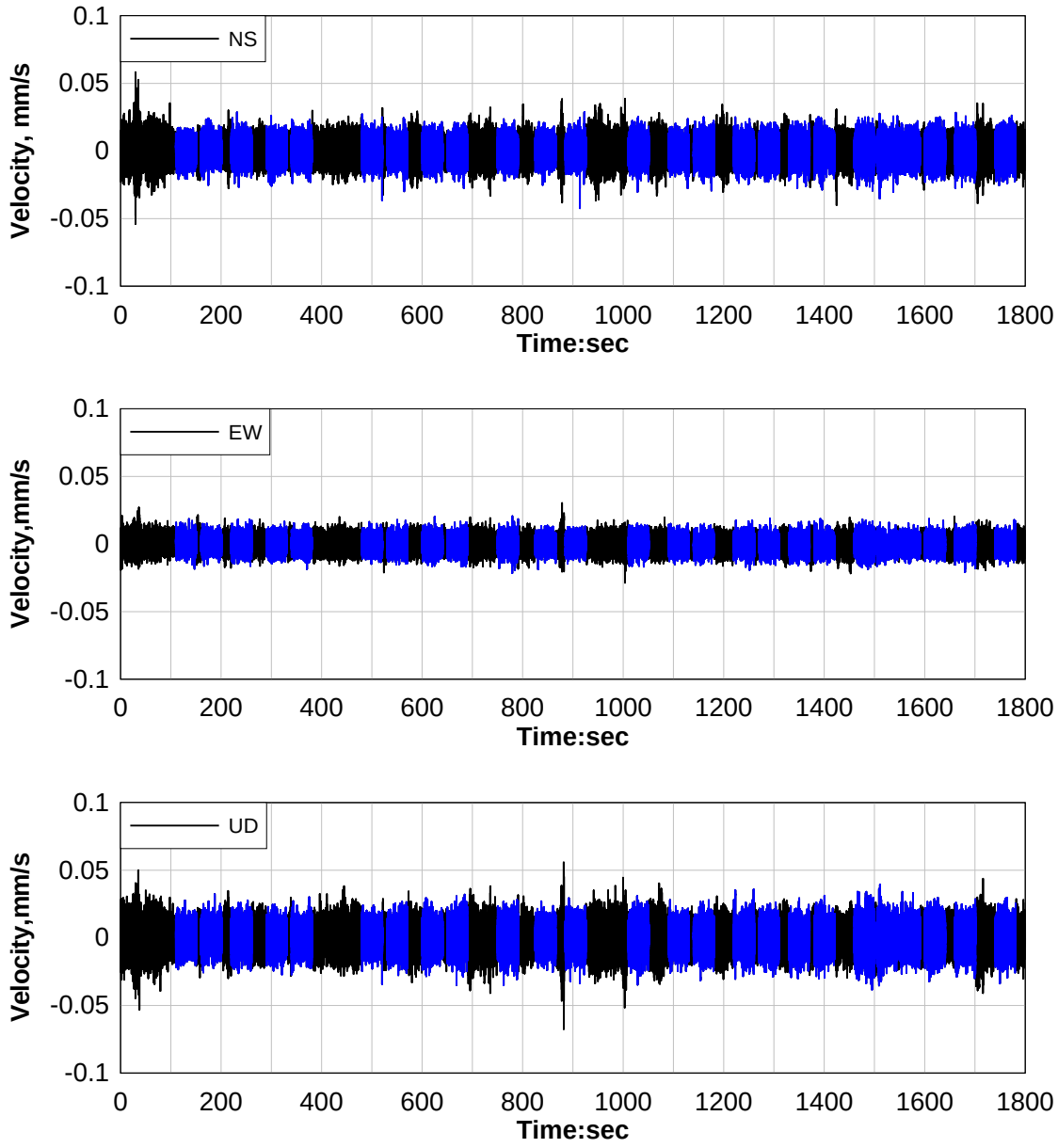

Figure 4.1: 25 window selections marked by blue color from total time history of microtremor data (30 min) at MT16-Mirpur 10 DRS.

Filter assignment

Before running the H/V process over the recorded signal, it is necessary to remove any bad signal (spike noise) from the overall waveform that is generated by near source effects such as footsteps, manual or mechanical digging, tractors etc. Time history data of each window 40.96 sec has been passed through a Band Pass filter in the range between 0.05 Hz to 25 Hz to reduce the distortion of peak amplitudes.

Smoothing option of the H/V ratio

Smoothing option can be used in order to remove a very spiky or sharp spectrum of H/V ratio produced over the range of frequencies. The smoothing option has different types, namely; Konno & Ohmachi, Constant and Proportional filters. The Konno & Ohmachi smoothing is recommended as it accounts for the different number of points at low frequencies by the SESAME guideline. In DPLOT software, the "smoothing" is the number of points over which the data of each window have been smoothed. This value varies 5 to 40 based on justification.

Time history data is not suitable to estimate the dynamic properties (predominant frequency and amplification ratio). So, transformation of time domain data to frequency domain data is required with Fourier Transformation. Fast Fourier Transformation (FFT) has been used to transfer time domain data of each window to frequency domain data.

Only the Fourier Spectrum along three subsequent directions is not appropriate to estimate the predominant frequency and amplification. So, Horizontal to Vertical spectral ratio (H/V) is required to determine the dynamic properties of soil. The two horizontal spectrums (North-South and East-West) have been merged with a quadratic mean using equation 4.1 and then divided by the vertical spectrum (Up-Down) to calculate the H/V spectral ratio of each window. Figure 4.2 represents detail procedures to calculate H/V spectral ratio of window 1 only. The geometric mean H/V spectral ratio of 25 windows has been calculated using equation 4.2. Then standard deviation of H/V spectral ratio has been calculated using equation 4.3. Frequency (Hz) verses average H/V spectral ratio as well as the plus and minus one standard deviation curves have been plotted on logarithmic and linear scale. After smoothing the corresponding curves, the output result, as shown in Figure 4.3, shows the H/V spectral ratio is the black continuous curve and it lies between the upper and lower standard deviation curves (dashed curve). From this graph, it has been observed that the range of frequency where in the H/V amplification is maximum. This range of frequency contains the predominant frequency (f_0) of the site. The peak value in the H/V solid curve represents the average value for the wave amplification factor (A_0) at that site. Seismic vulnerability index (K_g) has been determined using the predominant frequency (f_0) and amplification factor (A_0) of this site as, $K_g = \frac{A_0^2}{f_0}$.

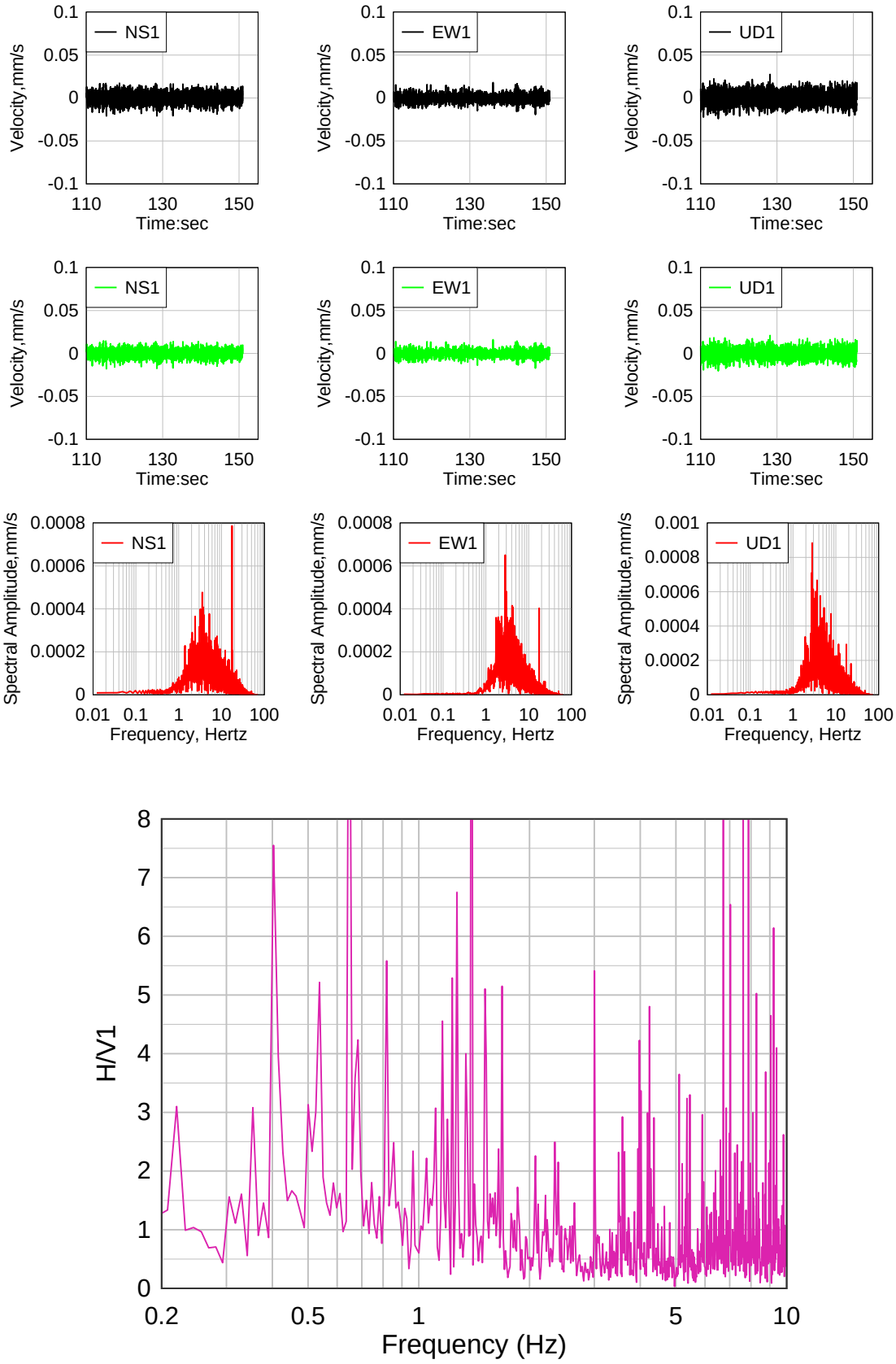

Figure 4.2: Time History data of window 1 from 110s to 150.96s (1st row), Band Pass Filter data (2nd row), FFT of window 1 in NS, EW and UD direction (3rd row) and H/V1 spectral ratio vs Frequency (Hz) of window 1 of MT16- Mirpur 10 DRS site.

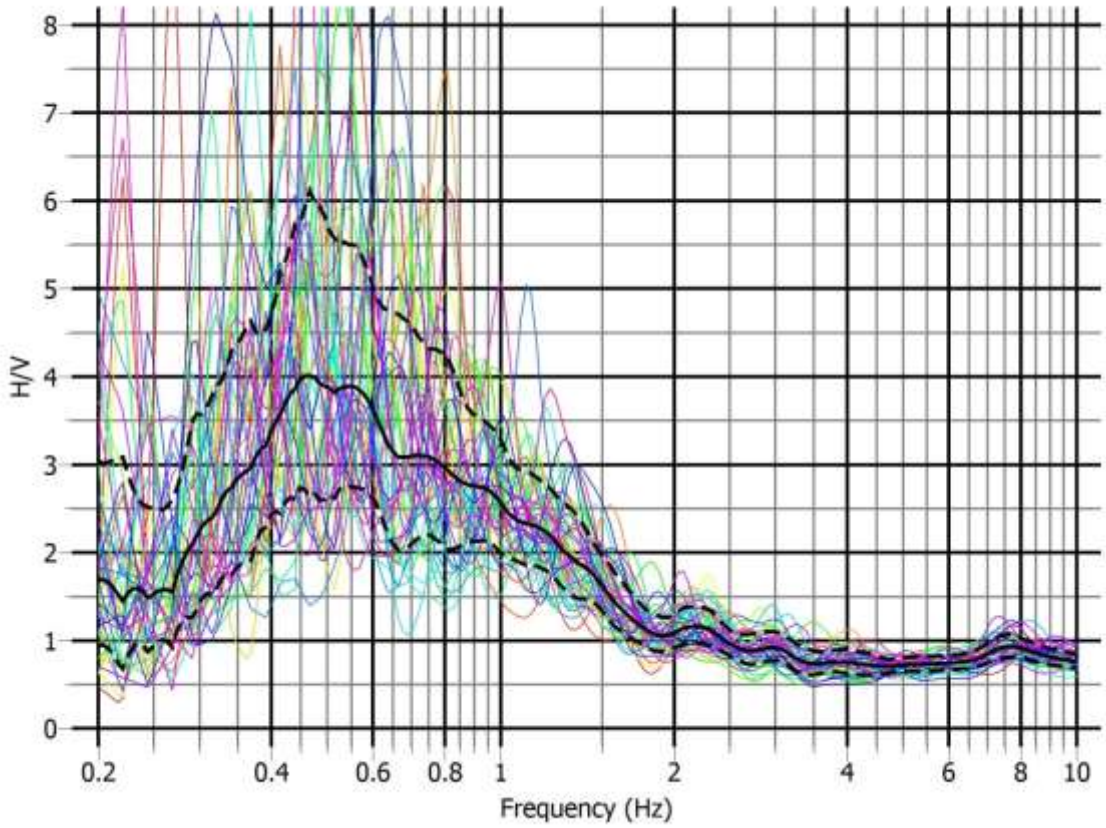

Figure 4.3: H/V spectral ratio curve of MT16- Mirpur 10 DRS site

4.3 CRITERIA OF THE H/V SPECTRAL RATIO ANALYSIS

The SESAME guidelines have three conditions for H/V spectral ratio curve reliability and five out of six criteria for identification of a peak frequency, f_0, as a clear peak. These criteria are depicted in Figure 4.4. The reliable curve criteria test the amount of variability in the standard deviation of the H/V amplitude and therefore determine whether the measured curve is a true representation of the H/V spectral ratio at this site. The criteria for a clear peak determine if the frequency band within which a spectral peak is located is stable and whether the peak may be considered prominent.

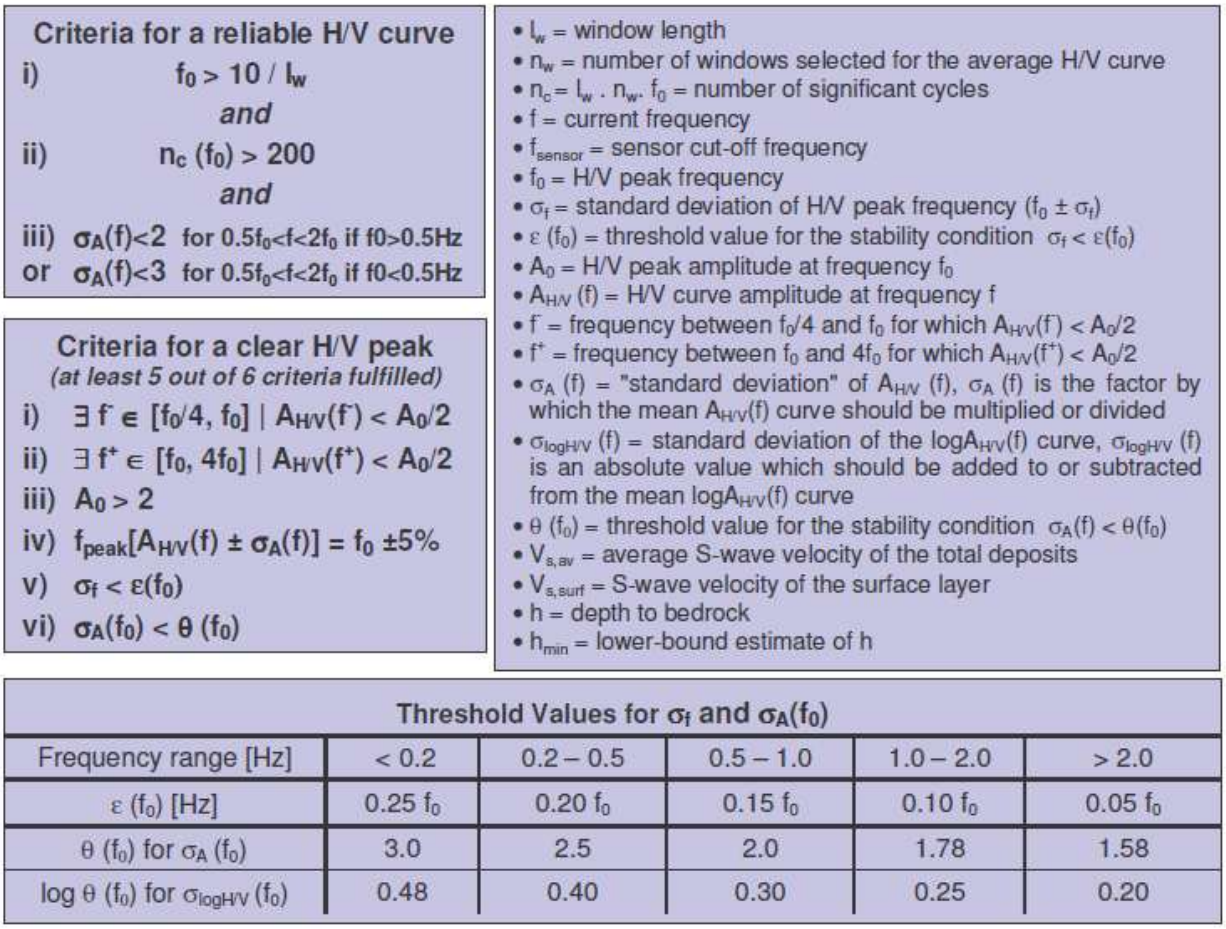

Figure 4.4: H/V Spectral Ratio testing criteria set forth by SESAME. Clockwise from top left panel: Criteria for reliable curve, variable list and description, threshold values for standard deviation of frequency and amplitude, and criteria for clear peak. Image is from SESAME, WP12 (2004).

4.3.1 Conditions for Curve Reliability (3 out of 3 must be satisfied)

i. f_0 must be greater than 10 divided by the window length. This condition requires that at the frequency (range) of interest, there should be at least 10 cycles in each window.

ii. The number of significant cycles must be greater than 200. The second condition determines if the overall recording duration contains sufficient data to be analyzed.

iii. This criteria requires an acceptably low level of scattering between all windows. Large standard deviation values often mean that ambient vibrations are strongly non-stationary and undergo some kind of perturbation, which may significantly affect the physical meaning of the HVSR peak frequency. The spectral standard

deviation of the amplitude has to be less than a particular value in a particular frequency range that depends on the f_0. If f_0 is greater than 0.5 Hz, the standard deviation of the amplitude must be less than 2 within the range of 0.5 f_0 to $2f_0$. If f_0 is less than 0.5 Hz, the standard deviation of the amplitude must be less than 3 within the range of 0.5 f_0 to $2f_0$.

4.3.2 Criteria for a Clear H/V Peak (at least 5 out of 6 criteria fulfilled)

The "clarity" concept may be related to several characteristics: the amplitude of the spectral ratio peak and its relative value with respect to the spectral ratio values in the surrounding frequency bands, the relative value of the standard deviation of the peak amplitude and frequency, and the standard deviation of estimates from individual windows.

i. Between $f_0/4$ and f_0, there exist a frequency at which the spectral ratio amplitude is less than $A_0/2$.
ii. Between f_0 and $4f_0$, there exists a frequency at which the spectral ratio amplitude at that frequency is less than $A_0/2$.
iii. A_0 must be greater than 2.
iv. For frequency stability, the frequency of the peak in the HVSR curves corresponding to mean + and − one standard deviation, is at most 5% higher or lower than f_0.
v. $\sigma_f < \varepsilon(f_0)$ The standard deviation of the peak frequency must be below the threshold value as determined through the threshold value table in Figure 4.4.
vi. $\sigma_A(f_0) < \theta(f_0)$ The standard deviation of the amplitude at the peak frequency must be less than the threshold value as determined through the threshold value table in Figure 4.4.

4.4 H/V SPECTRAL RATIO ANALYSIS

The details of the analysis for one example, for MT16-Mirpur 10 DRS site have been shown in Figure 4.5. The site has been mostly undisturbed with minimal external influences to the full waveform data. This site is located in Dhaka City on alluvial deposits and Madhupur Terrace (Middle). This site is in close proximity to residential housing or industrial structure. However, microtremor data have been collected on holiday for this

site to avoid noise as well as industrial origin. Therefore, it is expected this location to be an example of an ideal installation site to collect ambient noise data for gas network area.

MT16: Mirpur 10 DRS (23°48'25.5"N, 90°22'08.1"E)

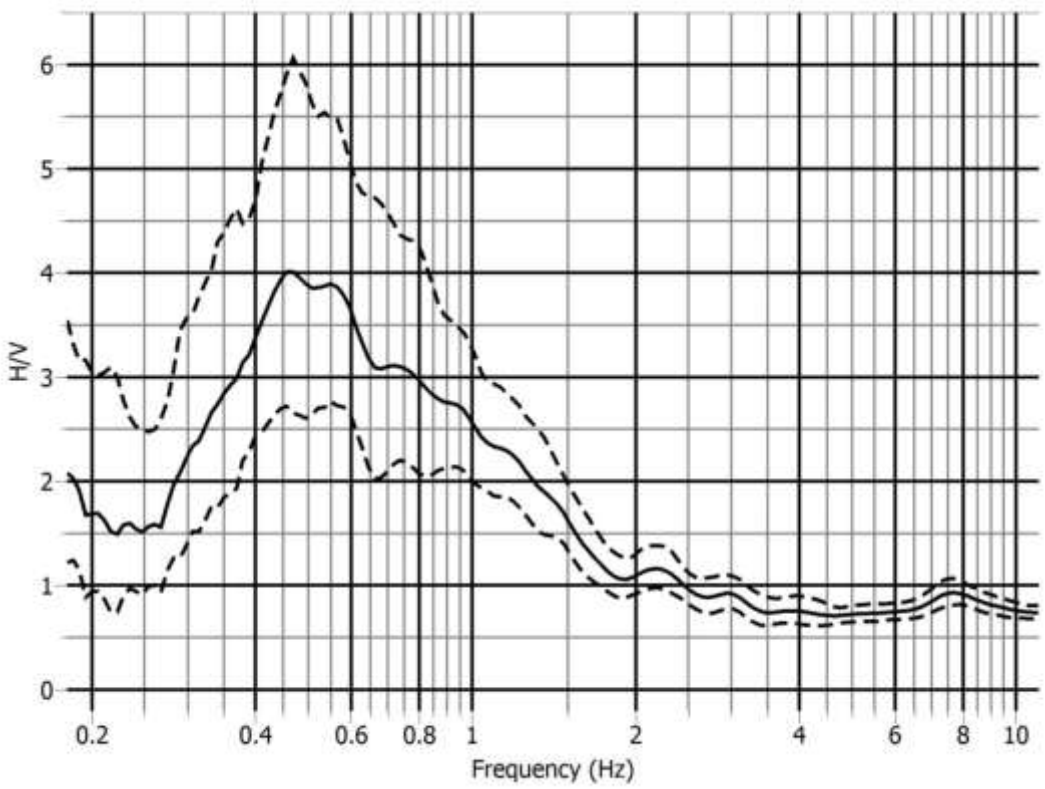

f_0=0.46 Hz; A_0 = 4.0; $A_{H/V}$ = (2.66, 6.0); $\sigma_A(f_0)$ = 1.50 & 1.50

i) f_0=0.46 Hz > (10/40.96=0.24 Hz); ii) n_c > 200; iii) $\sigma_A(f)$ < 3; at 0.23 Hz <f< 0.92 Hz

Satisfies all three criteria of Reliable H/V Curve

i) Between 0.115 to 0.46 Hz, $A_{H/V}(f^-) < A_0/2$

ii) Between 0.46 to 1.84 Hz, $A_{H/V}(f^+) < A_0/2$

iii) $A_0 > 2.0$

iv) Between 0.437 Hz to 0.483 Hz, f_{peak} = (0.45 Hz, 0.47 Hz)

v) $\sigma_f = 0.090 < \varepsilon(f_0) = 0.092$

vi) $\sigma_A(f_0) = 1.50 < \Theta(f_0) = 2.5$

Satisfies six out of six criteria of Clear H/V Peak

Reliable curve and Clear low frequency peak

Figure 4.5: Details of the analysis for one example, for MT16-Mirpur 10 DRS site

Table 4.1 Result output of H/V spectral ratio curve at MT16-Mirpur 10 DRS

Sl. No	ID	Location	Latitude	Longitude	f_0	σ_f	A_0	$\sigma_A(f_0)$
16	MT16	Mirpur 10 DRS	23°48'25.5"N	90°22'08.1"E	0.46	0.090	4.0	1.50

Window length 40.96 sec and total 25 windows (Figure 4.2) have been used for the analysis of H/V spectral ratio. Each window of data undergoes a Fourier transform to calculate amplitude spectra of three components. H/V spectral ratio of each window is calculated as combined horizontal components with a quadratic mean divided by vertical component. H/V spectral ratios for all windows are then averaged to generate the H/V spectral ratio curve as displayed by Figure 4.3. A peak frequency of interest is seen for investigation as listed in Table 4.1. The clarity of the peak frequency and the reliability of the spectral curve are then tested in accordance to the guidelines set forth by the SESAME project by Bard & SESAME Participants (2004).

4.4.1 SESAME Criteria for Reliable Curve

The three criteria for a reliable curve must be satisfied for it to be considered reliable for interpretation.

i) $f_0 > 10/l_w$; Criteria (i) for a reliable curve states there have to be at least 10 wave periods in each window. We have $f_0 = 0.46$ Hz, which is greater than the value of $\frac{10}{40.96 \text{ sec}}$ therefore, criteria (i) for a reliable curve is true. For this example, we test the highest peak observed.

ii) $n_c(f_0) > 200$ where the number of significant cycles $n_c = l_w \times n_w \times f_0$ is $40.96 \times 25 \times 0.46 \approx 471$. Therefore, criteria (ii) for a reliable curve is true.

iii) $\sigma_A(f) < 3$ for $0.5f_0 < f < 2f_0$ if $f_0 < 0.5$ Hz translates into $\sigma_A(f) \leq 3$ within the frequency range 0.23 Hz to 0.92 Hz. At f = 0.80 Hz, $\sigma_A(f) = 1.416$. Therefore, criteria (iii) for reliable curve is true.

In conclusion, all three criteria for a reliable curve are true. Therefore we proceed to test for the criteria for clear peak.

4.4.2 SESAME Criteria for Clear Peak

i) $\exists f^- \in \left[\frac{f_0}{4}, f_0\right] \mid A_{H/V}(f^-) < \frac{A_0}{2}$ states there exist a frequency f^- between $\frac{f_0}{4}$,(0.115 Hz) and f_0, (0.46 Hz) at which the amplitude of the H/V spectral ratio curve at the H/V spectral ratio curve is less than $\frac{A_0}{2}$ where, $\frac{A_0}{2}$ is 2.0. There exists a frequency f^- between 0.18 Hz and 0.28 Hz at which the amplitude is less than $\frac{A_0}{2}$; therefore criteria (i) for a clear peak is true.

ii) $\exists f^+ \in [f_0, 4f_0] \mid A_{H/V}(f^+) < \frac{A_0}{2}$ states there exists f^+ a frequency between f_0, (0.46 Hz) and $4f_0$, (1.84 Hz) for which the amplitude of f^+ is less than $\frac{A_0}{2}$ where $\frac{A_0}{2}$ is 2.0. There exists a frequency between 1.30 Hz and 1.84 Hz for which the amplitude of f^+ is less than $\frac{A_0}{2}$; therefore, criteria (ii) for a clear peak is true.

iii) $A_0 > 2$ where, A_0 is 4.0; therefore, criteria (iii) for a clear peak is true.

iv) $f_{peak}\,[A_{H/V}\,(f) \pm \sigma_A(f)] = f_0 \pm 5\%$ requires that the frequency of the peak for the two curves that represent the H/V spectral ratio + and - its standard deviation is within 5% of f_0, where $f_0 \pm 5\%$ is the range of 0.437 Hz to 0.483 Hz. We measure f_{peak} to be 0.45 Hz; therefore, criteria (iv) for a clear peak is true.

v) $\sigma_f < \varepsilon(f_0)$ states that the σ_f of 0.090 should be less than the threshold value for the stability condition which as shown in Figure 4.4 is $\varepsilon(f_0)$, $0.20f_0$ which is $0.20 \times 0.46 = 0.092$ Hz; therefore, criteria (v) for a clear peak is true.

vi) $\sigma_A(f_0) < \Theta(f_0)$states that the $\sigma_A(f_0)$ of 1.50 should be less than the threshold value for the stability condition which as shown in Figure 4.4 is $\Theta(f_0) = 2.5$; therefore, criteria (vi) for a clear peak is true.

At least 5 of the 6 criteria must be fulfilled for the peak to be identified as a clear peak. 6 of the 6 criteria for clear peak are fulfilled for the peak near 0.46 Hz frequency of Mirpur 10 DRS site; therefore, the peak is clear. This routine process is performed for each reliable curve and peak in each site for reliability and clarity as documented in Appendix A.

4.4.3 Unclear Peak Cases

Industrial signals: In some cases an industrial region or factory nearby the site, the recorded signal may become dominated by the noise from the industrial sources. This will show sharp peaks in the Fourier Transform of the recorded signal. Therefore, and as a recommendation, any signal containing sharp peaks can be discarded because it is 95 % probability that it is coming from an industrial source (SESAME, WP12, 2004).

Unclear low frequency peaks: Due to various conditions, the recorded signal may exhibit a low frequency an unclear peak. Such conditions include cases with meteorological interference, such as wind blowing or cases with soil impedance contrast or cases with low sensitivity of the soil sensor. A fuzzy, unclear low frequency peak (i.e., at frequencies lower than 1 Hz) of H/V curve does not satisfy criterion i) and possibly ii) of the amplitude (SESAME, WP12, 2004).

Broad or multiple peaks: For this case it can be either changed the parameters related to the smoothing band in order to transform the signal into a "clear" H/V ratio curve. Or if it could have been caused by an industrial signal, therefore must go back and check for industrial signals. A broad peak, or a multiplicity of local maxima, of H/V curve does not satisfy the above criteria i, ii and possibly v of clear peak (SESAME, WP12, 2004).

Two peaks: It can happen due to two soil layers impedance contrasts in the form of two layers one is thick and the other is shallow. Therefore the geological condition of the site should be checked. The two frequencies, f_0 and f_1 (with $f_0 < f_1$), may then be interpreted as characteristics at each scale, f_0 being the fundamental frequency (SESAME, WP12, 2004).

Flat Peak: If the amplitude values lying between around 0.5 and 2.0, without any clear peak, the H/V curve is flat. It is very likely that the local underground structure does not exhibit any sharp impedance contrast at any depth. It does not necessarily mean, however, that there is no site amplification (SESAME, WP12, 2004).

4.5 RESULTS AND DISCUSSIONS

The measurements consisted of a total of 58 microtremor measurements. Each measurement consists of thirty minutes recording. Following the SESAME recommendations (SESAME WP12, 2004), frequency peaks with amplitude greater than 2 has been measured. The threshold value is adequate in the study area, since it has been found that flat H/V spectral ratio curve has no clear frequency peaks with amplitude below 2. 46 out of 58 microtremor measurements have been considered to determine the site fundamental period and amplification factor. The analysis of microtremor measurements is shown in Appendix A. These 46 curves produced reliable curves. 22 out of these 46 measured peaks may be classified as clear peaks according to the SESAME criteria. The analyses of microtremor measurements have produced a wide variety of HVSR graphs: some spectral ratio curves show multiple peaks occurring at a range of frequencies, some graphs show no peaks or simple clear single peaks. It is not possible to determine the fundamental frequency and amplification factor for 12 sites. No peak has been found due to stiff soil stratum overlaying very hard soil stratum or bedrock at unknown depth from Microtremor measurements of MT4, MT12, MT20, MT22, MT23, MT24, MT41, MT42, MT46 and MT54 sites. On the other hand, MT9 site has produced no peak due to flat curve and MT47 site has produced unreliable curve as well as no peak. Table 4.2 shows the geographic coordinates for the 58 sites and the fundamental frequency and amplification factor for the 46 sites.

Out of 46 reliable curves, 22 clear peaks as well as 24 peaks that failed 2 or more clear peak criteria has been documented. The original criteria for a clear peak have been developed for single station analysis. However, since microtremor observation data-set consists of very closely spaced stations, it has been considered that there is still valuable information contained in peaks that may fail two or more criteria, yet are consistently observed over a significant lateral extent along the gas network area of Dhaka City. The distribution of the number of spectral peaks that pass the criteria for reliable curve and clear peak in accordance to the SESAME guidelines is shown in Figure 4.6 together with additional peaks that failed two or more criteria but has been consistently observed.

Table 4.2 Serial no, ID of each site, latitude, longitude, peak frequency, peak frequency error, amplitude, standard deviation of the amplitude of the peak, how many SESAME reliable curve/clear peak criteria failed and comments on curve/clear peak

Sl. No	ID	Location	Latitude	Longitude	f_0	σ_f	A_0	$\sigma_A(f_0)$	Condition failed		Comments	
									Curve	Peak	Curve	Peak
1	MT1	Monnu Textile Mill High School	23°53'39.8"N	90°24'01.9"E	0.42	0.086	5.66	1.76	0	i, v	Reliable	Unclear broad low frequency
2	MT2	Tongi TBS	23°54'17.47"N	90°24'18.71"E	0.51	0.075	2.81	1.50	0	i, ii	Reliable	Unclear broad low frequency
3	MT3	Kamarpara Mini DRS	23°52'50.8"N	90°24'00.9"E	0.48	0.081	4.20	1.64	0	ii	Reliable	Unclear low frequency
4	MT4	Uttara DRS	23°52'26.8"N	90°23'58.3"E	-	-	-	-	-	-	-	No Peak
5	MT5	Uttarkhan	23°52'45.0"N	90°25'29.3"E	0.75	0.127	2.72	1.36	0	i, v	Reliable	Unclear broad low frequency
6	MT6	Uttara 3rd Phase	23°50'55.3"N	90°22'22.0"E	0.41	0.075	3.88	1.69	0	i	Reliable	Unclear low frequency
7	MT7	Hazi Camp	23°51'04.1"N	90°24'41.3"E	0.44	0.084	2.38	1.55	0	i, ii	Reliable	Unclear broad low frequency
8	MT8	Baunia	23°50'57.0"N	90°23'18.7"E	0.59	0.120	2.91	1.40	0	v	Reliable	Clear low frequency
9	MT9	Joarsahara DRS	23°49'48.9"N	90°25'08.0"E	-	-	-	-	-	-	Flat Curve	No Peak
10	MT10	Balurghat	23°49'46.4"N	90°23'19.1"E	1.48	0.205	4.85	1.29	0	v	Reliable	Clear peak
11	MT11	Mirpur Mini DRS	23°49'57.6"N	90°21'49.2"E	0.46	0.070	3.12	1.46	0	i	Reliable	Unclear low frequency
12	MT12	Sadullapur	23°51'26.2"N	90°18'35.2"E	-	-	-	-	-	-	-	No Peak
13	MT13	MAWTS	23°49'30.3"N	90°21'51.0"E	0.46	0.069	2.72	1.54	0	i, ii	Reliable	Unclear broad low frequency
14	MT14	Mirpur Bangla School	23°48'51.8"N	90°22'02.6"E	0.44	0.111	2.60	1.38	0	i, v	Reliable	Unclear broad low frequency

Table 4.2 Serial no, ID of each site, latitude, longitude, peak frequency, peak frequency error, amplitude, standard deviation of the amplitude of the peak, how many SESAME reliable curve/clear peak criteria failed and comments on curve/clear peak (Continue)

Sl. No	ID	Location	Latitude	Longitude	f_0	σ_f	A_0	$\sigma_A(f_0)$	Condition failed		Comments	
									Curve	Peak	Curve	Peak
15	MT15	Bhasantek DRS	23°48'22.3"N	90°23'16.2"E	0.58	0.122	2.80	1.49	0	i, ii, v	Reliable	Unclear broad low frequency
16	MT16	Mirpur 10 DRS	23°48'25.5"N	90°22'08.1"E	0.46	0.090	4	1.50	0	0	Reliable	Clear low frequency
17	MT17	German Technical Training Center	23°48'08.2"N	90°21'28.9"E	0.44	0.071	2.75	1.53	0	i	Reliable	Unclear low frequency
18	MT18	Banani Rail Crossing	23°48'44.0"N	90°24'13.7"E	0.50	0.082	7.88	2.09	0	i	Reliable	Unclear low frequency
19	MT19	Banani Rail Station	23°47'44.8"N	90°24'03.7"E	0.46	0.096	3.15	1.52	0	i, v	Reliable	Unclear broad low frequency
20	MT20	Banani Play Ground	23°47'37.0"N	90°24'29.7"E	-	-	-	-	-	-	-	No Peak
21	MT21	Baridhara DRS	23°48'58.7"N	90°24'58.7"E	0.44	0.095	2.52	1.48	0	i, v	Reliable	Unclear broad low frequency
22	MT22	Jamuna Future Park	23°48'47.8"N	90°25'16.5"E	-	-	-	-	-	-	-	No Peak
23	MT23	Between US Embassy & JFP	23°48'24.5"N	90°25'18.4"E	-	-	-	-	-	-	-	No Peak
24	MT24	US Embassy	23°47'48.8"N	90°25'24.2"E	-	-	-	-	-	-	-	No Peak
25	MT25	Shahzadpur	23°46'29.8"N	90°25'34.2"E	0.45	0.100	3.35	1.34	0	i, v	Reliable	Unclear broad low frequency
26	MT26	Gulshan Avenue	23°46'59.6"N	90°25'01.2"E	0.92	0.144	2.05	1.29	0	i, v	Reliable	Unclear broad low frequency
27	MT27	Gulshan DRS	23°47'33.1"N	90°24'54.4"E	1.0	0.173	2.10	1.31	0	i, v	Reliable	Unclear broad peak
28	MT28	Tejgaon TBS	23°46'24.0"N	90°25'01.2"E	0.40	0.063	5.12	1.85	0	i	Reliable	Unclear low frequency
29	MT29	Nabisco (Phoenix)	23°46'16.1"N	90°24'03.9"E	0.42	0.082	4.50	1.70	0	0	Reliable	Clear low frequency

Table 4.2 Serial no, ID of each site, latitude, longitude, peak frequency, peak frequency error, amplitude, standard deviation of the amplitude of the peak, how many SESAME reliable curve/clear peak criteria failed and comments on curve/clear peak (Continue)

Sl. No	ID	Location	Latitude	Longitude	f_0	σ_f	A_0	$\sigma_A(f_0)$	Condition failed		Comments	
									Curve	Peak	Curve	Peak
30	MT30	BUTEX	23°45'37.8"N	90°23'58.6"E	0.46	0.090	2.66	1.51	0	i	Reliable	Unclear low frequency
31	MT31	Mirpur Bangla College	23°47'05.1"N	90°21'11.6"E	0.42	0.089	3.5	1.56	0	i, v	Reliable	Unclear broad low frequency
32	MT32	HBRI	23°46'52.5"N	90°21'11.7"E	0.44	0.073	3.20	1.54	0	i	Reliable	Unclear low frequency
33	MT33	Mirpur Mazar Road DRS	23°47'35.3"N	90°21'01.3"E	0.46	0.081	4.55	1.40	0	i	Reliable	Unclear low frequency
34	MT34	Amin Bazar DRS	23°47'20.7"N	90°19'05.8"E	0.44	0.066	9.05	1.67	0	0	Reliable	Clear low frequency
35	MT35	SMCH	23°46'06.8"N	90°22'09.1"E	0.42	0.092	3.03	1.55	0	i, v	Reliable	Unclear broad low frequency
36	MT36	BIM	23°45'24.2"N	90°22'30.6"E	0.48	0.083	3.18	1.52	0	i	Reliable	Unclear low frequency
37	MT37	Dhanmondi Play Ground	23°44'45.8"N	90°22'52.1"E	0.41	0.079	6.45	1.87	0	i	Reliable	Unclear low frequency
38	MT38	Sonargaon Hotel	23°45'10.1"N	90°23'59.5"E	0.56	0.122	2.75	1.46	0	i, ii, v	Reliable	Unclear broad low frequency
39	MT39	Rampura TV Station	23°46'00.1"N	90°25'28.2"E	0.63	0.112	3.13	1.49	0	i, ii, v	Reliable	Unclear broad low frequency
40	MT40	Teachers Training College	23°44'11.3"N	90°23'01.6"E	0.36	0.090	2.31	1.62	0	i, ii, v	Reliable	Unclear broad low frequency
41	MT41	Elephant Road (Mercantile Bank)	23°44'20.3"N	90°23'14.3"E	-	-	-	-	-	-	-	No Peak
42	MT42	Old RHD HQ	23°44'01.6"N	90°24'08.0"E	-	-	-	-	-	-	-	No Peak

Table 4.2 Serial no, ID of each site, latitude, longitude, peak frequency, peak frequency error, amplitude, standard deviation of the amplitude of the peak, how many SESAME reliable curve/clear peak criteria failed and comments on curve/clear peak (Continue)

Sl. No	ID	Location	Latitude	Longitude	f_0	σ_f	A_0	$\sigma_A(f_0)$	Condition failed		Comments	
									Curve	Peak	Curve	Peak
43	MT43	Jadughor	23°44'17.4"N	90°23'41.2"E	0.49	0.107	2.85	1.58	0	i, iv, v	Reliable	Unclear broad low frequency
44	MT44	Curzon Hall	23°43'41.0"N	90°24'07.2"E	0.41	0.079	2.49	1.41	0	i, ii	Reliable	Unclear broad low frequency
45	MT45	City Center DRS	23°43'30.1"N	90°24'35.3"E	0.42	0.080	2.71	1.73	0	i	Reliable	Unclear low frequency
46	MT46	AGB Colony	23°43'59.4"N	90°25'23.6"E	-	-	-	-	-	-	-	No Peak
47	MT47	BMK Stadium	23°43'34.3"N	90°25'43.7"E	0.53	0.096	2.63	1.93	iii	-	Unreliable	-
48	MT48	West Katasur	23°45'03.8"N	90°21'28.3"E	0.88	0.063	3.20	1.49	0	i	Reliable	Unclear low frequency
49	MT49	Majerchar DRS	23°44'09.2"N	90°20'06.0"E	0.90	0.167	3.76	1.30	0	v	Reliable	Clear low frequency
50	MT50	Hazaribag DRS	23°43'55.0"N	90°21'42.5"E	0.41	0.095	3.89	1.54	0	i, v	Reliable	Unclear broad low frequency
51	MT51	Zinzira DRS	23°47'33.1"N	90°23'52.9"E	0.40	0.079	2.72	1.38	0	i, ii	Reliable	Unclear broad low frequency
52	MT52	Postogola DRS	23°41'17.3"N	90°26'04.0"E	0.92	0.160	3.16	1.26	0	i, v	Reliable	Unclear broad low frequency
53	MT53	Nandipara TBS	23°44'44.5"N	90°26'41.1"E	1.06	0.153	3.49	1.48	0	i, v	Reliable	Unclear broad peak
54	MT54	Donia TBS	23°42'01.2"N	90°27'24.4"E	-	-	-	-	-	-	-	No Peak
55	MT55	Doleswar DRS	23°40'25.4"N	90°26'21.0"E	1.36	0.128	3	1.22	0	i	Reliable	Unclear Peak
56	MT56	Pangaon Valve Station	23°39'47.5"N	90°26'58.3"E	1.30	0.141	2.81	1.25	0	i, v	Reliable	Unclear broad peak
57	MT57	Demra CGS	23°42'46.7"N	90°30'11.7"E	1.50	0.139	4.38	1.30	0	i	Reliable	Unclear Peak
58	MT58	Joydevpur CGS	24°00'31.5"N	90°24'54.4"E	1.5	0.030	12.1	1.36	0	0	Reliable	Clear peak

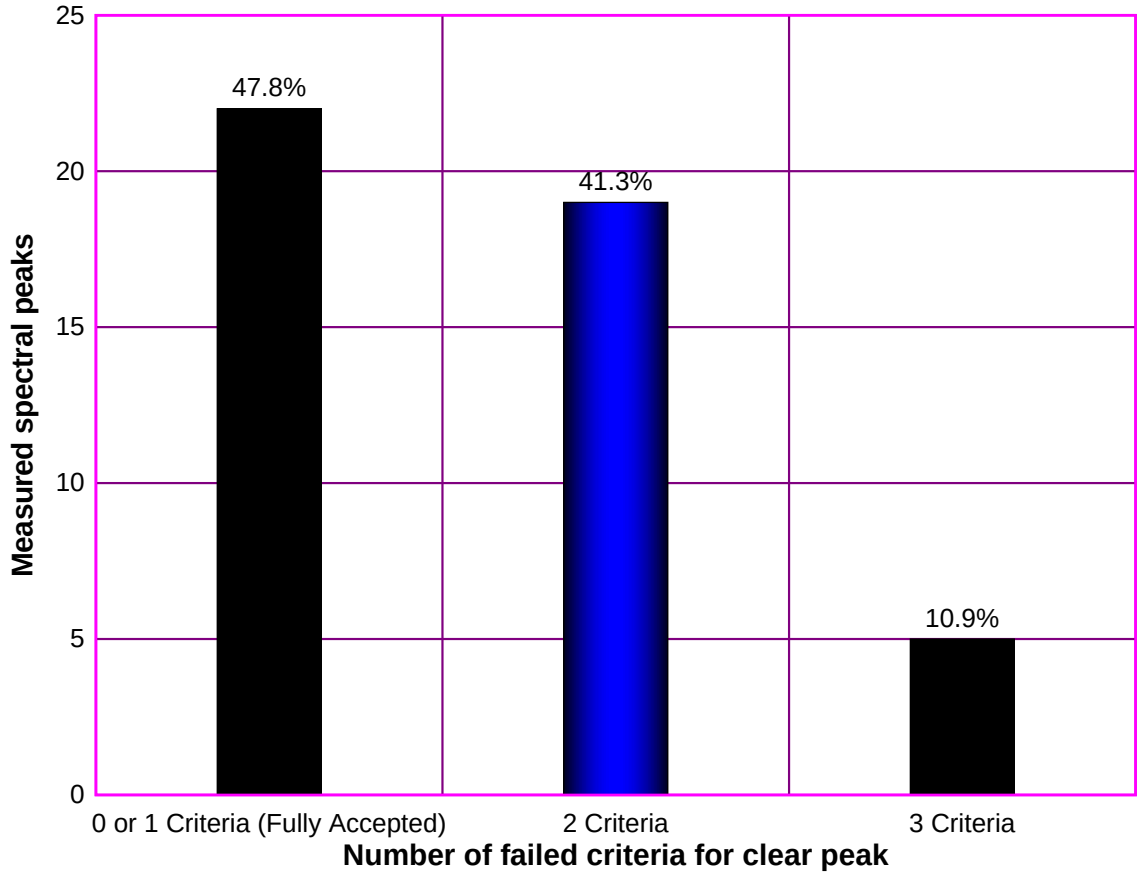

Figure 4.6: Distribution of number of spectral peaks that failed a specific number of clear peak criteria for the study Area. 22 clear peaks that failed 1 or no criterion, 19 peaks that failed 2 criteria, 5 peaks that failed 3 criteria.

Figure 4.7 shows the distribution of f_0 where the distribution of predominant frequencies is relatively uniform, ranging from 0.36 to 1.5 Hz. Obviously, the red color delineates high values of fundamental frequency located in the central part and the edge of northing, southing and easting part of the study area reaching 1.5 Hz while the blue color represents the low values of fundamental frequency in the round of central part of the study area reaching 0.36 Hz.

The total 46 reliable curves and clear peaks have been grouped with respect to the results in the frequencies ranges of $0.36\text{Hz} \leq f_0 \leq 0.50\text{Hz}$, $0.51\text{Hz} \leq f_0 \leq 1.0\text{Hz}$ and $1.0\text{Hz} < f_0 \leq 1.5\text{Hz}$. It has been observed a consistent peak in a frequency range $0.36\text{Hz} \leq f_0 \leq 0.50\text{Hz}$ covered the most part of the study area rounding the center point as shown in Figure 4.7 and Figure 4.8. The main reason for such a small range of results arises from the small differences in the near-surface geological conditions of the study area.

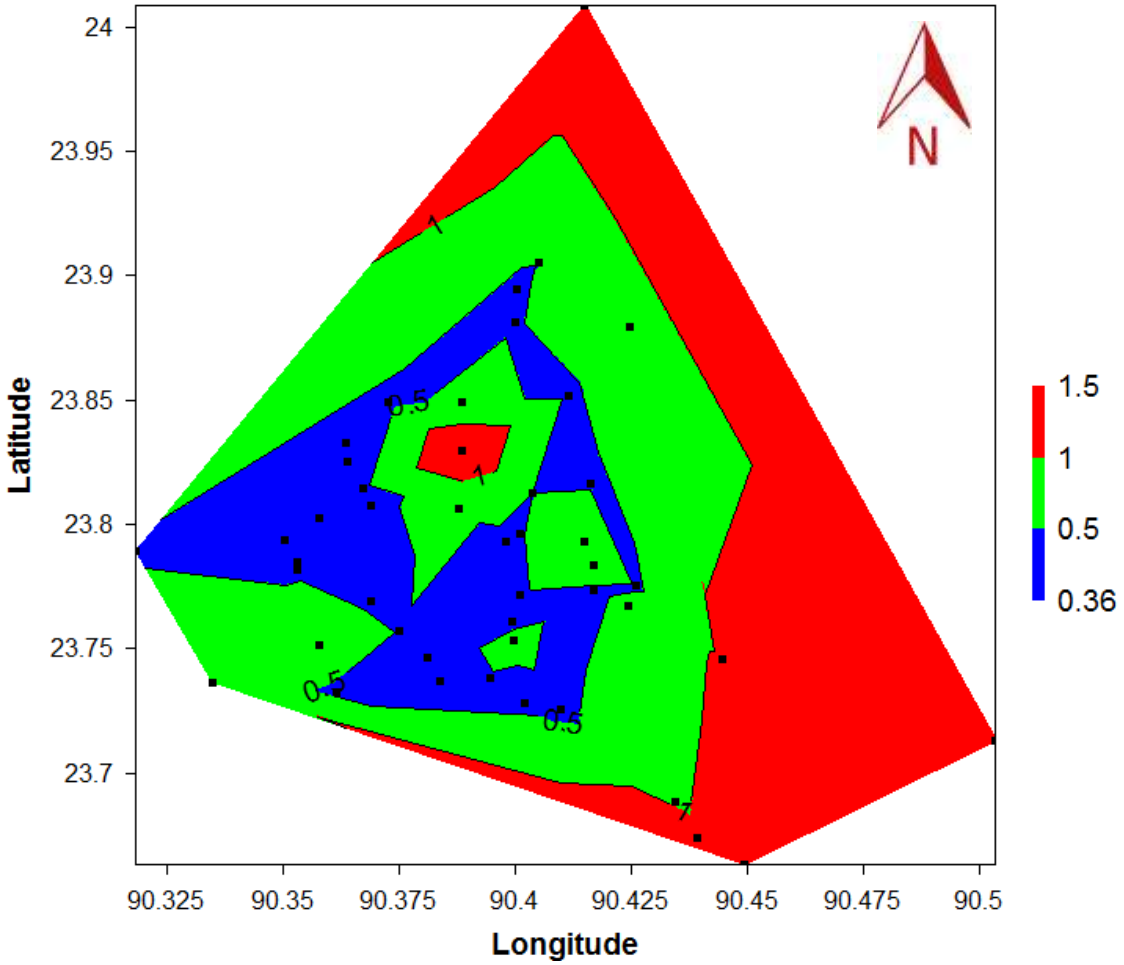

Figure 4.7: Distribution of the fundamental frequency (f_0) in the study area.

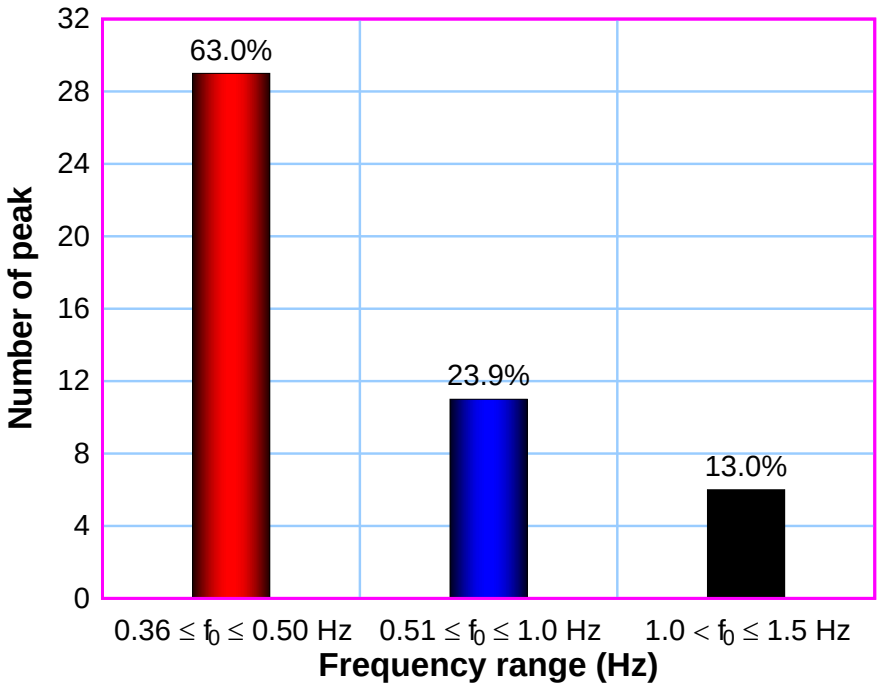

Figure 4.8: Distribution of number of peaks in specific frequency bands for the study area.

Dhaka is situated on the southern tip of the Madhupur tract which is a part of Pleistocene terrace. Two characteristic units cover the city and its surroundings, i.e., the Madhupur clay of Pleistocene age and the alluvial deposits of recent age. The Madhupur clay is the oldest sediment exposed in and around the city area. The alluvial deposits are characterized by flood plains, depression and abandoned channels (M. S. Islam et al. 2014). The topographic pattern is associated with the f_0 value. The residual soil thickness (h) is possibly estimated using the formula $f_0 = V_s/4h$, where V_s is shear wave velocity (Bard, 1998). It could be noted that the f_0 is related with the depth of bedrock. The smaller of f_0 value, the greater of depth of bedrock.

Figure 4.9 represents the amplification factor (A_0) or peak of H/V spectral ratio in investigation sites ranging from 2.05 to 12.1. The red color reveals the high values of amplification factor reaching 12.1 while the blue color illustrates the low values. High amplification factor ($A_0 > 4$) has been found in the northern part of the study area. In the majority of the study area, the H/V spectral ratio peak amplitudes are between 2 and 6. Amplification factors for the 190 investigated sites of Dhaka vary between 1.2 and 2.6 (Ansary et al., 2004). In general, low values are encountered for stiff soils and high values for soft soils. However, it is known that the amplitude of H/V spectral ratio peak is a less reliable parameter of microtremor measurements (Bard et al. 2005). It can be therefore used only as a rough indicator of impedance contrast between surface sediments and bedrock. Distribution of the high amplification factor in the study area measurements show that the topographic effect is not the only one factor controlling the amplification factor.

Different value of amplification factor (A_0) might be found in the same value of the predominant frequency (Figure 4.10). No correlation between predominant frequency and its amplitude (A_0) has been established. It can be noted that the variation of A_0 value is not strongly effected by the soil depth. Sheng Wang et al. (2002) explained that the variation of soil parameters (shear modulus, damping ratio and density) influenced the amplification factor. Yang Jun (2006) explained that the influence of the saturation state of the bedrock is insignificant; a change of the saturation state of the soil layer may have a marked impact on the amplification factor. It can be clearly stated that the geological factors are more dominant for A_0 variation.

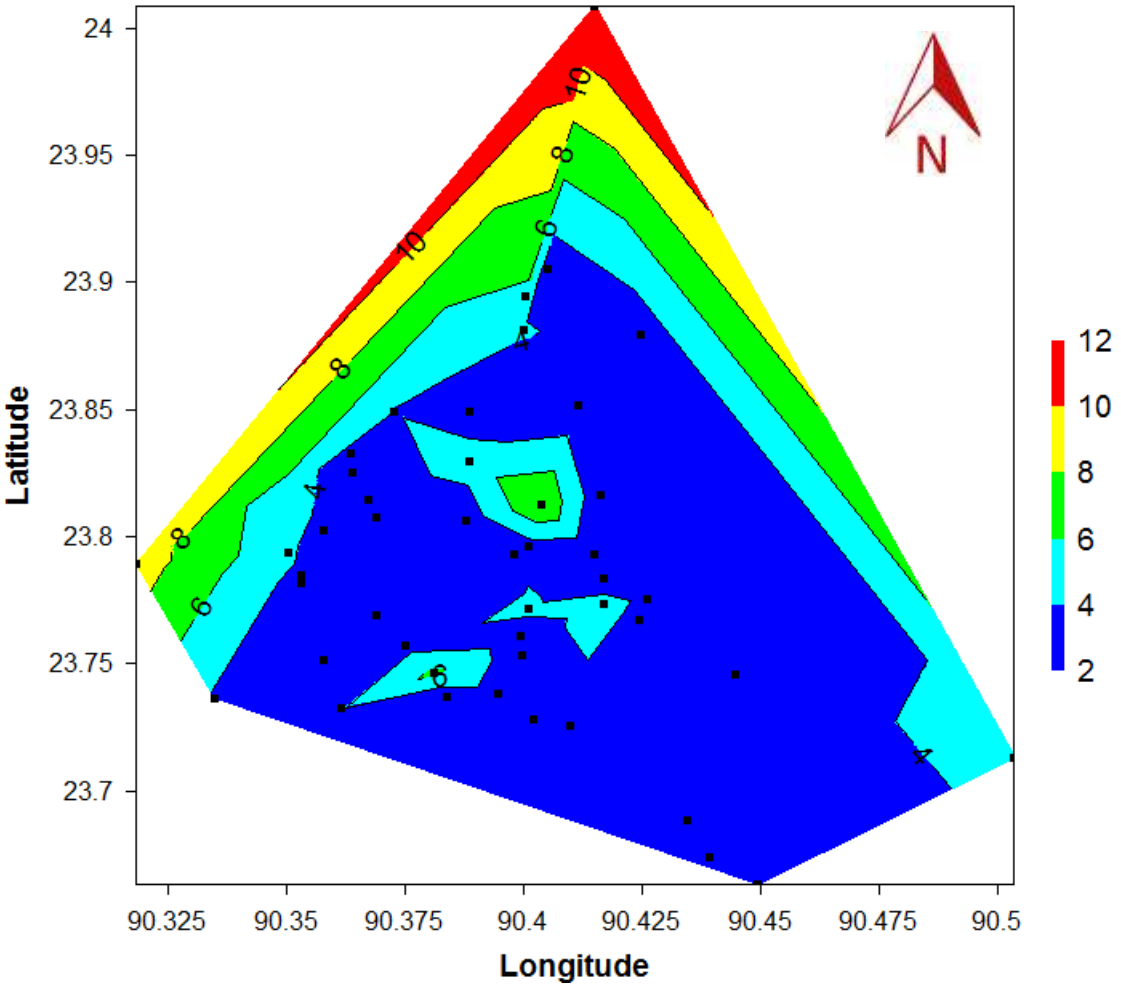

Figure 4.9: Distribution of the Amplification factor (A_0) in the study area.

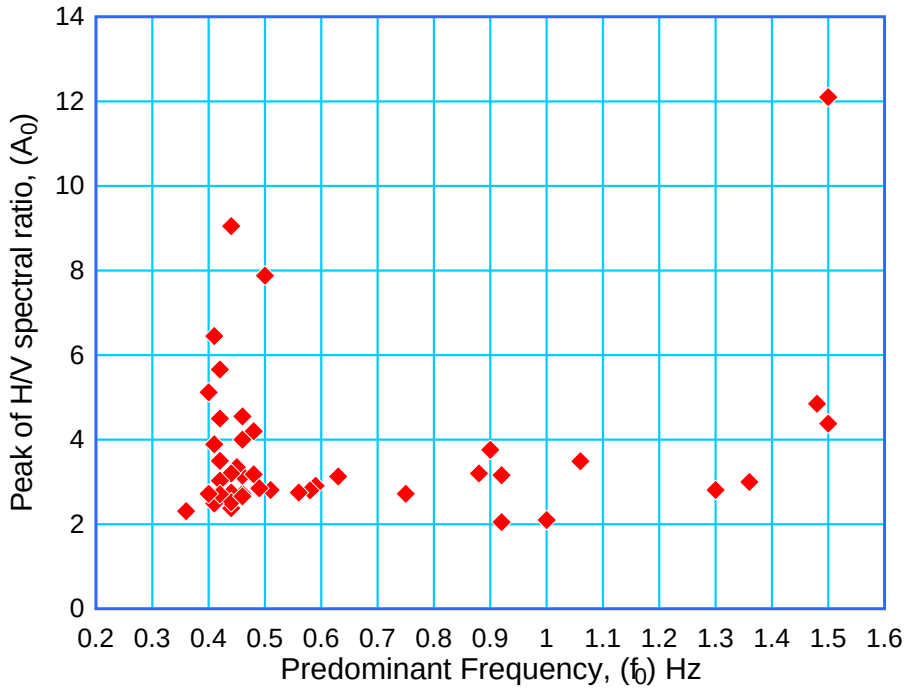

Figure 4.10: Predominant frequency vs. Peak of H/V spectral ratio graph.

At present, using the A_0 as site amplification parameter is still a hot debate among the experts (Nguyen et al., 2009). There is no ultimate correlation between the A_0 and the maximum spectral amplification of the site from strong motion. There might be some local relationships for a limited area and should only be regarded as a relative indicator of local site amplification since applied instruments or instrumental settings may also exert influence (Bard, 1998). Gosar (2010) explained that amplitude/amplification factor depends mainly on the impedance contrast and HVSR also does not provide any estimate of the actual bandwidth over which the ground motion is amplified. On the other hand, it is widely accepted in the scientific community that the predominant frequency (f_0) reflects the fundamental frequency of the site (Bard, 1998; Field et al. 1995; Lachet et al., 1994; Nakamura, 1989).

4.6 CALCULATION OF SEISMIC VULNERABILITY INDEX, K_g

Nakamura (1997) introduced a vulnerability index parameter (K_g), which combined amplification factor (A_0) and predominant frequency (f_0) to identify areas where greater seismic hazards and damage may be expected using H/V spectral ratio technique. Some studies like Pyi Soe Thein (2014), Daryono (2009), Huang H.C (2002) and Nakamura (2000) showed a good correlation between seismic vulnerability index (K_g) and the distribution of earthquake disaster damage. Thus, K_g value reflects local site effect and can be considered as an indicator which might be useful in selecting weak point of ground. Therefore, this index has been used for the detection of gas network areas of Dhaka City that are weak zone at the time of occurrence of earthquakes. Seismic vulnerability index is obtained from the peak value of H/V spectral ratio squared, divided by the value of the predominant frequency and is defined as:

$$K_g = \frac{A_0^2}{f_0} \qquad (4.4)$$

Where, K_g is the seismic vulnerability index, A_0 is the H/V spectral ratio peak and f_0 is the predominant frequency. K_g values for 46 locations of the study area are shown in Table 4.3.

Table 4.3 Seismic vulnerability index (K_g) value of gas network area of Dhaka City

Sl. No	ID	Location	Latitude	Longitude	Predominant Frequency, f_0 (Hz)	H/V Ratio, A_0	Vulnerability Index, $K_g = \frac{A_0^2}{f_0}$	*Remarks
1	MT1	Monnu Textile Mill High School	23°53'39.8"N	90°24'01.9"E	0.42	5.66	76.27	Very High
2	MT2	Tongi TBS	23°54'17.47"N	90°24'18.71"E	0.51	2.81	15.48	High
3	MT3	Kamarpara Mini DRS	23°52'50.8"N	90°24'00.9"E	0.48	4.20	36.75	Very High
4	MT4	Uttara DRS	23°52'26.8"N	90°23'58.3"E	-	-	-	-
5	MT5	Uttarkhan	23°52'45.0"N	90°25'29.3"E	0.75	2.72	9.86	Moderate
6	MT6	Uttara 3rd Phase	23°50'55.3"N	90°22'22.0"E	0.41	3.88	36.72	Very High
7	MT7	Hazi Camp	23°51'04.1"N	90°24'41.3"E	0.44	2.38	12.87	High
8	MT8	Baunia	23°50'57.0"N	90°23'18.7"E	0.59	2.91	14.35	High
9	MT9	Joarsahara DRS	23°49'48.9"N	90°25'08.0"E	-	-	-	-
10	MT10	Balurghat	23°49'46.4"N	90°23'19.1"E	1.48	4.85	15.89	High
11	MT11	Mirpur Mini DRS	23°49'57.6"N	90°21'49.2"E	0.46	3.12	21.16	High
12	MT12	Sadullapur	23°51'26.2"N	90°18'35.2"E	-	-	-	-
13	MT13	MAWTS	23°49'30.3"N	90°21'51.0"E	0.46	2.72	16.08	High
14	MT14	Mirpur Bangla School	23°48'51.8"N	90°22'02.6"E	0.44	2.60	15.36	High
15	MT15	Bhasantek DRS	23°48'22.3"N	90°23'16.2"E	0.58	2.80	13.52	High
16	MT16	Mirpur 10 DRS	23°48'25.5"N	90°22'08.1"E	0.46	4.00	34.78	Very High
17	MT17	German Technical Training Center	23°48'08.2"N	90°21'28.9"E	0.44	2.75	17.19	High
18	MT18	Banani Rail Crossing	23°48'44.0"N	90°24'13.7"E	0.50	7.88	124.19	Very High
19	MT19	Banani Rail Station	23°47'44.8"N	90°24'03.7"E	0.46	3.15	21.57	High
20	MT20	Banani Play Ground	23°47'37.0"N	90°24'29.7"E	-	-	-	-
21	MT21	Baridhara DRS	23°48'58.7"N	90°24'58.7"E	0.44	2.52	14.43	High
22	MT22	Jamuna Future Park	23°48'47.8"N	90°25'16.5"E	-	-	-	-
23	MT23	Between US Embassy & JFP	23°48'24.5"N	90°25'18.4"E	-	-	-	-

Table 4.3 Seismic vulnerability index (K_g) value of gas network area of Dhaka City (Continue)

Sl. No	ID	Location	Latitude	Longitude	Predominant Frequency, f_0 (Hz)	H/V Ratio, A_0	Vulnerability Index, $K_g = \frac{A_0^2}{f_0}$	*Remarks
24	MT24	US Embassy	23°47'48.8"N	90°25'24.2"E	-	-	-	-
25	MT25	Shahzadpur	23°46'29.8"N	90°25'34.2"E	0.45	3.35	24.94	High
26	MT26	Gulshan Avenue	23°46'59.6"N	90°25'01.2"E	0.92	2.05	4.57	Moderate
27	MT27	Gulshan DRS	23°47'33.1"N	90°24'54.4"E	1.00	2.10	4.41	Moderate
28	MT28	Tejgaon TBS	23°46'24.0"N	90°25'01.2"E	0.40	5.12	65.54	Very High
29	MT29	Nabisco (Phoenix)	23°46'16.1"N	90°24'03.9"E	0.42	4.50	48.21	Very High
30	MT30	BUTEX	23°45'37.8"N	90°23'58.6"E	0.46	2.66	15.38	High
31	MT31	Mirpur Bangla College	23°47'05.1"N	90°21'11.6"E	0.42	3.5	29.17	Very High
32	MT32	HBRI	23°46'52.5"N	90°21'11.7"E	0.44	3.20	23.27	High
33	MT33	Mirpur Mazar Road DRS	23°47'35.3"N	90°21'01.3"E	0.46	4.55	45.00	Very High
34	MT34	Amin Bazar DRS	23°47'20.7"N	90°19'05.8"E	0.44	9.05	186.14	Very High
35	MT35	SMCH	23°46'06.8"N	90°22'09.1"E	0.42	3.03	21.86	High
36	MT36	BIM	23°45'24.2"N	90°22'30.6"E	0.48	3.18	21.07	High
37	MT37	Dhanmondi Play Ground	23°44'45.8"N	90°22'52.1"E	0.41	6.45	101.47	Very High
38	MT38	Sonargaon Hotel	23°45'10.1"N	90°23'59.5"E	0.56	2.75	13.50	High
39	MT39	Rampura TV Station	23°46'00.1"N	90°25'28.2"E	0.63	3.13	15.55	High
40	MT40	Teachers Training College	23°44'11.3"N	90°23'01.6"E	0.36	2.31	14.82	High
41	MT41	Elephant Road (Mercantile Bank)	23°44'20.3"N	90°23'14.3"E	-	-	-	-
42	MT42	Old RHD HQ	23°44'01.6"N	90°24'08.0"E	-	-	-	
43	MT43	Jadughor	23°44'17.4"N	90°23'41.2"E	0.49	2.85	16.58	High
44	MT44	Curzon Hall	23°43'41.0"N	90°24'07.2"E	0.41	2.49	15.12	High
45	MT45	City Center DRS	23°43'30.1"N	90°24'35.3"E	0.42	2.71	17.48	High
46	MT46	AGB Colony	23°43'59.4"N	90°25'23.6"E	-	-	-	-
47	MT47	BMK Stadium	23°43'34.3"N	90°25'43.7"E	-	-	-	-

Table 4.3 Seismic vulnerability index (K_g) value of gas network area of Dhaka City (Continue)

Sl. No	ID	Location	Latitude	Longitude	Predominant Frequency, f_0 (Hz)	H/V Ratio, A_0	Vulnerability Index, $K_g = \frac{A_0^2}{f_0}$	*Remarks
48	MT48	West Katasur	23°45'03.8"N	90°21'28.3"E	0.88	3.20	11.64	Moderate
49	MT49	Majerchar DRS	23°44'09.2"N	90°20'06.0"E	0.90	3.76	15.71	High
50	MT50	Hazaribag DRS	23°43'55.0"N	90°21'42.5"E	0.41	3.89	36.91	Very High
51	MT51	Zinzira DRS	23°47'33.1"N	90°23'52.9"E	0.40	2.72	18.50	High
52	MT52	Postogola DRS	23°41'17.3"N	90°26'04.0"E	0.92	3.16	10.85	Moderate
53	MT53	Nandipara TBS	23°44'44.5"N	90°26'41.1"E	1.06	3.49	11.49	Moderate
54	MT54	Donia TBS	23°42'01.2"N	90°27'24.4"E	-	-	-	-
55	MT55	Doleswar DRS	23°40'25.4"N	90°26'21.0"E	1.36	3.00	6.62	Moderate
56	MT56	Pangaon Valve Station	23°39'47.5"N	90°26'58.3"E	1.30	2.81	6.07	Moderate
57	MT57	Demra CGS	23°42'46.7"N	90°30'11.7"E	1.50	4.38	12.79	High
58	MT58	Joydevpur CGS	24°00'31.5"N	90°24'54.4"E	1.50	12.10	97.61	Very High

* Remarks on Low (0 to ≤ 2.5), Moderate (< 2.5 to ≤ 12.5), High (< 12.5 to ≤ 25) and Very High (>25)

To calculate soil vulnerability index (K_g), the value of shear strain (γ) need to be considered. According to Ishihara ground soil becomes plastic state at about $\gamma \cong 1000 \times 10^{-6}$; and for $\gamma > 10{,}000 \times 10^{-6}$ catastrophic landslide or very large deformation will be occured. Nakamura (1997) had outlined the formulation in detail, but in summary it can be written as follows:

$$\gamma = \frac{A_0^2}{f_0} \times \frac{a_b}{\pi^2 v_b} \qquad (4.5)$$

In this equation, $\frac{A_0^2}{f_0}$ is called soil vulnerability index (K_g), a_b is the basement ground acceleration and v_b is the shear wave velocity of bedrock.

The common base rock under the Dhaka region is situated at a depth of approximately 10 km (Khan, 1990). The peak ground acceleration of Dhaka is 0.2 g (BNBC, Draft 2017). Assuming a_b = 0.2 g and bedrock shear wave velocity, v_b = 800 m/s, (BNBC, Draft 2017) for $\gamma > 1000 \times 10^{-6}$ then the K_g value > 4.0; and for $\gamma > 10{,}000 \times 10^{-6}$ the K_g value > 40.0. Based on the above criteria, for the value of K_g > 4.0 has been found to spread throughout the study area and for the value of K_g > 40 has been found only at several sites of the study area (Figure 4.11). The seismic vulnerability index value has been classified into four major types of damage. These are Low (0 to ≤ 4.0), Moderate (< 4.0 to ≤ 20), High (< 20 to ≤ 40) and Very High (>40). Thus, the higher Kg values (Kg > 40) in the site of gas network area has been considered as weak zones which may cause very high damage to infrastructure located in those area during an earthquake.

Figure 4.12 illustrate the distribution of vulnerability index (K_g) having values ranging from 4.41 to 186.14. The red color demonstrates the high values of vulnerability index reaching K_g > 40 while the green color indicates the values of the vulnerability index being 4 < K_g ≤ 20 may cause moderate damage. Seismic vulnerability index is also related to geological and geomorphological conditions. The high seismic vulnerability index indicates that the sediment areas are composed by alluvial material causes large damage. The low seismic vulnerability index indicates that the areas are very stiff as well as thick sediment deposit. Seismic vulnerability index (K_g) in the study area has found that the high values are scattered in the alluvial deposits area having a high seismic vulnerability indication.

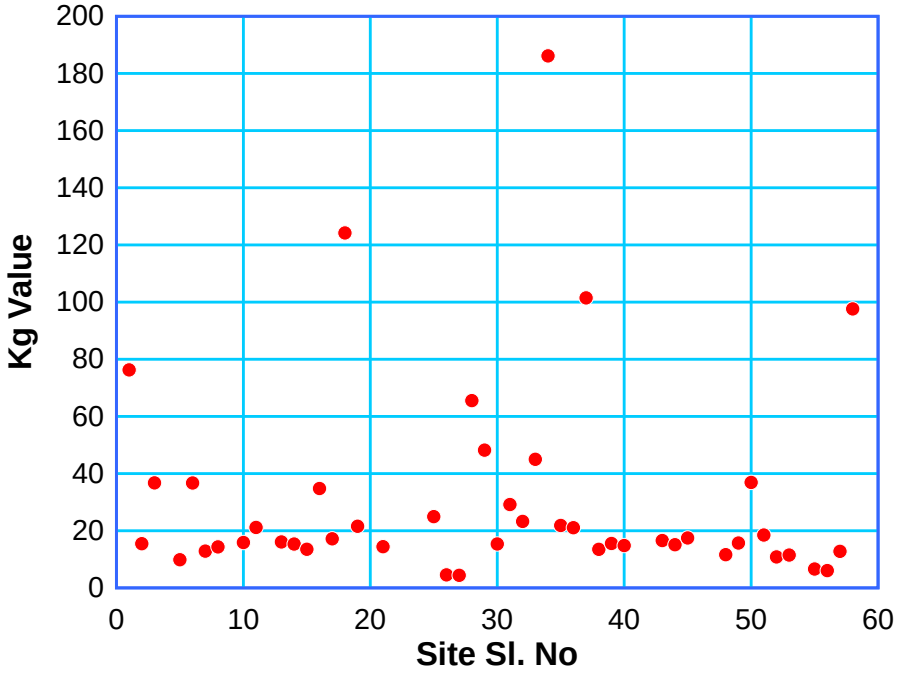

Figure 4.11: Distribution of vulnerability index (K_g)

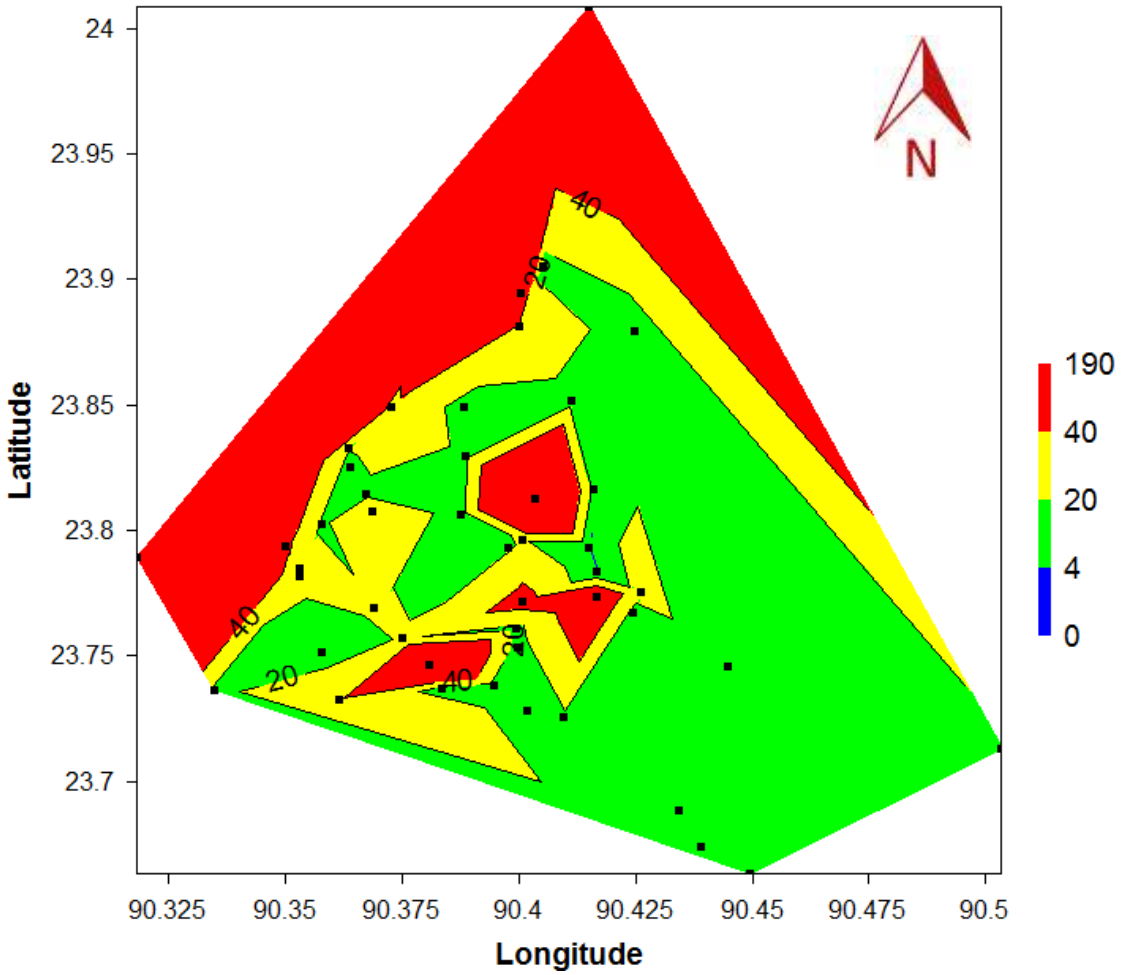

Figure 4.12: Contour map of the K_g value based on bedrock shear wave velocity 800 m/s in the study areas. The higher K_g values appear in the northern area.

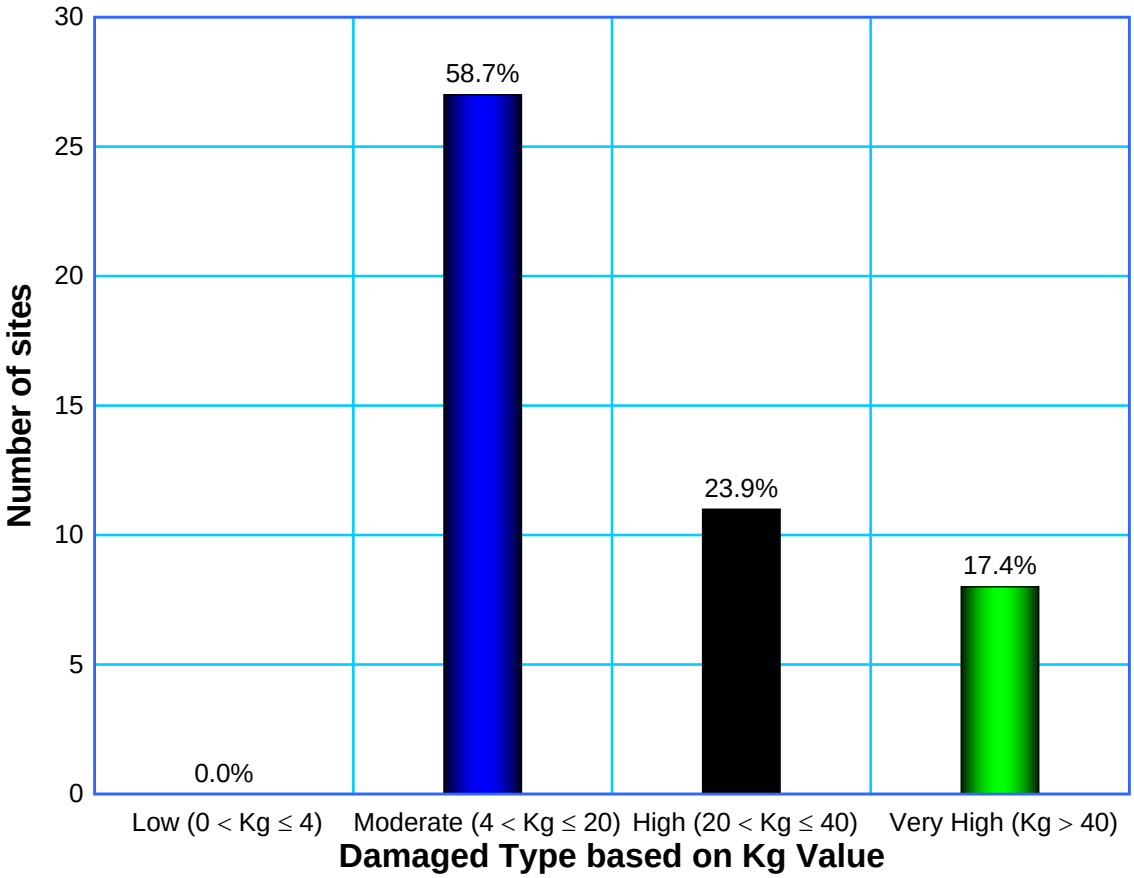

Figure 4.13: Distribution of damage area based on vulnerability index (K_g)

Figure 4.13, shows about 17.4% of research area of gas network are most vulnerable causing very high damage during earthquake. There are also 0% low, 58.7% moderate and 23.9% high damage area of 46 investigated sites. Table 4.3 demonstrates the highest K_g value at Amin Bazar DRS and Banani Rail Crossing. Most of the zones having higher Vulnerability Index (K_g) are situated in reclaimed area.

The engineering bedrock is the layer that has sufficiently large impedance ratio to the surface layer or hard deposit that expands widely in the region. Behavior outside this boundary does not affect the result of the seismic ground response analysis. Satoh et al. (1995a) defined their engineering bedrock as the layer of sedimentary rock of Pliocene or earlier age with an S wave velocity of 500 m/sec or larger and a SPT (Standard Penetration Test) blow count of 50 or more. From an engineering point of view, it is desirable to predict ground motions directly on the engineering bedrock on which foundation systems of important buildings and civil engineering structures will be constructed. Assuming a_b = 0.2 g (BNBC, Draft 2017) and engineering bedrock shear

wave velocity, v_b = 500 m/s, (Satoh et al., 1995a) for $\gamma > 1000 \times 10^{-6}$ then the K_g value > 2.5; and for $\gamma > 10{,}000 \times 10^{-6}$ the K_g value > 25.0. Based on the above criteria, for the value of K_g > 2.5 has been found spread throughout the study area and for the value of K_g > 25 has been found only at some sites of the study area (Figure 4.11). In that case, the seismic vulnerability index value has been classified into four major types. These are Low (0 to ≤ 2.5), Moderate (< 2.5 to ≤ 12.5), High (< 12.5 to ≤ 25) and Very High (>25). Thus, the higher Kg values (Kg > 25) in the site of gas network area has been considered as weak zones which may damage at very high scale during an earthquake and liquefaction potential exists.

Figure 4.14 shows the red color demonstrates the high values of vulnerability index K_g > 25 in the northern part of the study area may cause very high damage while the green color indicates the values of the vulnerability index being 2.5 < K_g ≤ 12.5 may cause moderate damage.

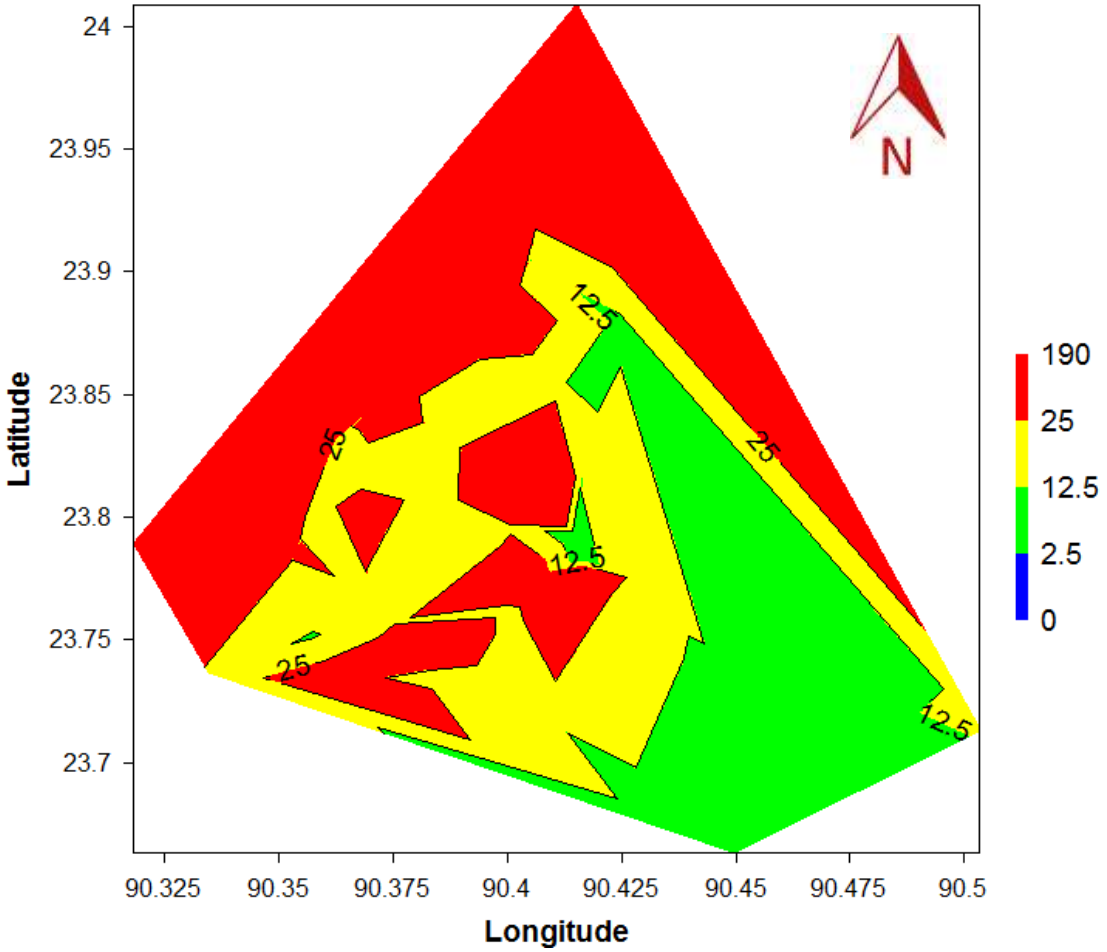

Figure 4.14: Contour map of the K_g value based on engineering bedrock shear wave velocity 500 m/s in the study areas. The higher K_g values appear in the northern area.

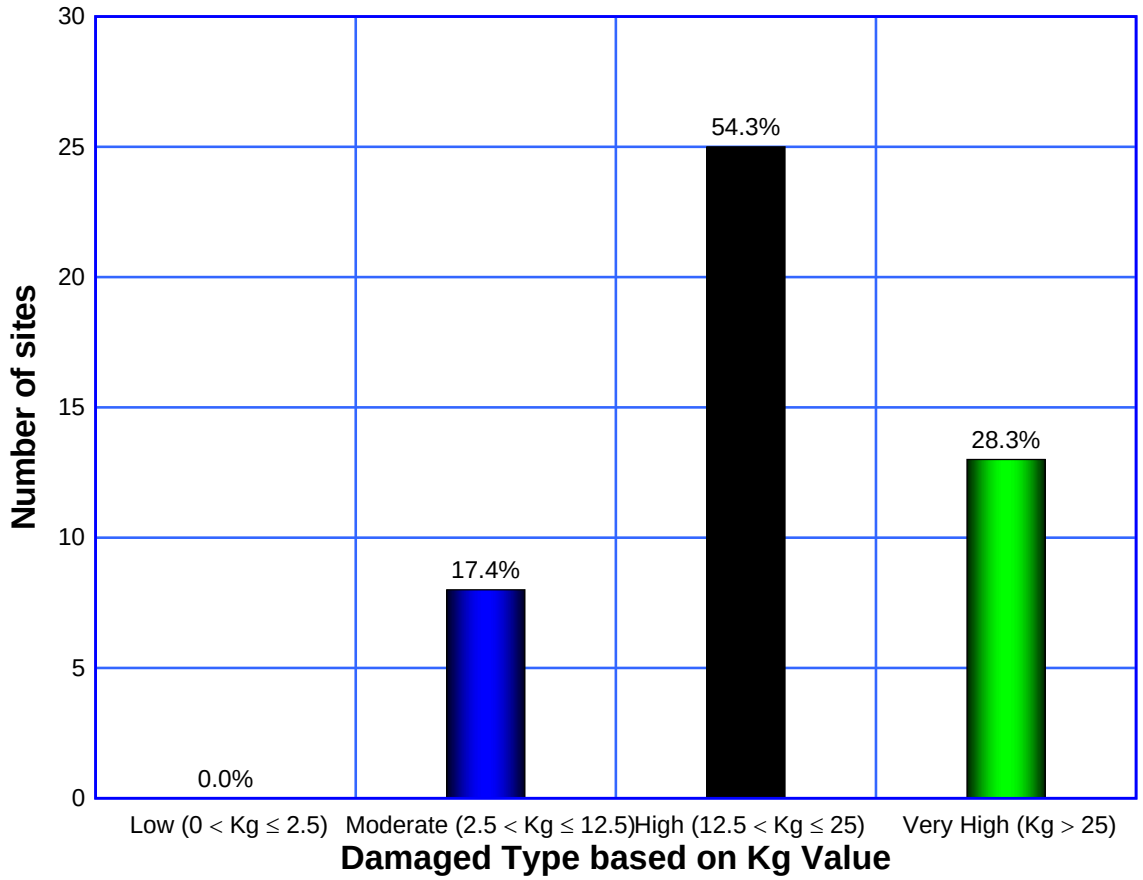

Figure 4.15: Distribution of damage area based on vulnerability index (K_g)

Figure 4.15 represents about 28.3% of research area of gas network are most vulnerable causing very high damage during earthquake. There are also 0% low, 17.4% moderate and 54.3% high damage area of 46 investigated sites.

To further ensure this, research on the acceleration of seismic waves in the basement need to be estimated. Vulnerability Index together with the acceleration of seismic waves in the basement has been suggested by Nakamura (2000) to calculate the value of shear strain (γ) of surface soil layers. Damaging earthquakes will occur when the limits are exceeded due to the shear strain deformation surface layer of soil. Soil is plastic at $\gamma = 1000 \times 10^{-6}$, whereas at $\gamma > 10.000 \times 10^{-6}$, the ground will deform. Only predominant frequency is not effective to classify a site due to Nakamura's vulnerability index. Both predominant frequency and amplification factor of H/V spectral ratio are required to estimate vulnerability type. However, at present, using the A_0 as site amplification parameter is still a hot debate among the experts (Nguyen, F. et. al, 2009).

4.7 CONCLUDING REMARKS

Chapter 4 represents detail of microtremor data analysis methodology based on SESAME guidelines to produce H/V spectral ratio curve with an example. Based on SESAME interpretation criteria, 46 out of 58 microtremor measurements have produced reliable curve and clear peak. Predominant frequencies and amplitude factors have been determined from these 46 reliable curves and peaks. Seismic vulnerability index (K_g) of the study area has also been calculated using the results output predominant frequencies and amplitude factors. A brief discussion of the results output predominant frequencies, amplitude factors and K_g values and relation with geological topographic pattern have been included. Contour map has been developed based on bedrock velocity 800 m/s for Kg > 40 and engineering bedrock velocity 500 m/s for Kg > 25 indicating very high damage during earthquake.

CHAPTER 5
CONCLUSIONS AND RECOMMENDATIONS

5.1 GENERAL

The purpose of this research is to apply microtremor horizontal to vertical (H/V) spectral ratio technique for assessment seismic vulnerability index (K_g) of gas network area in Dhaka city. Fifty eight locations in and around gas network area of Dhaka city have been selected for microtremor observation. The selected location points are superimposed on the geological map of Banladesh and geomorphological map of Dhaka city to identify geology and geomorphic units. Microtremor data has been collected and analyzed in order to determine the dynamic properties of soil, which are predominant frequency and amplification factor according to the guideline of SESAME. Finally, seismic vulnerability index (K_g) of site soil using Nakamura's technique has been calculated from predominant frequency and amplification factor parameter for the purpose of this research. The gas network of Dhaka city consists of different diameter (20 mm to 400 mm) of gas pipes with different pressure (50 psi to 300 psi) beneath the ground soil about 1 m to 3 m. The study has been carried out by measuring the microtremor at 58 sites scattered in gas network area of Dhaka city. The study area is situated latitude from 23˚40′ N to 23˚55′ N and longitude from 90˚18′ E to 90˚27′ E. The study area is situated on the southern tip of the Madhupur tract which is a part of Pleistocene terrace. Following conclusions may be made from the project.

5.2 CONCLUSIONS

- The frequencies of the study area have been grouped ranges of $0.36\text{Hz} \leq f_0 \leq 0.50\text{Hz}$, $0.51\text{Hz} \leq f_0 \leq 1.0\text{Hz}$ and $1.0\text{Hz} < f_0 \leq 1.5\text{Hz}$. It has been observed a consistent peak in a frequency range $0.36\text{Hz} \leq f_0 \leq 0.50\text{Hz}$ covered the most part of the study area. The lowest predominant frequency is 0.36 Hz at MT 40-Teachers Training College and the maximum predominant frequency is 1.50 Hz at MT57-Demra CGS and MT58-Joydevpur CGS. The soils of Dhaka city are mainly Madhupur clay and alluvial deposits. The predominant frequency is associated with the depth of bedrock. The low

frequencies correspond to soft soil sites and the high frequencies correspond to stiff soil sites.

- The amplification factors (A_0) or peaks of H/V spectral ratio for the 46 sites vary from 2.05 and 12.1. The lowest amplification factor is 2.05 at MT26-Gulshan Avenue site and the maximum amplification factor is 12.01 at MT58-Joydevpur CGS site. Low values are encountered for stiff soil site and high values for relatively soft soil site.

- Seismic vulnerability index (K_g) is calculated from the predominant frequency and amplification factor for 46 sites. Seismic vulnerability index (K_g) is an index indicating the level of vulnerability of a layer of soil to deform at the time of occurrence of earthquakes. The range of seismic vulnerability index (K_g) value is determined assuming the basement ground acceleration, a_b = 0.2 g and bedrock shear wave velocity, v_b = 800 m/s. It has been observed that the K_g value > 4.0 for $\gamma > 1000 \times 10^{-6}$ and the K_g value > 40.0 for $\gamma > 10{,}000 \times 10^{-6}$. The value of K_g > 4.0 has been found to spread throughout the study area and the value of K_g > 40 has been found only at several points of the study area. The seismic vulnerability index (K_g) value has been classified into four major types of damage. These are Low (0 to ≤ 4.0), Moderate (< 4.0 to ≤ 20), High (< 20 to ≤ 40) and Very High (>40). Thus, the higher K_g values (K_g > 40) in the site of gas network area has been considered as weak zones which may damage during the earthquake. The high values of vulnerability index K_g > 40 in the northern part of the study area may cause very high damage while the low values of the vulnerability index being 4 < K_g ≤ 20 may cause moderate damage. 17.4% of research area of gas network is most vulnerable causing very high damage during earthquake. There are also 0% low, 58.7% moderate and 23.9% high damage area of 46 investigated sites.

- On the other hand, the range of seismic vulnerability index (K_g) value is also determined assuming the basement ground acceleration, a_b = 0.2 g and engineering bedrock shear wave velocity, v_b = 500 m/s. It has been found that the K_g value > 2.5 for $\gamma > 1000 \times 10^{-6}$ and the K_g value > 25.0 for $\gamma > 10{,}000 \times 10^{-6}$. The value of K_g > 2.5 has been found to spread throughout the study area and the value of K_g > 25 has been found only at some location of the study area. In that case, the seismic

vulnerability index value has been classified into four major types of damage. These are Low (0 to ≤ 2.5), Moderate (< 2.5 to ≤ 12.5), High (< 12.5 to ≤ 25) and Very High (>25). Thus, the higher Kg values (Kg > 25) in the site of gas network area has been considered as weak zones which may damage during the earthquake. The high values of vulnerability index $K_g > 25$ in the northern part of the study area may cause very high damage while the low values of the vulnerability index being $2.5 < K_g \leq 12.5$ may cause moderate damage. 28.3% of research area of gas network is most vulnerable causing very high damage during earthquake. There are also 0% low, 17.4% moderate and 54.3% high damage area of 46 investigated sites.

- Seismic vulnerability index (K_g) is also related to geological and geomorphological conditions. The high seismic vulnerability index indicates that the sediment areas are composed by alluvial material causes large damage and liquefaction potential exists. The low seismic vulnerability index indicates that the areas are very stiff as well as thick sediment deposit. Seismic vulnerability index (K_g) in the study area has been found that the high values are scattered in the soft alluvial deposits area having a high seismic vulnerability indication. However, this observation is limited to a small number of sites and additional work is required.

5.3 RECOMMENDATIONS

Although the study covers the objectives of the research, more significant study would be needed to cover other aspects of the research. Specific recommendations are follows:

- Compare microtremor data with strong motion earthquake data.
- Compare microtremor data with Rayleigh wave.
- Investigation of microtremor H/V technique in Bangladesh using reference site where exposed rock is found.
- Liquefaction Potential Analysis is required using H/V Technique. In order to compare result Liquefaction based on Shear Wave Velocity and Standard Penetration Test (SPT) should be carried in the microtremor test location. Laboratory analysis such as Grain Size Analysis, Atterberg's Limit Test, Direct Shear Test, Cyclic Loading Test and Shaking Table test are required to compare the actual soil behavior with the microtremor estimated behavior.

REFERENCES

Aki, K. (1957). Space and time spectra of stationery stochastic waves, with special reference to microtremors, Bull. Of earthquake research institute 35, PP. 415-456.

Aki, K. (1993). Local site effects on weak and strong ground motion, Tectonophysics, 218, PP. 93-111.

Alam. M.K., Hasan, A.K.M.S., Khan, M.R., and Whitney, J.W. (1990). Geological map of Bangladesh. Geological Survey of Bangladesh, Dhaka.

Alfaro, A., Pujades, L., Goula, X., Susagna, T., Navarro, M., Sánchez, J. and Canas, J. A. (2001). Preliminary Map of Soil's Predominant Periods in Barcelona Using Microtremors, Pure appl. Geophys. 158, PP. 2499-2511.

Ali, M. H. and Choudhury, J. R. (1992). Tectonics and earthquake occurrence in Bangladesh, 36th Annual Convention, IEB, Dhaka.

Andrej Gosar (2017). Study on the applicability of the microtremor HVSR method to support seismic microzonation in the town of Idrija (W Slovenia), Nat. Hazards Earth Syst. Sci., 17, 925–937, 2017.

Ansary, M. A., Yamazaki, F. and Katayama, T. (1996). Application of microtremor measurements to the estimation of site amplification characteristics, Bulletin of Earthquake Resistant Structure Research Center, IIS, University of Tokyo, No. 29, PP. 95-113.

Ansary, M. A. Noor and M. A. Rashid (2004). Site amplification characteristics of Dhaka city, Journal of Civil Engineering (IEB), 32 (1) (2004) 1-16.

Arai, H. and Tokimatsu, K. (2004). S-wave velocity profiling by inversion of microtremor H/V spectrum. Bull. Seism. Soc. Am., 94, 1, PP. 53-63.

Arai, H. and Tokimatsu, K. (2000). Effects of Rayleigh and Love Waves on microtremors H/V spectra. Proc. 12th World Conf. on Earthquake Engineering, paper 2232, CD-ROM.

Asskar, J. C., Naghizadehrokni, M. and Rezaei, S. (2015). Liquefaction assessment by microtremor measurements in Babol city. Fifth International Conference on Geotechnique, Construction Materials and Environment, Nov 16-18, 2015 Osaka, Japan.

Asskar, J. C., Rezaei, S. and Farrokhzad, F. (2013). Evaluation of site response characteristics using microtremors GRADEVINAR 65 (2013) 8, 731-741.

Asten, M.W. (1978). Geological control on the three-component spectra of Rayleigh-wave microseisms. Bulletin of the Seismological Society of America, 68(6), 1623–1636.

Bard, P. Y. (1998). Microtremor measurements: A tool for site effect estimation?, Proceedings of the second international symposium on the effects of surface geology on seismic motion, Yokohama, Japan, December 1998, PP. 1251-1279.

Bard, P. Y. (2004). Effects of surface geology on ground motion: Recent results and remaining issues, Proceedings of the 10th European Conference on Earthquake Engineering, Vienna, Austria, August 28 - September 2, 1994, PP. 305-325.

Bard, P.-Y., & SESAME Participants (2004). The SESAME project: an overview and main results. Proceedings of the 13th world conference on earthquake engineering, Vancouver.

Bard, P.-Y., Atakan, K., Azzara, R. M., Cara, F., Cultrera, G., Dimitriou, P., Others (2004). Site effects assessment using ambient excitations (SESAME). Europeam Commission -Research General Directorate, WP04 (Project No. EVG1-CT-2000-00026 SESAME).

Bard, P.-Y., Jongmans, D., Ohrnberger, M., & Wathelet, M. (2005). Site effects assessment using ambient excitations (SESAME). Europeam Commission Research General Directorate, Final Repo (Project No. EVG1-CT-2000-00026 SESAME).

Bilham, R., Gaur, V. K. and Molnar, P. (2001). Himalayan Seismic Hazard, SCIENCE, 293.

BNBC (Draft 2017). Bangladesh National Building Code, 2017. HBRI-BSTI.

Bolt, B. A. (1987). Site specific study of seismic intensity and ground motion parameters for proposed Jamuna river bridge, Bangladesh, A report on Jamuna bridge study.

Bonnefoy-Claudet, S., Cornou, C., Kristek, J., Ohrnberger, M., Wathelet, M., Bard, P.Y. and Cotton, F. (2004). Simulation of seismic ambient noise: I. Results of H/V and array techniques on canonical models. Proceedings of the 13th world conference on earthquake engineering, Vancouver.

Bonnefoy-Claudet, S., Baize, S., Bonilla, L. F., Berge-Thierry, C., Pasten, C., Campos, J. and Verdugo, R. (2009). Site effect evaluation in the basin of Santiago de Chile using ambient noise measurements. Geophysical Journal International, 176(3), 925–937.

Borcherdt RD (1970). Effects of local geology on ground motion near San Francisco Bay. Bulletin of the Seismological Society of America 60: 29–61.

Borcherdt RD and Gibbs JF (1976). Effects of local geological conditions in the region on ground motions and the intensities of the 1906 earthquakes. Bulletin of the Seismological Society of America 66: 467–500.

Borcherdt RD, Glassmoyer G, Der Kiureghian A and Cranswick E (1989). Results and data from seismologic and geologic studies following earthquakes of 7 December near Spitak, Armenia, S.S.R.: U.S. Geological Survey Open-File Report 89–163A.

Bour, M., Fouissac, D., Dominique, P., & Martin, C. (1998). On the use of microtremor recordings in seismic microzonation; J. Soil Dyn. Earthq. Eng. 17,465-474.

Bouranta, E., Vallianatos, F., Hatzopoulos, J. N., Papadopoulos I. and Gaganis, P. (2013). Bulletin of the Geological Society of Greece, vol. XLVII 2013, Proceedings of the 13th International Congress, Chania, Sept. 2013.

Bullen, K. E. and Bolt, B. A. (1985). An introduction to the theory of seismology. Cambridge University Press.

Cara, F., Di Giulio, G., Milana, G., Bordoni, P., Haines, J., & Rovelli, A. (2010). On the stability and reproducibility of the horizontal-to-vertical spectral ratios on ambient noise: the case study of Cavola, northern Italy. Bulletin of the Seismological Society of America, 100(3), 1263-1275.

Cassidy, J. F., Rosenberger, A., Rogers, G.C., Little, T. E., Toth, J., Adams, J., Munro, P., Huffmann, S., Pierre, J. R., Asmis, H. and Pernica, G. (2007). Strong motion seismograph networks in Canada, Proceedings of the Canadian Conference on Earthquake Engineering, June 24-27th 2007, Ottawa.

CDMP (2011). Comprehensive Disaster Management Program (CDMP), Bangladesh, Seismic hazard and vulnerability mapping of Dhaka, Chittagong, and Sylhet city corporation areas, 2011.

Chatelain, J. C., Guillier, B., Cara, F., Duval, A. M., Atakan, K., Bard, P.Y. and The WP02 SESAME team (2007). Evaluation of the influence of experimental conditions on H/V results from ambient noise recordings. Bull. Earthquake Eng., doi: 10.1007/s10518-007-9040-7.

Chavez-Garcia F. J., & Cuenca, J. (1996). Site effects in Mexico City urban zone, a complementary study; J. Soil Dyn. Earthq. Eng., 15, 141-146.

Chaves-Garcia F. J., & Tejeda-Jacome, J. (2010). Site response in Tecoman, Colima, Mexico II Determination of subsoil structure and comparison with observations; J. Soil Dyn. Earthq. Eng. 30(8), 717-723.

Chouinard, L., Rosset., P., de la Puente, A., Madriz, R., Mitchell, D. and Adams, J. (2004). Seismic hazard analysis for Montreal, Proceedings of the 13th World Conference of Earthquake Engineering, Vancouver, BC, Paper 7010.

Daryono (2009). Eftek Tapek Lokal (Local site effect) di Graben Bantul Berdasarkan Pengakuran Mikrotremor. International Conference Earth Science and Technology. Yogjakarta.

Dimitriu, P. P., Papaioannou, Ch. and Theodulidis, N. P. (1998). EURO-SEISTEST strong motion array near Thessaloniki, Northern Greece: a case study of site effects. Bulletin of seismological society of America, No. 3, PP. 862-873.

Dravinski, M., Ding, G. and Wen, K. L. (1996). Analysis of spectral ratios for estimating ground motion in deep basins, Bull. Seism. Soc. Am., 86, PP. 843-847.

Ducellier, A., Kawase, H., & Matsushima, S. (2013). Validation of a new velocity structure inversion method based on horizontal-to-vertical (H/V) spectral ratios of earthquake motions in the Tohoku Area, Japan. Bulletin of the Seismological Society of America, 103(2 A), 958–970.

Dwa Desa Warnana, Ria Asih Aryani Soemitro, and Widya Utama, (2011). Application of microtremor HVSR method for assessing site effect in residual soil slope, International Journal of Basic & Applied Sciences IJBAS-IJENS Vol: 11 No: 04, 73-78.

Elcin Gok and Orhan Polat, (2012). Microtremor HVSR Study of Site Effects in Bursa City (Northern Marmara Region, Turkey), Earthquake Research and Analysis - New Frontiers in Seismology, Dr Sebastiano D'Amico (Ed.), ISBN: 978-953-307-840-3, http://www.intechopen.com/books/earthquakeresearch-and-analysis-new-frontiers-in-seismology/microtremor-hvsr-study-for-site-effect-in-bursa-westernanatolia-Turkey

Enomoto, T., Kuriyama, K., Navarro, M. and Iwatate, T. (2002). Site-effects evaluation by H/V spectra comparing microtremor with strongmotion records observed at ground surface and basement using borehole, 12th European Conference on Earthquake Engineering, paper 596. Londres.

Fäh, D., Kind, F. and Giardini, D. (2001). A theoretical investigation of average H/V ratios. Geophys. J. Int., 145, PP. 535-549.

Fäh, D., Kind, F. and Giardini, D. (2003). Investigation of local S-wave velocity structures from average H/V ratios, and their use for the estimation of site effects. Journal of Seismology, 7, PP. 449-467.

Field, E. H. and Jacob, K. H. (1993). The Theoretical Response of Sedimentary Layers to Ambient Seismic Noise, Geophysical Research Letter, 20, PP. 2925-2928.

Field, E. H. and Jacob, K. H. (1995). A comparison and test of various site-response estimation techniques, including three that are not reference-site dependent, Bulletin of the Seismological Society of America, 85, PP. 1127-1143.

Field, E. H., Clement, A. C., Jacob, K. H., Aharonian, V., Hough, S. E., Friberg, P. A., Babaian, T. O., Karapetian, S. S., Hovanessian, S. M. and Abramian, H. A. (1995). Earthquake site response study in Giumri (Formerly Leninakan), Armenian using ambient noise observation. Bull. Seism. Soc. Am., 85, PP. 349-353.

Flores, H., Aguirre, E. and Aguirre, J. (2003). SPAC: An Alternative Method to Estimate Earthquake Site Effects in Mexico City. Geofís, Int. Vol. 42 (2), PP. 227-236.

Frantti, G. (1963). The nature of high-frequency earth noise spectra. Geophysics, 28(4), 547–562.

Frantti, G., Willis, D., & Wilson, J. T. (1962). The spectrum of seismic noise. Bulletin of the Seismological Society of America, 52(1), 113–121.

Geological Survey of Bangladesh, GSB (2014). Geomorphological Map of Dhaka city, Preapared by GSB under the project of Comprehensive Disaster Management Programme (CDMP).

Ghayamghamian, M. R. and Kawakami, H. (1997). Segmental cross-spectrum in microtremor spectral ratio analysis. 7th International Conference on Structural Safety and Reliability, Kyoto, November 1997, 24-28, PP. 1487-1494.

Gosar, A, (2010). Site effects and soil-structure resonance study in the Kobarid basin (NW Slovenia) using microtremors. Nat. Hazards Earth Syst. Sci., 2010, 10, 761–772.

Guillier, B., Chatelain, J. L., Bonnefoy-Claudet, S., & Haghshenas, E. (2007). Use of Ambient Noise: From Spectral Amplitude Variability to H/V Stability. Journal of Earthquake Engineering, 11(6), 925–942. doi: 10.1080/13632460701457249.

Gutenberg, B. (1958). Two types of microseisms. Advances in Geophysics, 5, 53–92.

Haskell, N. A. (1953). The Dispersion of Surface Waves on Multilayered Media. Bull. Seism. Soc. Am., 43(1), PP. 17-34.

Hatem F. A. (2016). Seismic Microzonation and Site Effect Response of Al Auja District, Master of Urban and Regional Planning Engineering, Thesis, Faculty of Graduate Studies, An-Najah National University, Nablus, and Palestine.

Horike, M., Zhao, B. and Kawase, H. (2001). Comparison of site response characteristics inferred from microtremors and earthquake shear waves, Bulletin of the Seismological Society of America, 91, PP. 1526-1536.

Hough SE, Borcherdt RD, Friberg PA, Busby R, Field E and Jacob KH (1990). The role of sediment-induced amplification in the collapse of the Nimitz freeway during the October 17, 1989 Loma Prieta earthquake. Nature 344: 853–855.

Huang, H. C., (2002). Characteristics of earthquake ground motions and the H/V of microtremors in the southwestern part of Taiwan: Earthquake Engineering and Structural Dynamics, 31, 1815-1829.

Huang, H. C. and Tseng, Y. S. (2002). Characteristics of soil liquefaction using H/V of microtremors in Yuan-Lin area, Taiwan, TAO,Vol.13, No.3,325-338, September, 2002.

Ibs-von Seht, M. and J. Wohlenberg (1999). Microtremor measurements used to map thickness of soft sediments: Bulletin of the Seismological Society of America, 89, 250-259.

Ishihara, Kenji (1978), Introduction to Dnyamic Soil Mechanism, January (in Japanese).

Jensen, V.H. (2000). Seismic microzonation in Australia; J. Asian Earth Sci. 18, 3-15.

Kanai, K. and Tanaka, T. (1961). On microtremor VIII, Bull. Of earthquake research institute 39, PP. 97-114.

Kanai, K., Tanaka, T. and Osada, K. (1954). Measurements of Micro-tremors 1. Bulletin Earthquake Research Institute, Tokyo University, 32, PP. 199-210.

Kagami, H., Okada, S., Shiono, K., Oner, M., Dravinski, M. and Mal, A. K. (1986). Observation of 1 to 5 second microtremors and their application to earthquake engineering. Part III. A two-dimensional study of site effects in S. Fernando valley. Bulletin of seismological society of America, 76, PP. 1801-1812.

Katz, L. J. (1976). Microtremor analysis of local geological conditions: Bulletin of the Seismological Society of America, 66, 45-60.

Kelli Hardesty, Lorraine W. Wolf, and Paul Bodin (2010). Noise to signal: A microtremor study at liquefaction sites in the New Madrid Seismic Zone GEOPHYSICS, VOL. 75, NO. 3 MAY-JUNE 2010; P. B83–B90, 6 FIGS., 2TABLES.

Khalda Y. Ibrahim, Abu Elela A. Mohamed, Insaf S. Babiker and Abdel Hafiz G. Elmula (2015). Local Site Effects Evaluation for Atbara Area Using Microtremor Measurements. American Journal of Earth Sciences. Vol. 2, No. 5, 2015, pp. 134-141.

Khan, A. H. (1990). Geology of Bangladesh, University Press Limited.

Khandaker, M. H. (1989). Seismicity and tectonics of Bangladesh, International Centre for Theoretical physics, Trieste, Italy, May, 1989.

Kim, D. S. and Lee, J. S. (2007). Propagation and attenuation characteristics of various ground vibrations. Soil Dynamics and Earthquake Engineering, 19, PP. 115-126.

Konno, K. and Ohmachi, T. (1998). Ground motion characteristics estimated from spectral ratio between horizontal and vertical components of microtremor», Bull. Seism. Soc. Am., 88, N. 1, PP. 228-241.

Koller, M. G., Chatelain, J.-L., Guillier, B., Duval, A.-M., Atakan, K., Lacave, C., & Bard, P.-Y. (2004). Practical user guidelines and software for the implementation of the H/V ratio technique: measuring conditions, processing method and results interpretation. Proceedings of the 13th world conference in earthquake engineering, Vancouver.

Kramer, S.L. (1996). Geotechnical Earthquake Engineering, Prentice Hall, Inc., Pearson Education Pte. Ltd., Singapore, Chapter 5, PP.149-165.

Lachet, C. and Bard, P. Y. (1994). Numerical and theoretical investigations on the possibilities and limitations of Nakamura's technique, Journal of the Physics of the Earth, 42, PP. 377-397.

Lachet, C., Hatzfeld, D., Bard, P. Y., Theodulidis, C. P. and Savvaidis, A. (1996). Site effects and microzonation in the city of Thessaloniki (Greece): Comparison of different approaches, Bulletin of the Seismological Society of America, 86, PP. 1692-1703.

Lermo JF, Rodriguez M and Singh SK (1988) The Mexico earthquake of September 19, 1985: Natural period of sites in the valley of Mexico from microtremor measurements and from strong motion data. Earthquake Spectra 4: 805–814.

Lermo, L. and Chavez-Garcia, F. J. (1993). Site effect evaluation using spectral ratios with only one station, Bull. Seism. Soc. Am., 83, PP. 1574-1594.

Lermo, J. and Chavez-Garcia, F. J. (1994). Are Microtremors Useful in Site Response Evaluation? Bulletin of Seismological Society of America, 84, PP. 1350-1364.

Lermo, J. and Chavez-Garcia, F. J. (1994a). Are Microtremors Useful in Site Response Evaluation? Bulletin of Seismological Society of America, 84, PP. 1350-1364.

Lermo, J. and Chavez-Garcia, F. J. (1994b). Site effect evaluation at Mexico city: dominant period and relative amplification from strong motion and microtremor records, Soil dyn. Earthquake eng. 13, PP. 413-423., 84, PP. 1350-1364.

Longuet-Higgins, M. S. (1950). A theory of the origin of microseisms. Philosophical Transactions of the Royal Society of London A: Mathematical, Physical and Engineering Sciences, 243(857).

Malischewsky, P. G. and Scherbaum, F. (2004). Love's formula and H/V-ratio (ellipticity) of Rayleigh waves, Wave Motion, 40, PP. 57-67.

Martin G. Koller, Jean-Luc Chatelain, Bertrand Guillier, Anne-Marie Duval, Kuvvet Atakan, Corinne Lacave, Pierre-Yves Bard and the SESAME participants (2004). Practical User Guidelines and Software for the Implementation of the H/V Ratio Technique: Measuring Conditions, Processing Method and Results Interpretation, 13th World Conference on Earthquake Engineering, Vancouver, B.C., Canada, August 1-6, 2004, Paper No. 3132

McNamara, D. E. and Buland, R. P. (2004). Ambient noise levels in the continental United States. Bull. Seism. Soc. Am., 94, PP. 1517-1527.

Mohammad Shariful Islam, Hossain Md. Shahin, Suravi Banik1 and Fariha Azam (2014). Elasto-plastic constitutive model parameters and their application to bearing capacity estimation for Dhaka sub-soil. Journal of Civil Engineering (IEB), 42 (2) (2014) 171-188

Molnar, S. and Cassidy, J. F. (2006). A comparison of site response techniques using weak-motion earthquake and microtremors, Earthquake Spectra, 22, PP. 169-188.

Molnar, S., Cassidy, J. F., Monahan, P. A., Onur, T., Ventura, C.E. and Rosenberger, A. (2006a). Application of microtremor measurements for earthquake site response studies in southwestern British Columbia, Proceedings 100th Anniversary Earthquake conference, EERI/SSA, San Francisco, April 18-22, 2006.

Molnar, S., Rosenberger, A., Cassidy, J. F. and Rogers, G. C. (2006b). Internet Accelerograph recordings of low-level earthquakes in southwestern British Columbia from 2002 to 2003, Geological Survey of Canada Open File 5266, PP. 2.

Molnar, S., Rosenberger, A., Cassidy, J. F. Rogers, G. C. and Ristau, J. (2006c). Digital accelerograph recordings of the July 15 and 19, 2004 earthquakes, west of Vancouver Island, Geological Survey of Canada Open File 5010, PP.76.

Molnar, S., Rosenberger, A., Dosso, S. and Cassidy, J. (2006d). Earthquake and microtremor site response at Internet Accelerograph sites in British Columbia, Canada, Proceedings 1st European Earthquake Engineering and Seismology Conference, Geneva, Switzerland, September 4-8, 2006.

Molnar, S., Cassidy, J. F. Monahan, P. A. and Dosso, S. E. (2007). Comparison of geophysical methods to determine shear-wave velocity, Proceedings of the Canadian Conference on Earthquake Engineering, June 24-27th 2007, Ottawa, ON, Paper 1173.

Morales, J., Vidal, F., Peña, J. A., Alguacil, G. and Ibáñez, J. (1991). Microtremor study in the sediment filled basin of Zafarraya, Granada (Southern Spain), Bull. Seism. Soc. Am., 81, PP. 687- 693.

Morales, J., Seo, K., Samano, T., Peña, J. A., Ibañez, J. and Vidal, F. (1993). Site response on seismic motion in the Granada basin (southern Spain) based on microtremor measurements, J. Phys. Earth, 41, PP. 221-238.

Mucciarelli, M. (1998). Reliability and applicability range of the Nakamura's technique. Journ. Earthq. Eng., 2, 4, PP. 625-638.

Mucciarelli, M., Gallipoli, M. R. and Arcieri, M. (2003). The stability of the horizontal to vertical spectral ratio of triggered noise and earthquake recordings, Bulletin of the Seismological Society of America, 93 (3), PP. 1407-1413.

Nakamura, Y. (1989). A Method for Dynamic Characteristics of Sub-surface Using Microtremors on the Ground Surface, Quick Report of Railway Technical Research Institute, 30, No. 1, PP. 25-33 (in Japanese).

Nakamura, Y. and Samizo, M. (1989). Site Effect Evaluation of Surface Ground using Strong Motion Records (in Japanese), Proc. 20th JSCE Earthquake Eng. Symposium, 133-136.

Nakamura, Y. and Takizawa, T. (1990). Evaluation of Liquefaction of Surface Ground using Microtremor (in Japanese), Proc. 45th Annual Meeting of JSCE, I-519,1068-1069.

Nakamura, Y. (1996). Real Time Information Systems for Seismic Hazards Mitigation UrEDAS, HERAS and PIC, Quarterly Report of RTRI, Vol. 37, No. 3, 112-127.

Nakamura, Y. (1997). Seismic Vulnerability Indices For Ground and Structures Using Microtremor, World Congress on Railway Research in Florence, Italy, November 1997.

Nakamura, Y. (2000). Clear identification of fundamental idea of Nakamura's Technique and its applications, Proc. Of the 12th World Conference on Earthquake Engineering, Auckland, New Zealand, PP. 2656-2664.

Nakamura, Y. (2008). On the H/V spectrum. The 14th World Conference on Earthquake Engineering, 1-10.

Navarro, M., Enomoto, T., Sánchez, F. J., Matsuda, I., Iwatate, T., Posadas, A., Luzón, F., Vidal, F. and Seo, K. (2001). Surface Soil Effects Study Using Short-period Microtremor Observations in Almeria City, Southern Spain, Pure Appl. Geophys., 158, PP. 2481-2497.

Nguyen, F., Teerlynck, H., Van Rompaey, G., Van Camp, M., Jongmans, D. and Camelbeeck, T. (2009) Use of microtremor measurement for assessing site effects in Northern Belgium-interpretation of the observed intensity during the Ms5.0, June 11, 1938 Earthquake. Journal of Seismology, 8(1) 41-56, 2009.

Nogoshi, M. and Igarashi, T. (1970). On the propagation characteristics of microtremors. J. Seism. Soc. Japan, 23, PP. 264-280 (in Japanese with English abstract).

Nogoshi, M., and Igarashi, T. (1971). On the amplitude characteristics of microtremor (Part 2), Journal of the Seismological Society of Japan, 24, PP. 26-40.

Ohta, Y., Kagami, H., Goto, N. and Kudo, K. (1978). Observation of 1 to 5 second microtremors and their application to earthquake engineering. Part I. Comparison with long period accelerations at the Tokachi-Oki earthquake of 1968, Bull Seism. Soc. Am., 68, PP. 767-779.

Ohmachi, T., Nakamura, Y. and Toshinawa, T. (1991). Ground motion characteristics in the San Francisco Bay area detected by microtremor measurements, Proc. 2nd International Conference on Recent Advances in Geotech. Earth. Eng. & Soil Dyn. Saint Louis, Missouri, PP. 11-15 March: PP. 1643-1648.

Onur, T., Molnar, S., Cassidy, J. F., Ventura, C. E. and Hao, K. X. -S. (2004). Estimating site periods in Vancouver and Victoria, British Columbia using microtremor measurements and "SHAKE" analyses, Proceedings 57th Canadian Geotechnical Conference, Québec City, October 24-27, 2004.

Panou, A. A., Theodulidis, N., Hatzidimitriou, P., Stylianidis, K., & Papazachos, C. B. (2005). Ambient noise horizontal to vertical spectral ratio in site effects estimation and correlation with seismic damage distribution in urban environment: The case of the city of Thessaloniki (Northern Greece). Soil Dynamics and Earthquake Engineering, 25(4), 261–274.

Parolai, S., Bormann, P. and Milkereit, C. (2001). Assessment of the natural frequency of the sedimentary cover in the Cologne area (Germany) using noise measurements. Journal of Earthquake Engineering, 5, 4, PP. 541-56.

Parolai, S. and Galiana-Merino, J. J. (2006). Effect of transient seismic noise on estimates of H/V spectral ratios. Bull. Seism. Soc. Am., 96, PP. 228-236.

Parolai, S., Richwalski, S. M., Milkereit, C., & Bormann, P. (2004). Assessment of the stability of H/V spectral ratios from ambient noise and comparison with earthquake data in the Cologne area (Germany). Tectonophysics, 390(1), 57–73.

Parolai, S., Picozzi, M., Richwalski, S.M., and Milkereit, C. (2005). Joint inversion of phase velocity dispersion and H/V ratio curves from seismic noise recordings usinga genetic algorithm, considering higher modes. Geoph. Res. Lett., 32.

Parolai, S., Richwalski, S.M., Milkereit, C. and Fäh, D. (2006). S-wave velocity profiles for earthquake engineering purposes for the Cologne Area (Germany). Bull. Earthquake Eng., 4, PP. 65-94.

Picozzi, M., Parolai, S. and Richwalski, S. M. (2005) Joint inversion of H/V ratios and dispersion curves from seismic noise: Estimating the S-wave velocity of bedrock. Geoph. Res. Lett., 32.

Pujades, L., Canas, J. A., Mena, U., Espinoza, F., Alfaro, A. and Caselles, O. (2000). Seismic risk evaluation in Barcelona, Spain, Proc. Of the 12th World Conference on Earthquake Engineering, Auckland, New Zealand.

Pyi Soe Thein, Subagyo Pramumijoyo, Kirbani Sri Brotopuspito, Junji Kiyono, Wahyu Wilopo and Agung Setianto (2014). Strong Ground Motion Based on Microtremor and Empirical Stochastic Green's Function Computing at Palu City, Central Sulawesi Province, Indonesia, 2014 3rd International Conference on Geological and Environmental Sciences IPCBEE vol. 73 (2014) © (2014) IACSIT Press, Singapore, 10.7763/IPCBEE. 2014. V73. 11, 50-54.

Qadri, S. M. T., Nawaz, B., Riaz, S. H. S. and Sheikh, A. (2015). Ambient noise H/V spectral ratio in site effects estimation in Fateh jang area, Pakistan, Earthq Sci (2015) 28(1):87–95.

Rahman Md. Saidur (2011). Applicability of H/V Microtremor Technique for site Response Analysis in Dhaka City, M. Sc. Engg. Thesis, Department of Civil Engineering, BUET, Dhaka, Bangladesh.

Raymond Ng (2017). Site Characterization of the Los Angeles Basin Using Ambient Noise Spectral Ratio Measurements from a High Density Temporary Broadband Deployment, Thesis, Master of Science in Geological Sciences California State Polytechnic University, Pomona

Rodriguez, V. S. H. and Midorikawa, S. (2002). Applicability of the H/V Spectral Ratio of Microtremors in Assessing Site Effects on Seismic Motion, Earthquake Engineering and Structural Dynamics, 31, PP. 261-279.

Rogers AM, Borcherdt RD, Covington PA and Perkins DM (1984) A comparative ground response study near Los Angeles using recordings of Nevada nuclear tests and the 1971 San Fernando earthquake. Bulletin of the Seismological Society of America 74: 1925–1949.

Rosenberger, A., Rogers, G. C. and Cassidy, J. F. (2007). The new real-time reporting strong motion seismograph network in southwest BC: More strong motion instruments for less money, Proceedings of the Canadian Conference on Earthquake Engineering, June 24-27th 2007, Ottawa, ON.

Sato, T., Kawase, H., Matsui, M. and Kataoka, S. (1991). Array measurement of High frequency microtremors for underground structure estimation, Proc. 4th Int. conf. on seismic zonation II, PP. 409-416.

Satoh, T., T. Sato, and H. Lawase (1995a). Evaluation of local site effects and their removal from borehole records observed in the Sendai Region, Japan. Bull. Seismol. Soc. Am. 85, 1770-1789.

Sanchez-Sesma, F. J., Rodriguez, M., Iturraran-Viveros, U., Luzon, F., Campillo, M., Margerin, L., Rodriguez-Castellanos, A. (2011). A theory for microtremor H/V spectral ratio: Application for a layered medium. Geophysical Journal International, 186(1), 221–225.

Sayed SR Moustafa (2015), Microtremor Analysis of Marsa Matrouh Industrial Area Using Horizontal to Vertical Spectral Ratio Method, EJGE, Vol. 20 [2015], Bund. 6, 1591-1602.

Scherbaum, F., Hinzen, K. G. and Ohrnberger, M. (2003). Determination of shallow shear-wave velocity profiles in Cologne, Germany area using ambient vibrations. Geophys. J. Int., 152, PP. 597-612.

Seo, K. (1994). On the applicability of microtremors to engineering purpose, Preliminary report of the Joint ESG Research on Microtremors after the 1993 Kushiro-Oki (Hokkaido, Japan) earthquake. Proc. of 10th European Conf. on Earthq., 4, PP. 2643- 2648.

Seo, K. (1997). Comparison of measured microtremor with damage distribution. JICA Research and Development Project on Earthquake Disaster Prevention, 306-320, 306– 320.

SESAME WP03. (2003). Site Effects Assessment Using Ambient Excitations. H/V Technique: Data Processing. SESAME European research project. European

Commission-Research General Directorate Project No. EVG1-CT-2000-00026 SESAME, D09.03.

SESAME WP12, (2004). Guidelines for the implementation of the H/V spectral ratio technique on ambient vibrations. Measurements, processing and interpretation. SESAME European research project. European Commission. Research General Directorate Project No. EVG1-CT-2000-00026 SESAME, D23.12. http://sesame-fp5.obs.ujf grenoble.fr/SES_TechnicalDoc.htm.

Sheng Wang and Hong Hao,(2002). Effects of Random variations of Soil Properties on Site Amplification of seismic Ground Motion, Soil Dynamics and Earthquake Engineering, Vol 22, issue 7, September 2002, pp. 551-564

Siddiqqi, J., & Atkinson, G. M. (2002). Ground-motion amplification at rock sites across Canada as determined from the horizontal to vertical component ratio. Bulletin of the Seismological Society of America, 92(2), 877–884.

Singh SK, Lermo J, Dominguez T, Ordaz M, Espinoza JM, Mena F and Quass R, (1988) The Mexico earthquake of September 19, 1985: a study of amplification of seismic waves in the Valley of Mexico with respect to a hill zone site: Earthquake Spectra 4: 653–673.

Sneider, A. J., Motazedian, D. and Atkinson, G. M. (2005). Seismic soil amplification studies for Ontario Polaris stations, 1st Polaris-Polo Research Workshop, Queen's University, Kingston, January 6th, 2005.

Surve, G., & Mohan, G. (2010). Site response studies in Mumbai using (H/V) Nakamura technique. Natural Hazards, 54(3), 783-795.

Suzuki, T., Adachi, Y. and Tanaka, M. (1995). Application of Microtremor measurements to the estimation of earthquake ground motions in the Kushiro city during the Kushiro-Oki earthquake of 15 January 1993, Earthquake Eng. Struc. Dyn. 24, PP. 595-613.

Taga, N. (1993). Measurement of microtremors in Earthquake Ground Motion and Ground Condition, edited by The Architectural Institute of Japan.

Tamura, T., Nagai. O., Kokubo, H. and Sumita, H. (1993). Characteristics of wave group of microtremors obtained by array measurement, J. struc. consr. Eng, AIJ 449, PP. 83-91 (in Japanese).

Taniguchi, E. and Sawada, K. (1979). Attenuation with distance of traffic-induced vibrations. Soils and Foundations, 19, 2, PP. 16-28.

Tevas-Costa, P. and Matias, L. (1996). Seismic behavior estimation of thin alluvium layers using microtremor recordings. J. Soil Dyn. Earthq. Eng V.15, p.201-209.

Theodulidis, N., Culterera, G., Tento, A., Faeh, D., Atakan, K., Bard, P.-Y., Haghshenas, E. (2004). Empirical evaluation of the horizontal-to-vertical spectral ratio technique: results from the SESAME project. 13th World Conference on Earthquake Engineering.

Tokimatsu, K. and Miyadera, Y. (1992). Characteristics of Rayleigh waves in microtremors and their relation to the underground structures, J. struc. consr. Eng, AIJ 439, PP. 81-87 (in Japanese).

Ventura, C. E., Onur, T. and Hao, K. X-S. (2004). Site period estimations in the Fraser River delta using microtremor measurements–experimental and analytical studies, Proceedings of the 13th World Conference of Earthquake Engineering, Vancouver, BC, Paper 1075.

Vidal, F., Romacho, M. D., Feriche, M., Navarro, M. and Abeki, N. (1996). Seismic microzonation in Adra and Berja Towns, Almeria (Spain), Proc. of the 11th World Conference on Earthquake Engineering, Acapulco, Mexico, June 23-28, 1996.

Wakamatsu, K. and Yasui, Y. (1995). Possibility of estimation for amplification characteristics of soil deposits based on ratio of horizontal to vertical spectra of microtremors, J. struct. consr. Eng, AIJ 471, PP. 61-70 (in Japanese).

Welch, P. D. (1967). The use of fast Fourier transform for the estimation of power spectra: A method based on time averaging over short, modified periodograms. IEEE Transactions on audio and electroacoustics, 15(2), 70–73.

Woolery, E., and R. Street (2002). 3D near-surface soil response from H/V ambient-noise ratios: Soil Dynamics and Earthquake Engineering, 22, 865–876.

Yamanaka, H., Dravinski, M. and Kagami, H. (1993). Continuous measurements of microtremors on sediments and basement in Los Angeles, California, Bull. Seism. Soc. Am., 83, PP. 1595-1609.

Yamanaka, H., Takemura, M., Ishida, H. and Niwa, M. (1994). Characteristics of long period microtremors and their applicability in exploration of deep sedimentary layers, Bull. Seism. Soc. Am., 884, PP. 1831-1841.

Yang Jun, (2006). Frequency-Dependent Amplification of Unsaturated surface Soil Layer, Journal Geotech and Geoenvironmental Engineering, Vol 132, issue 4, April 2006, pp. 526-531.

Zhao, B., Horike, M. and Yoshihiro, T. (2000). Analytical study on reliability of seismic site-specific characteristics estimated from microtremor measurements. Proceeding of the 12th World Conference on Earthquake Engineering, 1522–1530.

APPENDIX- A

H/V SPECTRAL RATIO CURVE ANALYSIS

MT1: Monnu Textile Mill High School (23°53'39.8"N, 90°24'01.9"E)
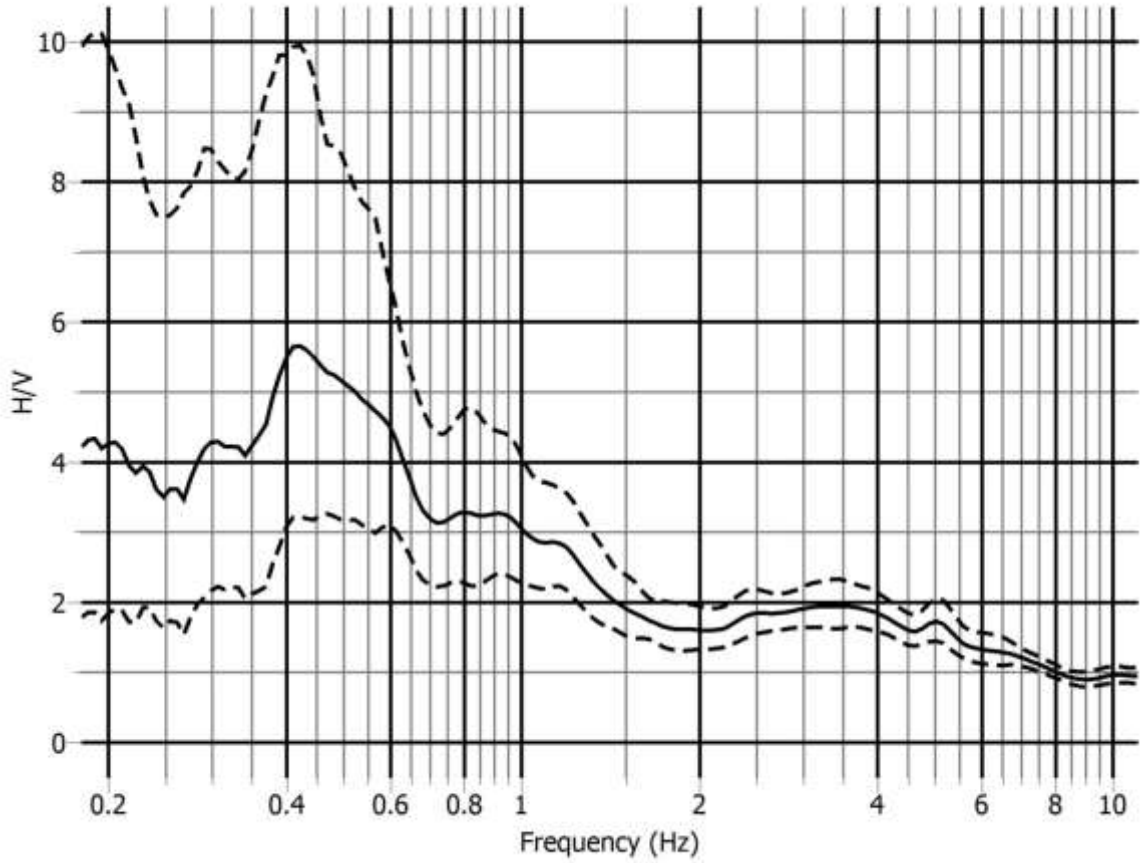
f_0=0.42 Hz; A_0 = 5.66; $A_{H/V}$ = (3.22,9.95); $\sigma_A(f_0)$ = 1.76 & 1.76
i) f_0=0.42 Hz > (10/40.96=0.24 Hz); ii) n_c > 200; iii) $\sigma_A(f)$ < 3; at 0.21 Hz <f< 0.84 Hz **Satisfies all three criteria of Reliable H/V Curve**
i) Between 0.105 to 0.42 Hz, $A_{H/V}(f^-) > A_0/2$, Not satisfy ii) Between 0.42 to 1.68 Hz, $A_{H/V}(f^+) < A_0/2$ iii) $A_0 > 2.0$ iv) Between 0.399 Hz to 0.441 Hz, f_{peak} = (0.405 Hz, 0.42 Hz) v) $\sigma_f = 0.086 > \varepsilon(f_0) = 0.084$, Not satisfy vi) $\sigma_A(f_0) = 1.76 < \Theta(f_0) = 2.5$ **Satisfies four out of six criteria of Clear H/V Peak**
Reliable curve and Unclear broad low frequency peak

MT2: Tongi TBS (23°54'17.47"N, 90°24'18.71"E)
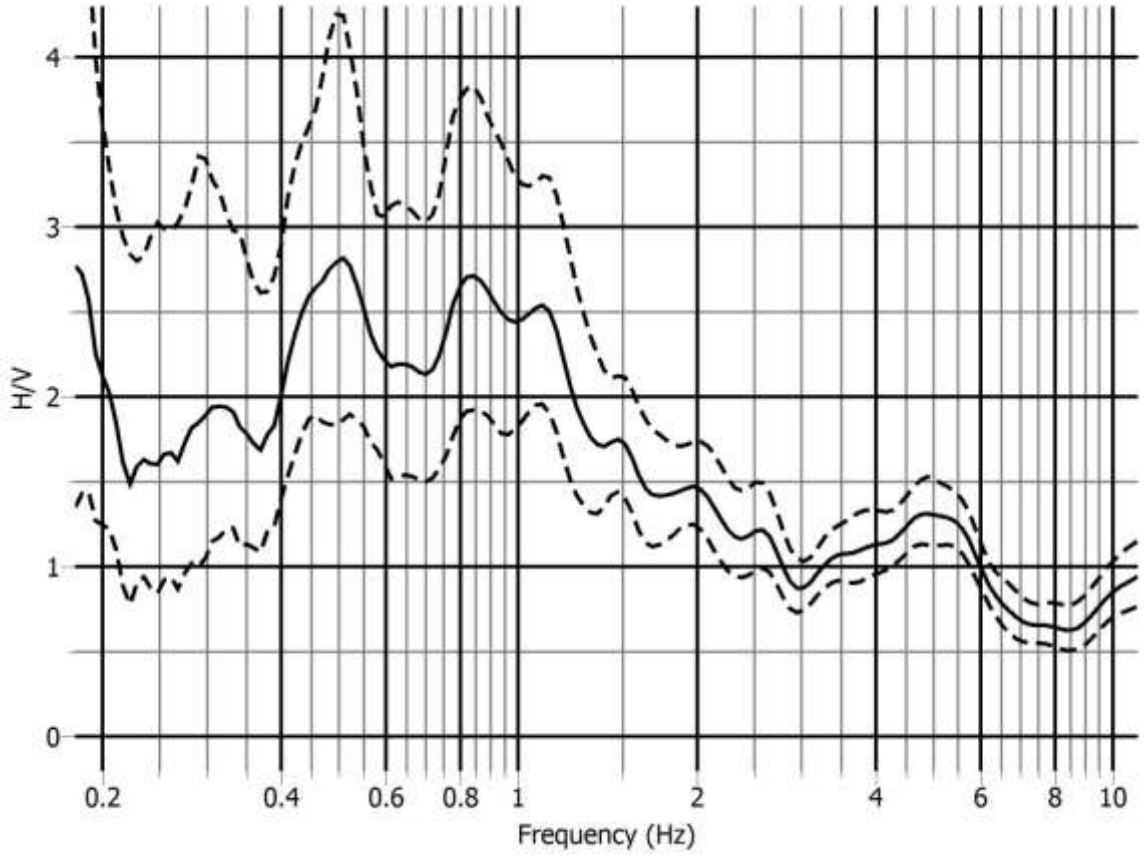
f_0=0.51 Hz; A_0 = 2.81; $A_{H/V}$ = (1.87,4.24); $\sigma_A(f_0)$ = 1.50 & 1.50
i) f_0=0.51 Hz > (10/40.96=0.24 Hz); ii) n_c > 200; iii) $\sigma_A(f)$ < 2; at 0.255 Hz <f< 1.02 Hz **Satisfies all three criteria of Reliable H/V Curve**
i) Between 0.127 to 0.51 Hz, $A_{H/V}(f^-) > A_0/2$, Not satisfy ii) Between 0.51 to 2.04 Hz, $A_{H/V}(f^+) > A_0/2$, Not satisfy iii) $A_0 > 2.0$ iv) Between 0.484 Hz to 0.535 Hz, f_{peak} = (0.525 Hz, 0.50 Hz) v) $\sigma_f = 0.075 < \varepsilon(f_0) = 0.0765$ vi) $\sigma_A(f_0) = 1.50 < \Theta(f_0) = 2$ **Satisfies four out of six criteria of Clear H/V Peak**
Reliable curve and Unclear broad low frequency peak

MT3: Kamarpara Mini DRS (23°52'50.8"N, 90°24'00.9"E)
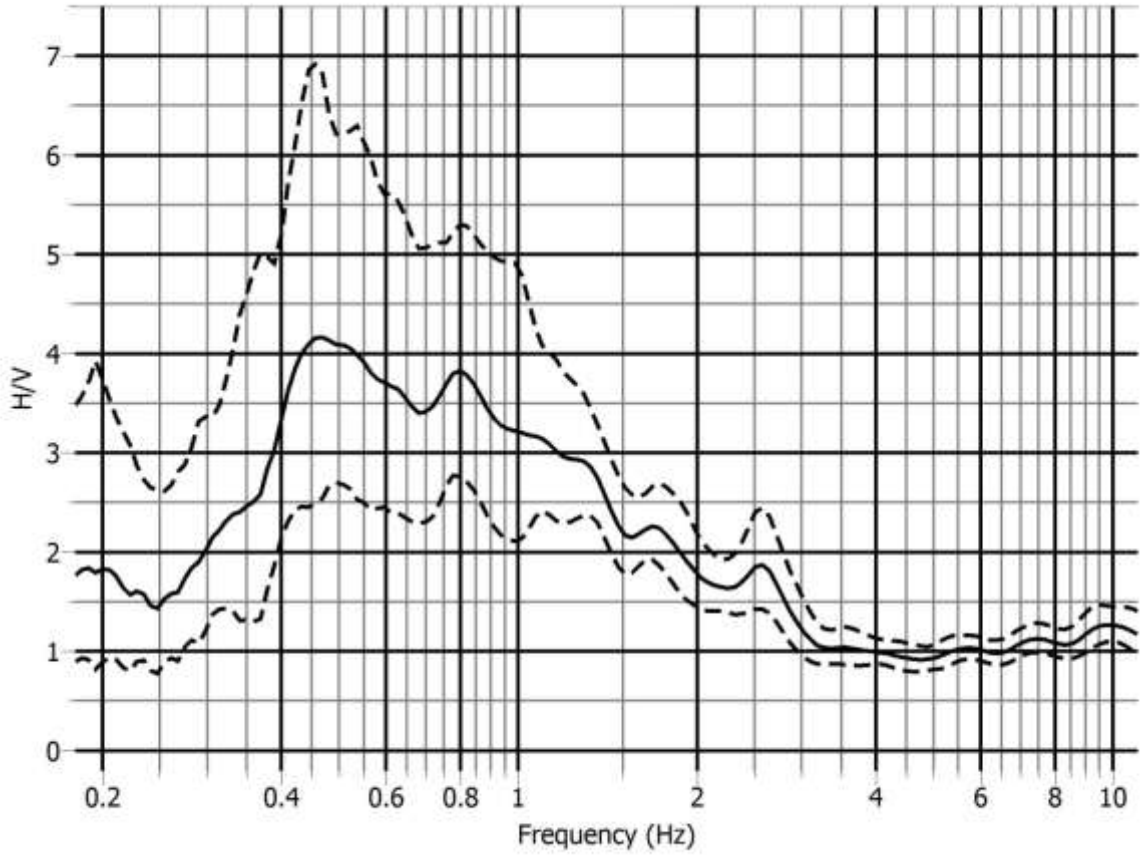
f_0=0.48 Hz; A_0 = 4.2; $A_{H/V}$ = (2.56,6.89); $\sigma_A(f_0)$ = 1.64 & 1.64
i) f_0=0.48 Hz > (10/40.96=0.24 Hz); ii) n_c > 200; iii) $\sigma_A(f)$ < 3; at 0.24 Hz <f< 0.96 Hz **Satisfies all three criteria of Reliable H/V Curve**
i) Between 0.12 to 0.48 Hz, $A_{H/V}(f^-) < A_0/2$ ii) Between 0.48 to 1.92 Hz, $A_{H/V}(f^+) > A_0/2$, Not satisfy iii) $A_0 > 2.0$ iv) Between 0.456 Hz to 0.504 Hz, f_{peak} = (0.50 Hz, 0.46 Hz) v) $\sigma_f = 0.081 < \varepsilon(f_0) = 0.096$ vi) $\sigma_A(f_0) = 1.64 < \Theta(f_0) = 2.5$ **Satisfies five out of six criteria of Clear H/V Peak**
Reliable curve and unclear low frequency peak

MT4: Uttara DRS (23°52'26.8"N, 90°23'58.3"E)

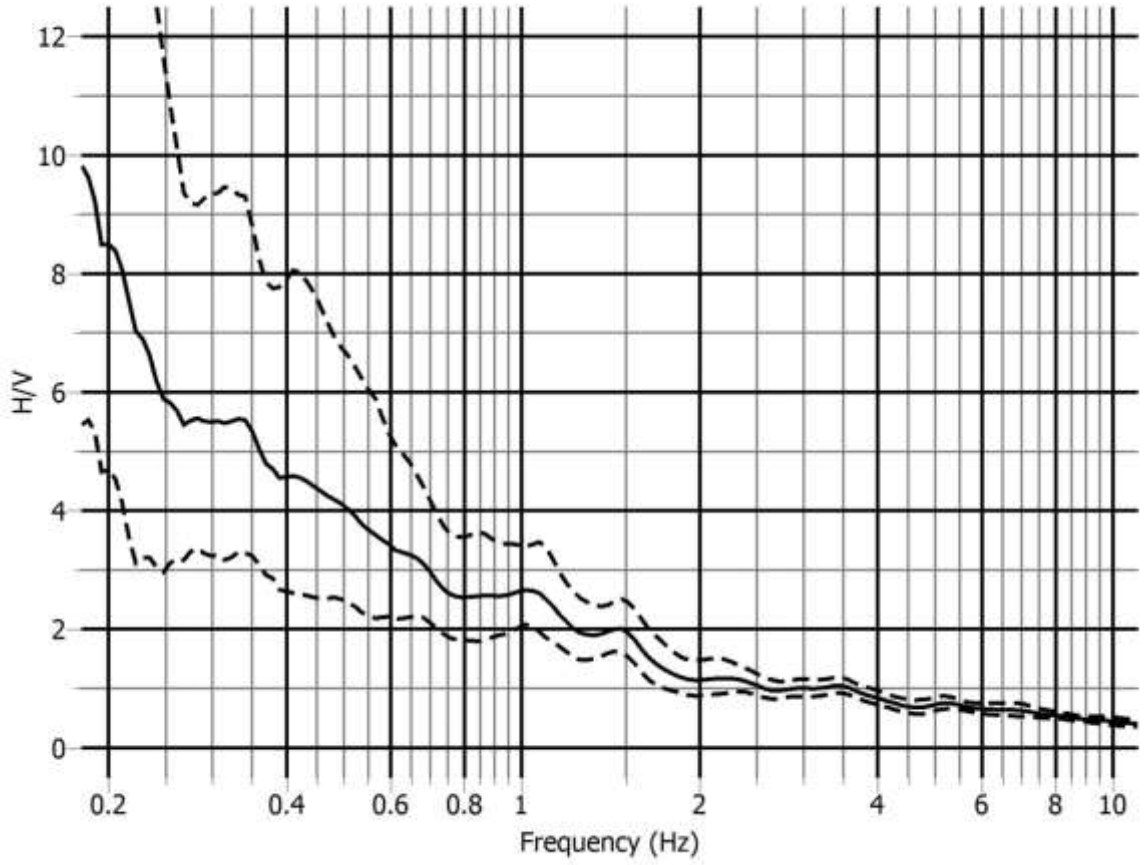

No peak has been found due to stiff soil stratum overlaying very hard soil stratum or bedrock at unknown depth

MT5: Uttarkhan (23°52'45.0"N, 90°25'29.3"E)

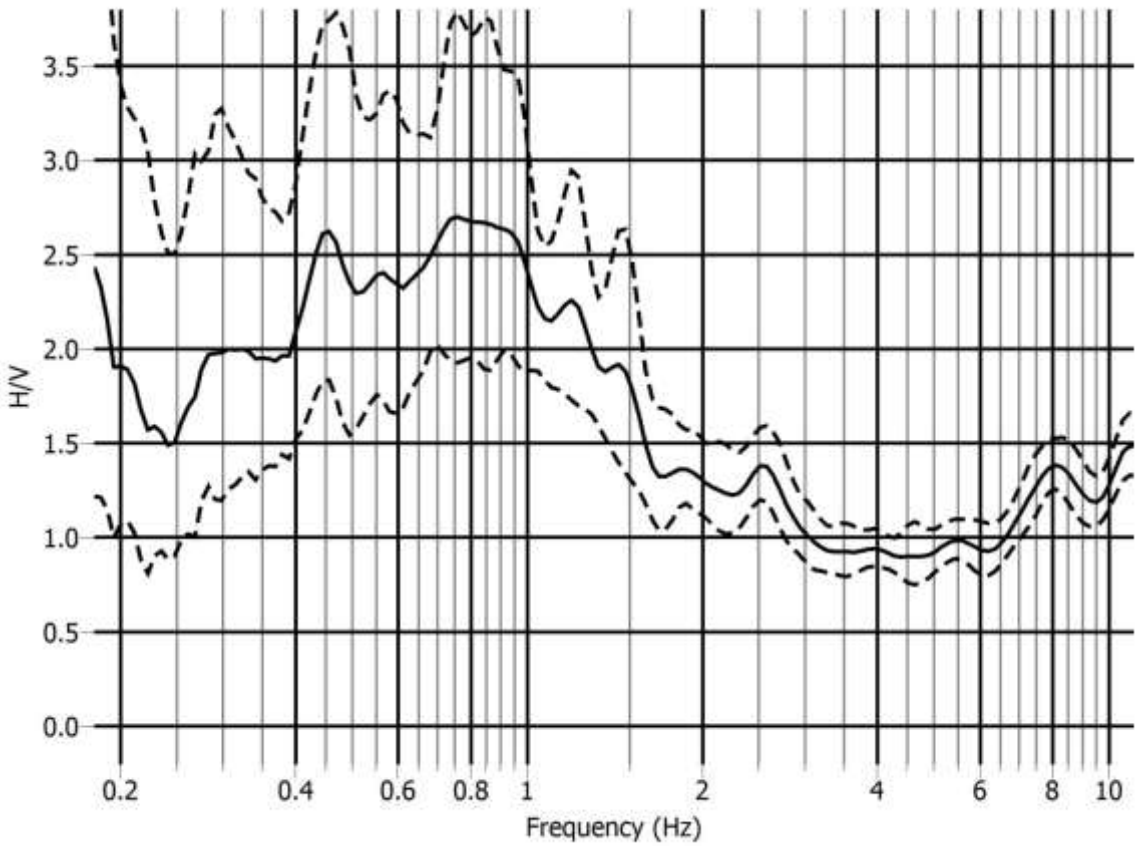

f_0=0.75 Hz; A_0 = 2.72; $A_{H/V}$ = (2.0,3.7); $\sigma_A(f_0)$ = 1.36 & 1.36

i) f_0=0.75 Hz > (10/40.96=0.24 Hz); ii) n_c > 200; iii) $\sigma_A(f)$ < 2; at 0.375 Hz <f< 1.50 Hz

Satisfies all three criteria of Reliable H/V Curve

i) Between 0.187 to 0.75 Hz, $A_{H/V}(f^-) > A_0/2$, Not satisfy

ii) Between 0.75 to 3.0 Hz, $A_{H/V}(f^+) < A_0/2$

iii) $A_0 > 2.0$

iv) Between 0.712 Hz to 0.787 Hz, f_{peak} = (0.715 Hz, 0.75 Hz)

v) $\sigma_f = 0.127 > \varepsilon(f_0) = 0.1125$, Not satisfy

vi) $\sigma_A(f_0) = 1.36 < \Theta(f_0) = 2$

Satisfies four out of six criteria of Clear H/V Peak

Reliable curve and Unclear broad low frequency peak

MT6: Uttara 3rd Phase (23°50'55.3"N, 90°22'22.0"E)
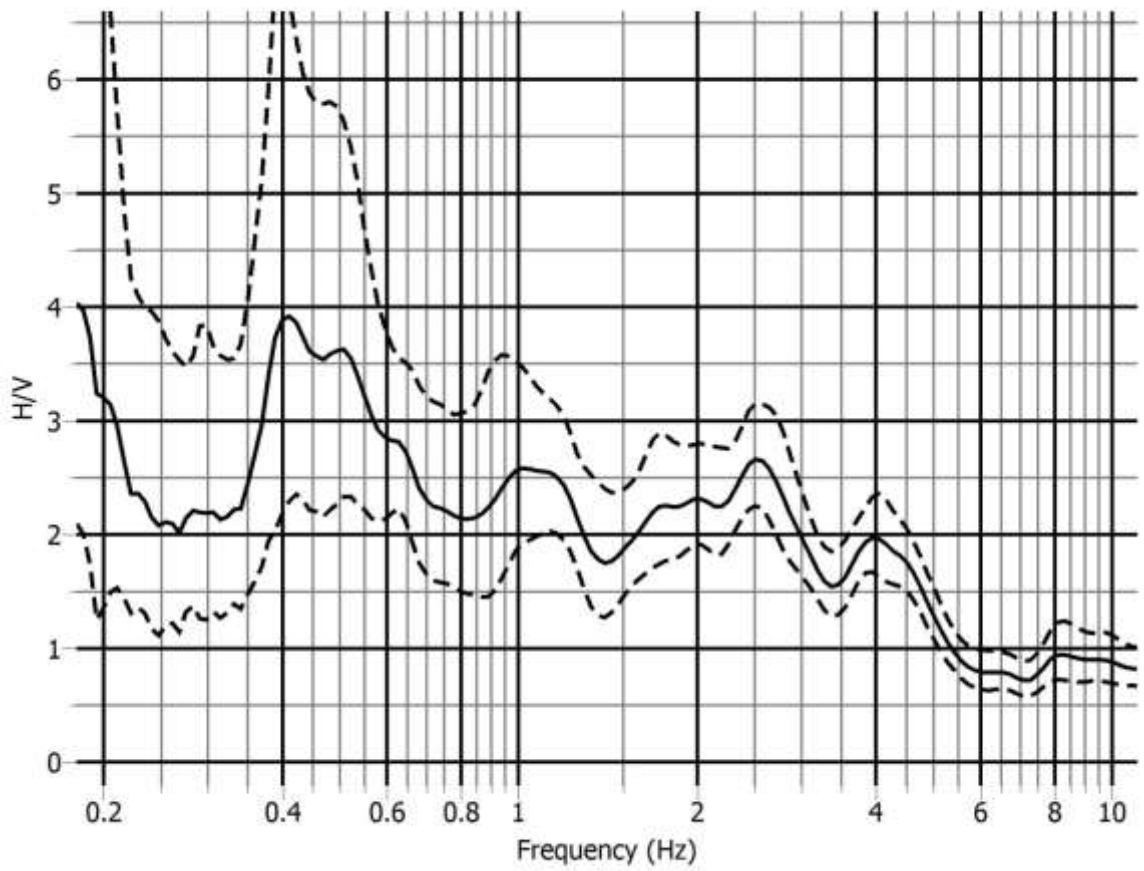
f_0=0.41 Hz; A_0 = 3.88; $A_{H/V}$ = (2.30,6.55); $\sigma_A(f_0)$ = 1.69 & 1.69
i) f_0=0.41 Hz > (10/40.96=0.24 Hz); ii) n_c > 200; iii) $\sigma_A(f)$ < 3; at 0.205 Hz <f< 0.82 Hz **Satisfies all three criteria of Reliable H/V Curve**
i) Between 0.102 to 0.41 Hz, $A_{H/V}(f^-) > A_0/2$, Not satisfy ii) Between 0.41 to 1.64 Hz, $A_{H/V}(f^+) < A_0/2$ iii) $A_0 > 2.0$ iv) Between 0.389 Hz to 0.430 Hz, f_{peak} = (0.42 Hz, 0.40 Hz) v) $\sigma_f = 0.075 < \varepsilon(f_0) = 0.082$ vi) $\sigma_A(f_0) = 1.69 < \Theta(f_0) = 2.5$ **Satisfies five out of six criteria of Clear H/V Peak**
Reliable curve and Unclear low frequency peak

MT7: Hazi Camp (23°51'04.1"N, 90°24'41.3"E)
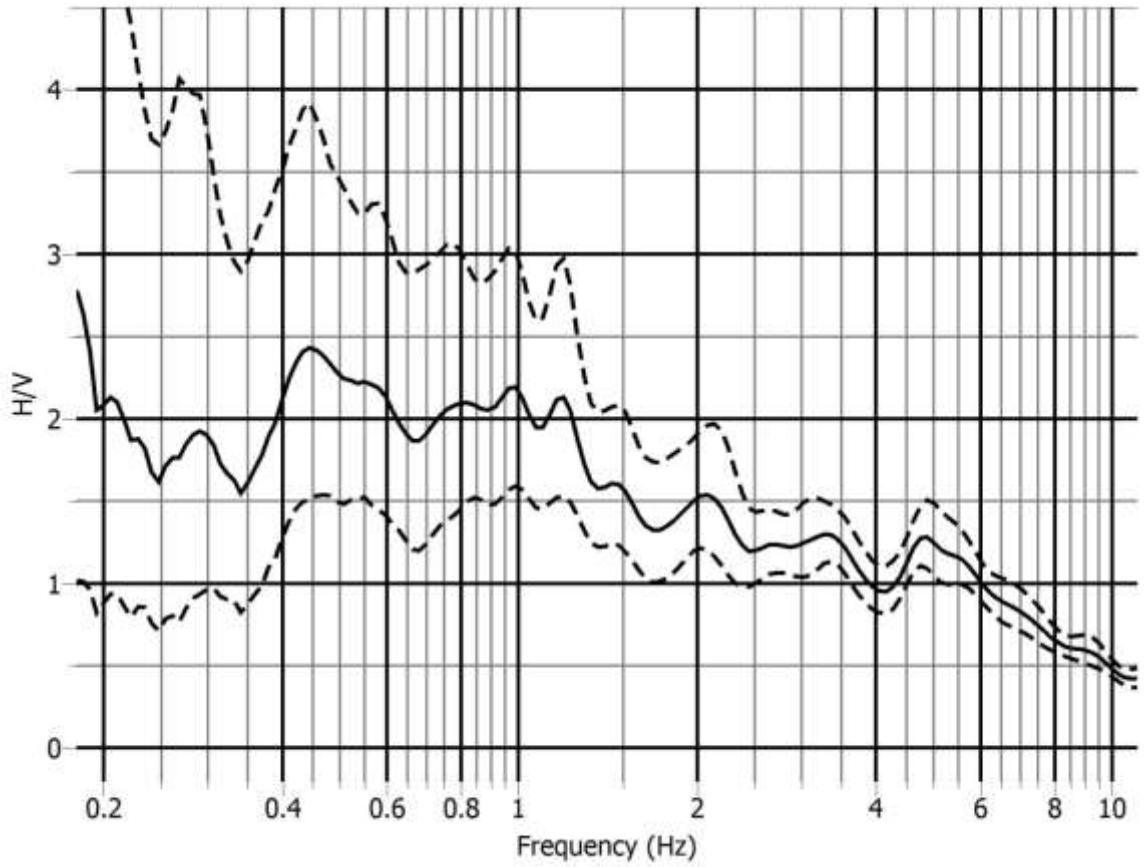
f_0=0.44 Hz; A_0 = 2.38; $A_{H/V}$ = (1.54, 3.69); $\sigma_A(f_0)$ = 1.55 & 1.55
i) f_0=0.44 Hz > (10/40.96=0.24 Hz); ii) n_c > 200; iii) $\sigma_A(f)$ < 3; at 0.22 Hz <f< 0.88 Hz **Satisfies all three criteria of Reliable H/V Curve**
i) Between 0.11 to 0.44 Hz, $A_{H/V}(f^-) > A_0/2$, Not satisfy ii) Between 0.44 to 1.76 Hz, $A_{H/V}(f^+) > A_0/2$, Not satisfy iii) $A_0 > 2.0$ iv) Between 0.418 Hz to 0.462 Hz, f_{peak} = (0.455 Hz, 0.44 Hz) v) $\sigma_f = 0.084 < \varepsilon(f_0) = 0.09$ vi) $\sigma_A(f_0) = 1.55 < \Theta(f_0) = 2.5$ **Satisfies four out of six criteria of Clear H/V Peak**
Reliable curve and Unclear broad low frequency peak

MT8: Baunia (23°50'57.0"N, 90°23'18.7"E)

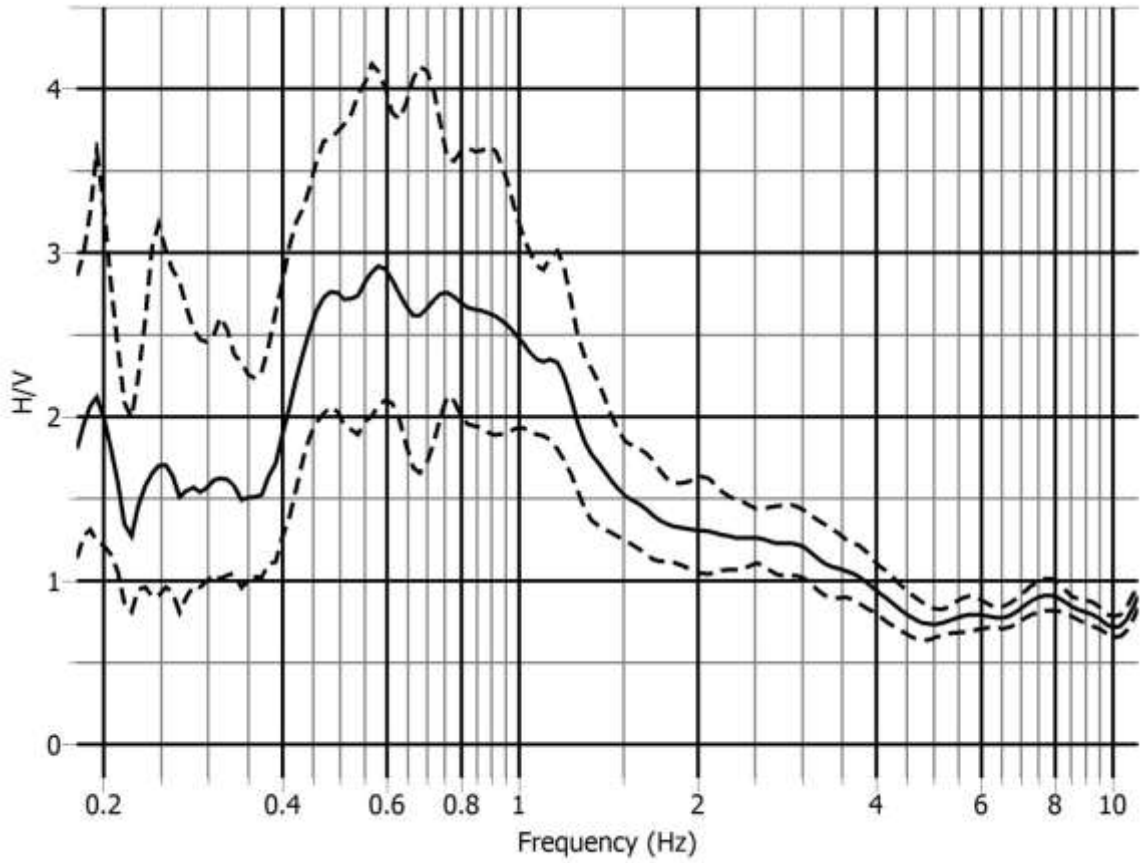

f_0=0.59 Hz; A_0 = 2.91; $A_{H/V}$ = (2.08,4.08); $\sigma_A(f_0)$ = 1.40 & 1.40

i) f_0=0.59 Hz > (10/40.96=0.24 Hz); ii) n_c > 200; iii) $\sigma_A(f)$ < 2; at 0.295 Hz <f< 1.18 Hz

Satisfies all three criteria of Reliable H/V Curve

i) Between 0.147 to 0.59 Hz, $A_{H/V}(f^-) < A_0/2$

ii) Between 0.59 to 2.36 Hz, $A_{H/V}(f^+) < A_0/2$

iii) $A_0 > 2.0$

iv) Between 0.56 Hz to 0.62 Hz, f_{peak} = (0.60 Hz, 0.56 Hz)

v) $\sigma_f = 0.120 > \varepsilon(f_0) = 0.0885$, Not Satisfy

vi) $\sigma_A(f_0) = 1.40 < \Theta(f_0) = 2$

Satisfies five out of six criteria of Clear H/V Peak

Reliable curve and Clear low frequency peak

MT9: Joarsahara DRS (23°49'48.9"N, 90°25'08.0"E)

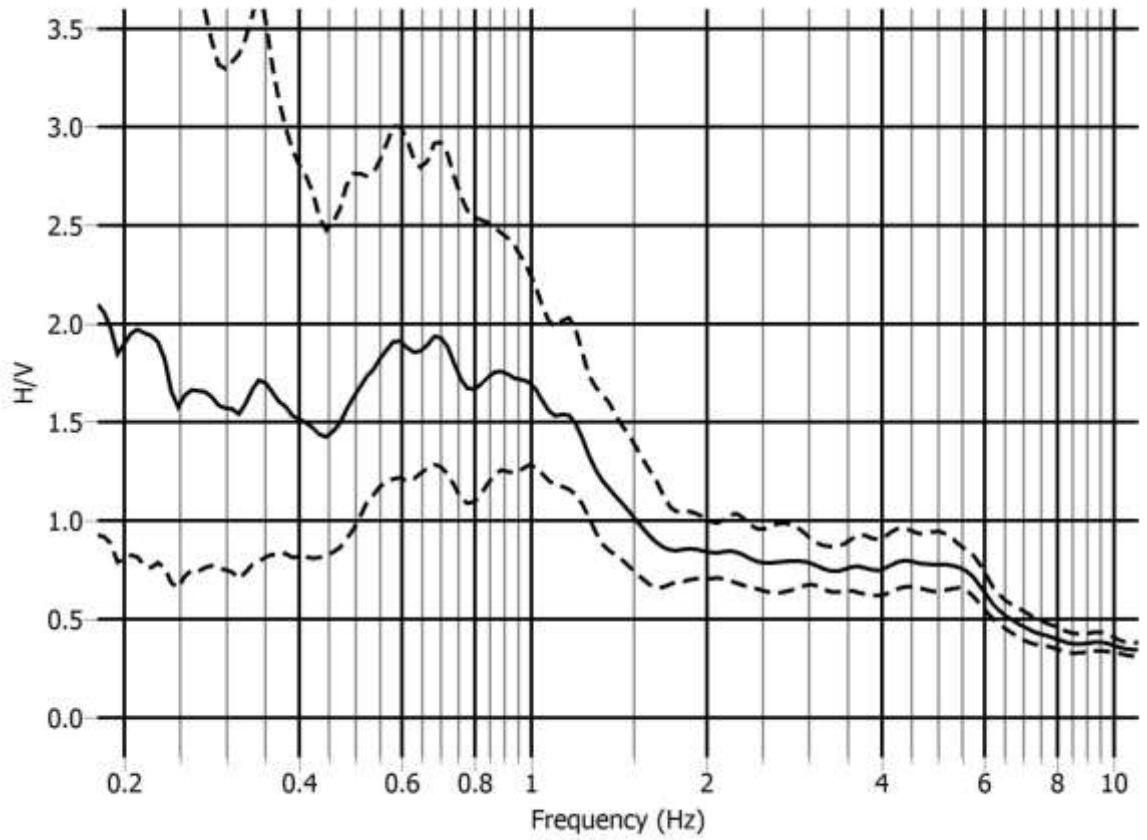

Flat curve and No peak have been found, since $A_0 < 2$ and stiff soil overlaying hard soil stratum or bedrock at unknown depth.

MT10: Balurghat (23°49'46.4"N, 90°23'19.1"E)

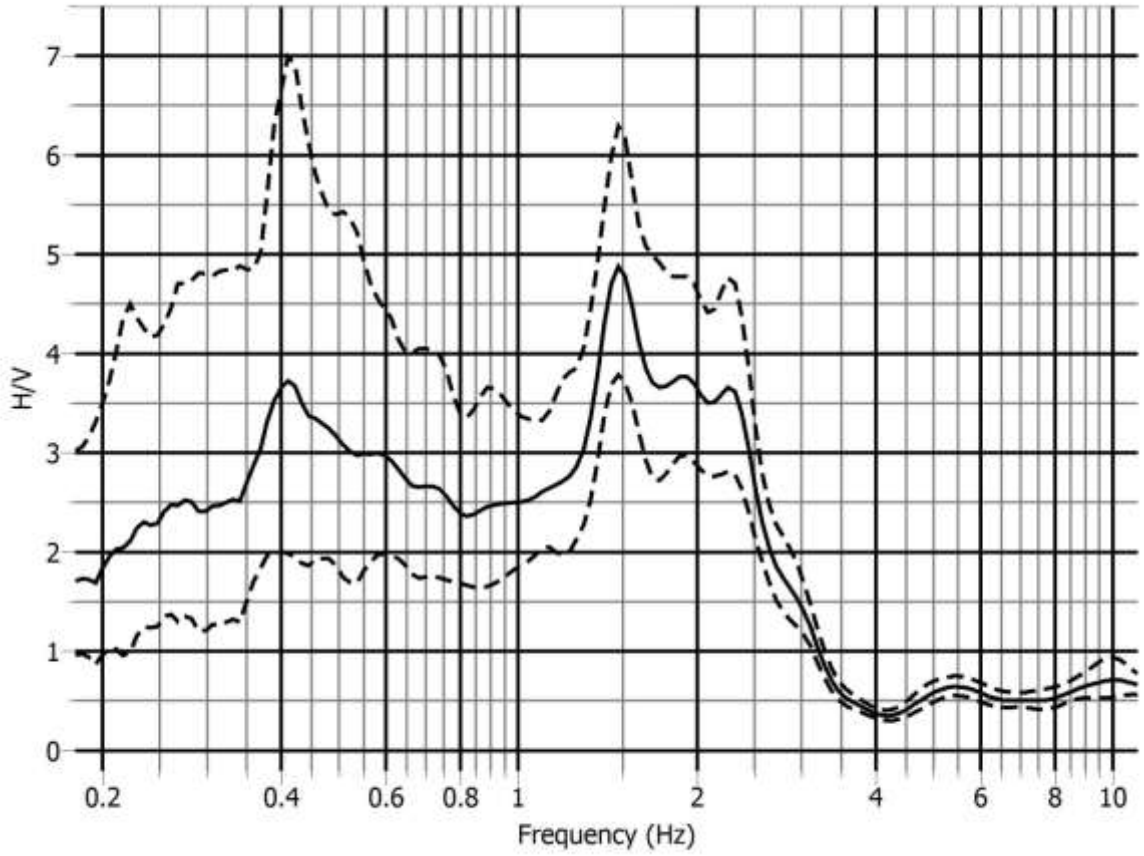

Peak 1: f_0=0.41 Hz; A_0 =3.7; $A_{H/V}$ = (2,7); $\sigma_A(f_0)$ = 1.85 & 1.89

i) f_0=0.41 Hz > (10/41=0.24 Hz); ii) n_c > 200; iii) $\sigma_A(f)$ < 3; at 0.205 Hz <f< 0.82 Hz

Satisfies all three criteria of Reliable H/V Curve

i) Between 0.103 to 0.41 Hz, $A_{H/V}(f^-) > A_0/2$, Not satisfy
ii) Between 0.41 to 1.64 Hz, $A_{H/V}(f^+) > A_0/2$, Not satisfy
iii) $A_0 > 2.0$
iv) Between 0.3895 Hz to 0.4305 Hz, f_{peak} = (0.39 Hz, 0.41 Hz)
v) $\sigma_f = 0.205 > \varepsilon(f_0) = 0.082$, Not satisfy
vi) $\sigma_A(f_0) = 1.89 < \Theta(f_0) = 2.5$

Satisfies three out of six criteria of clear H/V peak

Peak 2: f_0=1.48 Hz; A_0 =4.85; $A_{H/V}$ = (3.75,6.26), $\sigma_A(f_0)$ = 1.29 & 1.29

i) f_0=1.48 Hz > (10/41=0.24 Hz); ii) n_c > 200; iii) $\sigma_A(f)$ < 2; at 0.74 Hz <f< 2.96 Hz

Satisfies all three criteria of Reliable H/V Curve

i) Between 0.37 to 1.48 Hz, $A_{H/V}(f^-) < A_0/2$
ii) Between 1.48 to 5.92 Hz, $A_{H/V}(f^+) < A_0/2$
iii) $A_0 > 2.0$
iv) Between 1.406 Hz to 1.554 Hz, f_{peak} = (1.48 Hz, 1.48 Hz)
v) $\sigma_f = 0.205 > \varepsilon(f_0) = 0.148$, Not Satisfy
vi) $\sigma_A(f_0) = 1.29 < \Theta(f_0) = 1.78$

Satisfies five out of six criteria of Clear H/V Peak

Reliable curve, Two peak where frequency of peak 2 > peak 1, and Peak 2 is clear peak

MT11: Mirpur Mini DRS (23°49'57.6"N, 90°21'49.2"E)
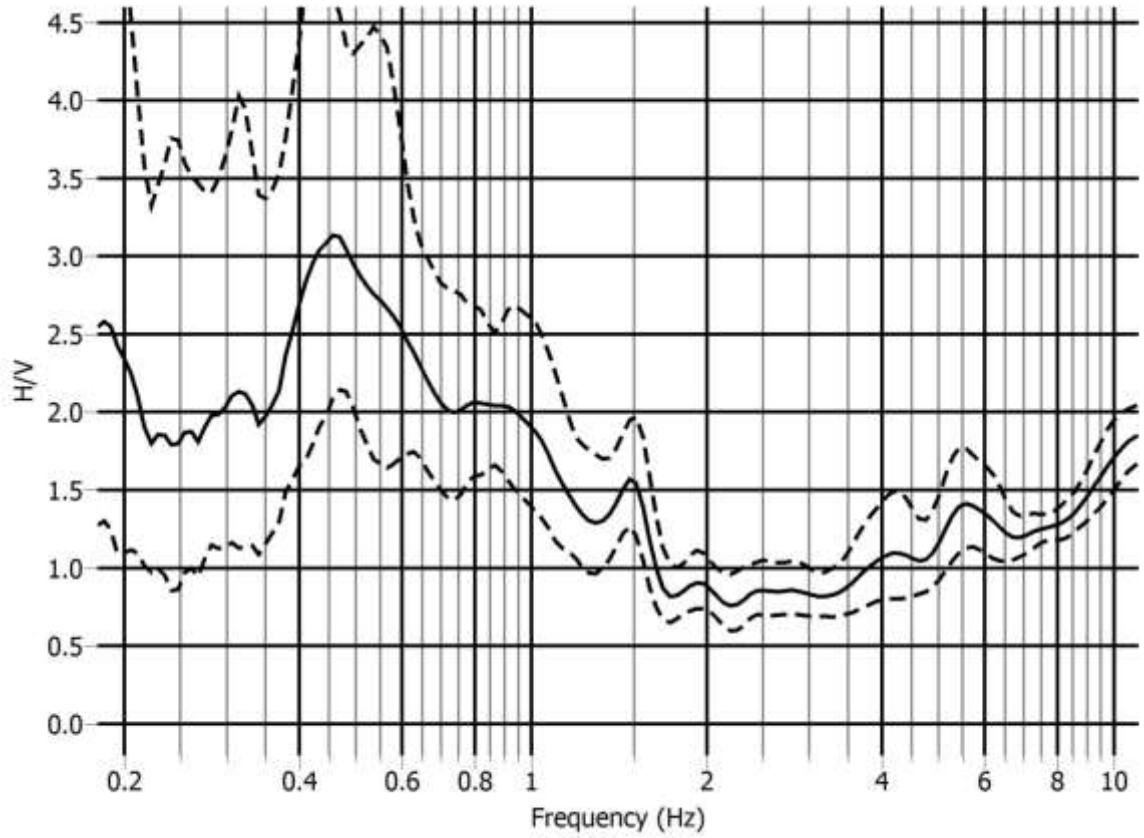
f_0=0.46 Hz; A_0 = 3.12; $A_{H/V}$ = (2.13, 4.57); $\sigma_A(f_0)$ = 1.46 & 1.46
i) f_0=0.46 Hz > (10/40.96=0.24 Hz); ii) n_c > 200; iii) $\sigma_A(f)$ < 3; at 0.23 Hz <f< 0.92 Hz **Satisfies all three criteria of Reliable H/V Curve**
i) Between 0.115 to 0.46 Hz, $A_{H/V}(f^-) > A_0/2$, Not satisfy ii) Between 0.46 to 1.84 Hz, $A_{H/V}(f^+) < A_0/2$ iii) $A_0 > 2.0$ iv) Between 0.437 Hz to 0.483 Hz, f_{peak} = (0.47 Hz, 0.44 Hz) v) $\sigma_f = 0.07 < \varepsilon(f_0) = 0.092$ vi) $\sigma_A(f_0) = 1.46 < \Theta(f_0) = 2.5$ **Satisfies five out of six criteria of Clear H/V Peak**
Reliable curve and Unclear low frequency peak

MT12: Sadullapur (23°51'26.2"N, 90°18'35.2"E)

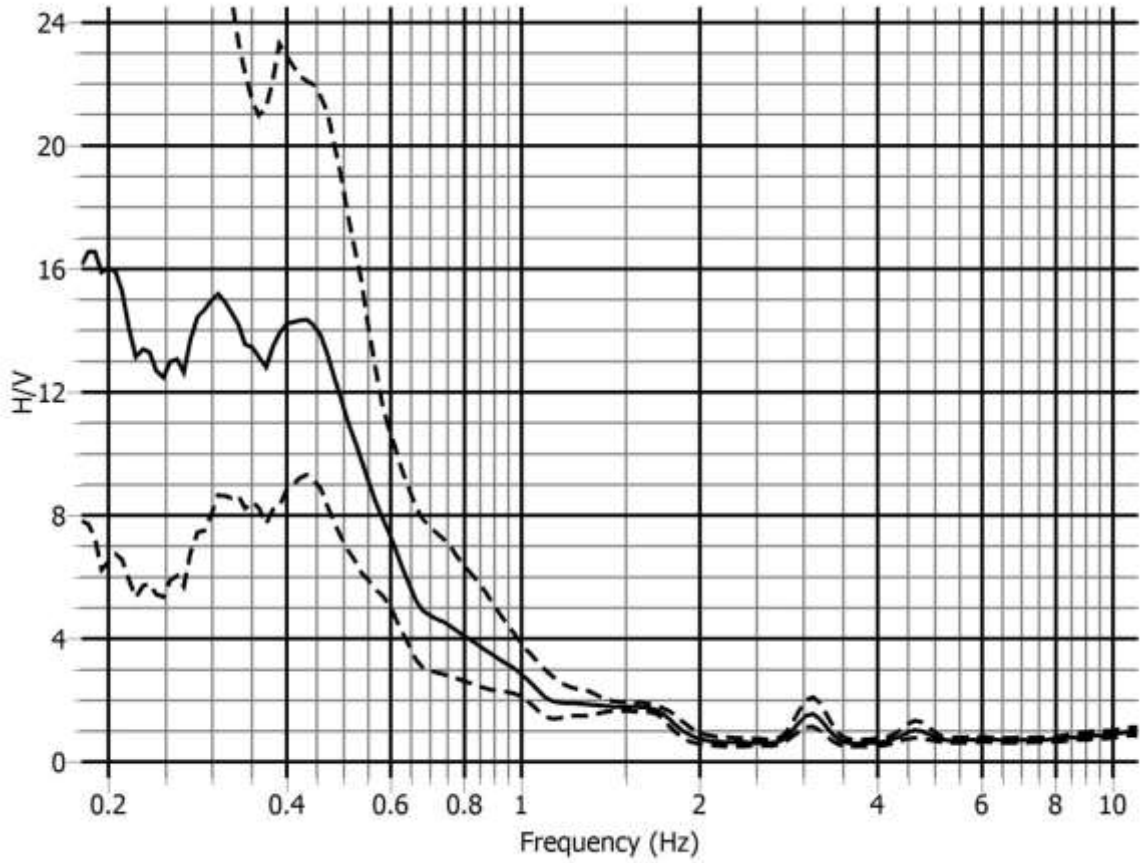

No peak has been found due to stiff soil stratum overlaying very hard soil stratum or bedrock at unknown depth

MT13: MAWTS (23°49'30.3"N, 90°21'51.0"E)

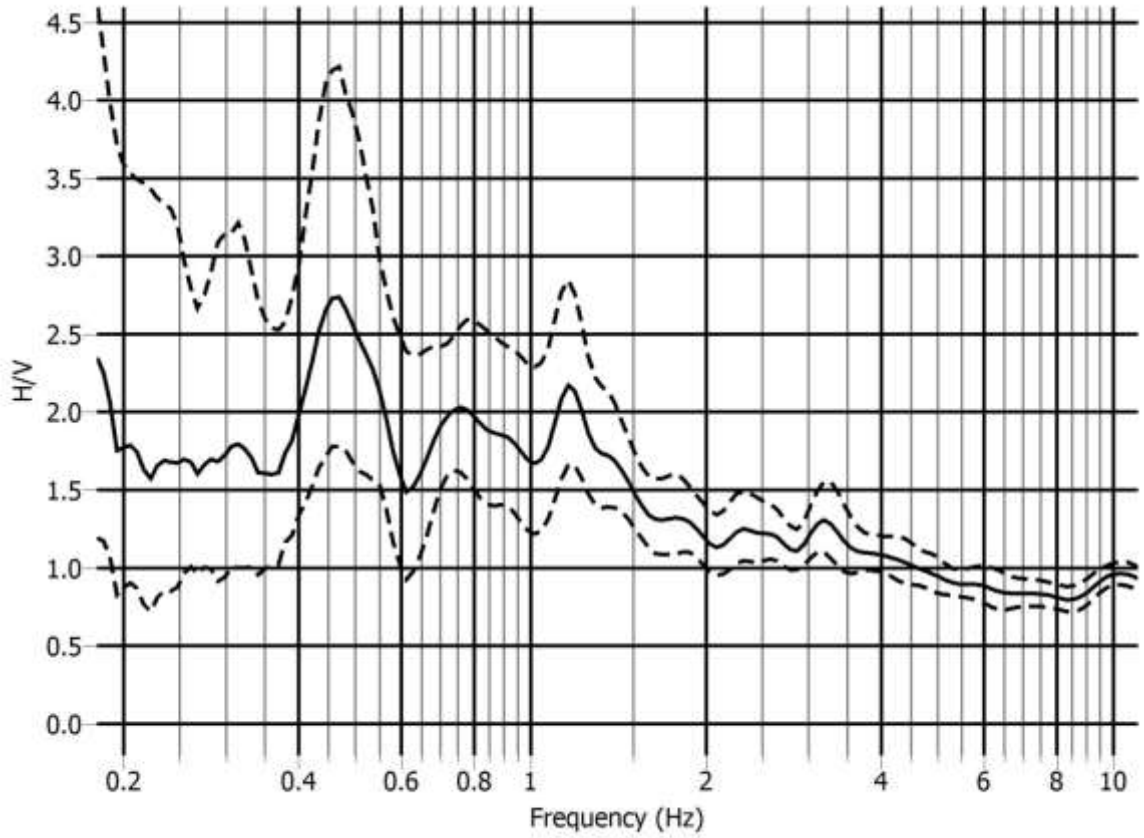

f_0=0.46 Hz; A_0 = 2.72; $A_{H/V}$ = (1.76,4.20); $\sigma_A(f_0)$ = 1.54 & 1.54

i) f_0=0.46 Hz > (10/40.96 = 0.24 Hz); ii) n_c > 200; iii) $\sigma_A(f)$ < 3; at 0.23 Hz <f< 0.92 Hz

Satisfies all three criteria of Reliable H/V Curve

i) Between 0.115 to 0.46 Hz, $A_{H/V}(f^-) > A_0/2$, Not satisfy

ii) Between 0.46 to 1.84 Hz, $A_{H/V}(f^+) > A_0/2$, Not satisfy

iii) $A_0 > 2.0$

iv) Between 0.437 Hz to 0.483 Hz, f_{peak} = (0.46 Hz, 0.47 Hz)

v) $\sigma_f = 0.069 < \varepsilon(f_0) = 0.092$

vi) $\sigma_A(f_0) = 1.54 < \Theta(f_0) = 2.5$

Satisfies four out of six criteria of Clear H/V Peak

Reliable curve and Unclear broad low frequency peak

MT14: Mirpur Bangla School (23°48'51.8"N, 90°22'02.6"E)

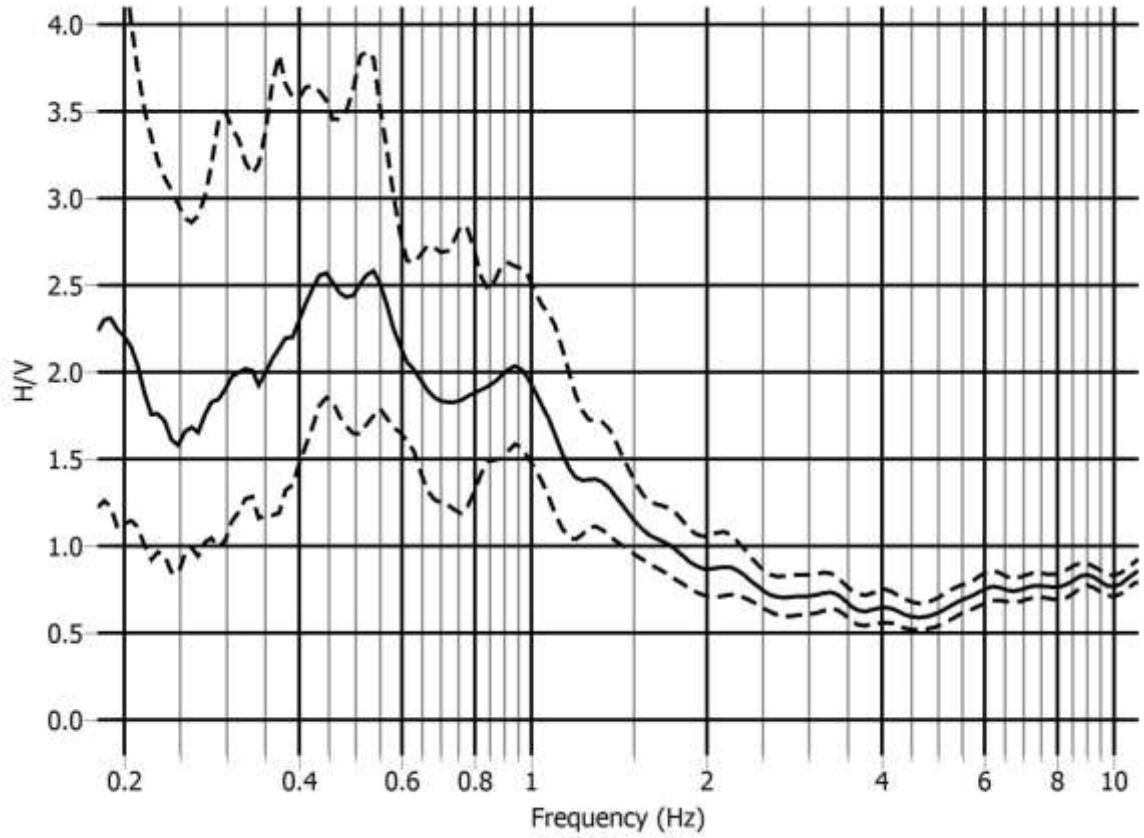

f_0=0.44 Hz; A_0 = 2.60; $A_{H/V}$ = (1.88,3.60); $\sigma_A(f_0)$ = 1.38 & 1.38

i) f_0=0.44 Hz > (10/40.96=0.24 Hz); ii) n_c > 200; iii) $\sigma_A(f)$ < 3; at 0.22 Hz <f< 0.88 Hz

Satisfies all three criteria of Reliable H/V Curve

i) Between 0.11 to 0.44 Hz, $A_{H/V}(f^-) > A_0/2$, Not satisfy

ii) Between 0.44 to 1.76 Hz, $A_{H/V}(f^+) < A_0/2$

iii) $A_0 > 2.0$

iv) Between 0.418 Hz to 0.462 Hz, f_{peak} = (0.45 Hz, 0.42 Hz)

v) $\sigma_f = 0.111 > \varepsilon(f_0) = 0.09$, Not satisfy

vi) $\sigma_A(f_0) = 1.38 < \Theta(f_0) = 2.5$

Satisfies four out of six criteria of Clear H/V Peak

Reliable curve and Unclear broad low frequency peak

MT15: Bhasantek DRS (23°48'22.3"N, 90°23'16.2"E)

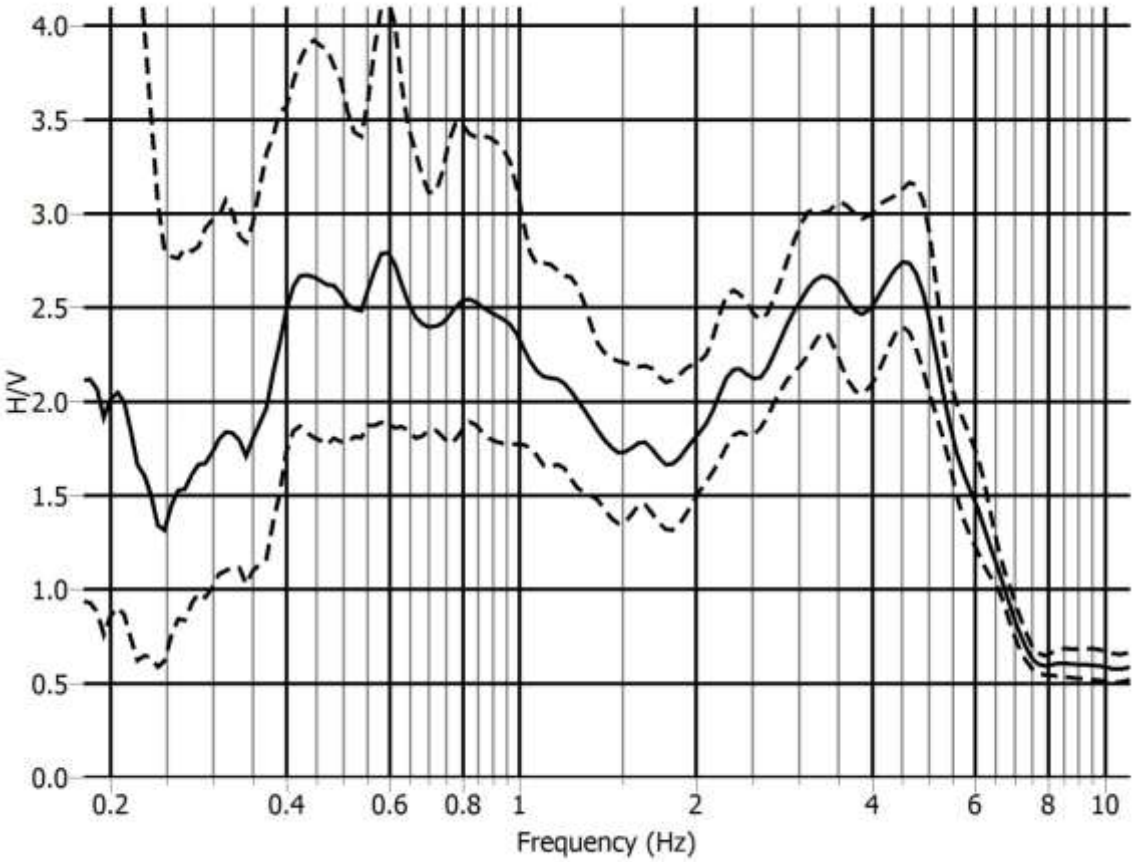

Peak 1: f_0=0.58 Hz; A_0 = 2.80; $A_{H/V}$ = (1.88, 4.17); $\sigma_A(f_0)$ = 1.49 & 1.49

i) f_0=0.58 Hz > (10/40.96=0.24 Hz); ii) n_c > 200; iii) $\sigma_A(f)$ < 2; at 0.29 Hz <f< 1.16 Hz

Satisfies all three criteria of Reliable H/V Curve

i) Between 0.145 to 0.58 Hz, $A_{H/V}(f^-) > A_0/2$, Not satisfy

ii) Between 0.58 to 2.32 Hz, $A_{H/V}(f^+) > A_0/2$, Not satisfy

iii) $A_0 > 2.0$

iv) Between 0.551 Hz to 0.609 Hz, f_{peak} = (0.58, 0.59 Hz)

v) $\sigma_f = 0.122 > \varepsilon(f_0) = 0.087$, Not satisfy

vi) $\sigma_A(f_0) = 1.49 < \Theta(f_0) = 2$

Satisfies three out of six criteria of Clear H/V Peak

Reliable curve and Unclear broad low frequency peak

MT16: Mirpur 10 DRS (23°48'25.5"N, 90°22'08.1"E)
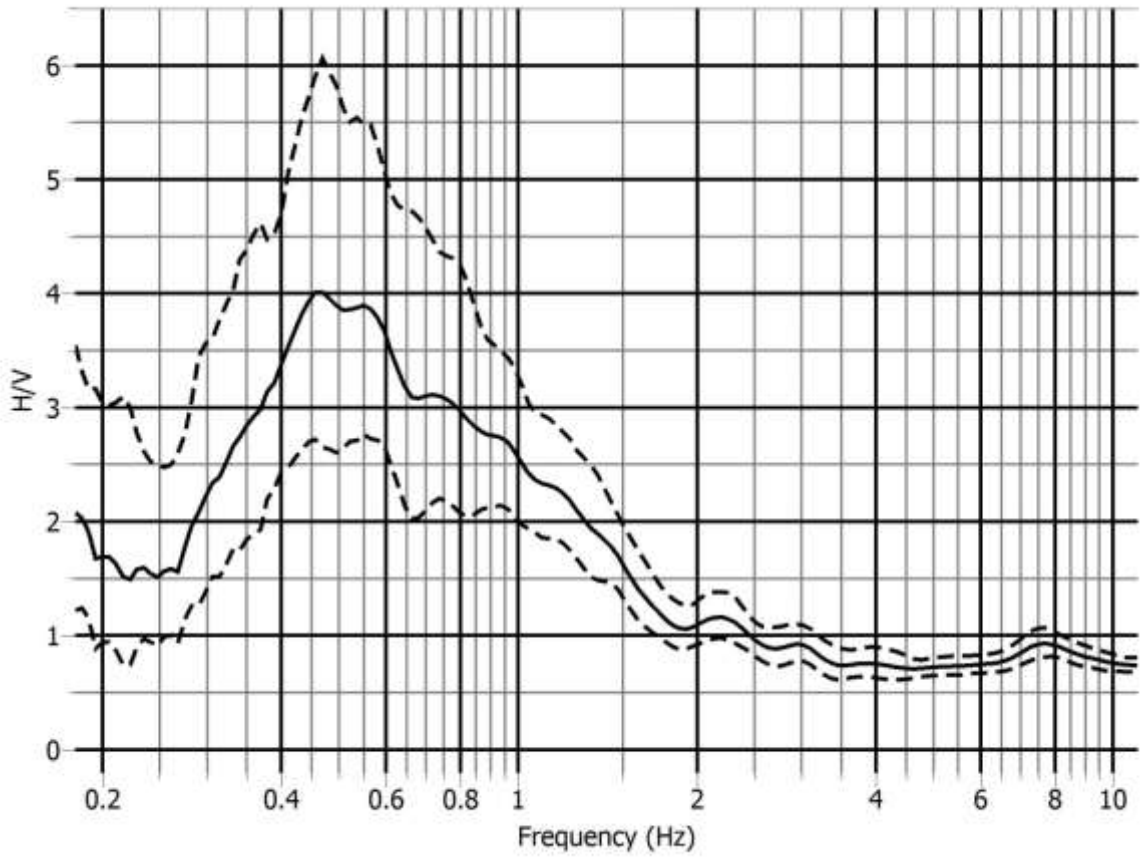
f_0=0.46 Hz; A_0 = 4.0; $A_{H/V}$ = (2.66, 6.0); $\sigma_A(f_0)$ = 1.50 & 1.50
i) f_0=0.46 Hz > (10/40.96=0.24 Hz); ii) n_c > 200; iii) $\sigma_A(f)$ < 3; at 0.23 Hz <f< 0.92 Hz **Satisfies all three criteria of Reliable H/V Curve**
vii) Between 0.115 to 0.46 Hz, $A_{H/V}(f^-) < A_0/2$ viii) Between 0.46 to 1.84 Hz, $A_{H/V}(f^+) < A_0/2$ ix) $A_0 > 2.0$ x) Between 0.437 Hz to 0.483 Hz, f_{peak} = (0.45 Hz, 0.47 Hz) xi) $\sigma_f = 0.090 < \varepsilon(f_0) = 0.092$ xii) $\sigma_A(f_0) = 1.50 < \Theta(f_0) = 2.5$ **Satisfies six out of six criteria of Clear H/V Peak**
Reliable curve and Clear low frequency peak

MT17: German Technical Training Center (23°48'08.2"N, 90°21'28.9"E)

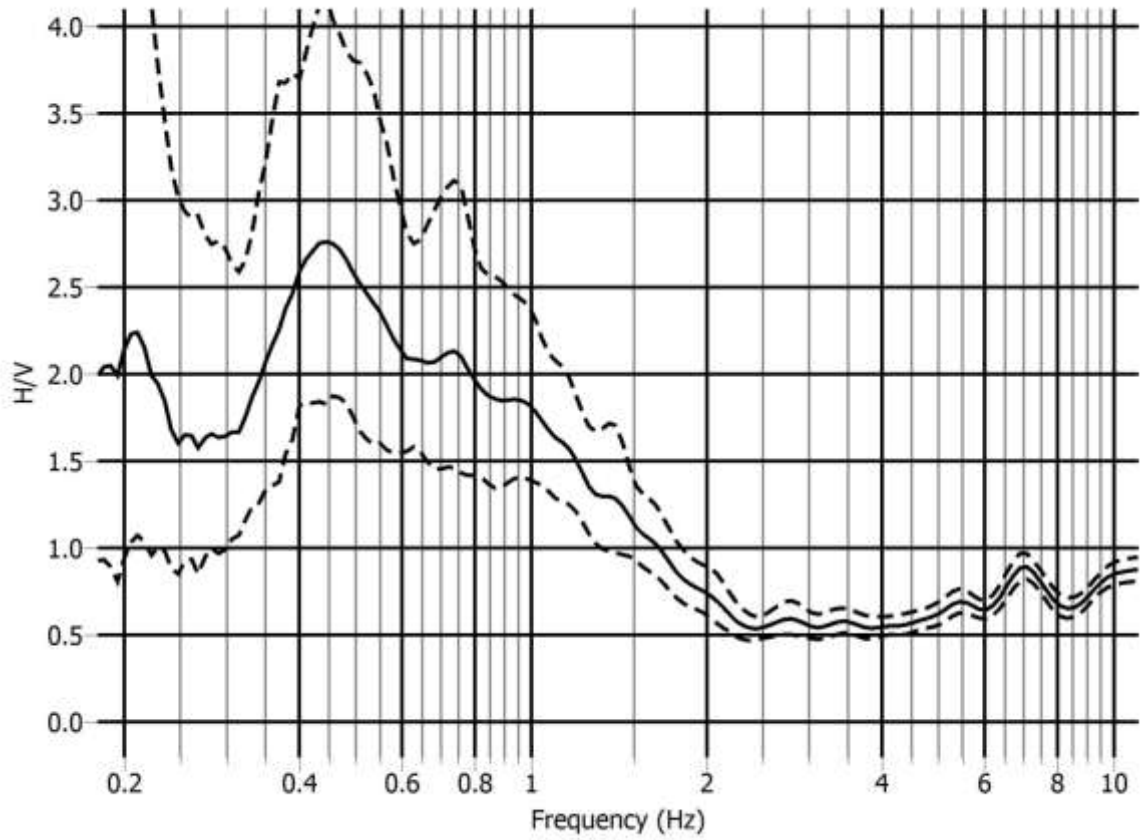

f_0=0.44 Hz; A_0 = 2.75; $A_{H/V}$ = (1.80, 4.22); $\sigma_A(f_0)$ = 1.53 & 1.53

i) f_0=0.44 Hz > (10/40.96=0.24 Hz); ii) n_c > 200; iii) $\sigma_A(f)$ < 3; at 0.22 Hz <f< 0.88 Hz

Satisfies all three criteria of Reliable H/V Curve

i) Between 0.11 to 0.44 Hz, $A_{H/V}(f^-) > A_0/2$, Not satisfy

ii) Between 0.44 to 1.76 Hz, $A_{H/V}(f^+) < A_0/2$

iii) $A_0 > 2.0$

iv) Between 0.418 Hz to 0.462 Hz, f_{peak} = (0.46 Hz, 0.43 Hz)

v) $\sigma_f = 0.071 < \varepsilon(f_0) = 0.088$

vi) $\sigma_A(f_0) = 1.53 < \Theta(f_0) = 2.5$

Satisfies five out of six criteria of Clear H/V Peak

Reliable curve and Unclear low frequency peak

MT18: Banani Rail Crossing (23°48'44.0"N, 90°24'13.7"E)
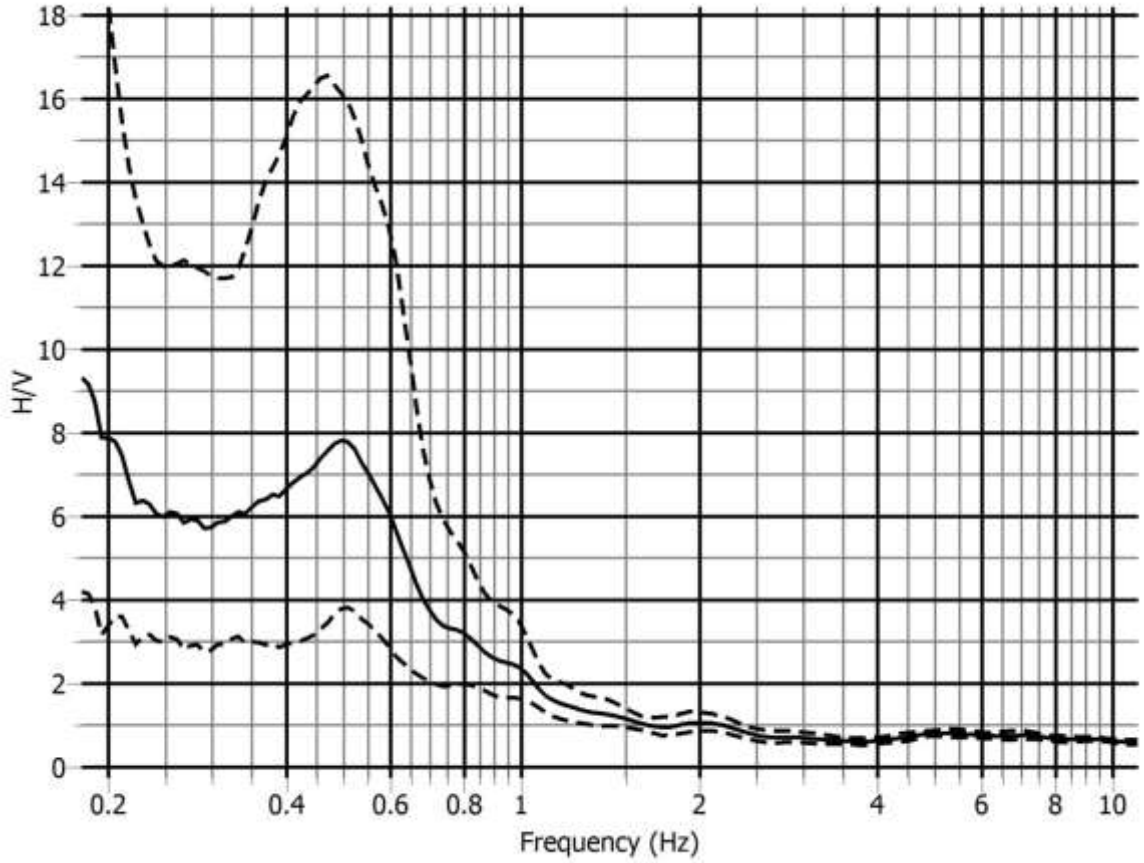
f_0=0.50 Hz; A_0 =7.88; $A_{H/V}$ = (3.76,16.51) $\sigma_A(f_0)$ = 2.09 & 2.09
i) f_0=0.50 Hz > (10/40.96=0.24 Hz); ii) n_c > 200; iii) $\sigma_A(f)$ < 3; at 0.25 Hz <f< 1.0 Hz **Satisfies all three criteria of Reliable H/V Curve**
i) Between 0.125 to 0.50 Hz, $A_{H/V}(f^-) > A_0/2$, Not satisfy ii) Between 0.50 to 2.0 Hz, $A_{H/V}(f^+) < A_0/2$ iii) $A_0 > 2.0$ iv) Between 0.475 Hz to 0.525 Hz, f_{peak} = (0.505 Hz, 0.475 Hz) v) $\sigma_f = 0.082 < \varepsilon(f_0) = 0.100$ vi) $\sigma_A(f_0) = 2.09 < \Theta(f_0) = 2.5$ **Satisfies five out of six criteria of Clear H/V Peak**
Reliable curve and Unclear low frequency peak

MT19: Banani Rail Station (23°47'44.8"N, 90°24'03.7"E)

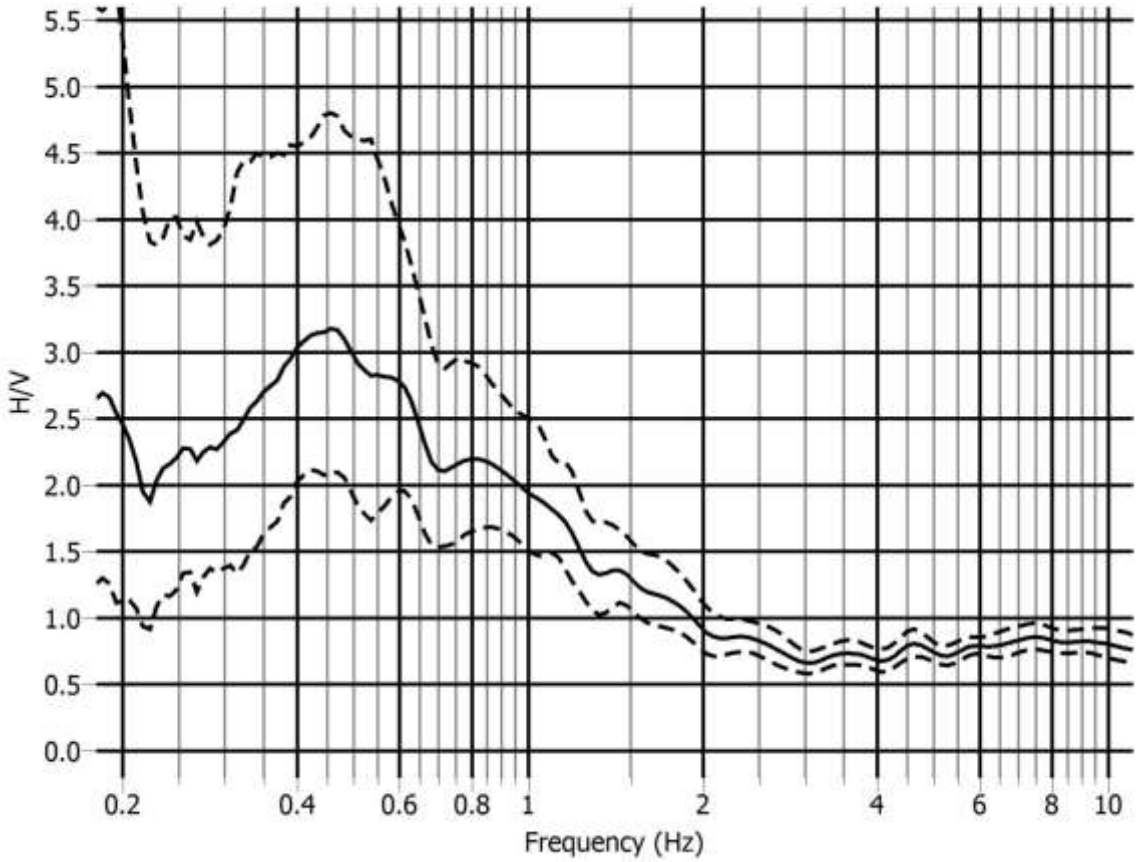

f_0=0.46 Hz; A_0 =3.15; $A_{H/V}$ = (2.07,4.79); $\sigma_A(f_0)$ = 1.52 & 1.52

i) f_0=0.46 Hz > (10/40.96=0.24 Hz); ii) n_c > 200; iii) $\sigma_A(f)$ < 3; at 0.23 Hz <f< 0.92 Hz

Satisfies all three criteria of Reliable H/V Curve

i) Between 0.115 to 0.46 Hz, $A_{H/V}(f^-) > A_0/2$, Not satisfy

ii) Between 0.46 to 1.84 Hz, $A_{H/V}(f^+) < A_0/2$

iii) $A_0 > 2.0$

iv) Between 0.437 Hz to 0.483 Hz, f_{peak} = (0.46 Hz, 0.45 Hz)

v) $\sigma_f = 0.096 > \varepsilon(f_0) = 0.092$, Not satisfy

vi) $\sigma_A(f_0) = 1.52 < \Theta(f_0) = 2.5$

Satisfies four out of six criteria of Clear H/V Peak

Reliable curve and Unclear broad low frequency peak

MT20: Banani Play Ground (23°47'37.0"N, 90°24'29.7"E)

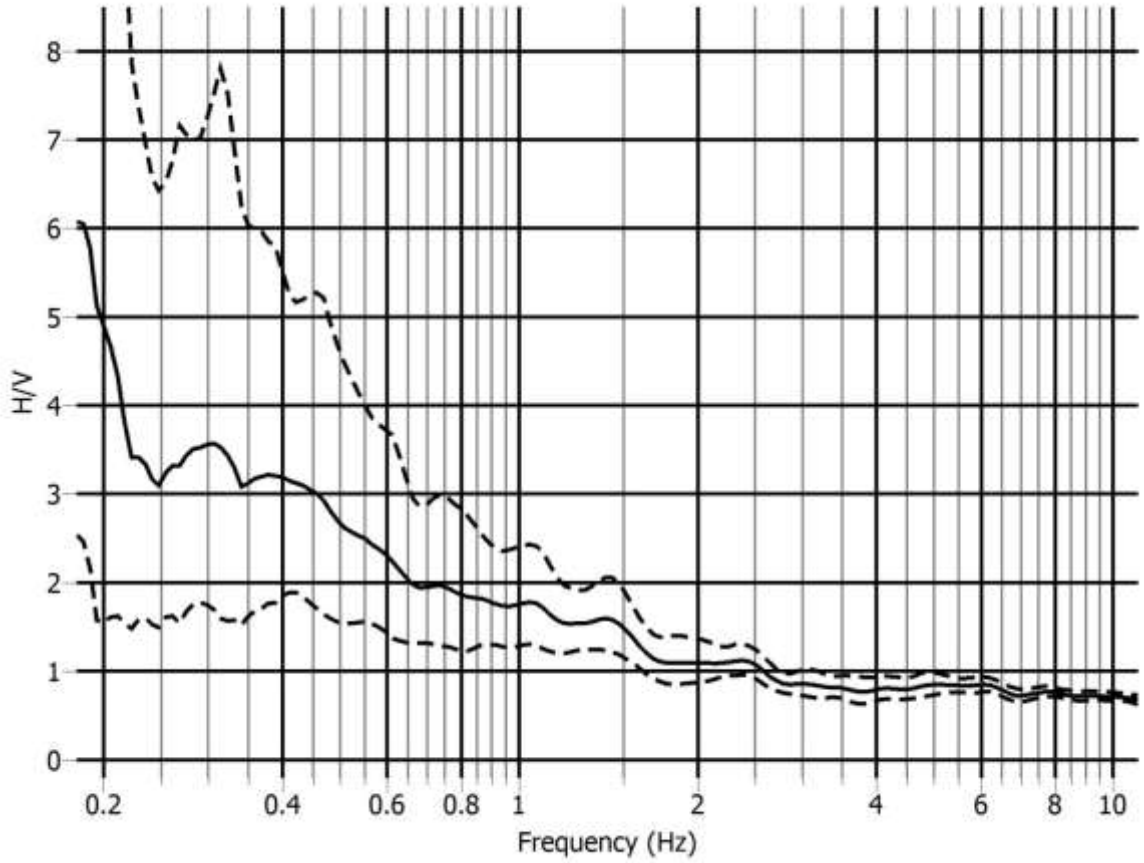

No peak has been found due to stiff soil stratum overlaying very hard soil stratum or bedrock at unknown depth

MT21: Baridhara DRS (23°48'58.7"N, 90°24'58.7"E)

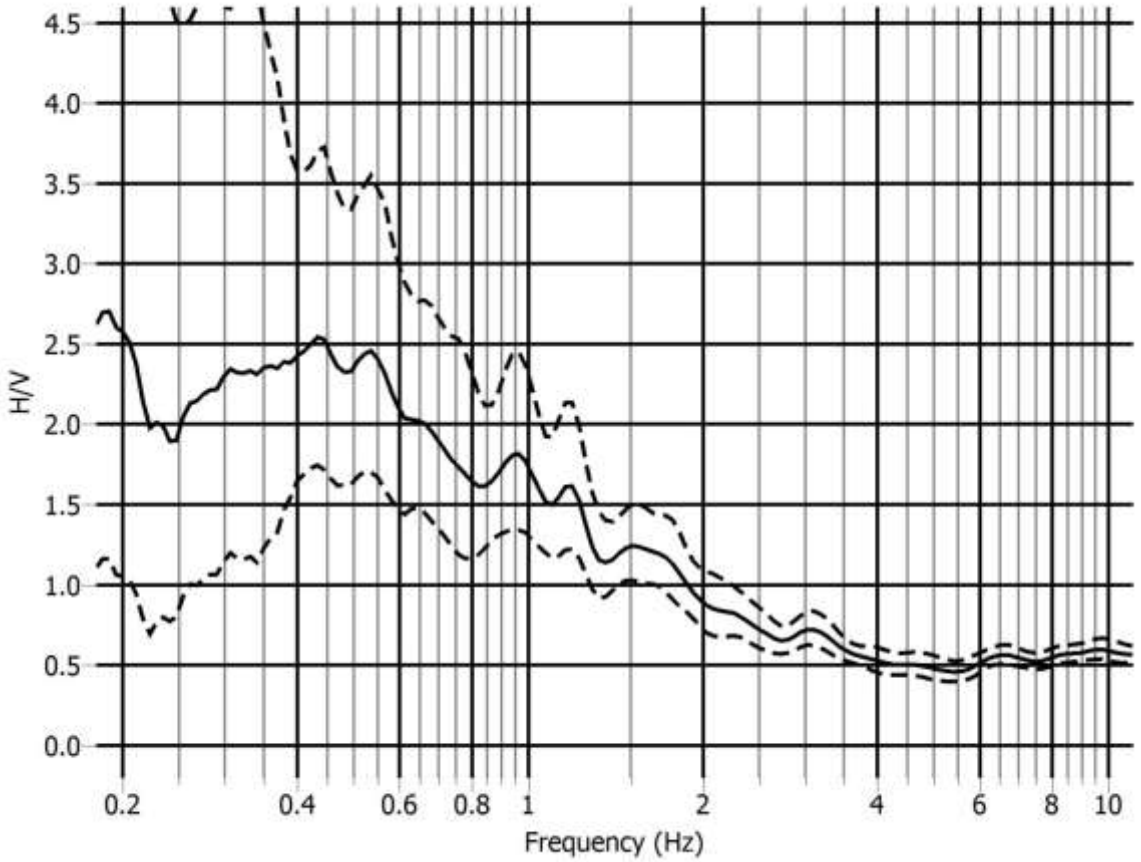

f_0=0.44 Hz; A_0 =2.52; $A_{H/V}$ = (1.7,3.73); $\sigma_A(f_0)$ = 1.48 & 1.48

i) f_0=0.44 Hz > (10/40.96=0.24 Hz); ii) n_c > 200; iii) $\sigma_A(f)$ < 3; at 0.22 Hz <f< 0.88 Hz

Satisfies all three criteria of Reliable H/V Curve

i) Between 0.11 to 0.44 Hz, $A_{H/V}(f^-) > A_0/2$, Not satisfy

ii) Between 0.44 to 1.76 Hz, $A_{H/V}(f^+) < A_0/2$

iii) $A_0 > 2.0$

iv) Between 0.418 Hz to 0.462 Hz, f_{peak} = (0.43 Hz, 0.45 Hz)

v) $\sigma_f = 0.095 > \varepsilon(f_0) = 0.088$, Not satisfy

vi) $\sigma_A(f_0) = 1.48 < \Theta(f_0) = 2.5$

Satisfies four out of six criteria of Clear H/V Peak

Reliable curve and Unclear broad low frequency peak

MT22: Jamuna Future Park (23°48'47.8"N, 90°25'16.5"E)
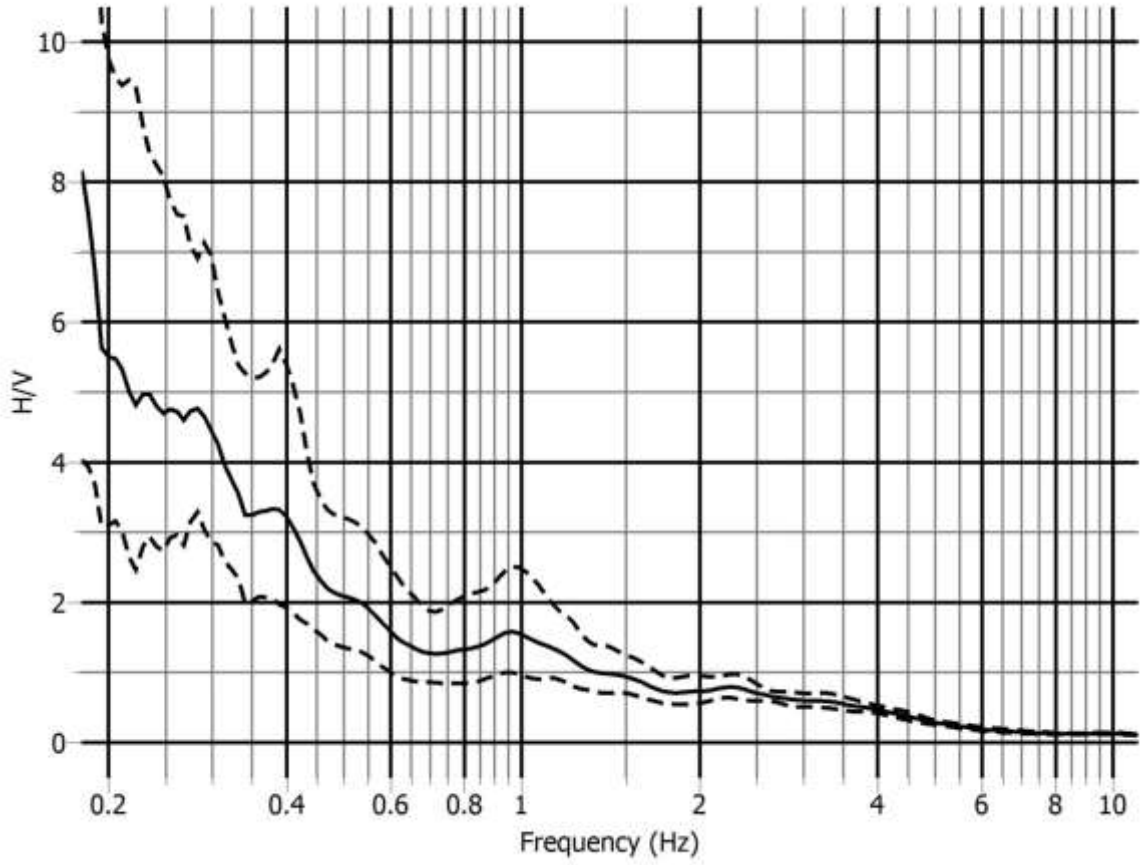
No peak has been found due to stiff soil stratum overlaying very hard soil stratum or bedrock at unknown depth

MT23: Between US Embassy & JFP (23°48'24.5"N, 90°25'18.4"E)

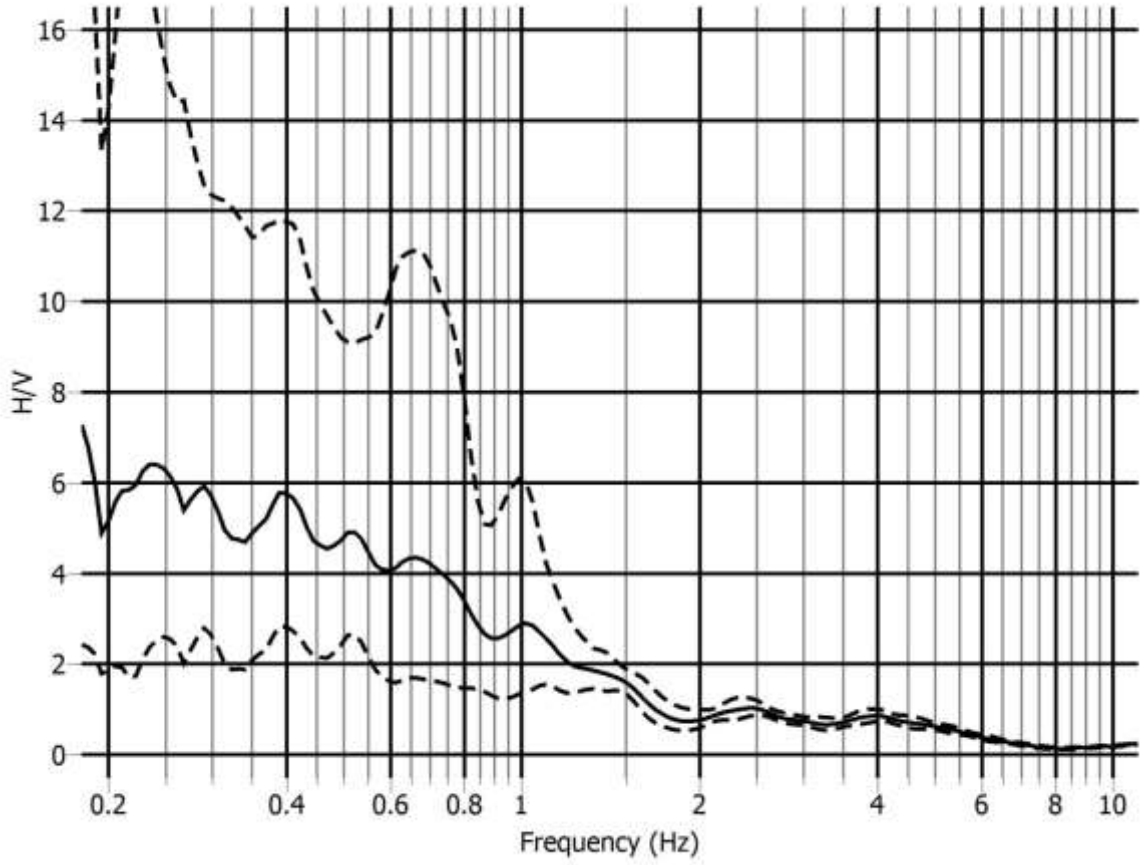

No peak has been found due to stiff soil stratum overlaying very hard soil stratum or bedrock at unknown depth

MT24: US Embassy (23°47'48.8"N, 90°25'24.2"E)

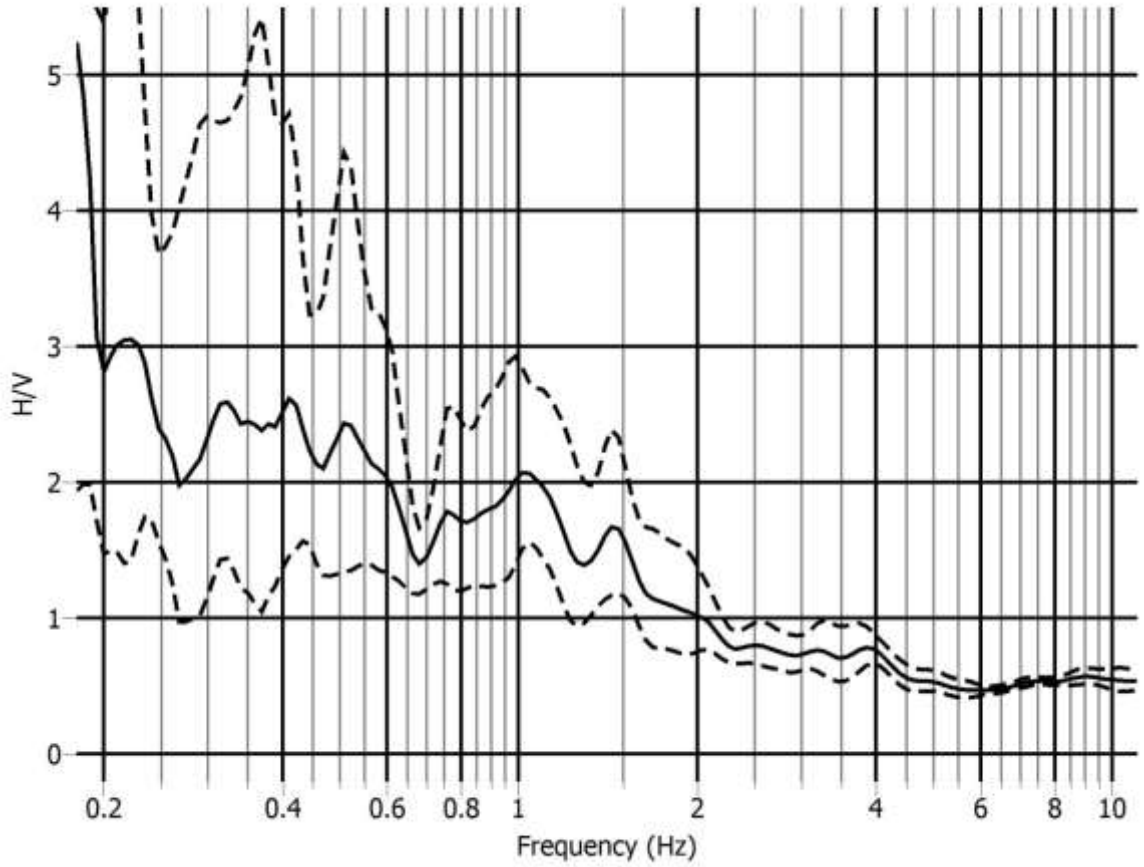

No peak has been found due to stiff soil stratum overlaying very hard soil stratum or bedrock at unknown depth

MT25: Shahzadpur (23°46'29.8"N, 90°25'34.2"E)

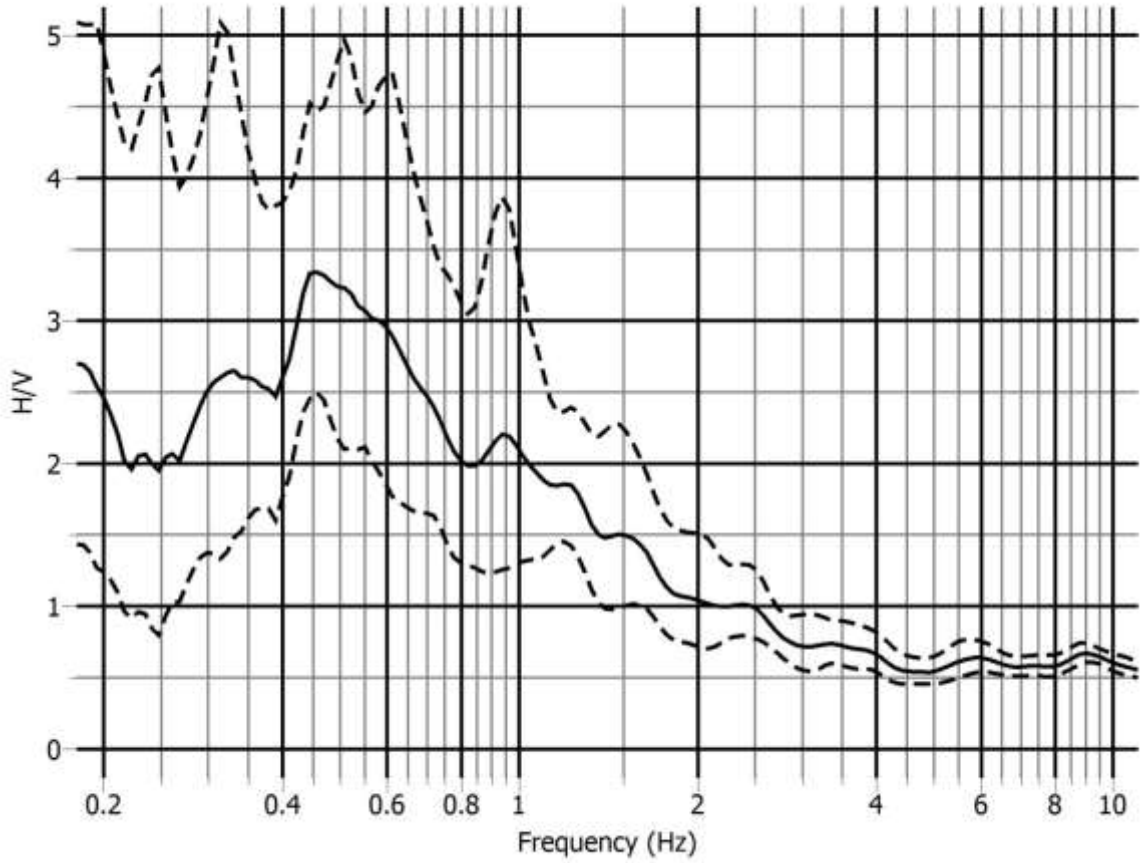

f_0=0.45 Hz; A_0 = 3.35; $A_{H/V}$ = (2.49,4.5); $\sigma_A(f_0)$ = 1.34 & 1.34

i) f_0=0.45 Hz > (10/40.96=0.24 Hz); ii) n_c > 200; iii) $\sigma_A(f)$ < 3; at 0.225 Hz <f< 0.90 Hz

Satisfies all three criteria of Reliable H/V Curve

i) Between 0.112 to 0.45 Hz, $A_{H/V}(f^-) > A_0/2$, Not satisfy

ii) Between 0.45 to 1.8 Hz, $A_{H/V}(f^+) < A_0/2$

iii) $A_0 > 2.0$

iv) Between 0.427 Hz to 0.472 Hz, f_{peak} = (0.46 Hz, 0.44 Hz)

v) $\sigma_f = 0.10 > \varepsilon(f_0) = 0.090$, Not satisfy

vi) $\sigma_A(f_0) = 1.34 < \Theta(f_0) = 2.5$

Satisfies four out of six criteria of Clear H/V Peak

Reliable curve and Unclear broad low frequency peak

MT26: Gulshan Avenue (23°46'59.6"N, 90°25'01.2"E)

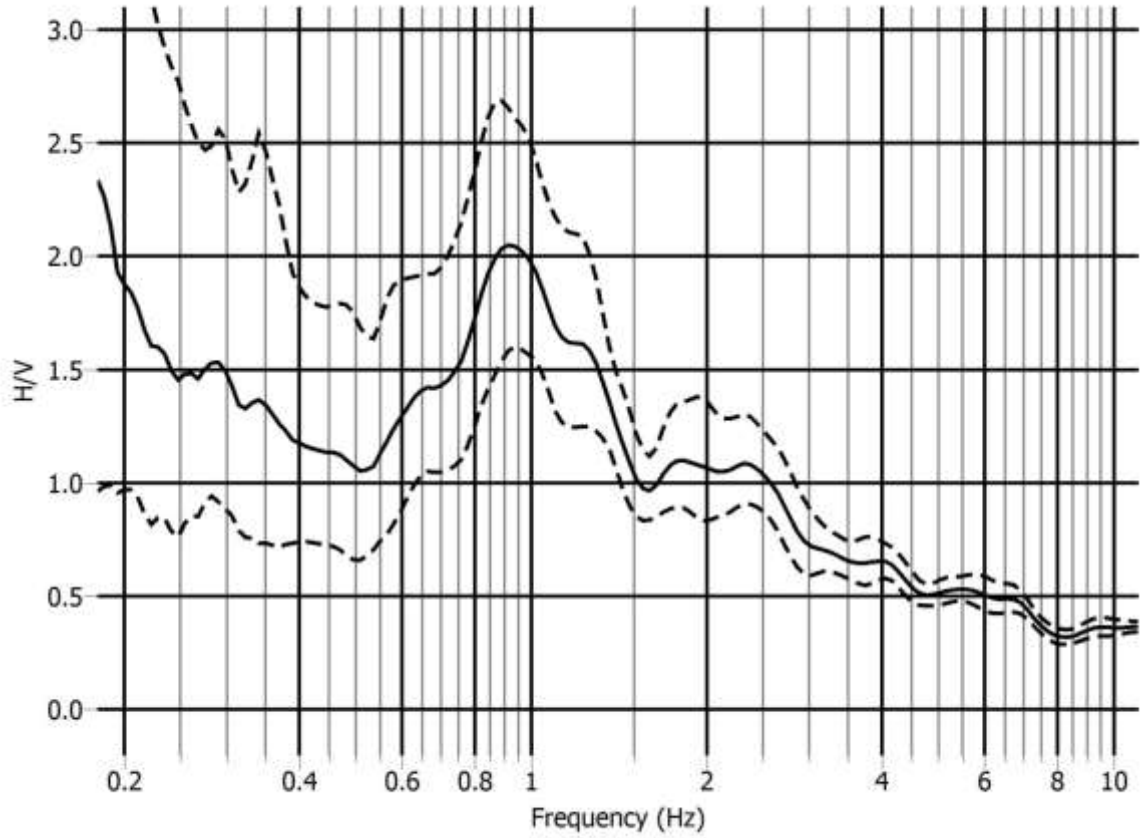

f_0=0.92 Hz; A_0 = 2.05; $A_{H/V}$ = (1.59, 2.65); $\sigma_A(f_0)$ = 1.29 & 1.29

i) f_0=0.92 Hz > (10/40.96=0.24 Hz); ii) n_c > 200; iii) $\sigma_A(f)$ < 2; at 0.46 Hz <f< 1.84 Hz

Satisfies all three criteria of Reliable H/V Curve

i) Between 0.23 to 0.92 Hz, $A_{H/V}(f^-) > A_0/2$, Not satisfy

ii) Between 0.92 to 3.68 Hz, $A_{H/V}(f^+) < A_0/2$

iii) $A_0 > 2.0$

iv) Between 0.874 Hz to 0.966 Hz, f_{peak} = (0.94 Hz, 0.89 Hz)

v) $\sigma_f = 0.144 > \varepsilon(f_0) = 0.138$, Not satisfy

vi) $\sigma_A(f_0) = 1.29 < \Theta(f_0) = 2$

Satisfies four out of six criteria of Clear H/V Peak

Reliable curve and Unclear broad low frequency peak

MT27: Gulshan DRS (23°47'33.1"N, 90°24'54.4"E)
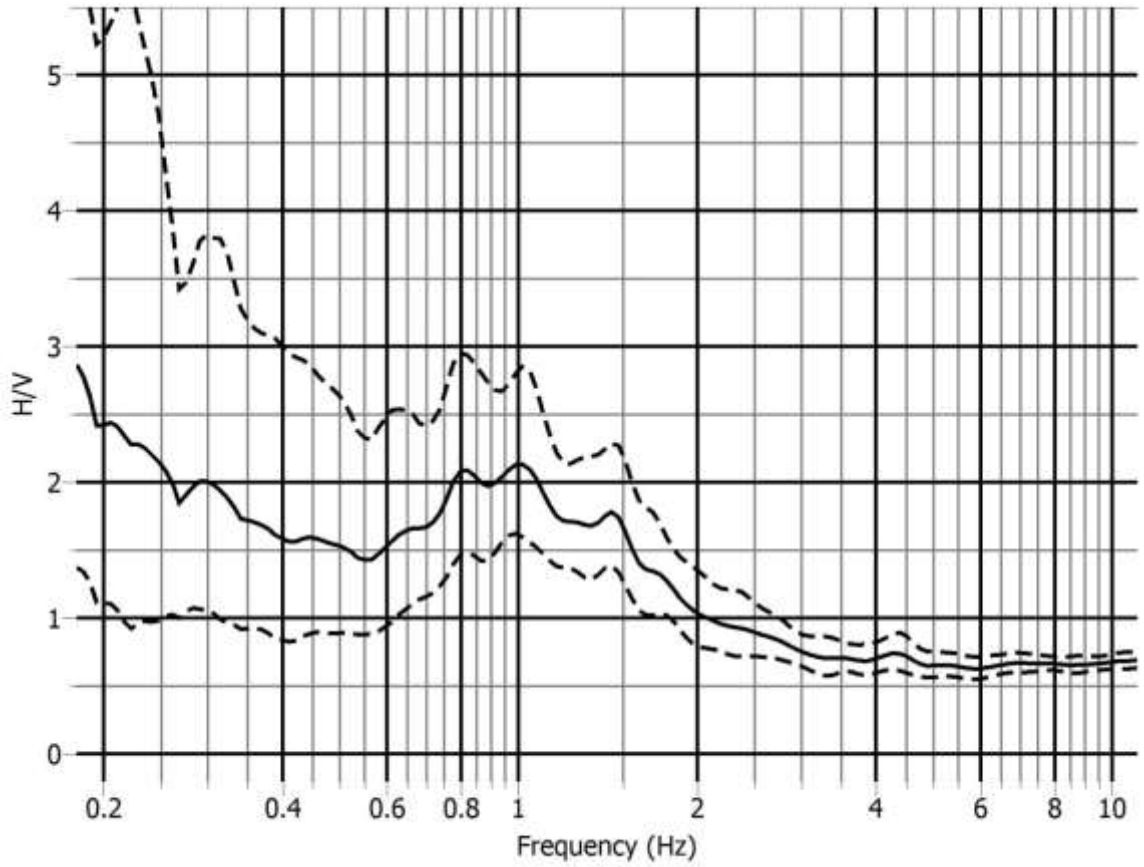
f_0=1.0 Hz; A_0 =2.1; $A_{H/V}$ = (1.6,2.75); $\sigma_A(f_0)$ = 1.31 & 1.31
i) f_0=1.0 Hz > (10/40.96=0.24 Hz); ii) n_c > 200; iii) $\sigma_A(f)$ < 2; at 0.50 Hz <f< 2.0 Hz **Satisfies all three criteria of Reliable H/V Curve**
i) Between 0.25 to 1.0 Hz, $A_{H/V}(f^-) > A_0/2$, Not satisfy ii) Between 1.0 to 4.0 Hz, $A_{H/V}(f^+) < A_0/2$ iii) $A_0 > 2.0$ iv) Between 0.95 Hz to 1.05 Hz, f_{peak} = (0.98 Hz, 1.01 Hz) v) $\sigma_f = 0.173 > \varepsilon(f_0) = 0.15$, Not satisfy vi) $\sigma_A(f_0) = 1.31 < \Theta(f_0) = 2$ **Satisfies four out of six criteria of Clear H/V Peak**
Reliable curve and Unclear broad peak frequency of 1.0 Hz.

MT28: Tejgaon TBS Gulshan TBS (23°46'24.0"N, 90°25'01.2"E)

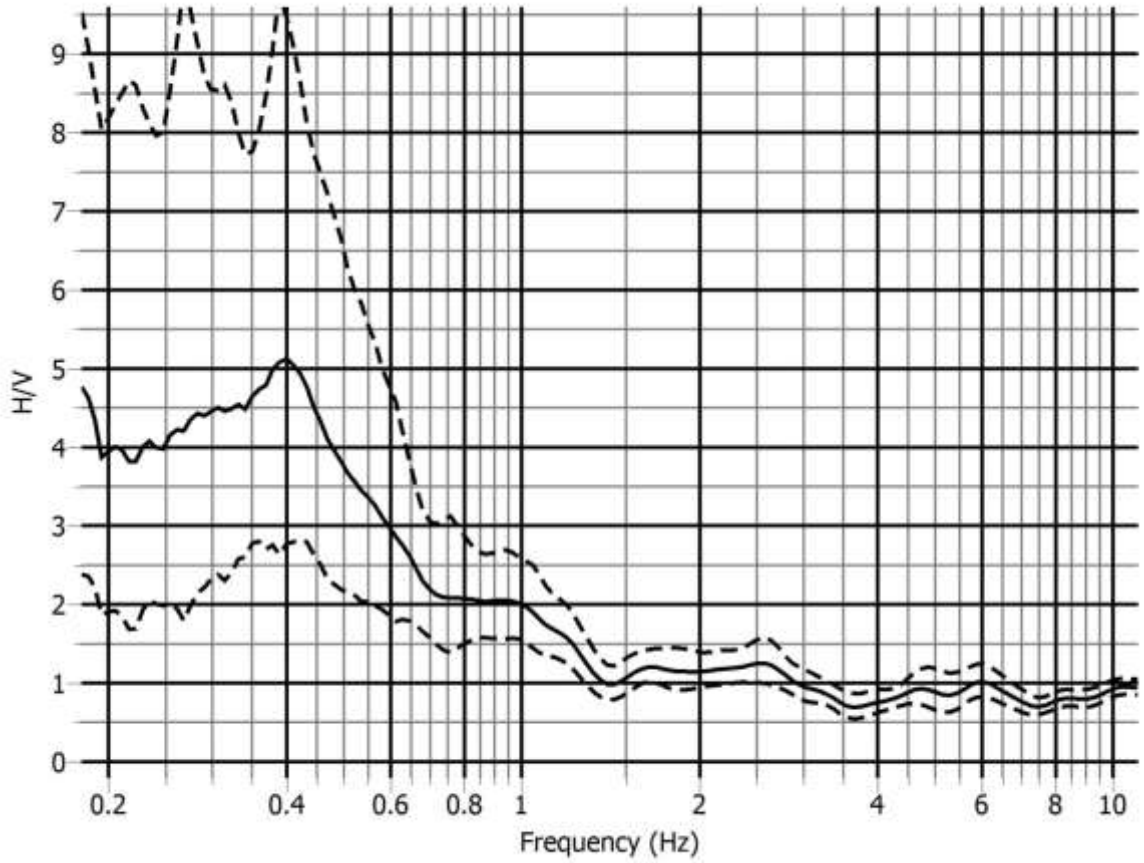

f_0=0.40 Hz; A_0 = 5.12; $A_{H/V}$ = (2.76,9.48); $\sigma_A(f_0)$ = 1.85 & 1.85

i) f_0=0.40 Hz > (10/40.96=0.24 Hz); ii) n_c > 200; iii) $\sigma_A(f)$ < 3; at 0.20 Hz <f< 0.80 Hz

Satisfies all three criteria of Reliable H/V Curve

i) Between 0.10 to 0.40 Hz, $A_{H/V}(f^-) > A_0/2$, Not satisfy

ii) Between 0.40 to 1.60 Hz, $A_{H/V}(f^+) < A_0/2$

iii) $A_0 > 2.0$

iv) Between 0.38 Hz to 0.42 Hz, f_{peak} = (0.42 Hz, 0.39 Hz)

v) $\sigma_f = 0.063 < \varepsilon(f_0) = 0.080$

vi) $\sigma_A(f_0) = 1.85 < \Theta(f_0) = 2.5$

Satisfies five out of six criteria of Clear H/V Peak

Reliable curve and Unclear low frequency peak

MT29: Nabisco (Phoenix) (23°46'16.1"N, 90°24'03.9"E)
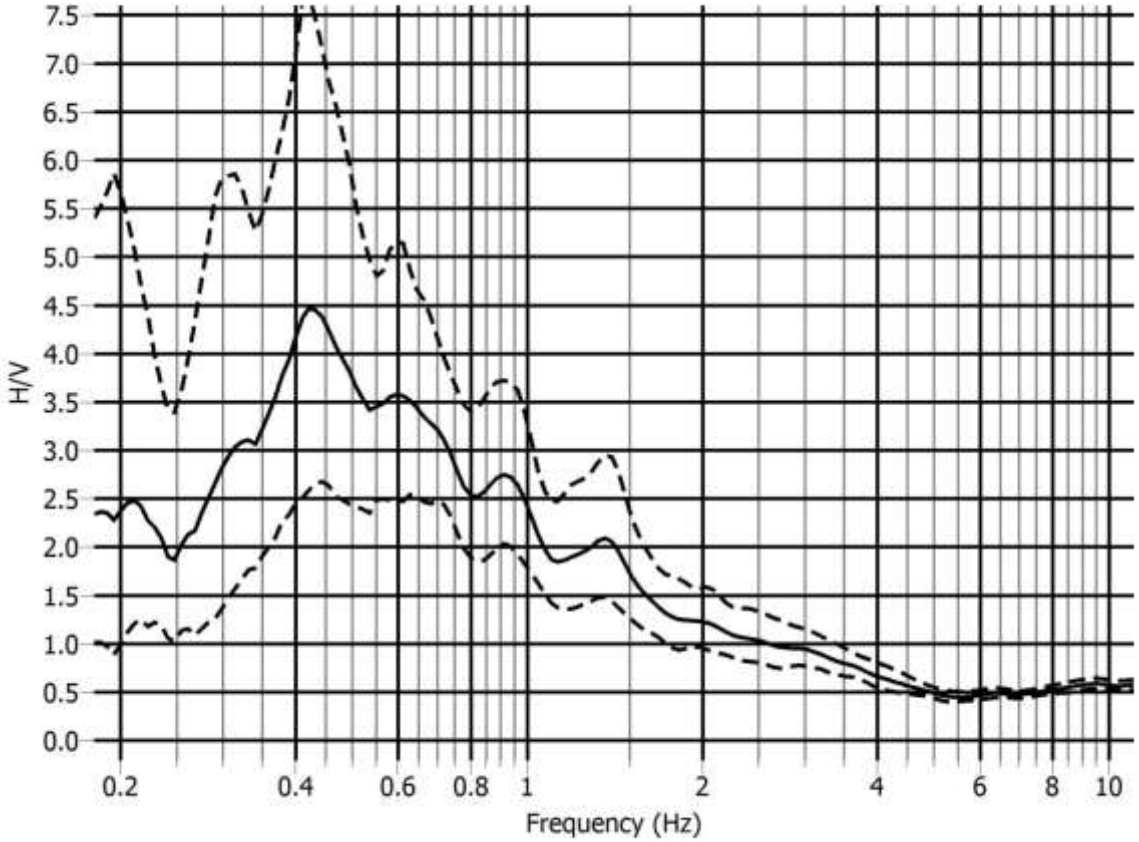
f_0=0.42 Hz; A_0 = 4.5; $A_{H/V}$ = (2.65,7.64); $\sigma_A(f_0)$ = 1.70 & 1.70
i) f_0=0.42 Hz > (10/40.96=0.24 Hz); ii) n_c > 200; iii) $\sigma_A(f)$ < 3; at 0.21 Hz <f< 0.84 Hz **Satisfies all three criteria of Reliable H/V Curve**
i) Between 0.105 to 0.42 Hz, $A_{H/V}(f^-) < A_0/2$ ii) Between 0.42 to 1.68 Hz, $A_{H/V}(f^+) < A_0/2$ iii) $A_0 > 2.0$ iv) Between 0.399 Hz to 0.441 Hz, f_{peak} = (0.44 Hz, 0.42 Hz) v) $\sigma_f = 0.082 < \varepsilon(f_0) = 0.084$ vi) $\sigma_A(f_0) = 1.70 < \Theta(f_0) = 2.5$ **Satisfies six out of six criteria of Clear H/V Peak**
Reliable curve and Clear low frequency peak

MT30: BUTEX (23°45'37.8"N, 90°23'58.6"E)

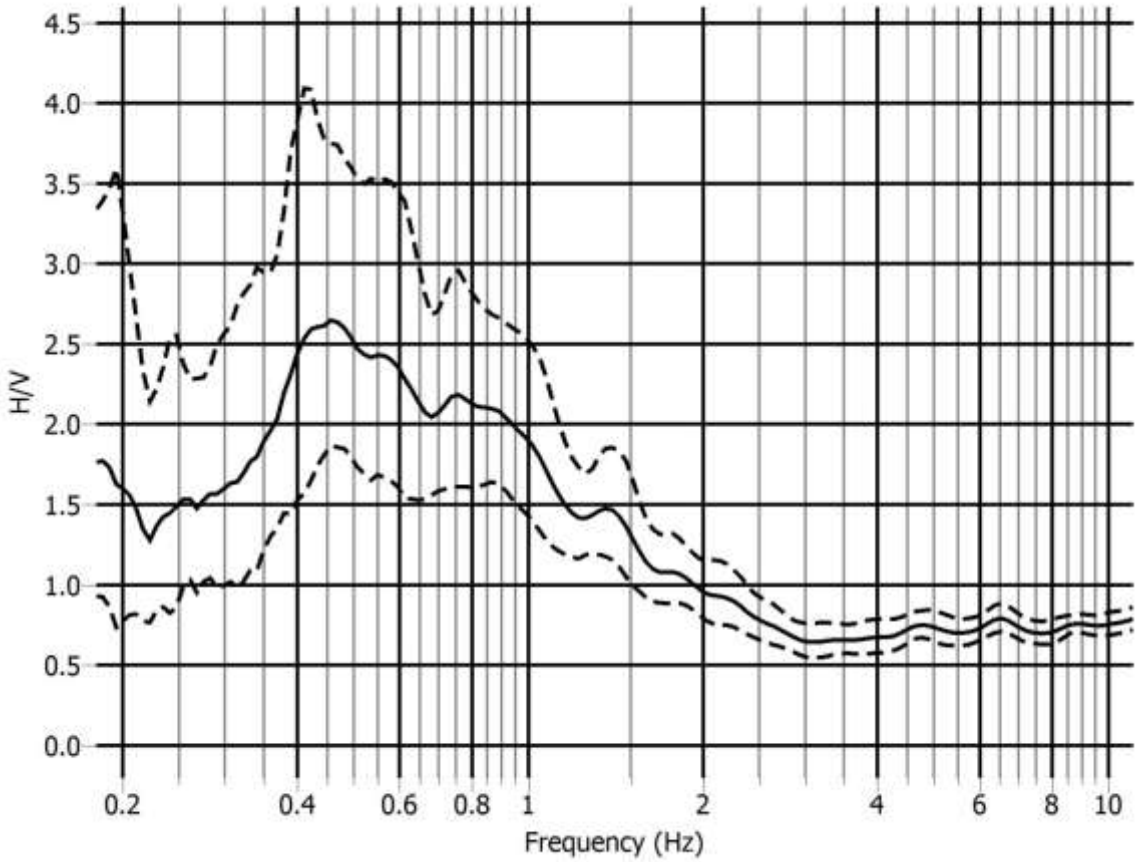

f_0=0.46 Hz; A_0 =2.66; $A_{H/V}$ = (1.76,4.03); $\sigma_A(f_0)$ = 1.51 & 1.51

i) f_0=0.46 Hz > (10/41=0.24 Hz); ii) n_c > 200; iii) $\sigma_A(f)$ < 3; at 0.23 Hz <f< 0.92 Hz

Satisfies all three criteria of Reliable H/V Curve

i) Between 0.115 to 0.46 Hz, $A_{H/V}(f^-) > A_0/2$, Not satisfy

ii) Between 0.46 to 1.84 Hz, $A_{H/V}(f^+) < A_0/2$

iii) $A_0 > 2.0$

iv) Between 0.437 Hz to 0.483 Hz, f_{peak} = (0.46 Hz, 0.42 Hz), Not Satisfy

v) $\sigma_f = 0.09 < \varepsilon(f_0) = 0.092$

vi) $\sigma_A(f_0) = 1.51 < \Theta(f_0) = 2.5$

Satisfies four out of six criteria of Clear H/V Peak

Reliable curve and Unclear low frequency peak

MT31: Mirpur Bangla College (23°47'05.1"N, 90°21'11.6"E)

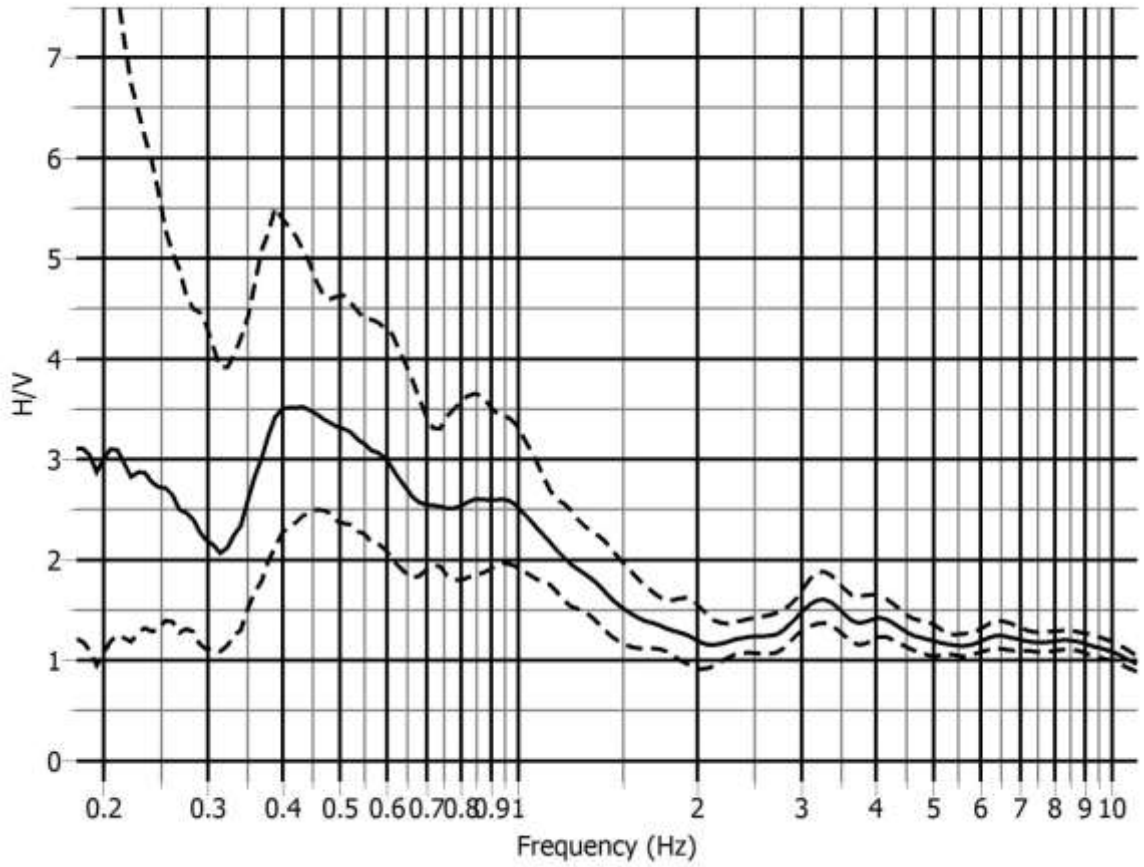

f_0=0.42 Hz; A_0 = 3.5; $A_{H/V}$ = (2.24,5.48) $\sigma_A(f_0)$ = 1.56 & 1.56

i) f_0=0.42 Hz > (10/41=0.24 Hz); ii) n_c > 200; iii) $\sigma_A(f)$ < 3; at 0.21 Hz <f< 0.84 Hz

Satisfies all three criteria of Reliable H/V Curve

i) Between 0.105 to 0.42 Hz, $A_{H/V}(f^-) > A_0/2$, Not Satisfy

ii) Between 0.42 to 1.68 Hz, $A_{H/V}(f^+) < A_0/2$

iii) $A_0 > 2.0$

iv) Between 0.399 Hz to 0.441 Hz, f_{peak} = (0.45 Hz, 0.39), Not Satisfy

v) $\sigma_f = 0.089 > \varepsilon(f_0) = 0.086$, Not satisfy

vi) $\sigma_A(f_0) = 1.56 < \Theta(f_0) = 2.5$

Satisfies three out of six criteria of Clear H/V Peak

Reliable curve and Unclear broad low frequency peak

MT32: HBRI (23°46'52.5"N, 90°21'11.7"E)

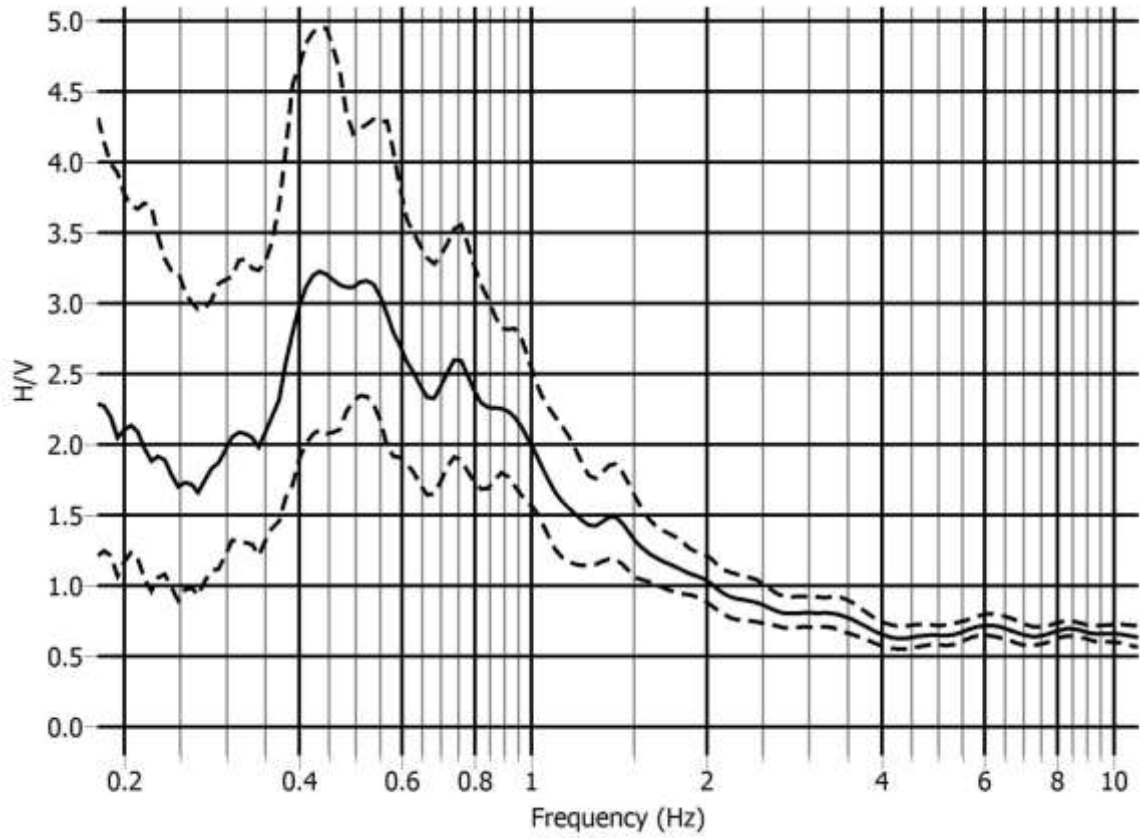

f_0=0.44 Hz; A_0 = 3.20; $A_{H/V}$ = (2.08, 4.92); $\sigma_A(f_0)$ = 1.54 & 1.54

i) f_0=0.44 Hz > (10/40.96=0.24 Hz); ii) n_c > 200; iii) $\sigma_A(f)$ < 3; at 0.22 Hz <f< 0.88 Hz

Satisfies all three criteria of Reliable H/V Curve

i) Between 0.11 to 0.44 Hz, $A_{H/V}(f^-) > A_0/2$, Not satisfy

ii) Between 0.44 to 1.76 Hz, $A_{H/V}(f^+) < A_0/2$

iii) $A_0 > 2.0$

iv) Between 0.418 Hz to 0.462 Hz, f_{peak} = (0.43 Hz, 0.45 Hz)

v) $\sigma_f = 0.073 < \varepsilon(f_0) = 0.088$

vi) $\sigma_A(f_0) = 1.54 < \Theta(f_0) = 2.5$

Satisfies five out of six criteria of Clear H/V Peak

Reliable curve and Unclear low frequency peak

MT33: Mirpur Mazar Road DRS (23°47'35.3"N, 90°21'01.3"E)

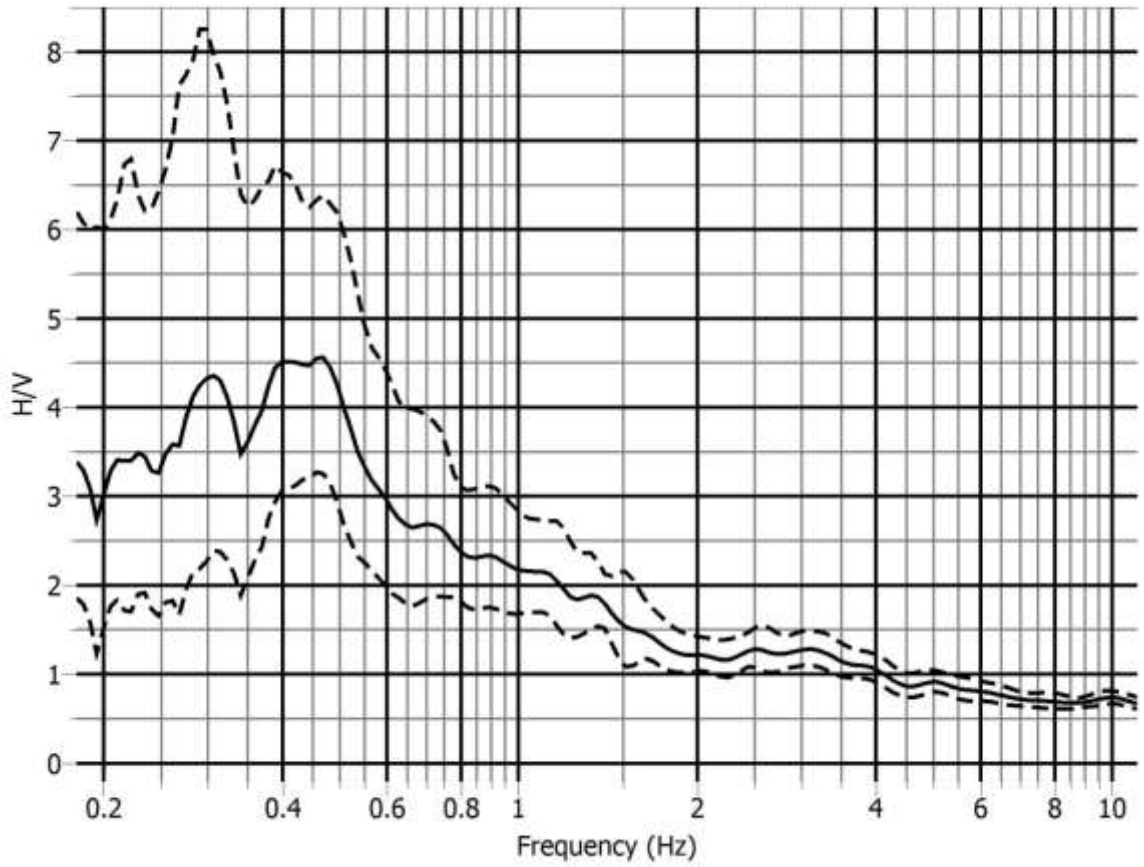

f_0=0.46 Hz; A_0 = 4.55; $A_{H/V}$ = (3.25,6.37); $\sigma_A(f_0)$ = 1.40 & 1.40

i) f_0=0.46 Hz > (10/40.96=0.24 Hz); ii) n_c > 200; iii) $\sigma_A(f)$ < 3; at 0.23 Hz <f< 0.92 Hz

Satisfies all three criteria of Reliable H/V Curve

i) Between 0.115 to 0.46 Hz, $A_{H/V}(f^-) > A_0/2$, Not satisfy

ii) Between 0.46 to 1.84 Hz, $A_{H/V}(f^+) < A_0/2$

iii) $A_0 > 2.0$

iv) Between 0.437 Hz to 0.483 Hz, f_{peak} = (0.46 Hz, 0.46 Hz)

v) $\sigma_f = 0.081 < \varepsilon(f_0) = 0.086$

vi) $\sigma_A(f_0) = 1.40 < \Theta(f_0) = 2.5$

Satisfies five out of six criteria of Clear H/V Peak

Reliable curve and Unclear low frequency peak

MT34: Amin Bazar DRS (23°47'20.7"N, 90°19'05.8"E)

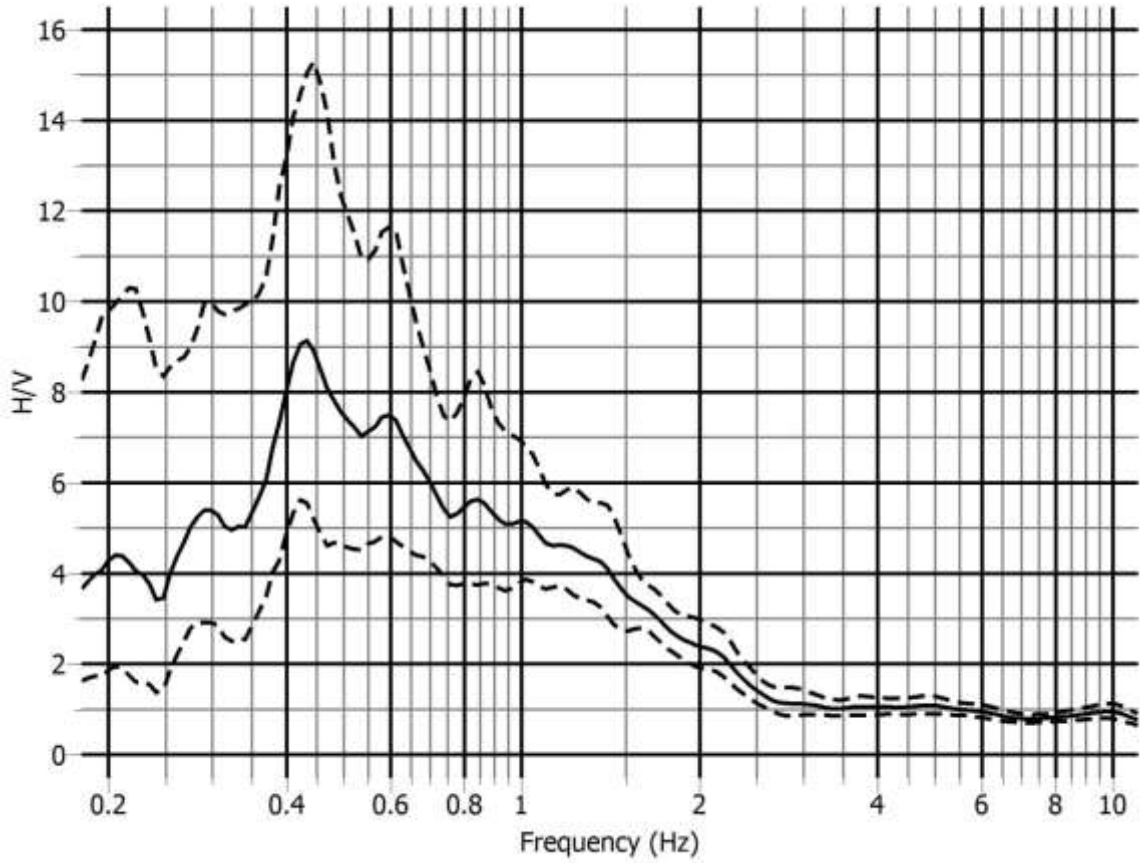

f_0=0.44 Hz; A_0 = 9.05; $A_{H/V}$ = (5.42,15.10); $\sigma_A(f_0)$ = 1.67 & 1.67

i) f_0=0.44 Hz > (10/40.96=0.24 Hz); ii) n_c > 200; iii) $\sigma_A(f)$ < 3; at 0.22 Hz <f< 0.88 Hz

Satisfies all three criteria of Reliable H/V Curve

i) Between 0.11 to 0.44 Hz, $A_{H/V} < A_0/2$

ii) Between 0.44 to 1.76 Hz, $A_{H/V} < A_0/2$

iii) $A_0 > 2.0$

iv) Between 0.418 Hz to 0.462 Hz, f_{peak} = (0.42 Hz, 0.447 Hz)

v) $\sigma_f = 0.066 < \varepsilon(f_0) = 0.088$

vi) $\sigma_A(f_0) = 1.67 < \Theta(f_0) = 2.5$

Satisfies six out of six criteria of Clear H/V Peak

Reliable curve and Clear low frequency peak

MT35: SMCH (23°46'06.8"N, 90°22'09.1"E)
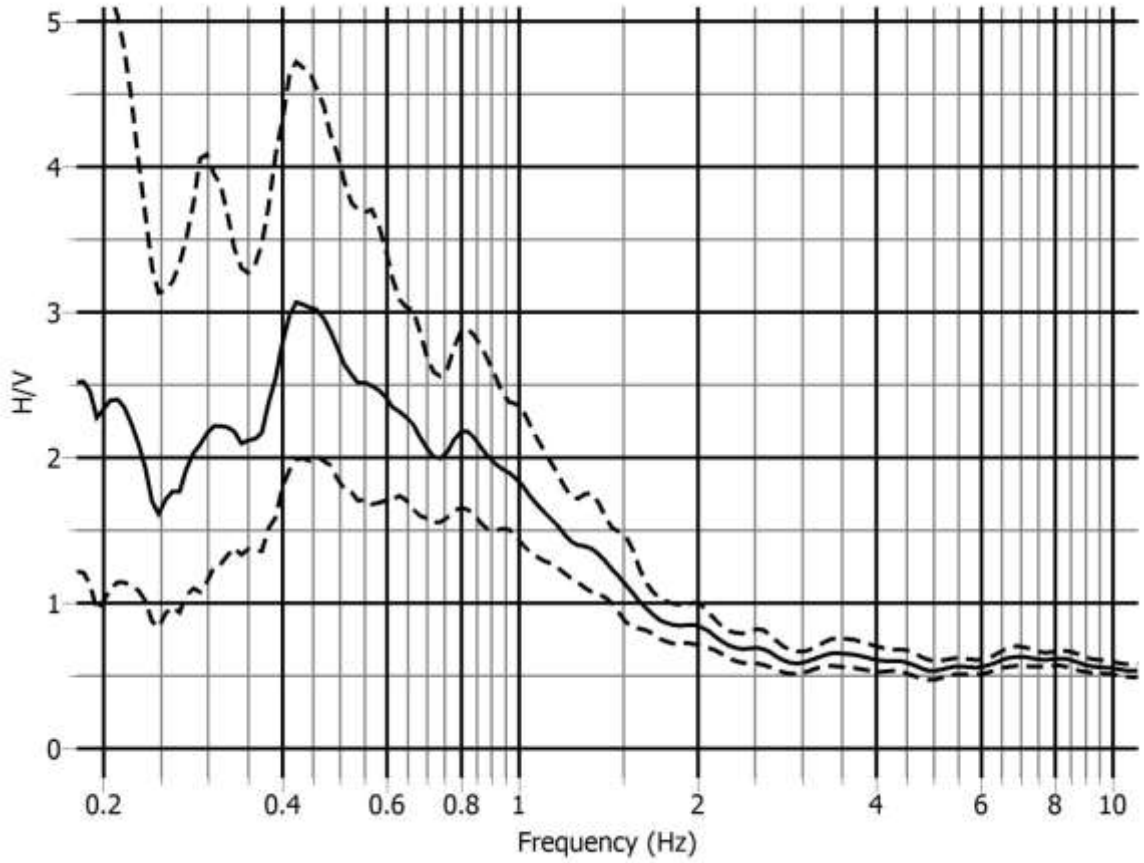
f_0=0.42 Hz; A_0 = 3.03; $A_{H/V}$ = (1.95,4.71); $\sigma_A(f_0)$ = 1.55 & 1.55
i) f_0=0.42 Hz > (10/40.96=0.24 Hz); ii) n_c > 200; iii) $\sigma_A(f)$ < 3; at 0.21 Hz <f< 0.84 Hz **Satisfies all three criteria of Reliable H/V Curve**
i) Between 0.105 to 0.42 Hz, $A_{H/V}(f^-) > A_0/2$, Not satisfy ii) Between 0.42 to 1.68 Hz, $A_{H/V}(f^+) < A_0/2$ iii) $A_0 > 2.0$ iv) Between 0.399 Hz to 0.441 Hz, f_{peak} = (0.43 Hz, 0.42 Hz) v) $\sigma_f = 0.092 > \varepsilon(f_0) = 0.084$, Not satisfy vi) $\sigma_A(f_0) = 1.55 < \Theta(f_0) = 2.5$ **Satisfies four out of six criteria of Clear H/V Peak**
Reliable curve and Unclear broad low frequency peak

MT36: BIM (23°45'24.2"N, 90°22'30.6"E)

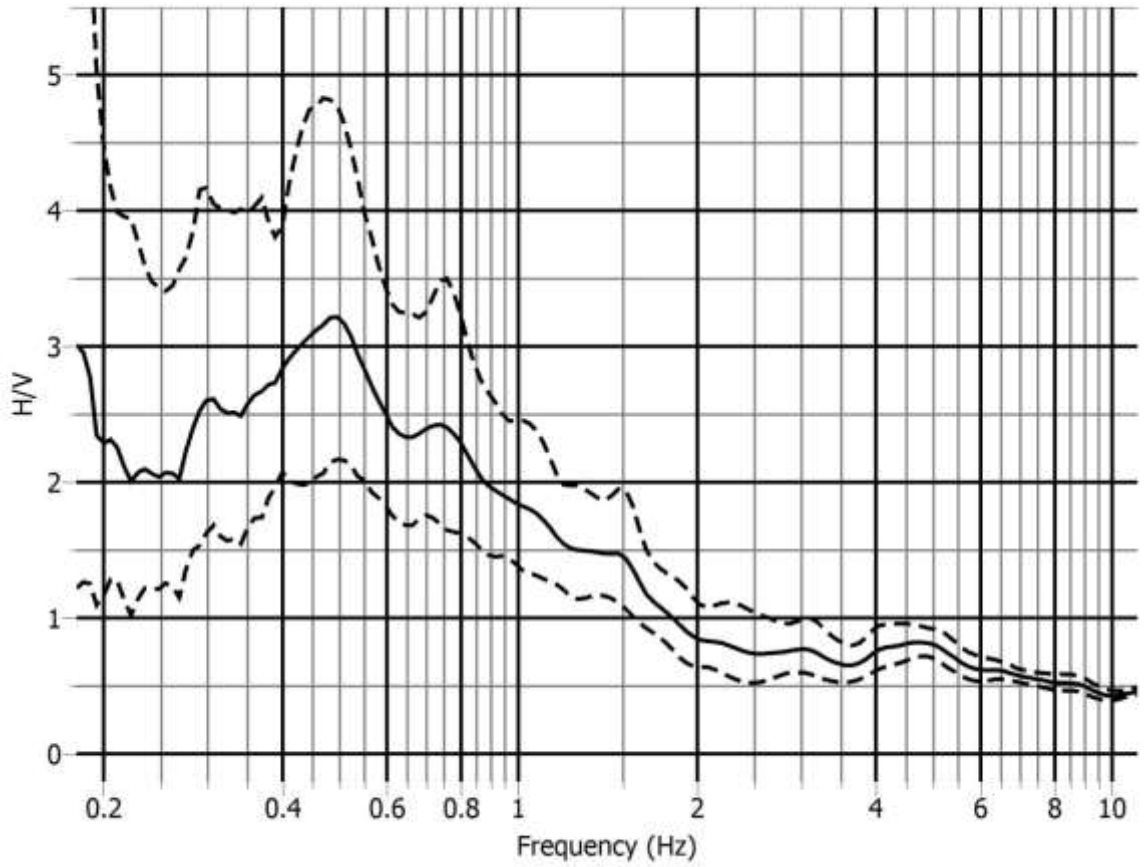

f_0=0.48 Hz; A_0 = 3.18; $A_{H/V}$ = (2.09,4.82); $\sigma_A(f_0)$ = 1.52 & 1.52

i) f_0=0.48 Hz > (10/40.96 = 0.24 Hz); ii) n_c > 200; iii) $\sigma_A(f)$ < 3; at 0.24 Hz <f< 0.96 Hz

Satisfies all three criteria of Reliable H/V Curve

i) Between 0.12 to 0.48 Hz, $A_{H/V}(f^-) > A_0/2$, Not satisfy

ii) Between 0.48 to 1.92 Hz, $A_{H/V}(f^+) < A_0/2$

iii) $A_0 > 2.0$

iv) Between 0.456 Hz to 0.504 Hz, f_{peak} = (0.50 Hz, 0.475 Hz)

v) $\sigma_f = 0.083 < \varepsilon(f_0) = 0.096$

vi) $\sigma_A(f_0) = 1.52 < \Theta(f_0) = 2.5$

Satisfies five out of six criteria of Clear H/V Peak

Reliable curve and Unclear low frequency peak

MT37: Dhanmondi Play Ground (23°44'45.8"N, 90°22'52.1"E)
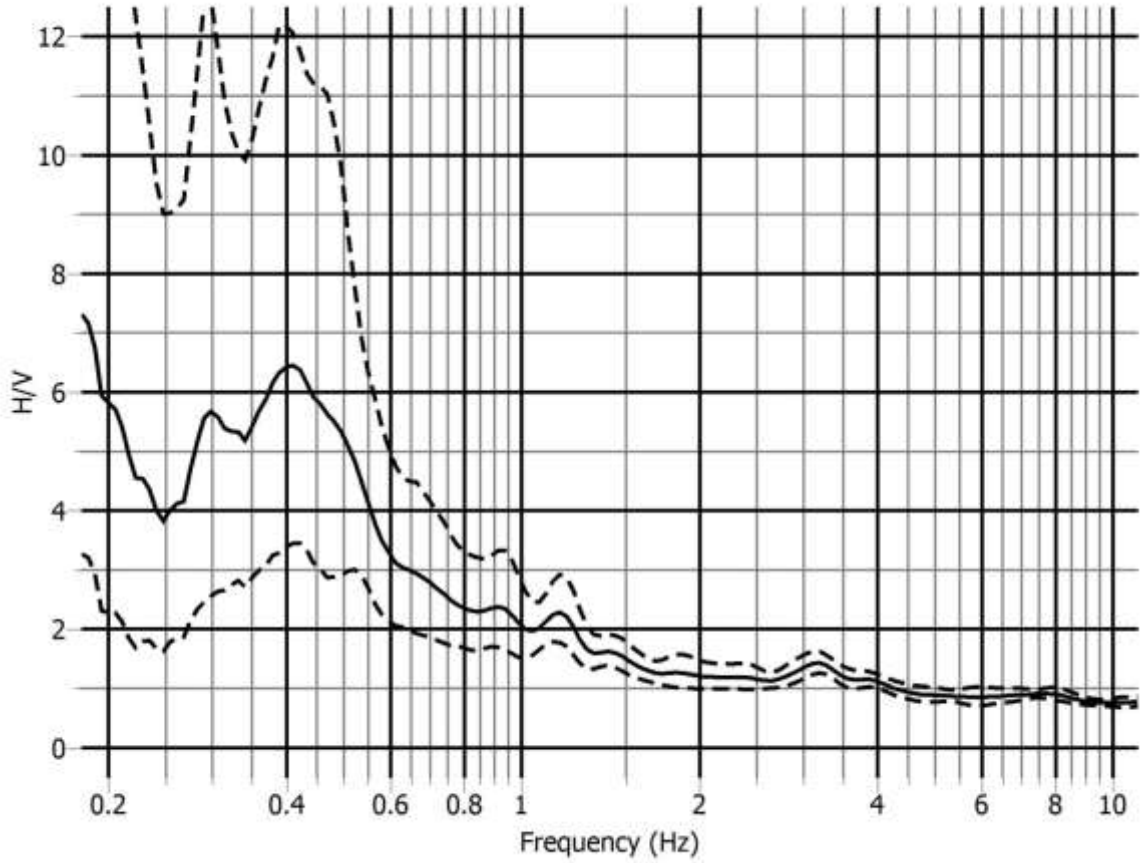
f_0=0.41 Hz; A_0 =6.45; $A_{H/V}$ = (3.44,12.10); $\sigma_A(f_0)$ = 1.87 & 1.87
i) f_0=0.41 Hz > (10/41=0.24 Hz); ii) n_c > 200; iii) $\sigma_A(f)$ < 3; at 0.205 Hz <f< 0.82 Hz **Satisfies all three criteria of Reliable H/V Curve**
i) Between 0.1025 to 0.41 Hz, $A_{H/V}(f^-) > A_0/2$, Not satisfy ii) Between 0.41 to 1.64 Hz, $A_{H/V}(f^+) < A_0/2$ iii) $A_0 > 2.0$ iv) Between 0.3895 Hz to 0.4305 Hz, f_{peak} = (0.42 Hz, 0.39 Hz) v) $\sigma_f = 0.079 < \varepsilon(f_0) = 0.082$ vi) $\sigma_A(f_0) = 1.87 < \Theta(f_0) = 2.5$ **Satisfies five out of six criteria of Clear H/V Peak**
Reliable curve and Unclear low frequency peak

MT38: Sonargaon Hotel (23°45'10.1"N, 90°23'59.5"E)

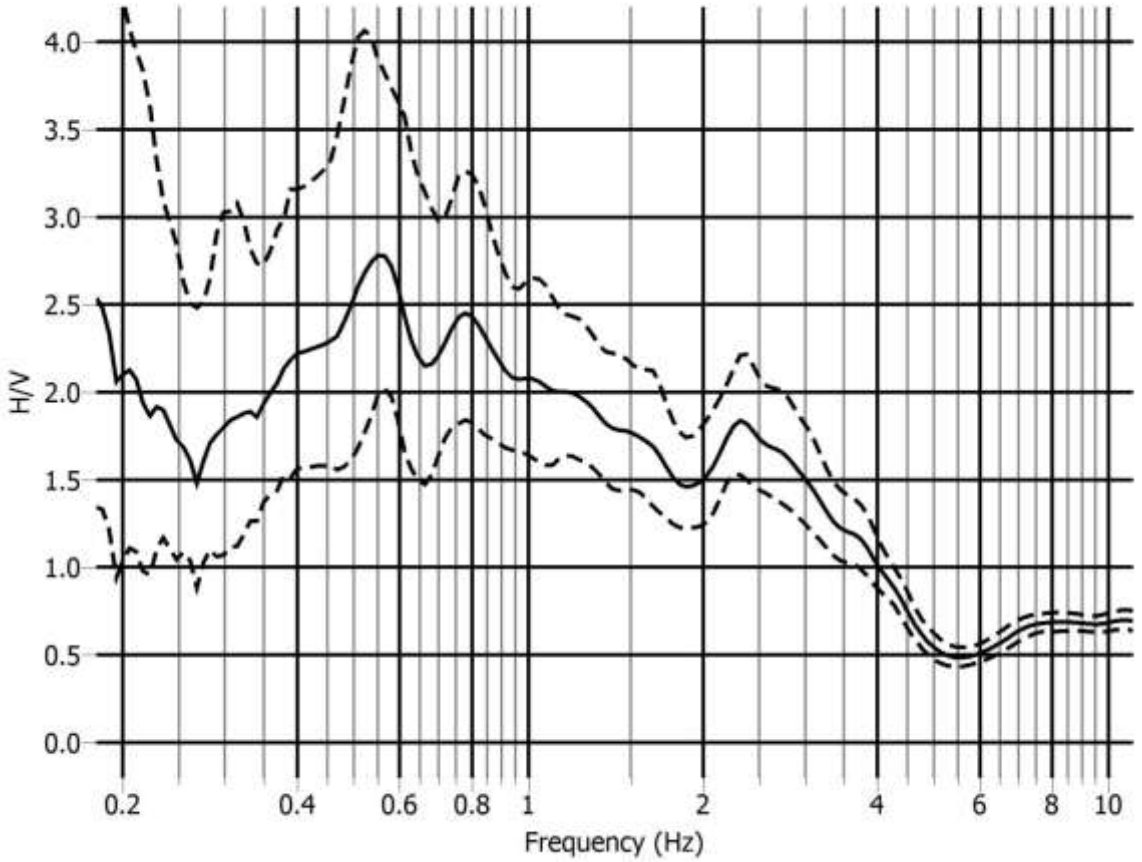

f_0=0.56 Hz; A_0 = 2.75; $A_{H/V}$ = (2.0,4.02); $\sigma_A(f_0)$ = 1.37 & 1.46

i) f_0=0.56 Hz > (10/40.96=0.24 Hz); ii) n_c > 200; iii) $\sigma_A(f)$ < 2; at 0.28 Hz <f< 1.12 Hz

Satisfies all three criteria of Reliable H/V Curve

i) Between 0.14 to 0.56 Hz, $A_{H/V}(f^-) > A_0/2$, Not satisfy

ii) Between 0.56 to 2.24 Hz, $A_{H/V}(f^+) > A_0/2$, Not satisfy

iii) $A_0 > 2.0$

iv) Between 0.532 Hz to 0.588 Hz, f_{peak} = (0.57 Hz, 0.52 Hz), Not satisfy

v) $\sigma_f = 0.122 > \varepsilon(f_0) = 0.084$, Not satisfy

vi) $\sigma_A(f_0) = 1.46 < \Theta(f_0) = 2$

Satisfies two out of six criteria of Clear H/V Peak

Reliable curve and Unclear broad low frequency peak

MT39: Rampura TV Station (23°46'00.1"N, 90°25'28.2"E)

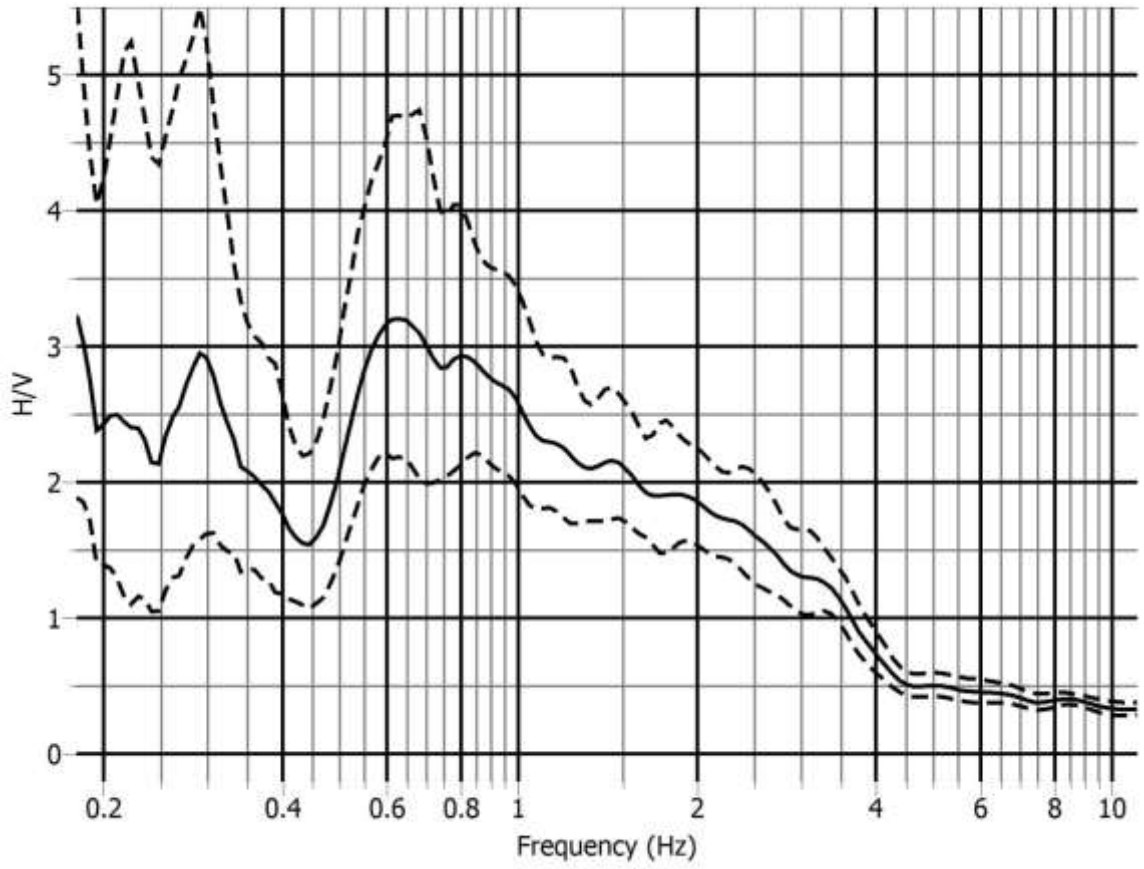

f_0=0.63 Hz; A_0 = 3.13; $A_{H/V}$ = (2.1,4.68); $\sigma_A(f_0)$ = 1.49 & 1.49

i) f_0=0.63 Hz > (10/40.96=0.24 Hz); ii) n_c > 200; iii) $\sigma_A(f)$ < 2; at 0.315 Hz <f< 1.26 Hz

Satisfies all three criteria of Reliable H/V Curve

i) Between 0.1575 to 0.63 Hz, $A_{H/V}(f^-) < A_0/2$, Not satisfy

ii) Between 0.63 to 2.52 Hz, $A_{H/V}(f^+) < A_0/2$, Not satisfy

iii) $A_0 > 2.0$

iv) Between 0.598 Hz to 0.661 Hz, f_{peak} = (0.60 Hz, 0.62 Hz)

v) $\sigma_f = 0.112 > \varepsilon(f_0) = 0.0945$, Not satisfy

vi) $\sigma_A(f_0) = 1.49 < \Theta(f_0) = 2$

Satisfies three out of six criteria of Clear H/V Peak

Reliable curve and Unclear broad low frequency peak

MT40: Teachers Training College (23°44'11.3"N, 90°23'01.6"E)
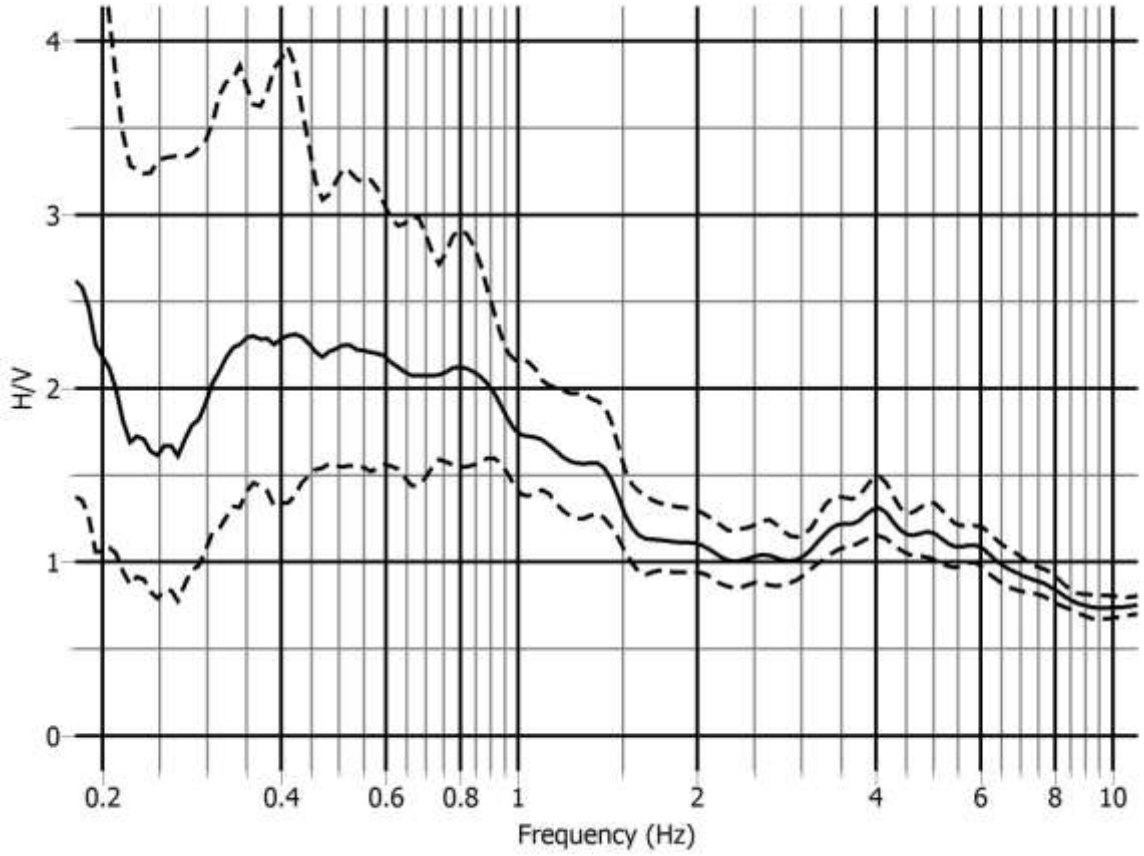
f_0=0.36 Hz; A_0 = 2.31; $A_{H/V}$ = (1.43,3.74); $\sigma_A(f_0)$ = 1.62 & 1.62
i) f_0=0.36 Hz > (10/40.96=0.24 Hz); ii) n_c > 200; iii) $\sigma_A(f)$ < 3; at 0.18 Hz <f< 0.72 Hz **Satisfies all three criteria of Reliable H/V Curve**
i) Between 0.09 to 0.36 Hz, $A_{H/V}(f^-) > A_0/2$, Not satisfy ii) Between 0.36 to 1.44 Hz, $A_{H/V}(f^+) > A_0/2$, Not satisfy iii) $A_0 > 2.0$ iv) Between 0.342 Hz to 0.378 Hz, f_{peak} = (0.36 Hz, 0.34 Hz) v) $\sigma_f = 0.09 > \varepsilon(f_0) = 0.072$, Not satisfy vi) $\sigma_A(f_0) = 1.61 < \Theta(f_0) = 2.5$ **Satisfies three out of six criteria of Clear H/V Peak**
Reliable curve and Unclear broad low frequency peak

MT41: Elephant Road (Mercantile Bank) (23°44'20.3"N, 90°23'14.3"E)

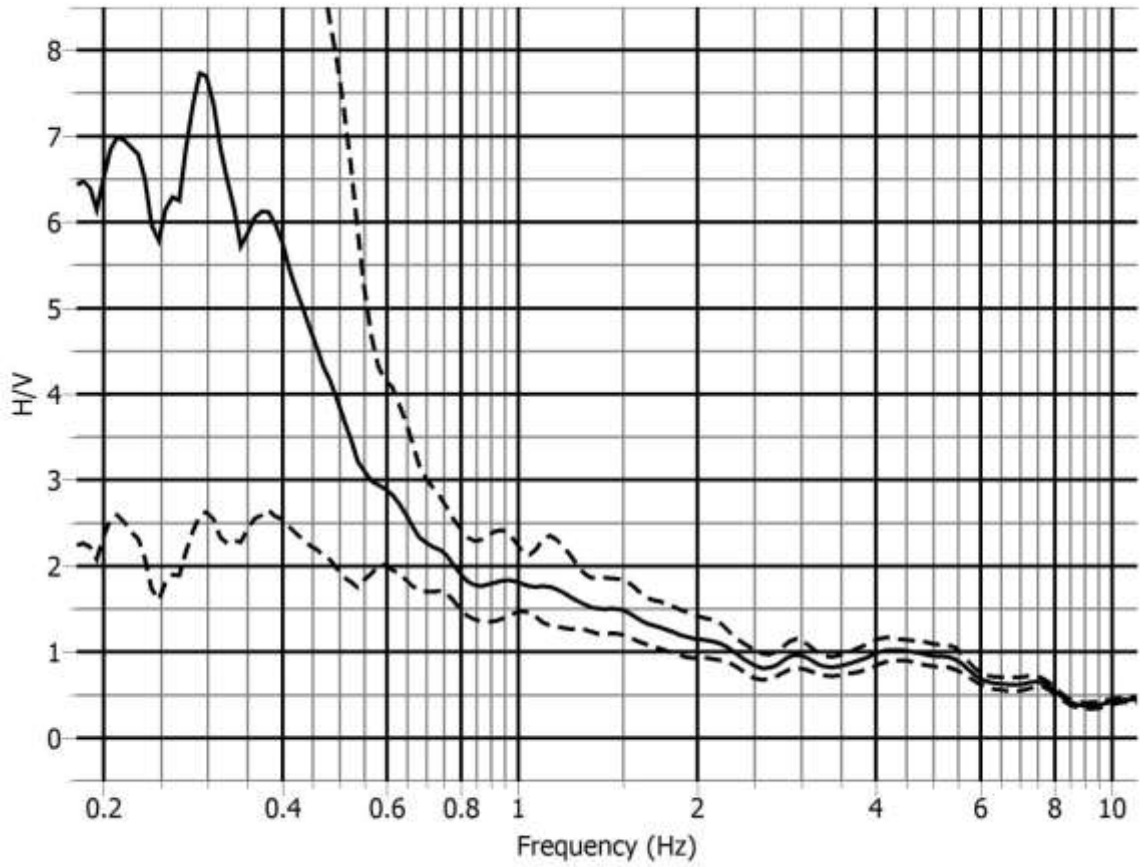

No peak has been found due to stiff soil stratum overlaying very hard soil stratum or bedrock at unknown depth

MT42: Old RHD HQ (23°44'01.6"N, 90°24'08.0"E)

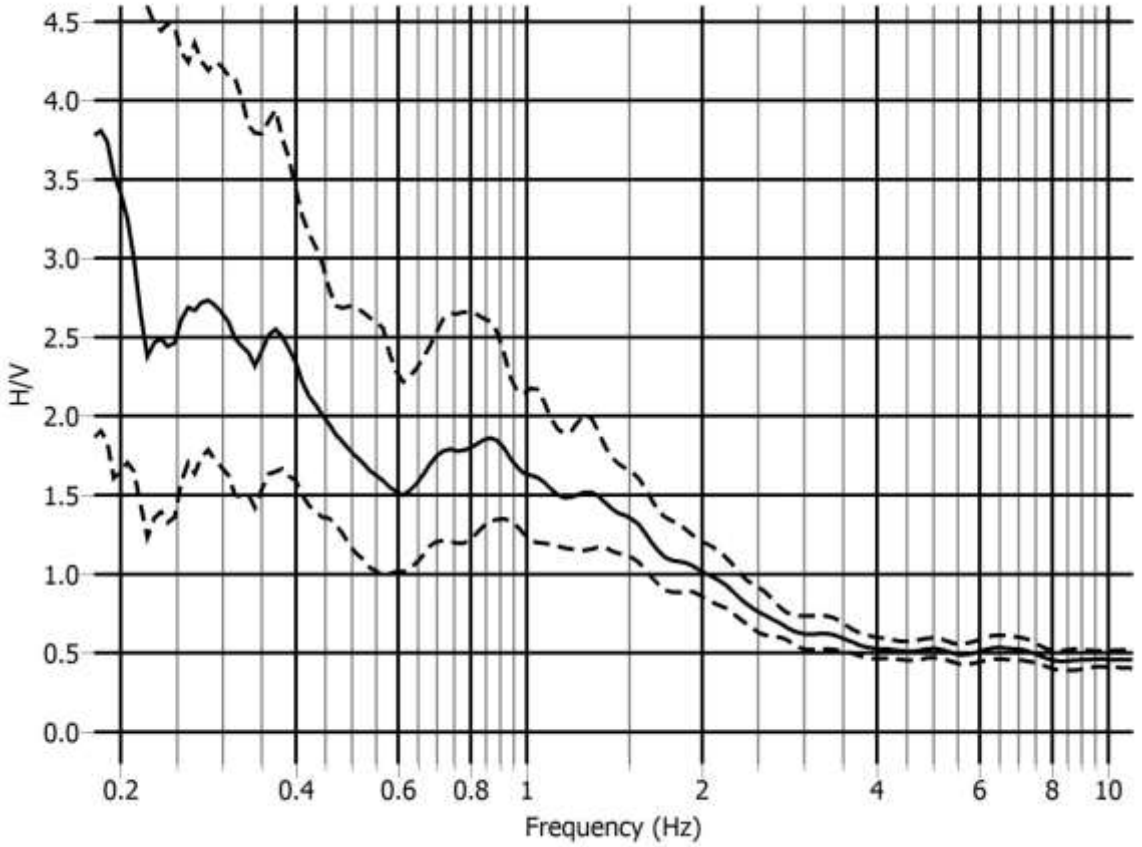

No peak has been found due to stiff soil stratum overlaying very hard soil stratum or bedrock at unknown depth

MT43: Jadughor (23°44'17.4"N, 90°23'41.2"E)

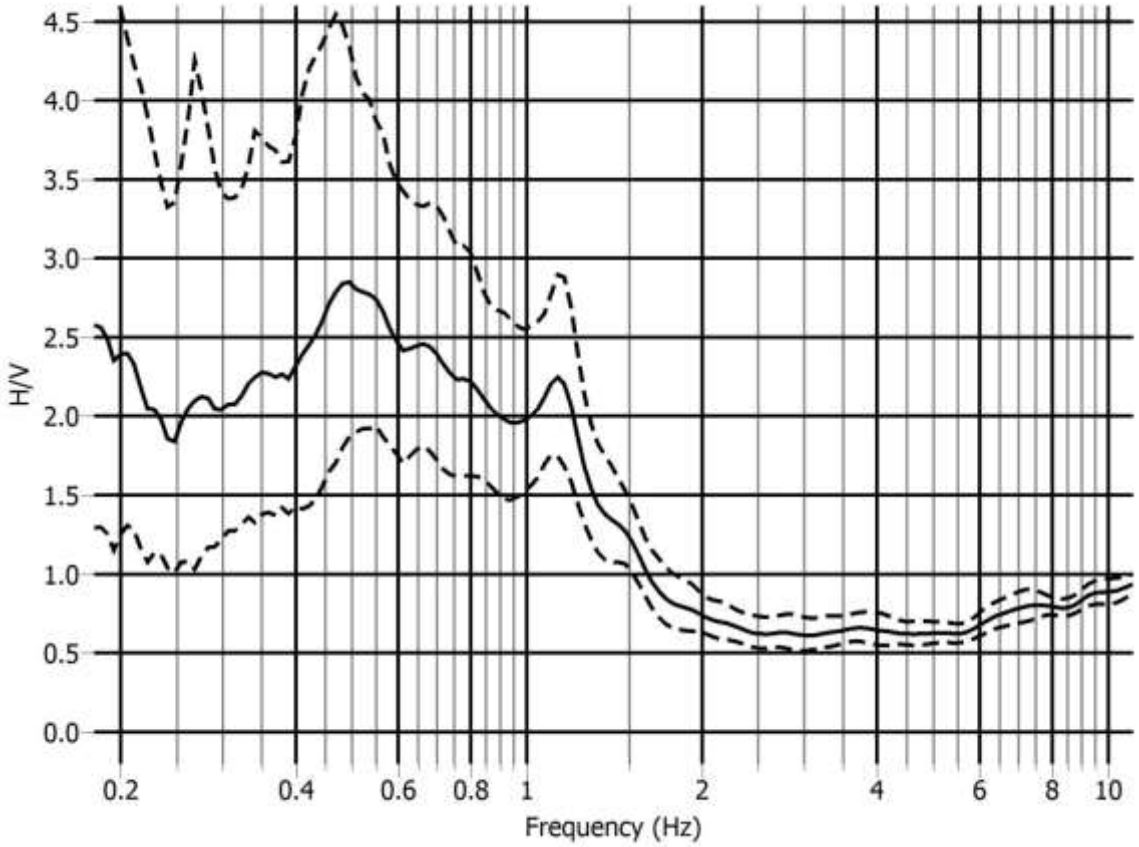

f_0=0.49 Hz; A_0 = 2.85; $A_{H/V}$ = (1.80, 4.51); $\sigma_A(f_0)$ = 1.58 & 1.58

i) f_0=0.49 Hz > (10/40.96=0.24 Hz); ii) n_c > 200; iii) $\sigma_A(f)$ < 3; at 0.245 Hz <f< 0.98 Hz

Satisfies all three criteria of Reliable H/V Curve

i) Between 0.123 to 0.49 Hz, $A_{H/V}(f^-) > A_0/2$, Not satisfy

ii) Between 0.49 to 1.96 Hz, $A_{H/V}(f^+) < A_0/2$

iii) $A_0 > 2.0$

iv) Between 0.466 Hz to 0.515 Hz, f_{peak} = (0.54 Hz, 0.47 Hz), Not satisfy

v) $\sigma_f = 0.107 > \varepsilon(f_0) = 0.098$, Not satisfy

vi) $\sigma_A(f_0) = 1.58 < \Theta(f_0) = 2.5$

Satisfies three out of six criteria of Clear H/V Peak

Reliable curve and Unclear broad low frequency peak

MT44: Curzon Hall (23°43'41.0"N, 90°24'07.2"E)

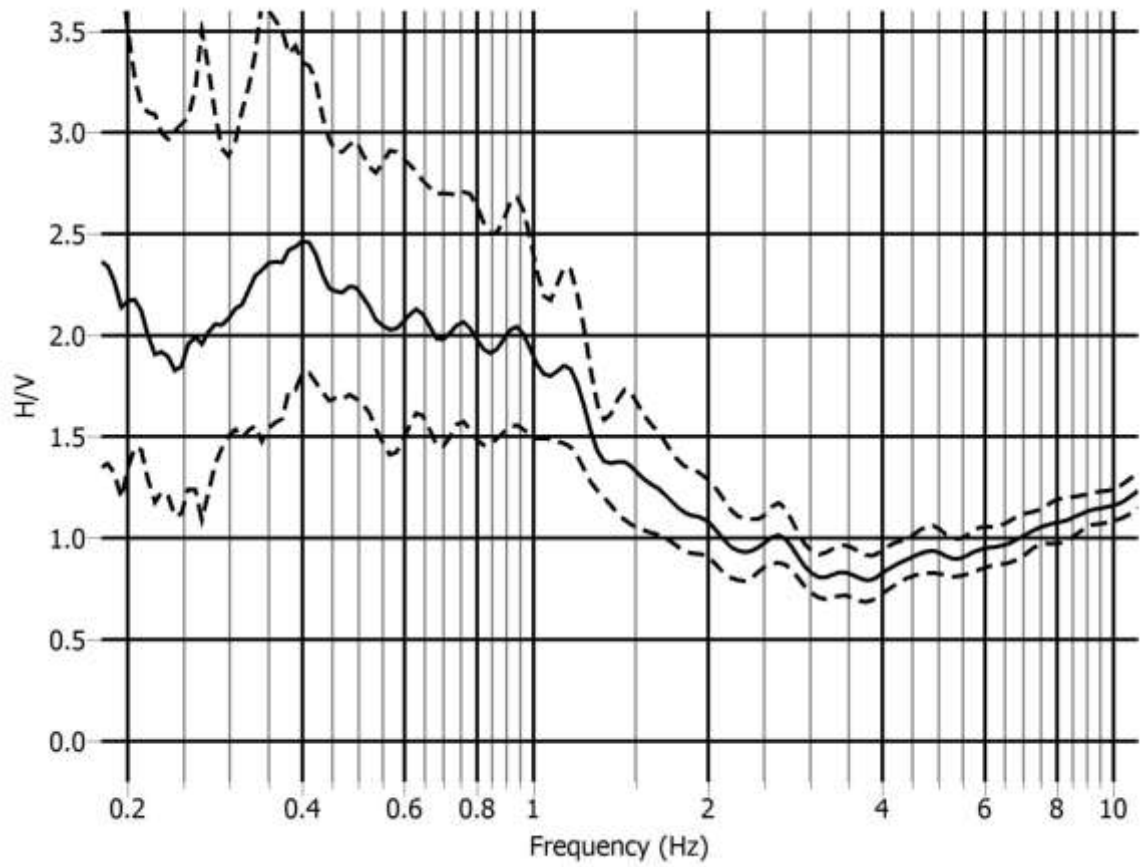

f_0=0.41 Hz; A_0 = 2.49; $A_{H/V}$ = (1.76, 3.52); $\sigma_A(f_0)$ = 1.41 & 1.41

i) f_0=0.41 Hz > (10/40.96=0.24 Hz); ii) n_c > 200; iii) $\sigma_A(f)$ < 3; at 0.205 Hz <f< 0.82 Hz

Satisfies all three criteria of Reliable H/V Curve

i) Between 0.1025 to 0.41 Hz, $A_{H/V}(f^-) > A_0/2$, Not satisfy

ii) Between 0.41 to 1.64 Hz, $A_{H/V}(f^+) > A_0/2$, Not satisfy

iii) $A_0 > 2.0$

iv) Between 0.3895 Hz to 0.4305 Hz, f_{peak} = (0.405 Hz, 0.39 Hz)

v) $\sigma_f = 0.079 < \varepsilon(f_0) = 0.082$

vi) $\sigma_A(f_0) = 1.41 < \Theta(f_0) = 2.5$

Satisfies four out of six criteria of Clear H/V Peak

Reliable curve and Unclear broad low frequency peak

MT45: City Center DRS (23°43'30.1"N, 90°24'35.3"E)

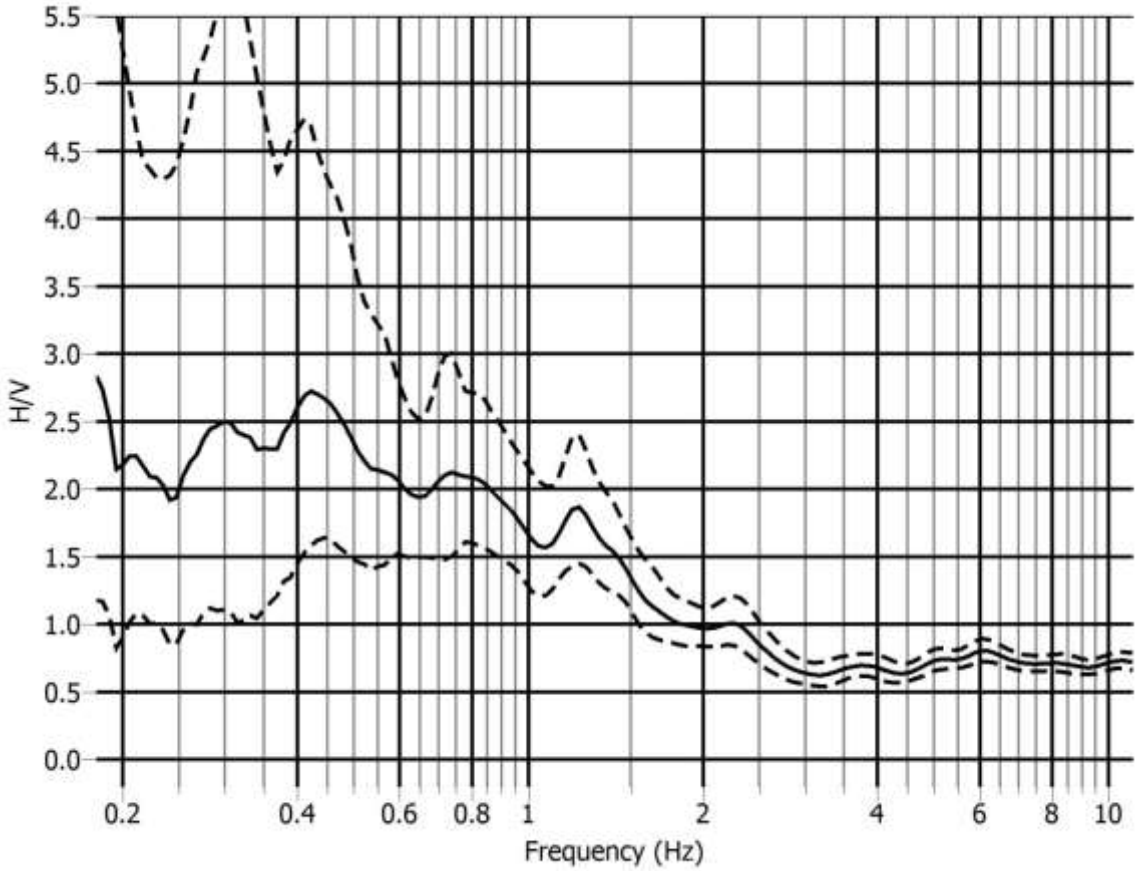

f_0=0.42 Hz; A_0 =2.71; $A_{H/V}$ = (1.57,4.69); $\sigma_A(f_0)$ = 1.73 & 1.73

i) f_0=0.42 Hz > (10/41=0.24 Hz); ii) $n_c > 200$; iii) $\sigma_A(f) < 3$; at 0.21 Hz <f< 0.84 Hz

Satisfies all three criteria of Reliable H/V Curve

i) Between 0.105 to 0.42 Hz, $A_{H/V}(f^-) > A_0/2$, Not satisfy

ii) Between 0.42 to 1.68 Hz, $A_{H/V}(f^+) < A_0/2$

iii) $A_0 > 2.0$

iv) Between 0.399 Hz to 0.441 Hz, f_{peak} = (0.44 Hz, 0.41 Hz)

v) $\sigma_f = 0.08 < \varepsilon(f_0) = 0.084$

vi) $\sigma_A(f_0) = 1.73 < \Theta(f_0) = 2.5$

Satisfies five out of six criteria of Clear H/V Peak

Reliable curve and Unclear low frequency peak

MT46: AGB Colony (23°43'59.4"N, 90°25'23.6"E)

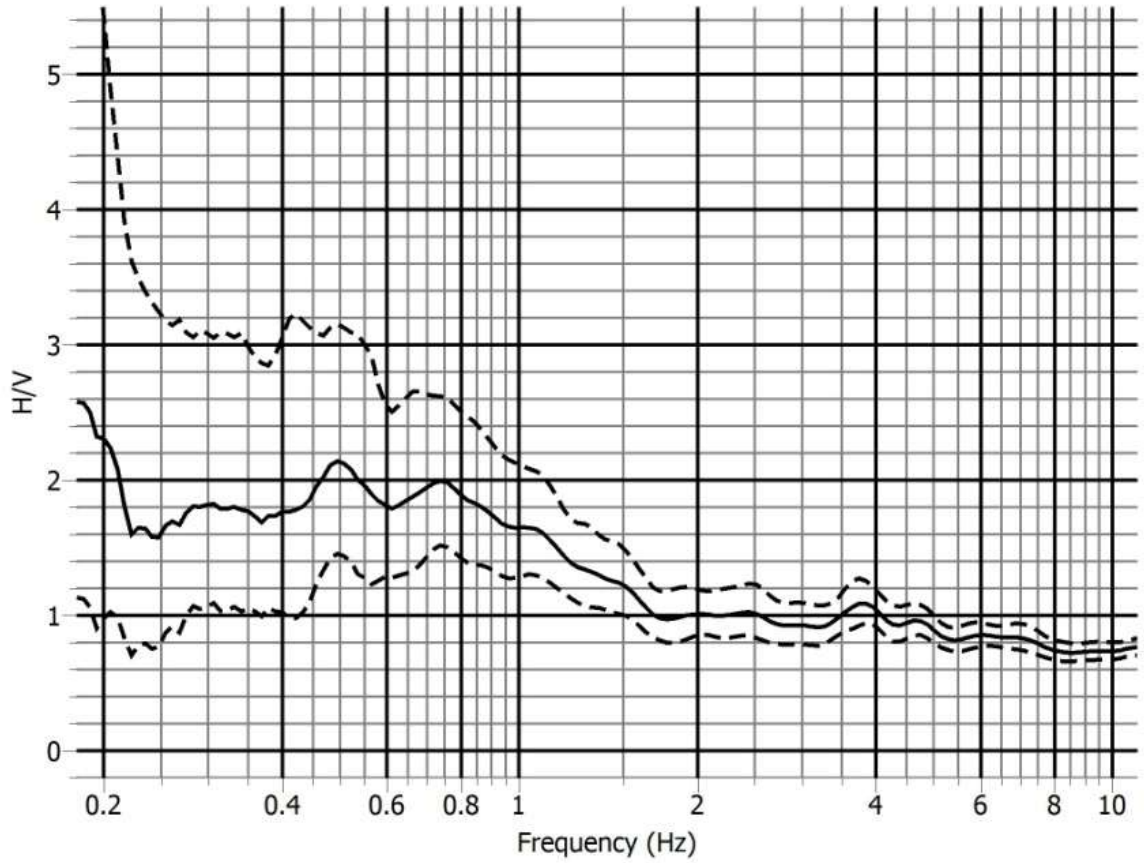

No peak has been found due to stiff soil stratum overlaying very hard soil stratum or bedrock at unknown depth

MT47: BMK Stadium (23°43'34.3"N, 90°25'43.7"E)
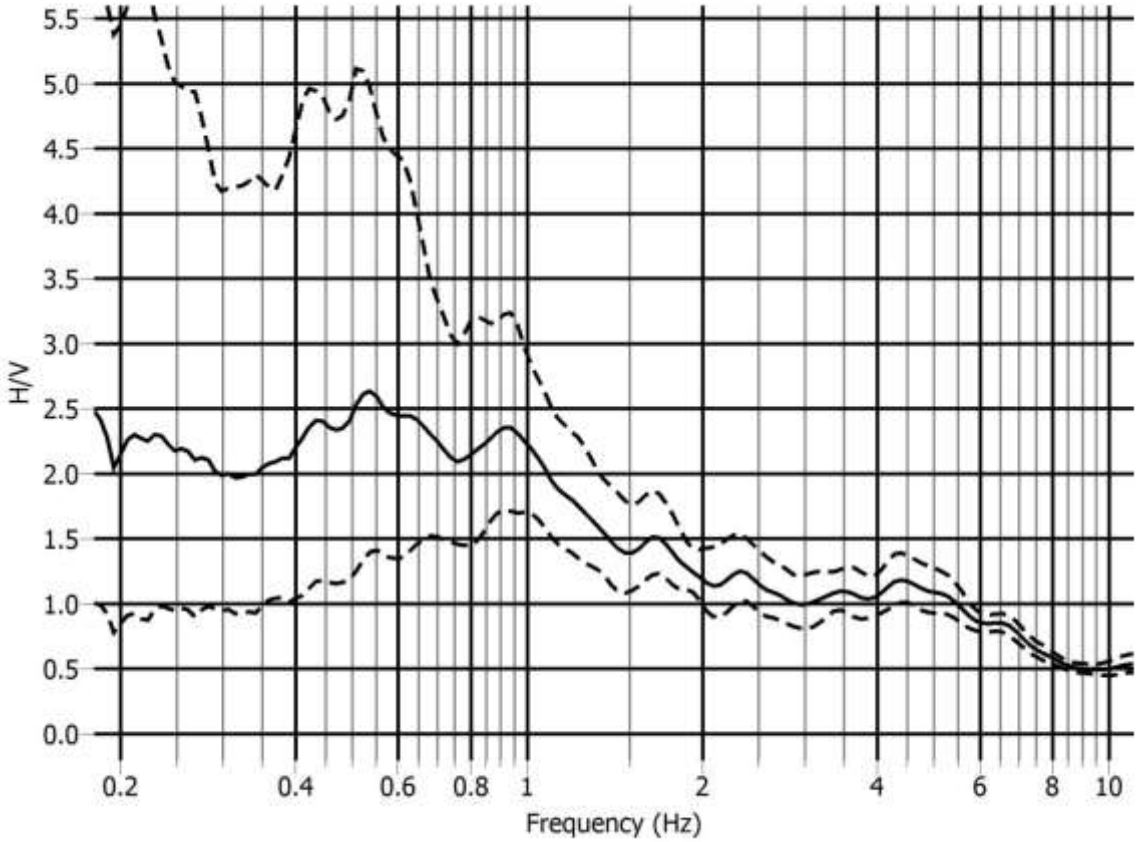
f_0=0.53 Hz; A_0 = 2.63; $A_{H/V}$ = (1.36,5.09); $\sigma_A(f_0)$ = 1.93 & 1.93
i) f_0=0.53 Hz>(10/40.96=0.24 Hz); ii) n_c > 200; iii) $\sigma_A(f)$ > 2; at 0.265 Hz <f< 1.06 Hz, Not satisfy **Satisfies two criteria of Reliable H/V Curve**
None Reliable curve and no interpretation.

MT48: West Katasur (23°45'03.8"N, 90°21'28.3"E)

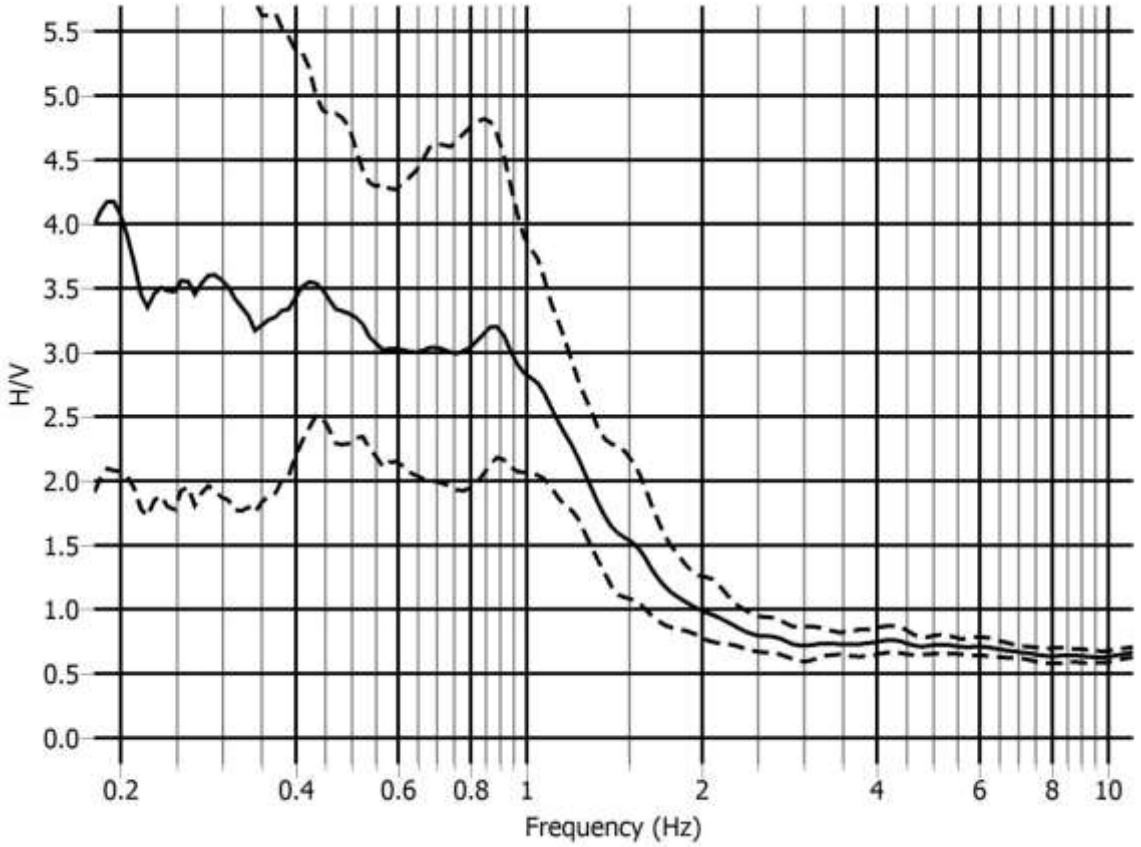

f_0=0.88 Hz; A_0 = 3.20; $A_{H/V}$ = (2.15,4.77); $\sigma_A(f_0)$ = 1.49 & 1.49

i) f_0=0.88 Hz > (10/40.96=0.24 Hz); ii) n_c > 200; iii) $\sigma_A(f)$ < 2; at 0.44 Hz <f< 1.76 Hz

Satisfies all three criteria of Reliable H/V Curve

i) Between 0.22 to 0.88 Hz, $A_{H/V}(f^-) > A_0/2$, Not satisfy

ii) Between 0.75 to 3.0 Hz, $A_{H/V}(f^+) < A_0/2$

iii) $A_0 > 2.0$

iv) Between 0.836 Hz to 0.924 Hz, f_{peak} = (0.89 Hz, 0.85 Hz)

v) $\sigma_f = 0.063 < \varepsilon(f_0) = 0.132$

vi) $\sigma_A(f_0) = 1.49 < \Theta(f_0) = 2$

Satisfies five out of six criteria of Clear H/V Peak

Reliable curve and Unclear low frequency peak

MT49: Majerchar DRS (23°44'09.2"N, 90°20'06.0"E)

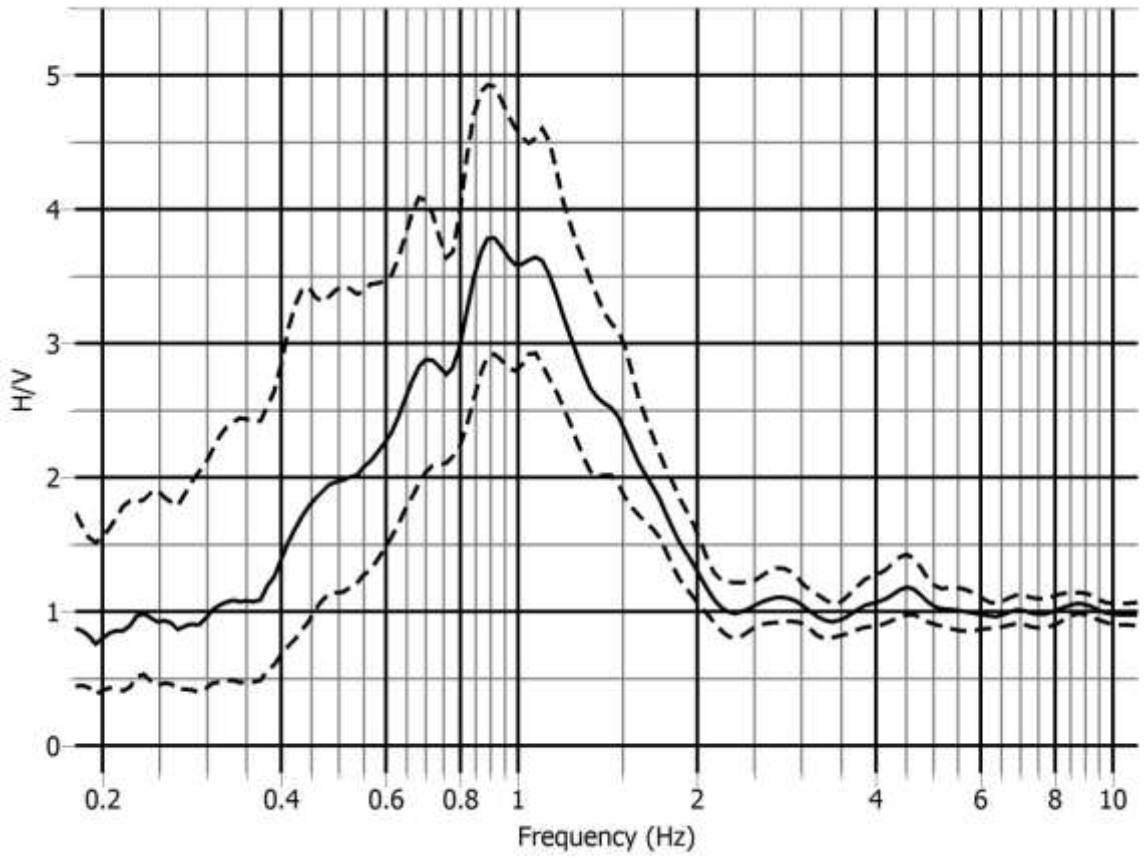

f_0=0.90 Hz; A_0 = 3.76; $A_{H/V}$ = (2.88, 4.90); $\sigma_A(f_0)$ = 1.30 & 1.30

i) f_0=0.90 Hz > (10/40.96=0.24 Hz); ii) n_c > 200; iii) $\sigma_A(f)$ < 2; at 0.45 Hz <f< 1.80 Hz

Satisfies all three criteria of Reliable H/V Curve

i) Between 0.225 to 0.90 Hz, $A_{H/V}(f^-) < A_0/2$

ii) Between 0.90 to 3.60 Hz, $A_{H/V}(f^+) < A_0/2$

iii) $A_0 > 2.0$

iv) Between 0.855 Hz to 0.945 Hz, f_{peak} = (0.91 Hz, 0.90 Hz)

v) $\sigma_f = 0.167 > \varepsilon(f_0) = 0.135$, Not satisfy

vi) $\sigma_A(f_0) = 1.30 < \Theta(f_0) = 2$

Satisfies five out of six criteria of Clear H/V Peak

Reliable curve and Clear low frequency peak

MT50: Hazaribag DRS (23°43'55.0"N, 90°21'42.5"E)

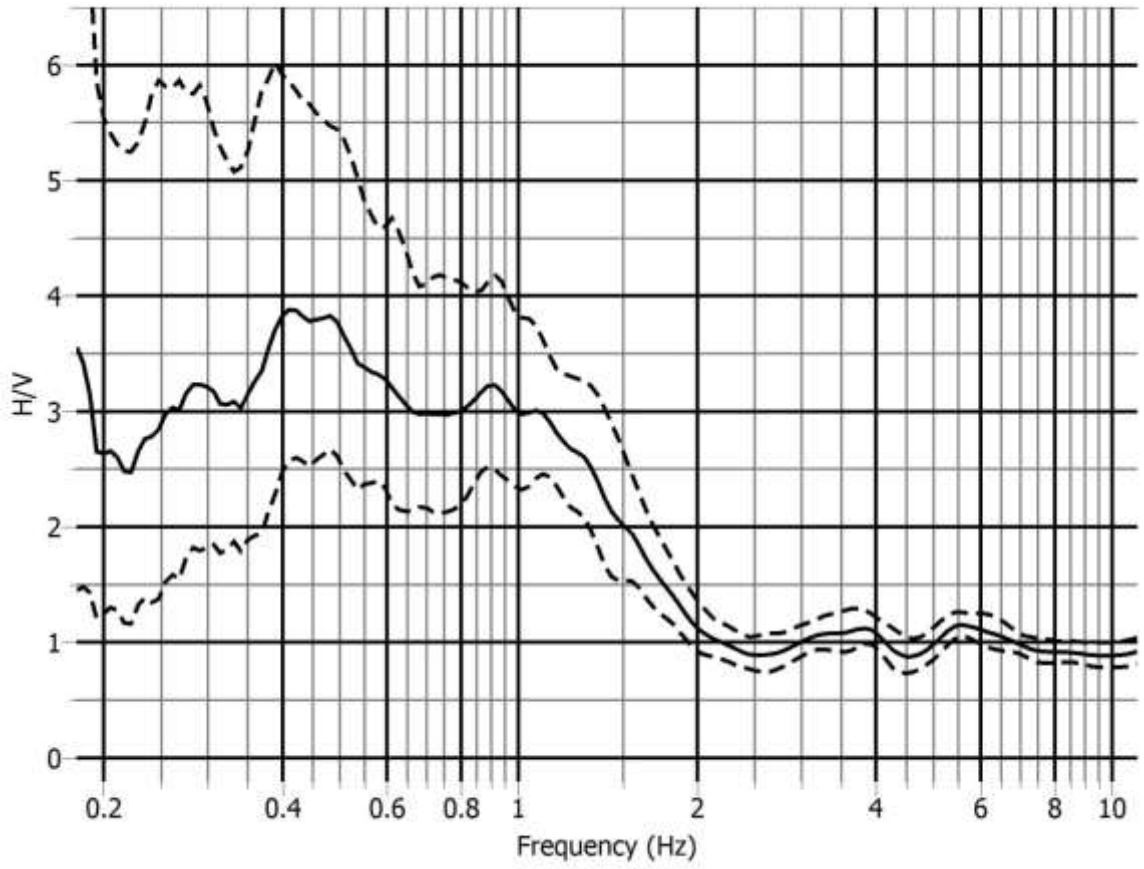

f_0=0.41 Hz; A_0 =3.89; $A_{H/V}$ = (2.52,6.0); $\sigma_A(f_0)$ = 1.54 & 1.54

i) f_0=0.41 Hz > (10/40.96=0.24 Hz); ii) n_c > 200; iii) $\sigma_A(f)$ < 3; at 0.205 Hz <f< 0.82 Hz

Satisfies all three criteria of Reliable H/V Curve

i) Between 0.1025 to 0.41 Hz, $A_{H/V}(f^-) > A_0/2$, Not satisfy

ii) Between 0.41 to 1.64 Hz, $A_{H/V}(f^+) < A_0/2$

iii) $A_0 > 2.0$

iv) Between 0.3895 Hz to 0.4305 Hz, f_{peak} = (0.42 Hz, 0.39 Hz)

v) $\sigma_f = 0.095 > \varepsilon(f_0) = 0.084$, Not satisfy

vi) $\sigma_A(f_0) = 1.54 < \Theta(f_0) = 2.5$

Satisfies four out of six criteria of Clear H/V Peak

Reliable curve and Unclear broad low frequency peak

MT51: Zinzira DRS (23°47'33.1"N, 90°23'52.9"E)
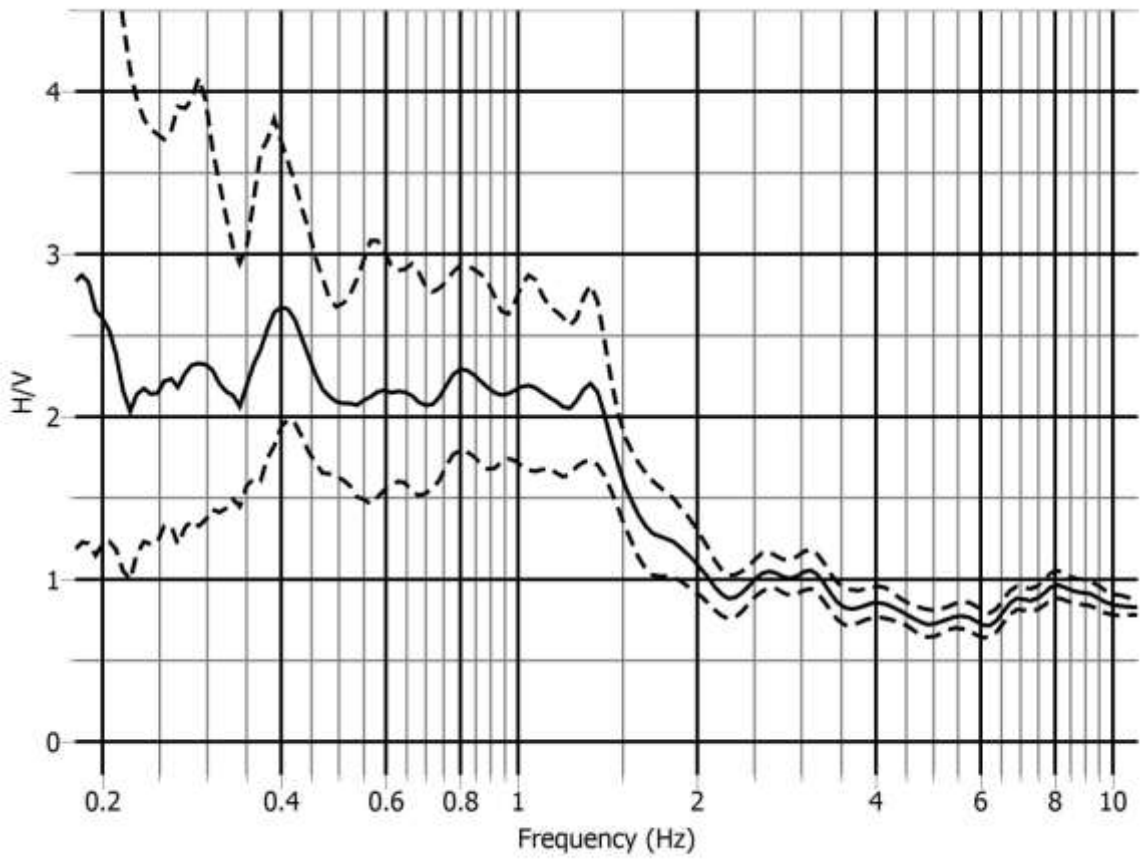
f_0=0.40 Hz; A_0 = 2.72; $A_{H/V}$ = (1.97,3.76); $\sigma_A(f_0)$ = 1.38 & 1.38
i) f_0=0.40 Hz > (10/40.96=0.24 Hz); ii) n_c > 200; iii) $\sigma_A(f)$ < 3; at 0.20 Hz <f< 0.80 Hz **Satisfies all three criteria of Reliable H/V Curve**
i) Between 0.10 to 0.40 Hz, $A_{H/V}(f^-) > A_0/2$, Not satisfy ii) Between 0.40 to 1.60 Hz, $A_{H/V}(f^+) > A_0/2$, Not satisfy iii) A_0 > 2.0 iv) Between 0.38 Hz to 0.42 Hz, f_{peak} = (0.41 Hz, 0.39 Hz) v) $\sigma_f = 0.079 < \varepsilon(f_0) = 0.080$ vi) $\sigma_A(f_0) = 1.38 < \Theta(f_0) = 2.5$ **Satisfies four out of six criteria of Clear H/V Peak**
Reliable curve and Unclear broad low frequency peak

MT52: Postogola DRS (23°41'17.3"N, 90°26'04.0"E)

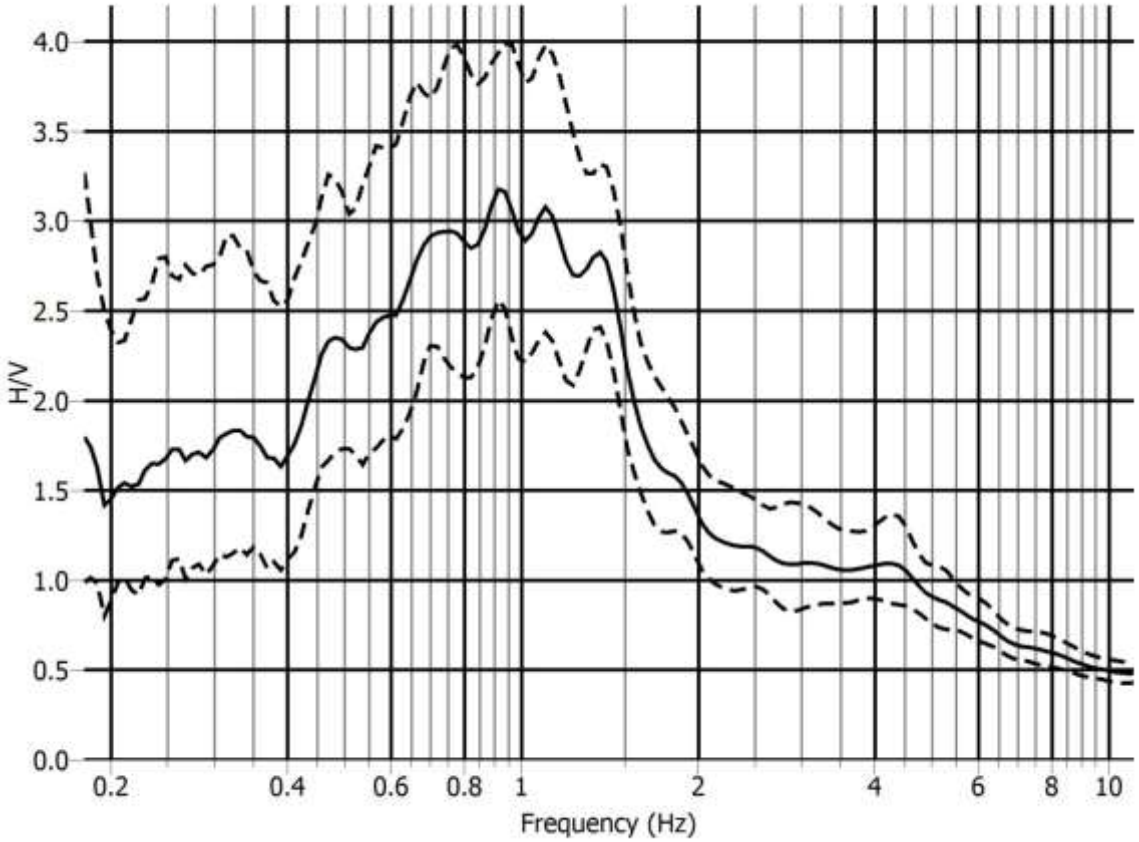

f_0=0.92 Hz; A_0 = 3.16; $A_{H/V}$ = (2.51, 4.0); $\sigma_A(f_0)$ = 1.26 & 1.26

i) f_0=0.92 Hz > (10/40.96=0.24 Hz); ii) n_c > 200; iii) $\sigma_A(f)$ < 2; at 0.46 Hz <f< 1.84 Hz

Satisfies all three criteria of Reliable H/V Curve

i) Between 0.23 to 0.92 Hz, $A_{H/V}(f^-) > A_0/2$, Not satisfy

ii) Between 0.92 to 3.68 Hz, $A_{H/V}(f^+) < A_0/2$

iii) $A_0 > 2.0$

iv) Between 0.874 Hz to 0.966 Hz, f_{peak} = (0.92 Hz, 0.95 Hz)

v) $\sigma_f = 0.160 > \varepsilon(f_0) = 0.138$, Not satisfy

vi) $\sigma_A(f_0) = 1.26 < \Theta(f_0) = 2$

Satisfies four out of six criteria of Clear H/V Peak

Reliable curve and Unclear broad low frequency peak

MT53: Nandipara TBS (23°44'44.5"N, 90°26'41.1"E)

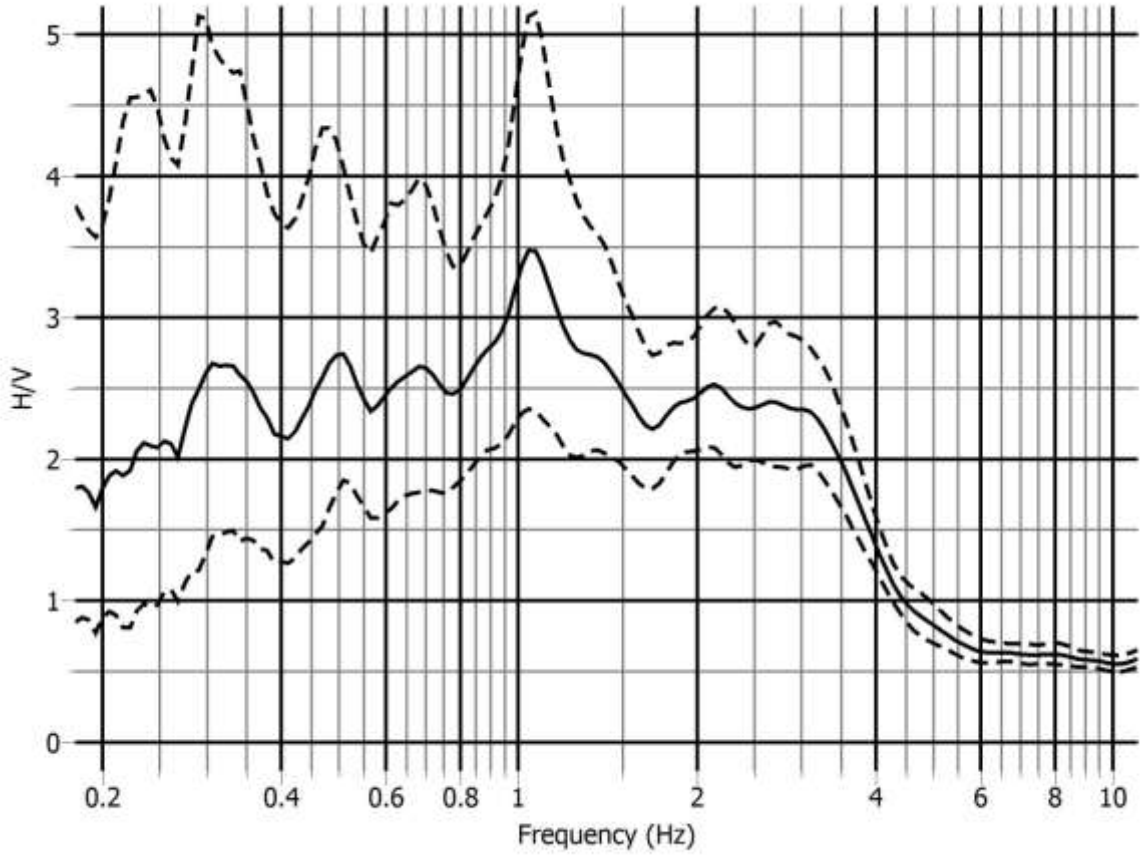

f_0=1.06 Hz; A_0 = 3.49; $A_{H/V}$ = (2.35,5.16); $\sigma_A(f_0)$ = 1.48 & 1.48

i) f_0=1.06 Hz > (10/40.96=0.24 Hz); ii) n_c > 200; iii) $\sigma_A(f)$ < 2; at 0.53 Hz <f< 2.12 Hz

Satisfies all three criteria of Reliable H/V Curve

i) Between 0.265 to 1.06 Hz, $A_{H/V}(f^-) > A_0/2$, Not satisfy

ii) Between 1.06 to 4.24 Hz, $A_{H/V}(f^+) < A_0/2$

iii) $A_0 > 2.0$

iv) Between 1.01 Hz to 1.11 Hz, f_{peak} = (1.06 Hz, 1.09 Hz)

v) $\sigma_f = 0.153 > \varepsilon(f_0) = 0.106$, Not satisfy

vi) $\sigma_A(f_0) = 1.48 < \Theta(f_0) = 1.78$

Satisfies four out of six criteria of Clear H/V Peak

Reliable curve and Unclear broad peak

MT54: Donia TBS (23°42'01.2"N, 90°27'24.4"E)

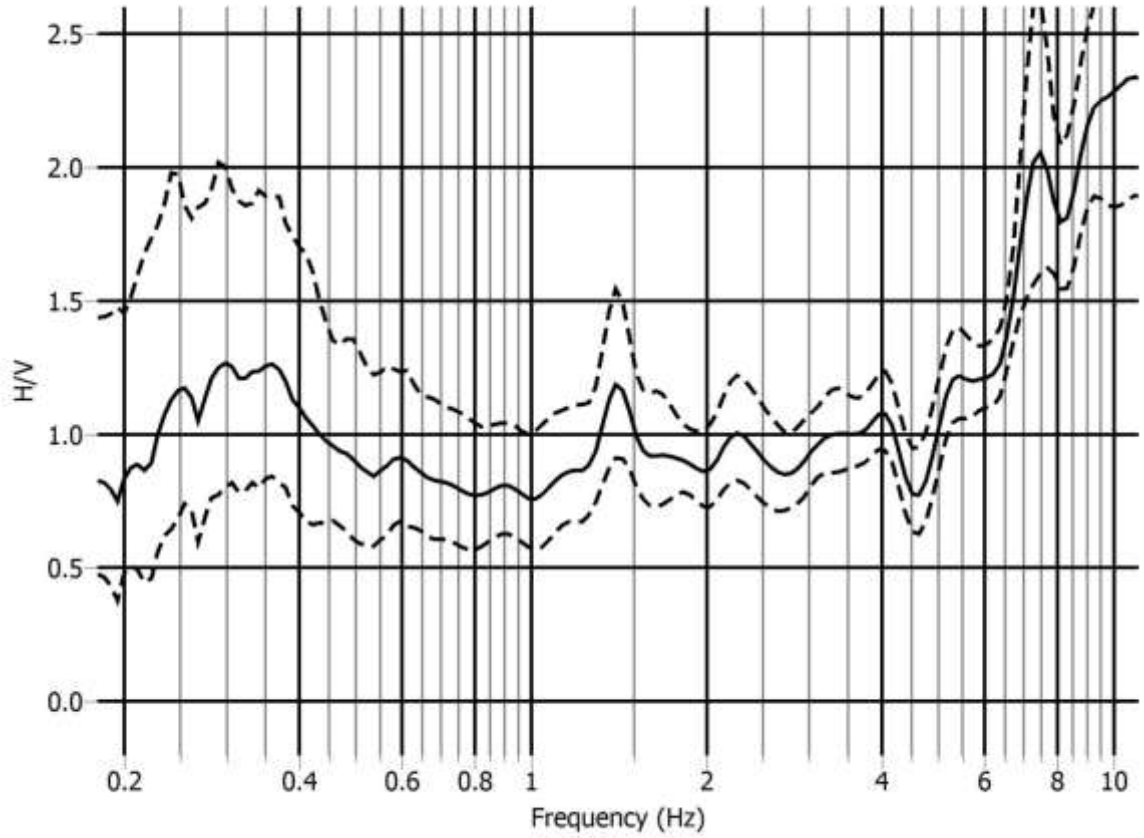

Could not read clearly for interpretation.

MT55: Doleswar DRS (23°40'25.4"N, 90°26'21.0"E)

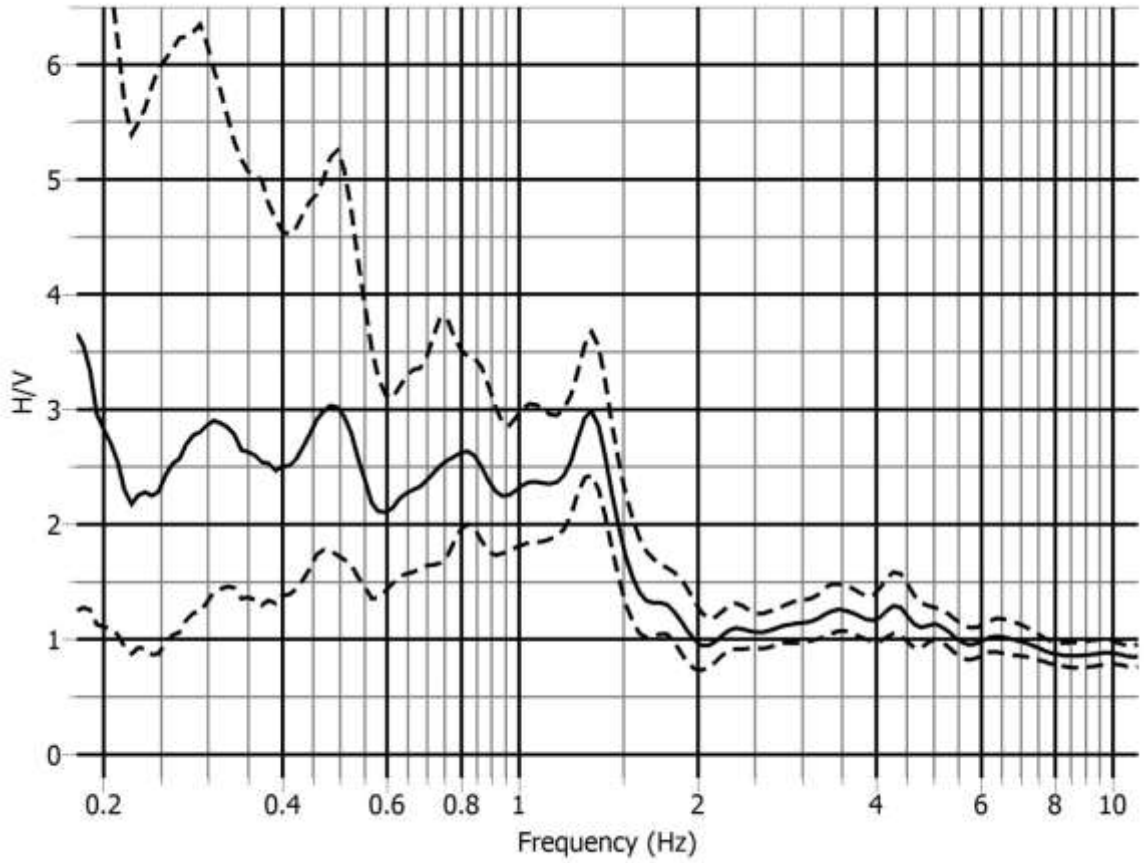

f_0=1.36 Hz; A_0 =3; $A_{H/V}$ = (2.46,3.65); $\sigma_A(f_0)$ = 1.22 & 1.22

i) f_0=1.36 Hz > (10/40.96=0.24 Hz); ii) n_c > 200; iii) $\sigma_A(f)$ < 2; at 0.68 Hz <f< 2.72 Hz

Satisfies all three criteria of Reliable H/V Curve

i) Between 0.34 to 1.36 Hz, $A_{H/V}(f^-) > A_0/2$, Not satisfy

ii) Between 1.43 to 5.72 Hz, $A_{H/V}(f^+) < A_0/2$

iii) $A_0 > 2.0$

iv) Between 1.292 Hz to 1.428 Hz, f_{peak} = (1.35 Hz, 1.36 Hz)

v) $\sigma_f = 0.128 < \varepsilon(f_0) = 0.136$

vi) $\sigma_A(f_0) = 1.22 < \Theta(f_0) = 1.78$

Satisfies five out of six criteria of Clear H/V Peak

Reliable curve and Unclear Peak

MT56: Pangaon Valve Station (23°39'47.5"N, 90°26'58.3"E)
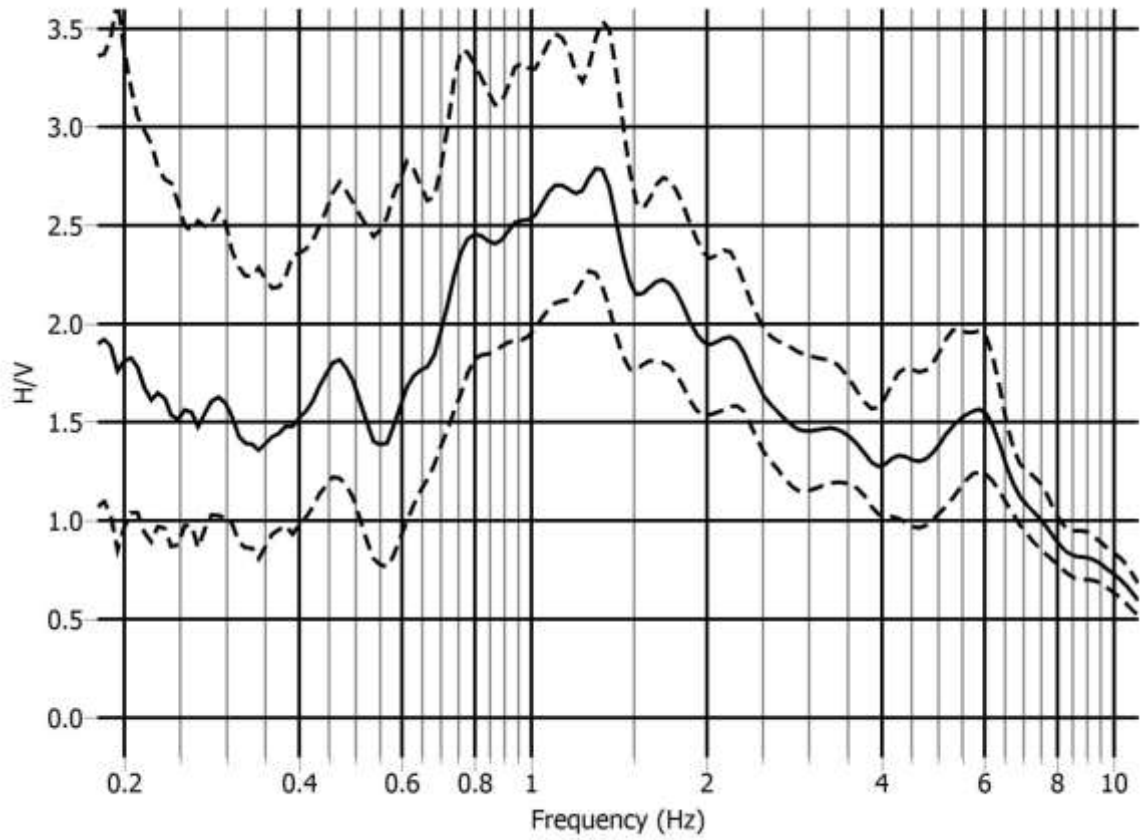
f_0=1.30 Hz; A_0 = 2.81; $A_{H/V}$ = (2.25, 3.51); $\sigma_A(f_0)$ = 1.25 & 1.25
i) f_0=1.30 Hz > (10/40.96=0.24 Hz); ii) n_c > 200; iii) $\sigma_A(f)$ < 2; at 0.65 Hz <f< 2.60 Hz **Satisfies all three criteria of Reliable H/V Curve**
i) Between 0.325 to 1.30 Hz, $A_{H/V}(f^-) > A_0/2$, Not satisfy ii) Between 1.30 to 5.20 Hz, $A_{H/V}(f^+) < A_0/2$ iii) $A_0 > 2.0$ iv) Between 1.235 Hz to 1.365 Hz, f_{peak} = (1.26 Hz, 1.34 Hz) v) $\sigma_f = 0.141 > \varepsilon(f_0) = 0.130$, Not satisfy vi) $\sigma_A(f_0) = 1.25 < \Theta(f_0) = 1.78$ **Satisfies four out of six criteria of Clear H/V Peak**
Reliable curve and Unclear broad Peak

MT57: Demra CGS (23°42'46.7"N, 90°30'11.7"E)
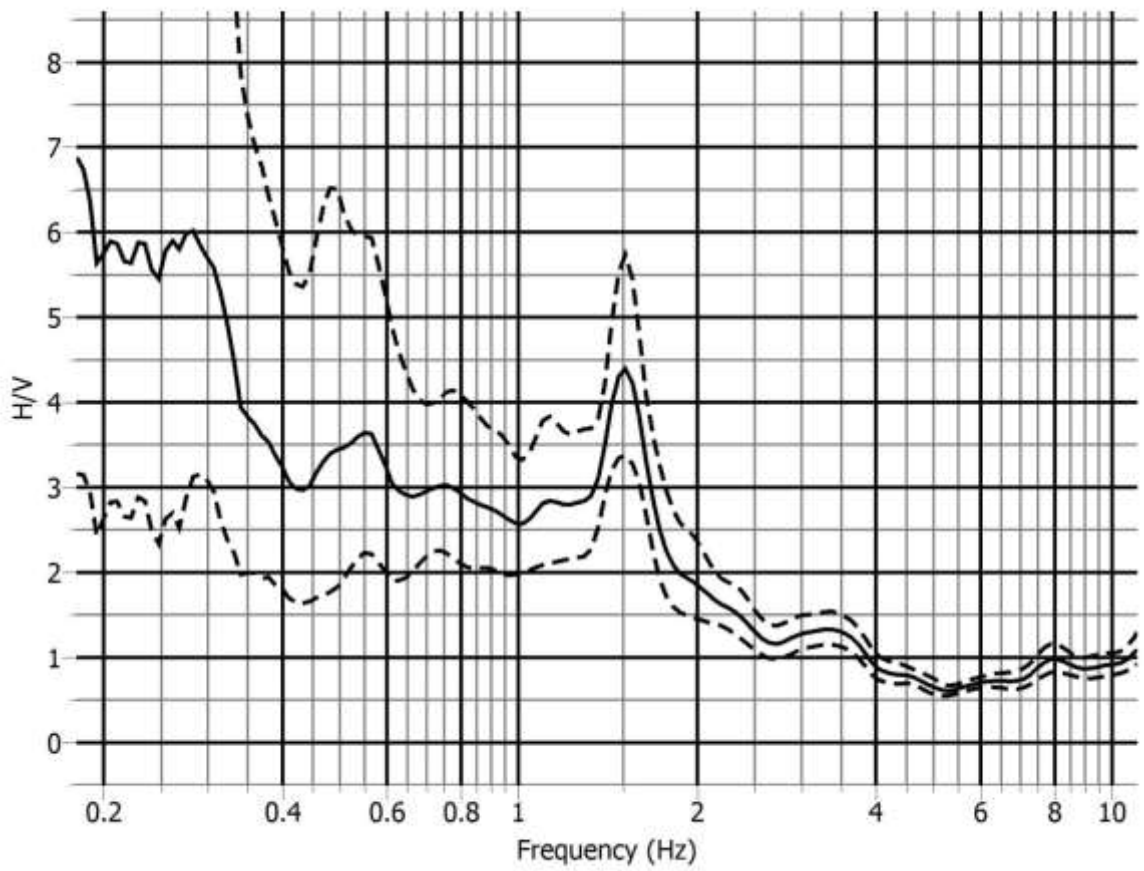
f_0=1.5 Hz; A_0 =4.38; $A_{H/V}$ = (3.36,5.71); $\sigma_A(f_0)$ = 1.30 & 1.30
i) f_0=1.5 Hz > (10/40.96=0.24 Hz); ii) n_c > 200; iii) $\sigma_A(f)$ < 2; at 0.75 Hz <f< 3 Hz **Satisfies all three criteria of Reliable H/V Curve**
i) Between 0.375 to 1.5 Hz, $A_{H/V}(f^-) > A_0/2$, Not satisfy ii) Between 1.5 to 6 Hz, $A_{H/V}(f^+) < A_0/2$ iii) $A_0 > 2.0$ iv) Between 1.425 Hz to 1.575 Hz, f_{peak} = (1.495 Hz, 1.505 Hz) v) $\sigma_f = 0.139 < \varepsilon(f_0) = 0.15$ vi) $\sigma_A(f_0) = 1.30 < \Theta(f_0) = 1.78$ **Satisfies five out of six criteria of Clear H/V Peak**
Reliable curve and unclear Peak

MT58: Joydevpur CGS (24°00'31.5"N, 90°24'54.4"E)

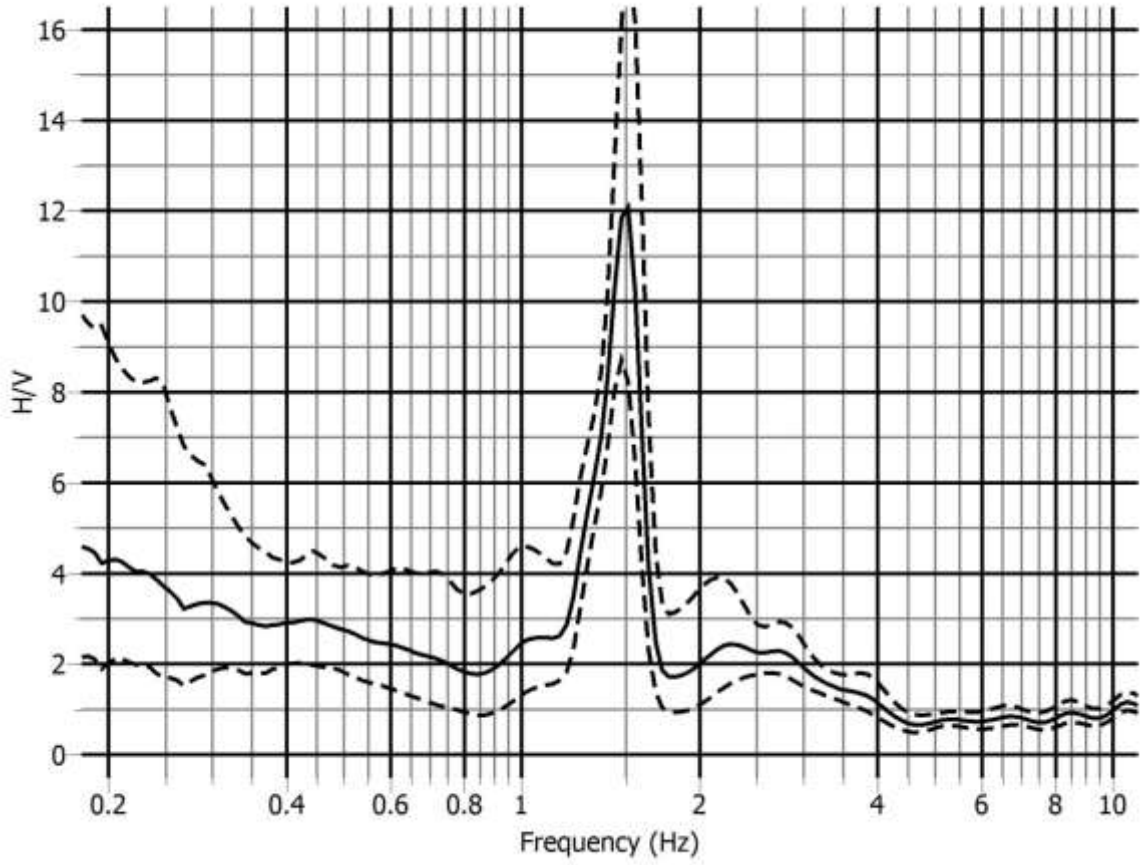

f_0=1.5 Hz; A_0 =12.1; $A_{H/V}$ = (8.9,16.46); $\sigma_A(f_0)$ = 1.36 & 1.36

i) f_0=1.50 Hz > (10/40.96=0.24 Hz); ii) n_c > 200; iii) $\sigma_A(f)$ < 2; at 0.75 Hz <f< 3.0 Hz

Satisfies all three criteria of Reliable H/V Curve

i) Between 0.375 to 1.5 Hz, $A_{H/V}(f^-) < A_0/2$

ii) Between 1.5 to 6.0 Hz, $A_{H/V}(f^+) < A_0/2$

iii) $A_0 > 2.0$

iv) Between 1.425 Hz to 1.575 Hz, f_{peak} = (1.49Hz, 1.52 Hz)

v) $\sigma_f = 0.03 < \varepsilon(f_0) = 0.15$

vi) $\sigma_A(f_0) = 1.36 < \Theta(f_0) = 1.78$

Satisfies six out of six criteria of Clear H/V Peak

Reliable curve and Clear peak

Note: Peak has been amplified due to a nearly piling work.